

---

# **Optimal Design of Power-to-X Processes**

---

## **Optimales Design von Power-to-X-Prozessen**

---

Von der Fakultät für Maschinenwesen der Rheinisch-Westfälischen  
Technischen Hochschule Aachen zur Erlangung des akademischen Grades  
eines Doktors der Ingenieurwissenschaften genehmigte Dissertation

vorgelegt von

Jannik Burre

Berichter: Universitätsprofessor Alexander Mitsos, Ph.D.  
Associate Professor Mariano Martín Martín, PhD

Tag der mündlichen Prüfung: 28. März 2022

Diese Dissertation ist auf den Internetseiten  
der Universitätsbibliothek online verfügbar.

Titel: Optimal Design of Power-to-X Processes

Autor: Jannik Burre

Reihe: Aachener Verfahrenstechnik Series  
AVT.SVT - Process Systems Engineering  
Band 25 (2022)

Herausgeber: Aachener Verfahrenstechnik  
Forckenbeckstraße 51  
52074 Aachen  
Tel.: +49 (0)241 80 97717  
Fax.: +49 (0)241 80 92326  
E-Mail: [secretary.svt@avt.rwth-aachen.de](mailto:secretary.svt@avt.rwth-aachen.de)  
<https://www.avt.rwth-aachen.de>

---

## Vorwort

Die vorliegende Arbeit entstand während meiner Zeit als wissenschaftlicher Mitarbeiter am Lehrstuhl für Systemverfahrenstechnik (SVT) der RWTH Aachen University.

Mein Dank gilt zuallererst meinem Doktorvater, Professor Alexander Mitsos, Ph.D., für die herausragende Betreuung, die inspirierenden Ideen und die motivierenden Gespräche. Weiterhin danke ich Professor Mariano Martín Martín, PhD, für die Übernahme des Koreferats. Professor Dr.-Ing. Robert Pitz-Paal danke ich für die Übernahme des Prüfungsvorsitzes.

Ich danke dem Bundesministerium für Bildung und Forschung (BMBF) für die zur Verfügung gestellten Fördermittel innerhalb des Projekts Kopernikus Power-to-X und NAMOSYN und dem Projektträger Jülich (PtJ) für die Organisation und Aufsicht der Projekte.

Ein besonderer Dank geht an meine gesamten Kolleg:innen der SVT, insbesondere für deren große Unterstützung, für die fachlichen und nicht fachlichen Diskussionen und generell für die tolle gemeinsame Zeit am Institut, auf hoher See und bei diversen sonstigen Veranstaltungen. Besonders danke ich meinen ehemaligen Bürokolleg:innen Eduardo Schultz, Chryssa Kappatou, Adrian Caspari, Jan Schulze und Johannes Faust für die vielen lustigen Momente. Andreas Bremen und Matthias Leitl danke ich für die starke Unterstützung im Prozessentwicklungs-Team. Andrea König und Philipp Ackermann danke ich für die super Zusammenarbeit im Event-Team.

Des Weiteren geht ein ganz großer Dank an meinen langjährigen Projektpartner und zweiten Betreuer Dominik Bongartz für die vielen Dinge, die ich von ihm lernen konnte. Ich danke Luisa Brée, Kosan Roh, Christoph Kabatnik, Sarah Deutz, Simon Völker, Christian Gierlich, Anja Fink, Ruiyan Sun, Chalachew Mebrahtu, Ole Osterthun und Ahmad Omari für die tolle Zusammenarbeit in verschiedensten Projekten.

Nicht unwesentlich zu meiner reibungslosen Zeit an der SVT beigetragen haben zudem das gesamte Team um Petra Eissa, Wanda Frohn, Jutta Friedrich, Sascha Gerhards und Didem Uslu, denen ich dafür herzlich danken möchte. Des Weiteren bedanke ich mich bei meinen gesamten studentischen Hilfskräften und Studierenden, die mich bei meiner Forschung tatkräftig unterstützt haben, insbesondere Philipp Dürr, Sven Dörner, Huixin Shi, Julian Ufert und Mohamed Al-Khatib. Meinem Mitbewohner Jens Berger danke ich dafür, dass er mir den Übergang in den Feierabend so einfach gemacht hat.

Schließlich bedanke ich mich vor allem bei meiner Familie dafür, dass sie immer für mich da ist, mich in jeder Situation unterstützt hat und mir bei jeder Entscheidung und Unternehmung vertraut hat.

Aachen, im März 2022

*Jannik Burre*



---

# Contents

<b>Kurzfassung</b>	<b>VII</b>
<b>Summary</b>	<b>IX</b>
<b>Publications and Copyrights</b>	<b>XI</b>
<b>1. Introduction</b>	<b>1</b>
<b>2. Reaction Pathways for Dimethoxymethane Synthesis</b>	<b>5</b>
2.1. Established Pathway . . . . .	5
2.2. Oxidative Pathway . . . . .	5
2.3. Reductive Pathway . . . . .	6
2.4. Dehydrogenative Pathway . . . . .	7
2.5. Transfer-Hydrogenative Pathway . . . . .	7
<b>3. Benchmark Processes of Oxymethylene Ether Production</b>	<b>9</b>
3.1. Dimethoxymethane Production . . . . .	9
3.1.1. Process Description . . . . .	9
3.1.2. Model Description . . . . .	10
3.1.3. Process Efficiency . . . . .	11
3.2. OME <sub>3-5</sub> Production . . . . .	11
3.2.1. Synthesis Routes . . . . .	13
3.2.2. Process Description . . . . .	15
3.2.3. Model Description . . . . .	17
3.2.4. Results and Discussion . . . . .	22
3.3. Conclusion . . . . .	28
<b>4. Optimal Process Design of Dimethoxymethane Production</b>	<b>29</b>
4.1. Hierarchical Comparison of Reaction Pathways . . . . .	29
4.1.1. Process Design and Evaluation Accounting for TRL . . . . .	30
4.1.2. Results on Key Performance Indicators for DMM Production . . . . .	34
4.1.3. Conclusion . . . . .	45
4.2. Optimal Process Design for Reductive DMM Production . . . . .	47
4.2.1. Process Flowsheet for Reductive DMM Production . . . . .	48
4.2.2. Thermodynamic Modeling . . . . .	49
4.2.3. Process Modeling . . . . .	54
4.2.4. Problem Formulation and Objective Function . . . . .	57
4.2.5. Results and Discussion . . . . .	58
4.2.6. Conclusion . . . . .	61
4.3. Process Chains via Reductive DMM Production . . . . .	63
4.3.1. DMM Production from Renewable H <sub>2</sub> and CO <sub>2</sub> . . . . .	63

4.3.2. OME <sub>3-5</sub> Production from Renewable H <sub>2</sub> and CO <sub>2</sub> . . . . .	64
<b>5. MINLP Problem Formulations for Global Superstructure Optimization</b>	<b>67</b>
5.1. Problem Definition . . . . .	68
5.1.1. Simple Illustrative Example Problem . . . . .	68
5.1.2. Multiple-Disjunction Example Problem . . . . .	70
5.2. Problem Formulations . . . . .	71
5.2.1. Big-M . . . . .	72
5.2.2. Convex Hull . . . . .	72
5.2.3. MPEC . . . . .	74
5.2.4. Plus Function . . . . .	76
5.2.5. Direct MINLP . . . . .	76
5.2.6. Reduced-Space Formulation . . . . .	77
5.3. Results for the Example Problems . . . . .	78
5.3.1. Simple Illustrative Example Problem . . . . .	78
5.3.2. Multiple-Disjunction Example Problem . . . . .	80
5.3.3. Selective Branching for FS Formulations . . . . .	82
5.4. Application to Problems with Piecewise-Defined Functions . . . . .	83
5.5. Conclusion . . . . .	88
<b>6. Conclusion and Outlook</b>	<b>91</b>
<b>A. Reaction Kinetic Parameters for OME<sub>3-5</sub> Formation</b>	<b>95</b>
<b>B. DMM Pathway Comparison</b>	<b>97</b>
<b>C. PCP-SAFT EOS Parameters and Sensitivity Analysis</b>	<b>113</b>
<b>D. Material Balances and Energy Demand of Process Chains via Reductive DMM Production</b>	<b>115</b>
<b>E. MINLP Problem Formulations for Superstructure Optimization</b>	<b>117</b>
<b>Bibliography</b>	<b>141</b>

---

# Kurzfassung

Der zunehmende Anteil erneuerbarer Energiequellen im Stromnetz führt zu Abregelungen, die die volle Ausschöpfung des ökologischen und wirtschaftlichen Potenzials von erneuerbarem Strom verhindern. *Power-to-X*-Prozesse können diesen Strom für die Herstellung von Produkten nutzen, die sonst aus fossilen Quellen erzeugt würden. Für einen größtmöglichen Nutzen müssen diese Prozesse allerdings hinsichtlich maximaler Ressourceneffizienz optimiert sein. Der alleinige Austausch von Rohstoffen ist in der Regel nicht zielführend. Daher entwickeln wir zur Identifizierung und zum Design nachhaltiger Prozesskonzepte optimierungsbasierte Methoden, die wir auf die Herstellung von Dimethoxymethan (DMM oder OME<sub>1</sub>)—ein vielversprechender synthetischer Kraftstoff und Zwischenprodukt für die Herstellung von längerkettigen Oxymethylenethern (OME<sub>3-5</sub>)—anwenden.

Um die etablierten Prozesskonzepte zur DMM- und OME<sub>3-5</sub>-Produktion analysieren zu können, implementieren wir detaillierte Prozessmodelle. Mit diesen zeigen wir, dass selbst unter Berücksichtigung einer maximal möglichen Wärmeintegration diese Prozesse deutlich ineffizienter sind als die zur Produktion von anderen synthetischen Kraftstoffen. Für eine effiziente Produktion von DMM müssen also grundlegend neue Prozesse entwickelt werden.

*Power-to-X*-Prozesse befinden sich in der Regel auf einem unterschiedlichen Entwicklungsstand. Um einen fairen Vergleich und optimales Prozessdesign zu ermöglichen, entwickeln wir ein Framework, das optimierungsbasierte Methoden auf verschiedenen Hierarchieebenen einbezieht. Das Framework ermöglicht eine systematische Prozessentwicklung und -bewertung hinsichtlich drei Indikatoren: Produktionskosten, Exergieeffizienz und CO<sub>2</sub>-Fußabdruck. Bei dessen Anwendung auf fünf Reaktionswege für die DMM-Produktion haben wir die direkte CO<sub>2</sub>-Reduktion als am nachhaltigsten identifizieren können.

Für eine erfolgreiche industrielle Umsetzung sind detaillierte Prozessmodelle erforderlich. Da die hohe Komplexität solcher Modelle oft Schwierigkeiten für die deterministische Optimierung mit sich bringt, entwickeln wir für die reduktive DMM-Produktion ein hybrides Prozessmodell bestehend aus Gaußschen Prozessen und künstlichen neuronalen Netzen. Zur Lösung des nichtkonvexen Optimierungsproblems verwenden wir eine *reduced-space*-Formulierung und ein Hybrid aus der McCormick- und der *auxiliary variable*-Methode, die in unserem deterministischen globalen Solver MAiNGO implementiert sind.

Da die Entwicklung von *Power-to-X*-Prozessen oft diskrete Entscheidungen enthält, analysieren wir Problemformulierungen bzgl. ihrer Eignung für die globale Superstrukturoptimierung und wenden die vielversprechendste auf die Optimierung der reduktiven DMM-Produktion an. Für gemischt-ganzzahlige nichtlineare Probleme, die nichtkonvexe Funktionen enthalten, konnten wir diejenigen Formulierungen als vielversprechend identifizieren, die die Anzahl der Optimierungsvariablen reduzieren. Obwohl diese nichtkonvexe Terme mit sich bringen, bleiben die Relaxierungen für unsere Beispiele vergleichsweise eng. Um allgemeingültige Aussagen ableiten zu können, wäre allerdings deren Anwendung auf eine große Bibliothek von Benchmark-Problemen unterschiedlicher Komplexität notwendig.

Die Anwendung von optimierungsbasierten Methoden auf die DMM-Produktion hat großes Potenzial aufgezeigt. Es wurde aber auch Verbesserungspotenzial identifiziert—sowohl bzgl. der Methoden als auch der Produktion von DMM als *Power-to-X*-Prozess.





---

# Summary

The increasing share of renewable energy sources in the electricity grid causes curtailments, which prevent exploiting the full environmental and economic potential of renewable electricity. *Power-to-X* processes can utilize this electricity to produce certain products that would have been otherwise produced from fossil-based sources. To benefit the most, these Power-to-X processes need to be optimized for a maximum resource-efficiency. We demonstrate that the sole replacement of raw materials for industrial process concepts is not expedient. We therefore develop optimization-based methods to identify sustainable process concepts and support their optimal design. These methods are applied to the production of dimethoxymethane (referred to as DMM or OME<sub>1</sub>)—a promising synthetic fuel candidate and intermediate for the production of longer-chain oxymethylene ethers (OME<sub>3-5</sub>).

To analyze DMM and OME<sub>3-5</sub> production using established process concepts, we implement process models with detailed thermodynamic models from the open literature. Even by considering their maximum potential for heat integration, these process concepts have been found to be much less efficient than those for the production of other synthetic fuel candidates. Therefore, fundamentally new processes need to be designed.

Emerging Power-to-X processes are usually on a very different stage of development. To enable a fair comparison and support process design, we develop a methodology that incorporates optimization-based methods on different hierarchy levels. The methodology allows a systematic way to design and evaluate each candidate regarding three key performance indicators: production costs, exergy efficiency, and global warming impact. Applied to five reaction pathways for DMM production, we identified the direct reduction of CO<sub>2</sub> to be the most suitable one for sustainable DMM production at its current state.

For a successful implementation, detailed process models are necessary. As the complicated form of such models often cause difficulties for deterministic optimization, we develop a hybrid process model for reductive DMM production incorporating Gaussian processes and artificial neural networks. For solving the resulting nonconvex program, we use a *reduced-space* formulation and a hybrid between the McCormick and the auxiliary variable method implemented in our deterministic global solver MAiNGO. Only with these measures on both the modeling and algorithm level, convergence was possible.

As Power-to-X design problems often contain discrete decisions, we analyze different problem formulations regarding their suitability for global superstructure optimization and applied the most suitable one to the design problem for reductive DMM production. For mixed-integer nonlinear programming problems containing nonconvex functions, we identified such formulations as particularly promising that reduce the number of optimization variables. Although they introduce nonconvex terms, corresponding relaxations remain comparably tight for our example problems. However, a large library with benchmark problems of different complexity would be necessary to derive generally valid statements.

The application of optimization-based methods to DMM production has demonstrated great potential. However, also limitations and further improvement potential was identified—for both the methods and DMM production as a Power-to-X process.



---

# Publications and Copyrights

This thesis is partially based on the research performed by the author during his time at the Chair of Process Systems Engineering (AVT.SVT) at RWTH Aachen University between April 2017 and December 2021. Some parts of this thesis have already been published or submitted for publication as described in the following. Alexander Mitsos provided ideas and guidance as well as edits.

- The introduction in Chapter 1 is reproduced in part from J. Burre, D. Bongartz, L. Brée, K. Roh, and A. Mitsos. Power-to-X: Between Electricity Storage, e-Production, and Demand Side Management. *Chemie Ingenieur Technik*, 92, 74–84. 2020. © (2020) The Authors. Published by WILEY-VCH Verlag GmbH & Co. KGaA, Weinheim.
- The results of the analysis of the established process chain for DMM production in Section 3.1 are taken from D. Bongartz, J. Burre, and A. Mitsos. Production of Oxymethylene Dimethyl Ether from Hydrogen and Carbon Dioxide – Part I: Modeling and Analysis for OME<sub>1</sub>. *Industrial & Engineering Chemistry Research*, 58:4881–4889, 2019. © (2019) American Chemical Society.
- The analysis of the process chain for OME<sub>3-5</sub> production in Section 3.2 as well as Appendix A is reproduced in part from J. Burre, D. Bongartz, and A. Mitsos. Production of Oxymethylene Dimethyl Ether from Hydrogen and Carbon Dioxide – Part II: Modeling and Analysis for OME<sub>3-5</sub>. *Industrial & Engineering Chemistry Research*, 58:5567–5578, 2019. © (2019) American Chemical Society.  
Major parts of the publication are used in this thesis. D. Bongartz supported the implementation and testing of the property and process models and provided feedback on the text.
- Parts of the introduction in Chapter 1, as well as the introduction of reaction pathways for DMM synthesis in Chapter 2, and their comparison in Section 4.1 and Appendix B are reproduced in part from J. Burre, D. Bongartz, S. Deutz, C. Mebrahtu, O. Osterthun, R. Sun, S. Völker, A. Bardow, J. Klankermayer, R. Palkovits, and A. Mitsos. Comparing pathways for electricity-based production of dimethoxymethane as a sustainable fuel. *Energy & Environmental Science*, 14:3686–3699, 2021. © (2021) The Royal Society of Chemistry.  
Major parts of the publication are used in this thesis. D. Bongartz supported the development and optimization of processes and supervised the work together with A. Mitsos. S. Deutz and S. Völker calculated the impact on climate change supervised by A. Bardow and wrote corresponding sections of the manuscript. C. Mebrahtu, O. Osterthun, and R. Sun wrote the descriptions of the novel reaction pathways and provided fundamental information for the discussions regarding catalyst improvement potential under the supervision of J. Klankermayer and R. Palkovits.

- The considerations on the process optimization for reductive DMM production in Section 4.2 and Appendix C are reproduced in part from J. Burre, C. Kabatnik, M. Al-Khatib, D. Bongartz, A. Jupke, and A. Mitsos. Global Flowsheet Optimization for Reductive Dimethoxymethane Production using Data-Driven Thermodynamic Models. *Computers & Chemical Engineering*, 162:107806, 2022. © (2022) Elsevier.

Major parts of the publication are used in this thesis. M. Al-Khatib developed the superstructure model for distillation column sequencing. C. Kabatnik performed experiments, fitted parameters for the PCP-SAFT equation of state, and developed the mechanistic flash model under the supervision of A. Jupke. D. Bongartz supported the development of the process model and provided feedback on the text.

- The analysis of different MINLP formulations in Chapter 5 and Appendix E is reproduced in part from J. Burre, D. Bongartz, and A. Mitsos. Comparison of MINLP problem formulations for global superstructure optimization. *Optimization and Engineering*. 2022. © (2022) Springer Nature, and the accepted manuscript D. Bongartz, J. Burre, and A. Mitsos. Global Superstructure Optimization with Nonconvex Models: Comparison of MINLP Formulations. *Computer Aided Chemical Engineering*, April 8th, 2022. © (2022) Elsevier.

Major parts of the publication are used in this thesis. D. Bongartz supported the analysis of the results.

During his time at AVT.SVT, the author supervised or co-supervised the student theses of Karim Soliman, Philipp Dürr, R. Sager, S. Suh, T. Faruß, S. Dörner, S. Kratzsch, H. Shi, J. Ufert, and M. Al-Khatib. The work of all students is gratefully acknowledged. Some of the work described herein partially builds on the following theses:

- S. Dörner. Solvent screening and optimization based process design for the multi-phase OME<sub>1</sub> synthesis. Master thesis, Process Systems Engineering, RWTH Aachen University, 2020.

Sven Dörner developed process models for multi-phase DMM synthesis and evaluated them based on their minimum energy demand (similarly to the processes that are developed in Section 4.1).

- H. Shi. Deterministic global optimization of a process for renewable methylal production using hybrid models. Master thesis, Process Systems Engineering, RWTH Aachen University, 2021.

Huixin Shi developed the framework for the optimization of the reductive DMM production process using thermodynamic data-driven models and applied it to the reaction and vapor-liquid separation part of the process presented in Section 4.2.

- J. Ufert. Development and evaluation of distillation models for deterministic global optimization. Bachelor thesis, Process Systems Engineering, RWTH Aachen University, 2021.

Julian Ufert implemented different distillation models in C++ and evaluated their suitability for deterministic global optimization regarding both accuracy and computational performance. The most suitable model is used for the optimization in Section 4.2.

- M. Al-Khatib. Distillation column sequencing using deterministic global superstructure optimization. Master thesis, Process Systems Engineering, RWTH Aachen University, 2021.

Mohamed Al-Khatib implemented different representations for superstructures in C++ and evaluated their suitability for deterministic global optimization regarding both accuracy and computational performance. The most suitable model is used for the optimization in Section 4.2.

Additionally, the author contributed to the following publications and presentations that appeared or were submitted during the author’s time at AVT.SVT, but do not form part of this thesis:

- D. Bongartz, J. Burre, and A. Mitsos. Power-to-OME – Processes for the Production of Oxymethylene Dimethyl Ether from Hydrogen and Carbon Dioxide. *Chemie Ingenieur Technik*, 90:1155, 2018.
- S. Deutz, D. Bongartz, J. Burre, B. Heuser, A. Omari, A. Sternberg, J. Klankermayer, W. Leitner, A. Mitsos, S. Pischinger, A. Bardow. Das ökologische Potenzial von Oxymethylenether-Kraftstoffen. *Chemie Ingenieur Technik*, 90:1155, 2018.
- J. Burre, D. Bongartz, S. Deutz, A. Bardow, and A. Mitsos. Comparison of Processes for Producing OME<sub>1</sub> - An Efficient, Economic, and Environmentally Sustainable e-Fuel? *Sustainable Engineering Forum*, 249–250, 2019.
- K. Roh, A. Bardow, D. Bongartz, J. Burre, W. Chung, S. Deutz, D. Han, M. Hesselmann, Y. Kohlhaas, A. König, J. S. Lee, R. Meys, S. Völker, M. Wessling, J. H. Lee, and A. Mitsos. Early-Stage Evaluation of Emerging CO<sub>2</sub> Utilization Technologies at Low Technology Readiness Levels. *Green Chemistry*, 22:3842–3859, 2020.
- R. Sun, C. Mebrahtu, J.P. Hoffmann, D. Bongartz, J. Burre, C.H. Gierlich, P.J.C. Hausoul, A. Mitsos, and R. Palkovits. Hydrogen-efficient non-oxidative transformation of methanol into dimethoxymethane over a tailored bifunctional Cu catalyst. *Sustainable Energy & Fuels*, 5:117–126, 2021.
- D. Bongartz, J. Burre, A.L. Ziegler, and A. Mitsos. Power-to-OME<sub>1</sub> via Direct Oxidation of Methanol: Process Design and Global Flowsheet Optimization. *Computer Aided Chemical Engineering*, 50:273–278, 2021.
- S. Völker, S. Deutz, J. Burre, D. Bongartz, A. Omari, B. Lehrheuer, A. Mitsos, S. Pischinger, A. Bardow, and N. von der Assen. Blend for All or Pure for Few? Well-to-Wheel Life Cycle Assessment of Blending Electricity-Based OME<sub>3-5</sub> with Fossil Diesel. *Sustainable Energy & Fuels*, 6:1959–1973, 2022.



---

# 1. Introduction

On a global scale, the share of renewable energy sources (RES) in electricity production is still small but is growing continuously. In order to prevent economic losses and idle green resources caused by energy curtailments, corrective actions need to be taken. In this regard, the concept of *Power-to-X* is considered promising to effectively utilize electricity from RES with the goal of exploiting its environmental and economic potential. On the one hand, this can be realized by flexibly adapting the operation of industrial processes to the fluctuating electricity supply, also referred to as *demand side management* (DSM) [1]. On the other hand, Power-to-X processes can be designed to temporarily store renewable electricity, e.g., as a chemical, when supply exceeds demand (*e-Storage*). Once the demand exceeds supply, these processes release their stored low-carbon electricity again. Finally, Power-to-X processes can be designed to replace fossil-based products with such that can be produced from renewable electricity, also referred to as *e-Production*. e-Production can be used to make RES accessible for sectors that heavily rely on fossil resources, i.e., chemical industry, heating, and transportation [2]. This concept is called *sector coupling* and explicitly promising for that part of the transportation sector that can not be electrified directly (e.g., by battery electric vehicles (BEV)). For such applications, liquid fuels produced from biomass (*biofuels*) and/or renewable electricity (*e-fuels*) can be advantageous due to their comparatively high energy density.

In this regard, oxymethylene ethers ( $\text{OME}_n$ ,  $\text{CH}_3\text{O}(\text{CH}_2\text{O})_n\text{CH}_3$ ) of different chain length  $n$  have received considerable attention as full substitutes [3–5] or blend components [6–9] for diesel fuels. Currently, fossil diesel largely dominates fuel consumption in long-distance and heavy-duty transportation and will maintain its crucial role in the next decades, as highlighted by the International Energy Agency [10]. The addressable market for  $\text{OME}_n$  as a fuel alternative is therefore enormous and ideally complements the one for gasoline fuel alternatives such as ethanol from renewable resources [11].  $\text{OME}_n$  can be produced from renewable syngas via biomass gasification [12–14], or from renewable hydrogen ( $\text{H}_2$ ) and carbon dioxide ( $\text{CO}_2$ ) [15–19] potentially achieving carbon neutrality over their entire life cycle. Their volumetric energy density ( $\sim 20 \text{ MJ L}^{-1}$  [20]) is about 40 % lower than that of diesel, but it is similar to that of other e-fuels [21] and about one order of magnitude higher than that of Li-ion batteries for BEV [22]. This makes  $\text{OME}_n$  particularly suitable for long-distance and heavy-duty transportation. Both  $\text{OME}_1$  (methylal or dimethoxymethane, hereinafter referred to as DMM) with only one formaldehyde (FA) group incorporated and  $\text{OME}_{3-5}$  offer outstanding combustion characteristics (e.g., high thermodynamic efficiency [6, 8, 9], low pollutant emissions [4, 6–9]) but differ in production, infrastructure, and engine compatibility. Whereas  $\text{OME}_{3-5}$  has more diesel-like properties and can be combusted in conventional diesel engines, DMM needs to be either mixed with additives to gain engine compatibility [6] or blended with diesel [7, 23]. However, engine modifications seem to remain indispensable for both DMM and  $\text{OME}_{3-5}$  [3, 4, 24]. In addition to the potential direct application in internal combustion engines, DMM is a key intermediate in  $\text{OME}_{3-5}$  production via paraformaldehyde [25], trioxane [26, 27], or in

novel routes via gaseous formaldehyde [28, 29].

Compared to other e-fuel candidates, e.g., hydrogen, methanol, dimethylether (DME), both DMM and OME<sub>3-5</sub> production requires a high amount of renewable electricity [30]. Corresponding reaction pathways are rather hydrogen-inefficient, as significant amounts of water are formed as side products (e.g., within the production of the intermediate FA [16]). To decrease the amount of water produced within their value chains and in turn increase their resource efficiency, new catalysts have been developed both for DMM [31] and OME<sub>3-5</sub> [28, 29] synthesis. However, corresponding processes have not been developed yet. This may have two reasons: First, the reaction pathways that have become feasible with these new catalysts are at a very early stage of development and have therefore not received much attention. As only little information about corresponding reaction mechanisms and performance is available, process development and their fair comparison with more established process alternatives is difficult. Second, some of these reaction pathways require rather harsh operating conditions. This makes the application of complicated thermodynamic models inevitable and optimization-based process design challenging.

To approach these problems, several methods have been developed in the field of process systems engineering. The probably most well-known method for early-stage process development is the application of the Douglas hierarchy [32]. Whereas this hierarchical decision procedure provides a systematic way of designing a process based on general input information about the underlying design task, it does not explicitly differentiate between the quality and different type of input data. Such a differentiation is however crucial for the development and fair comparison of processes that are on a very different stage of development. Moreover, since heuristic methods tend to miss promising process alternatives, the use of optimization-based methods is desirable. Fortunately, the increasing interest in Power-to-X technologies has spurred research in this field. Many methods, guidelines, and frameworks for techno-economic analysis (TEA) [33], life cycle assessment (LCA) [34], and combined TEA and LCA [35] dedicated to technologies with varying technology readiness levels (TRL) have been published recently. However, none of them combines process evaluation based on TEA and LCA with optimization-based process design for technologies with different TRL to explicitly provide feedback for further catalyst development. This combined consideration is however key for the identification of promising reaction pathways and in turn for the design of Power-to-X processes with a high resource efficiency.

Optimization-based methods are essential to maximize the efficiency of Power-to-X processes. In this regard, deterministic optimization is a powerful tool to optimize a process based on a certain objective (e.g., maximization of efficiency) and constraints (e.g., fulfillment of safety measures). As such processes exhibit complex chemical and physical phenomena, among other things resulting from complicated thermodynamic models, corresponding optimization problems are usually nonconvex. Local optimization methods may therefore lead to suboptimal solutions and miss the real potential of a process candidate. In contrast, global optimization methods guarantee global optimality but are computationally demanding. Especially for process models that require complicated thermodynamic models, like many Power-to-X processes do given their need for harsh operating conditions to make CO<sub>2</sub> reactive, the optimization problem easily becomes computationally intractable. The presence of discrete decisions to also consider structural process alternatives (e.g., different distillation configurations) results in superstructure optimization problems, which makes global process optimization even more challenging. To still solve these complicated optimization problems, suitable problem formulations—potentially tailored to the applied



---

global solution algorithm—need to be utilized.

This thesis has the goal to provide optimization-based methods for the development of Power-to-X processes. To advance the production of a synthetic fuel that offers a high compatibility with today’s infrastructure, we develop corresponding methods and apply them to the production of DMM from renewable sources. In particular, we want to find the reaction pathway that allows the most sustainable production of DMM, which in turn could be used for more resource-efficient OME<sub>3-5</sub> production compared to conventional processes. To reach this goal, we develop a methodology that enables a fair comparison between reaction pathways and processes that are on a very different stage of development. To advance DMM production, we develop tailored process models for the most promising reaction pathway, which enable deterministic process optimization while keeping model accuracy high. As for optimal process design usually also discrete decisions need to be taken (e.g., distillation column sequencing, integration into the entire value chain with different process options) we analyze several mixed-integer nonlinear programming (MINLP) problem formulations to identify their characteristics and finally enable computationally efficient superstructure optimization for problems that contain nonconvex functions. Finally, we estimate the potential of the new reaction pathways for DMM synthesis to increase the efficiency of OME<sub>3-5</sub> production.

The thesis is organized as follows: In Chapter 2, background information about the available reaction pathways for DMM synthesis based on methanol are summarized. In Chapter 3, we implement detailed process models to analyze DMM and OME<sub>3-5</sub> production incorporating established process concepts, which we use for the process comparison with more advanced reaction pathways. In Chapter 4, we develop a hierarchical process development and evaluation methodology that allows a systematic comparison of processes that are on a different stage of development and apply it to DMM production. Based on this comparison, we develop data-driven process models that provide a high accuracy and can still be used for deterministic global optimization. As optimal design problems for Power-to-X processes often require discrete decisions and are therefore difficult to solve globally, we analyze conventional and rather unconventional MINLP formulations for nonconvex problems in Chapter 5. Finally, Chapter 6 summarizes the key results of the dissertation and proposes future research directions.



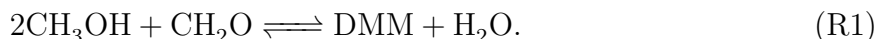
---

## 2. Reaction Pathways for Dimethoxymethane Synthesis

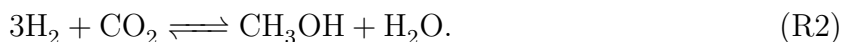
For an overview on available reaction pathways for DMM production as a potential Power-to-X process, this chapter provides background information on available reaction pathways for DMM synthesis from methanol,  $H_2$ , and  $CO_2$ . Commercial DMM production is based on the established reaction pathway (Section 2.1), whereas the more direct pathways (Section 2.2-2.5) have been proposed just recently. Herein, we present their key ideas. For more detailed information, we refer to the review article of Sun et al. [31].

### 2.1. Established Pathway

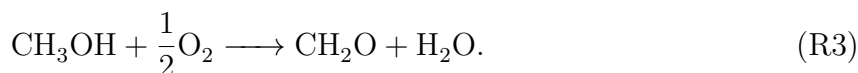
Currently, DMM is typically produced by the reaction of methanol with (typically aqueous) FA:



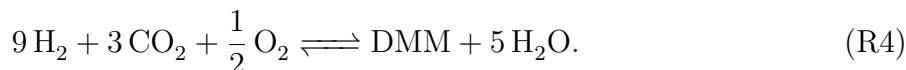
Thus, two intermediates are required: methanol and FA. Methanol can be produced directly from  $H_2$  and  $CO_2$  according to the reaction



FA is typically available as aqueous solution. It is produced from methanol either via partial oxidation or via combined partial oxidation and dehydrogenation [25]. Their overall reaction is



An alternative access to FA is via methanol dehydrogenation [36]. As the process concept for the established pathway intends to represent the state-of-the-art benchmark process for DMM production and methanol dehydrogenation is still at an early stage of development, we do not consider this (potentially beneficial) access to FA for the process concept of the established pathway. All in all, the overall reaction equation starting from  $H_2$  and  $CO_2$  is

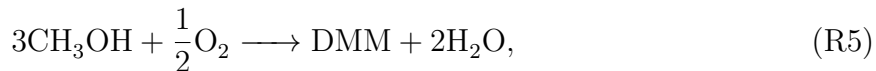


The process concept for the established reaction pathway is presented in Section 3.1.

### 2.2. Oxidative Pathway

The direct oxidation of methanol to DMM involves two sequential reactions occurring in the same reactor: in-situ methanol oxidation to FA and subsequent FA acetalization with

methanol to DMM. Both add up to the overall reaction equation



which is identical to the overall reaction equation of the established pathway both starting from methanol (Reaction (R1) + (R3)) and starting from  $\text{H}_2$  and  $\text{CO}_2$  (Reaction (R4)). The generated FA from methanol oxidation is directly trapped by methanol to yield DMM, thus avoiding the isolation and purification of FA. Within this reaction system, the production of one molecule of DMM is accompanied by the formation of two molecules of water (Reaction (R5)) [31].

In contrast to the established pathway, these water molecules are not bound to FA (resulting in methylene glycols), such that the formed water can be more easily removed from the reaction mixture and purged from the process.

For the experimental direct oxidation of methanol to DMM (Reaction (R5)), a gaseous substrate mixture of methanol and an oxidant (typically air) is fed into a fixed-bed reactor. The reactor is operated continuously under atmospheric pressure at temperatures between  $120^\circ\text{C}$  and  $240^\circ\text{C}$  and gas hourly space velocities (GHSV) between  $10.000\text{ mL h}^{-1}\text{ g}_{\text{cat}}^{-1}$  and  $40.000\text{ mL h}^{-1}\text{ g}_{\text{cat}}^{-1}$  [31]. To ensure safe operation, the applied methanol concentration should stay outside of the explosive range (7–36 % in air).

Extensive research on the direct oxidation of methanol toward DMM has resulted in a large number of bifunctional catalysts comprising redox and acidic active sites. The bifunctional nature of such catalysts plays a key role in directing the reaction network toward the selective formation of DMM. An appropriate ratio between redox and acidic properties is crucial for high DMM selectivities (80–99 % [31]). Among the reported catalysts, silica-modified and  $\text{TiO}_2$ -supported vanadium oxide (VTiSi) features a state-of-the-art performance with an DMM selectivity of up to 99 % at a methanol conversion of 51 % and a reaction temperature of  $140^\circ\text{C}$  (Appendix Tab. B.1) [37].

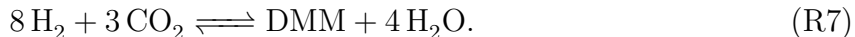
## 2.3. Reductive Pathway

The direct reduction of  $\text{CO}_2$  to DMM incorporates  $\text{CO}_2$  and  $\text{H}_2$  into methanol following the overall reaction equation



First, methyl formate (MF) is formed by a coupled  $\text{CO}_2$  hydrogenation and esterification with methanol. A further hydrogenation step of MF to methoxymethanol (MM) takes place, before a transacetalization with an additional methanol molecule leads to DMM [38–40].

In contrast to the aforementioned pathways, where FA is produced in a redox-inefficient oxidation step either in a dedicated process step (cf. established pathway) or in-situ (cf. oxidative pathway), FA formation is avoided in the reductive pathway. This results in a lower overall  $\text{H}_2$  consumption—the main cost driver of e-fuels—following the overall reaction equation starting from  $\text{H}_2$  and  $\text{CO}_2$



The experimental resource-efficient reduction of CO<sub>2</sub> toward DMM (Reaction (R6)) is enabled by a homogeneous ruthenium-based catalyst, which is dissolved together with a co-catalyst into a liquid methanol solution. Under high pressure (80 bar) and high temperature (80 °C), turnover numbers (the amount of substrate molecules converted into product molecules per active catalyst site, TON) of up to 214 toward DMM could be achieved [38]. Schieweck and Klankermayer [39] later exchanged the ruthenium-based catalyst by an earth abundant cobalt catalyst to perform the same reaction. A study by Siebert et al. [40] revealed further potential of the ruthenium system: By using a Design of Experiments approach, a TON of 786 for DMM could be achieved. Although TON and yield (product of selectivity and conversion) correlate linearly for a fixed catalyst concentration, a high TON does not necessarily mean a high yield. For low catalyst concentrations, product yield can be low although the TON of the catalyst is high. For industrial implementation, achieving a reasonable high DMM yield is key—preferably with only a small amount of catalyst thus high TON. For the reduction of CO<sub>2</sub> toward DMM, a maximum yield of 8.3 % (selectivity of 81.8 %, conversion of 10.8 %) has been achieved (Appendix Tab. B.1).

## 2.4. Dehydrogenative Pathway

A further non-oxidative pathway for DMM synthesis can be achieved by coupling the dehydrogenation of methanol to FA with the acetalization of FA with methanol [41]:

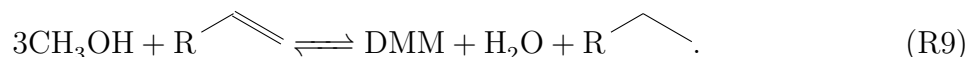


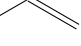
The prominent advantage of the dehydrogenative pathway is the replacement of the oxidative formation of FA by methanol dehydrogenation leading to the co-formation of valuable H<sub>2</sub> and less water. The produced molecular H<sub>2</sub> can be recycled to the methanol production process leading to the same overall savings in H<sub>2</sub> consumption as for the reductive pathway (cf. Reaction (R7)). No complex catalyst recycling needs to be realized due to the heterogeneous reaction system. In contrast to the oxidative pathway, the absence of an oxidizing agent further improves operational safety as only gaseous methanol need to be supplied.

The experimental dehydrogenation of methanol (Reaction (R8)) proceeds in a gas-phase fixed-bed reactor in the presence of a tailored Cu/H $\beta$  bifunctional catalyst. A high SiO<sub>2</sub>-to-Al<sub>2</sub>O<sub>3</sub> ratio (836) of the zeolite H $\beta$  ensures a high selectivity toward DMM (up to 80.3 %) at a conversion of 3.6 % [41]. This is possible even at mild reaction conditions due to the coupling of methanol dehydrogenation and FA acetalization. Temperatures at around 200 °C, atmospheric pressure, and a GHSV of 14.549 mL h<sup>-1</sup> g<sub>cat</sub><sup>-1</sup> are sufficient (Appendix Tab. B.1).

## 2.5. Transfer-Hydrogenative Pathway

Similar to methanol dehydrogenation, methanol transfer-hydrogenation releases one mole H<sub>2</sub> per mole DMM produced following the overall reaction



Starting with three equivalents of methanol, in a first step, the dehydrogenation of one methanol molecule takes place. The (formally) liberated molecular hydrogen is converted in-situ in the hydrogenation of a model liquid-organic hydrogen carrier substance (denoted by  $R$  ) . Thus, downstream purification of the off gas to access molecular hydrogen is omitted. A subsequent reaction between the FA molecule produced from methanol dehydrogenation and the second equivalent of methanol takes place to form MM. A third equivalent of methanol can then undergo a condensation reaction with MM leading to the desired product DMM [42].

Similar to the other non-oxidative pathways (reductive and dehydrogenative pathway), the transfer-hydrogenation of methanol toward DMM benefits from the same savings in overall  $H_2$  consumption (cf. Reaction (R7)). These savings are enabled by a beneficial  $H_2$  management via the regeneration of  $H_2$  from its carrier substance and its recycling.

The transfer-hydrogenation of methanol (Reaction (R9)) was published recently by Osterthun [42] and requires the presence of a homogeneous iridium catalyst and the presence of a Lewis acid. TONs up to 204 for DMM could be achieved for a system at 100 °C and 20 bar. A selectivity as high as 98.2 % at a methanol conversion of 0.9 % could be achieved so far (Appendix Tab. B.1).

---

## 3. Benchmark Processes of Oxymethylene Ether Production

To provide a benchmark for DMM and OME<sub>3-5</sub> production, this chapter presents process chains that contain only industrial process steps or state-of-the-art process steps from literature. Section 3.1 introduces the process chain for DMM production as well as corresponding models that have been developed to calculate its process efficiency. In Section 3.2, we develop process models required for estimating the process exergy efficiency of OME<sub>3-5</sub> production.

### 3.1. Dimethoxymethane Production

This section briefly presents the individual steps of the benchmark process chain for DMM production (Section 3.1.1), corresponding process models (Section 3.1.2), and the key results on process exergy efficiency (Section 3.1.3). For more detailed information, we refer to the original publication by Bongartz et al. [16].

#### 3.1.1. Process Description

On the basis of Reaction (R1), the benchmark process chain for DMM production is composed of three dedicated process steps: First, methanol is produced from renewable H<sub>2</sub> and CO<sub>2</sub>. Then, parts of the methanol is further converted to aqueous FA, which finally reacts with the rest of the methanol to DMM.

##### Methanol Production

For methanol production, a process for CO<sub>2</sub> hydrogenation is considered [43, 44]. Therein, H<sub>2</sub> and CO<sub>2</sub> enter the process at ambient temperature and pressures of 30 bar and 1 bar, respectively, before they react under high pressure (70 bar) to methanol. The heat released by the exothermic reaction (R2) covers the entire heat demand for distillative methanol purification and is further used for steam production.

##### Formaldehyde Production

For FA production, the BASF process is considered [25]. Therein, methanol is first evaporated before it undergoes a partial oxidation and dehydrogenation over a silver catalyst in a fixed bed reactor. The gaseous FA is then separated from its by-products in an absorption column using water. The heat released by the exothermic reaction (R3) covers the entire heat demand of the process and is further used, together with the heat from the combustion of the side products, for steam production.

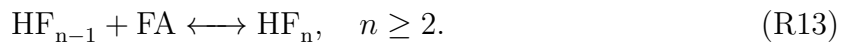
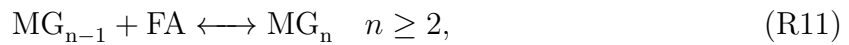
## DMM Production

For DMM production, a process concept based on the work of Weidert et al. [45] is used. Therein, a fixed-bed reactor with an acidic ion exchange resin (Amberlyst 15) as catalyst is used to enable the formation of DMM according Reaction (R1). A reaction temperature of about 60 °C, a pressure just higher than ambient pressure to avoid substrate evaporation, and methanol in excess enable almost perfect selectivity toward DMM at almost complete FA conversion. Product separation is achieved by a pressure swing distillation to break the azeotrope between methanol and DMM. The first distillation column additionally contains a reactive section for converting leftover FA and a vapor side draw for removing excess methanol. In contrast to the two upstream processes, a net heat demand for DMM separation remains.

### 3.1.2. Model Description

#### Thermodynamic Model

The high reactivity of FA in aqueous and methanolic solution requires a thermodynamic model that simultaneously considers phase equilibrium and oligomerisation reactions (R10) - (R13) toward methylene glycols ( $MG_n$ ) and hemiformals ( $HF_n$ ) to accurately represent the system's behavior [46].



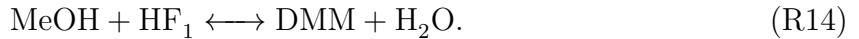
These reactions take place without the presence of the catalyst and therefore need to be considered in each process unit within the model. A corresponding thermodynamic model (based on the UNIFAC model [47]) has been developed and extended over the last decades [27, 48–54], which we provide (together with the process models presented hereafter) as Aspen Plus implementations on our homepage [55]. More details on the model implementation and its validation are given in Bongartz et al. [16].

#### Process Model

All process steps presented in Section 3.1.1 are implemented in Aspen Plus to enable detailed process analyses and finally estimate the exergy efficiency of the entire value chain for DMM production from renewable  $H_2$  and  $CO_2$  via established process concepts. The process model for methanol production contains a plug flow reactor model incorporating kinetics from Van-Dal and Bouallou [43] to model methanol formation according to Reaction (R2). The separation of methanol from water is modeled using a RadFrac model for distillation with column specifications from Otto [56]. Formaldehyde formation is modeled using the conversion reactor model RStoic with a methanol conversion of 98 % and a selectivity of 90 % toward FA [25]. The partial oxidation and dehydrogenation of methanol



produces water and carbon monoxide (CO) as side products. The absorption column is modeled using a RadFrac model with chemical reactions (R10) - (R13) implemented in the *Chemistry* section of Aspen Plus. The process model for DMM production contains a plug flow reactor model incorporating kinetics from Drunsel et al. [57] to model DMM formation according to



The distillation columns for DMM purification via pressure swing distillation are modeled using RadFrac models, of which the first one contains a kinetically controlled reactive section to reach full conversion of FA. Similarly to the absorption column in the FA process, the oligomerisation reactions are considered in all relevant columns. All column specifications are taken from Drunsel et al. [57]. For heat integration, two different cases are considered: 1) pinch-based heat integration within each individual process step and subsequent steam export (base case), and 2) pinch-based heat integration within the entire process chain.

### 3.1.3. Process Efficiency

To evaluate the process performance of the benchmark process chain for DMM production, the exergy efficiency  $\eta_{\text{Ex}}$  is calculated as

$$\eta_{\text{Ex}} = \frac{\dot{n}_{\text{DMM}} \hat{e}_{\text{DMM}}}{\dot{n}_{\text{H}_2} \hat{e}_{\text{H}_2} + \dot{n}_{\text{CO}_2} \hat{e}_{\text{CO}_2} + P_{\text{el}} + \dot{E}_{\text{Q}}}, \quad (3.1)$$

where  $\dot{n}_i$  is the molar flow of component  $i$ ,  $\hat{e}_i$  is the molar exergy of component  $i$ ,  $P_{\text{el}}$  is the electricity demand for pumping and compression, and  $\dot{E}_{\text{Q}}$  is the exergy flow of the net heat demand of the process chain. An ambient temperature of 25 °C is assumed. For details about the calculation of molar exergies, we refer to the original publication by Bongartz et al. [16].

The resulting exergy efficiency for DMM production from renewable H<sub>2</sub> and CO<sub>2</sub> considering established process concepts is 73 % (Fig. 3.1) and in good agreement with literature data [19]. However, it is 13-17 percentage points lower than that of alternative synthetic fuels [21]. These losses are mainly attributed to the low exergy efficiency of the FA production process, in which valuable H<sub>2</sub> is converted to water. If heat integration within the entire process chain is considered, the exergy efficiency can be increased by 1 percentage point to 74 %. In terms of efficiency, this increase does not seem significant. In terms of heat demand, however, this corresponds to a reduction of about 63 % yielding a net heat demand of 1.46 MJ kg<sup>-1</sup> produced DMM. Given the much lower exergy efficiency compared to other synthetic fuel candidates, the sole replacement of raw materials is for DMM production as a Power-to-X process with established process concepts not useful.

## 3.2. OME<sub>3-5</sub> Production

Nowadays, OME<sub>3-5</sub> is produced industrially in China at a scale of more than 240 000 ta<sup>-1</sup> [58]. Since their production is based on coal and future mobility is supposed to be environmentally friendly, novel production processes need to be based on a renewable feedstock.

Due to increasing interest in OME<sub>n</sub> as a synthetic fuel, much effort is being spent on new

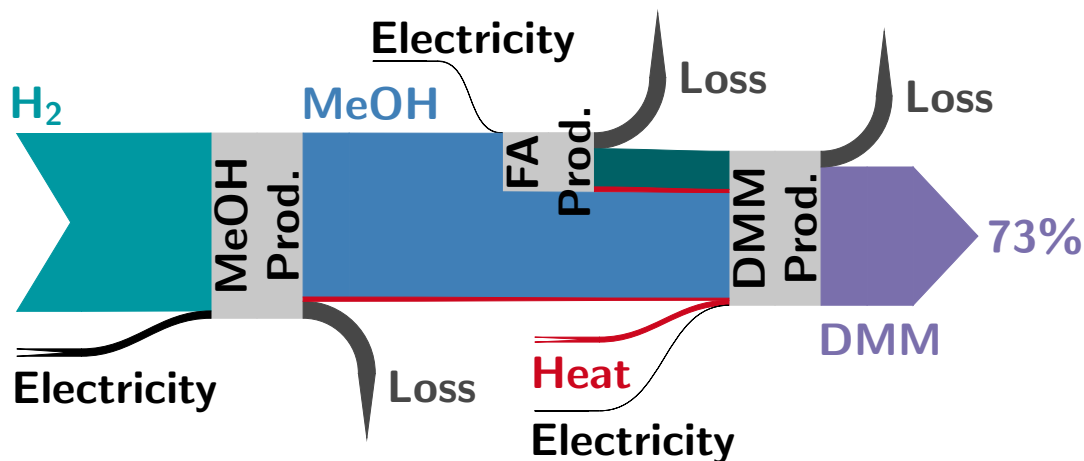


**Figure 3.1.:** Exergy flow diagram of the value chain for DMM production from  $H_2$  and  $CO_2$  via established process concepts. A pinched-base heat integration within the individual process steps and steam export is considered. An overall process exergy efficiency of 73 % is reached.

synthesis routes [59]. However, just very few publications analyze entire process chains for the production of  $OME_{3-5}$ . Recently, Schmitz et al. [60] investigated the economic potential of a process chain for the production of  $OME_{3-5}$  from methanol. In order to include methanol also as a renewable feedstock, they consider a methanol price ranging from 100  $US\$t^{-1}$  to 500  $US\$t^{-1}$ , where the lower and upper limit reflect the price for methanol produced from natural gas and biomass, respectively [60]. The economic assessment is based on material balances assuming a yield of 100% for the trioxane, DMM, and  $OME_{3-5}$  plant and 88% for methanol towards FA. The energy demands for the isolated processes are either extrapolated from literature or assumed to be equal to similar processes within the chain. For the calculation of investment cost, a general costing model for refineries is used. Considering these process assumptions along with a low methanol price and low investment cost,  $OME_{3-5}$  production using their benchmark process chain is found to be competitive with conventional diesel. Jacob and Maus [58] use the results to compare the process developed by Schmitz et al. [60] with the coal-based production process in China, a novel route by Schmitz et al. [61], a perspective route using DME and FA, as well as with the production of DMM. The coal-based production process and the perspective route was found to be cheaper by 16% and 45%, respectively. Also Ouda et al. [62] propose a process chain starting from methanol only. There, formaldehyde is being produced in a first reactor at high temperature by methanol dehydrogenation. This avoids the formation of water, such that its subsequent step, i.e.,  $OME_{3-5}$  synthesis, is based on a water-free feed. However, in this step, water is produced as a byproduct and shifts reaction equilibrium towards the educts. In a subsequent article, Ouda et al. [63] propose a detailed process concept including separation via distillation and evaluate its economic potential and its efficiency. However, process models used are rather simple and the proposed distillation sequence differ from other publications (e.g., [61, 64]). The same reaction to form  $OME_{3-5}$  from methanol and formaldehyde is considered in a holistic evaluation of biomass-based  $OME_{3-5}$  production by Zhang et al. [65, 66]. There, Aspen Plus® models for each process step have been implemented, the most relevant process parameters identified, and their influence on  $OME_{3-5}$  yield analyzed. Mahbub et al. [67] extend this analysis by a life-

cycle assessment taking into account biomass production, biomass transportation, chemical conversion, fuel mixing, fuel dispensing, and vehicle combustion. It is shown that the total life-cycle green house gas emissions can be reduced by up to 86% compared to fossil diesel.

The process efficiency, the economic competitiveness, as well as the GWI reduction potential for OME<sub>3-5</sub> production via formaldehyde and methanol has been assessed greatly in literature. In contrast to such an aqueous route, the hydrous one via trioxane and DMM is beneficial in the following: It avoids water formation, saves energy and unit operations for its removal, and shifts reaction equilibrium to OME<sub>3-5</sub>. However, trioxane is known to be expensive to purchase and its conventional stand-alone production energy intensive [68, 69]. By considering a novel trioxane process and integrating it into the entire value chain, these drawbacks do not necessarily hold anymore, as methanol and formaldehyde production is accompanied by significant steam generation. [70] deals with corresponding analyses. Due to the benefits and just little detailed information in literature about OME<sub>3-5</sub> production starting from H<sub>2</sub> and CO<sub>2</sub> via trioxane and DMM, we implement detailed models from literature using Aspen Plus<sup>®</sup> and conduct process simulations and analyses. This reveals the potential and limits of integrating trioxane production into the value chain, such that improvements for future production concepts can be derived systematically. We explicitly provide the implementations of process models in Aspen Plus<sup>®</sup> via our homepage[55], which can be used as a basis for further OME analyses respecting some constraints and limits given in Section 3.2.3.1. Such model implementations including highly complex thermodynamics have not been published by anybody else before.

Section 3.2 is organized as follows: Section 3.2.1 introduces the variety of different synthesis routes for OME<sub>3-5</sub> production by distinguishing between the aqueous and anhydrous ones. Corresponding benefits and challenges are discussed and the potential of the anhydrous route highlighted. Subsequently, in Section 3.2.2 both intermediate processes for the chain growth of DMM, i.e., trioxane and OME<sub>3-5</sub> production, are described. Section 3.2.3 introduces the thermodynamic model used in this study, as well as its coupled reaction kinetics, and the unit operation models used in Aspen Plus<sup>®</sup>. The process results for the entire process chain are presented in Section 3.2.4, before Section 3.3 concludes the key findings for the benchmark process chain for OME<sub>3-5</sub> production.

### 3.2.1. Synthesis Routes

As indicated in Figure 3.2, for the production of OME<sub>n</sub> with different chain lengths two main elements need to be provided: methoxy groups and formaldehyde molecules. The former constitute the end groups of OME<sub>n</sub> and may be taken from methanol, DMM, or DME. The formaldehyde molecules for chain growth may be provided from aqueous or methanolic FA, paraformaldehyde (PF), or solid trioxane (TRI). The process analyzed in this work is solely based on H<sub>2</sub> produced from renewable energy and CO<sub>2</sub> from biomass, flues gas, or directly captured from air. The provision of these raw materials are not discussed on process level within this section. Instead, they are considered in a concluding exergy efficiency analysis of the entire production process.

Figure 3.2 gives an overview of routes starting from the CO<sub>2</sub> sources air, biomass, and flue gas, as well as sources for H<sub>2</sub>, i.e., water via electrolysis and biomass via gasification. A discussion of all these routes is out of the scope of this investigation. In order to provide a basis of information about the process steps affecting OME<sub>3-5</sub> directly, we focus on the synthesis reactions from different methoxy and formaldehyde sources. In general, all routes

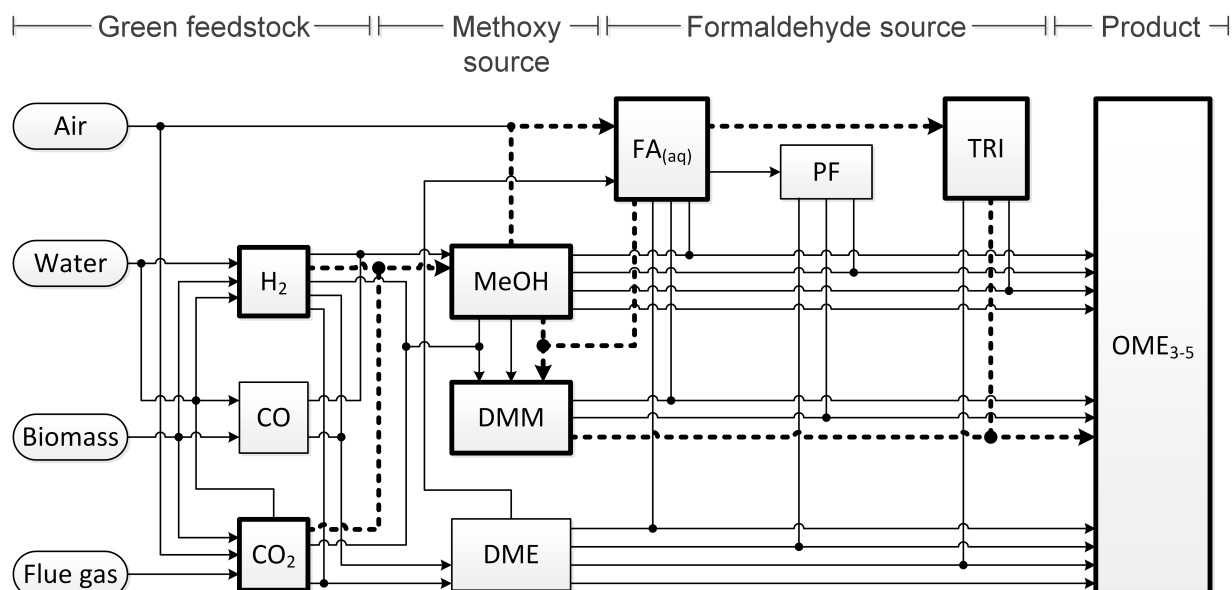


**Figure 3.2.:** Flow diagram with possible synthesis routes for OME<sub>3-5</sub> production from renewable H<sub>2</sub> and green CO<sub>2</sub>. The dashed, bold path corresponds to the anhydrous process chain considered in this section.

can be classified either as an anhydrous or aqueous synthesis route [71], i.e., distinguishing whether water is formed in the OME<sub>3-5</sub> formation reaction or not.

Within the majority of currently discussed synthesis routes, water is produced as a byproduct, e.g., in the synthesis of OME<sub>3-5</sub> from methanol and aqueous FA (formalin). The synthesis of OME<sub>3-5</sub> from methanol and aqueous FA has recently received a lot of attention as only three process steps are involved: methanol, FA, and OME<sub>3-5</sub> production [60, 61, 71–76]. This is particularly promising in terms of capital costs and utility demand, which make this process route highly attractive for industrial production. However, its main shortcoming is the need for removing water, which is produced as a byproduct and additionally introduced into the system by the aqueous FA feed. The presence of water lowers the selectivity towards OME<sub>3-5</sub>, as methylene glycols are formed in a competing reaction. Schmitz et al. recently published a process, where water is removed either by adsorption [61] or via membranes [77]. The process concept has been proven feasible in lab-scale and is continuously improved in academia and industry.

By using PF instead of formalin, no water is introduced into the OME<sub>3-5</sub> synthesis. However, water is still produced stoichiometrically depending on the chain length distribution of PF [78]. Oestreich et al. [79] perform reaction equilibrium experiments using PF and methanol, coming to the conclusion that this reaction's obstacle is the formation of a significant amount of byproducts. For an innovative OME<sub>3-5</sub> production process they propose an extractive separation of OME with hydrocarbons yielding a high extraction selectivity. By exchanging methanol with DMM as the methoxy source, the reaction selectivity towards OME<sub>3-5</sub> increases significantly [78, 80–84]. However, the production of PF from aqueous FA via vacuum distillation [85] requires several steps under various temperatures and is thus rather complex. Additionally, under given conditions PF is in solid state, which makes its handling challenging.

Utilizing trioxane as formaldehyde source the presence of water in OME<sub>3-5</sub> synthesis,

and hence its complex removal, is truly avoided. In this regard, the production of OME<sub>3-5</sub> from DMM and trioxane is an intensively investigated process [86–90]. A corresponding process can be composed of comparatively simple unit operations and is characterized by its high selectivity towards OME<sub>3-5</sub>: Selectivities of up to 70% are reported as well as a high stability of the catalyst’s activity [91–96]. In contrast, some publications mention the high energy demand of the conventional trioxane production process and its high complexity [69]. Therefore, trioxane is often considered as an unfavorable and expensive intermediate in OME<sub>3-5</sub> synthesis [68]. However, it remains unclear whether these drawbacks still hold for a novel production process based on distillation [97, 98], which eventually benefits from heat integration with the entire value chain. This question is the subject of the following investigation.

The other synthesis routes indicated in Figure 3.2 (e.g., synthesis from DME [99–102]) are much less discussed in literature and, thus, no suitable data for detailed process analyses is available.

### 3.2.2. Process Description

The objective in Section 3.2 is the evaluation of the anhydrous OME<sub>3-5</sub> production route starting from H<sub>2</sub> and CO<sub>2</sub>. Special attention is given to the integrability of a promising trioxane process into the entire process chain and whether this overcomes the shortcomings of the conventional trioxane production. This analysis requires detailed process information, e.g., heat flows and temperature levels of all heat sinks and sources, as we perform a pinch-based heat integration. For formaldehyde containing processes it is essential to use detailed models as its reactive behavior influences such process characteristics significantly. Due to that, each of the process chain’s five intermediate steps are modeled. Part one of our two-part article [16] introduces the processes for methanol, FA, and DMM production and is not discussed in further detail here. The two subsequent steps, i.e., trioxane and OME<sub>3-5</sub> production, are described in the following.

#### 3.2.2.1. Trioxane Production Process

Conventionally, trioxane is synthesized from aqueous FA in a highly energy intensive process consisting of several intermediate steps including FA concentration, reaction, trioxane extraction, separation, and purification [69]. At least five columns and one reactor is necessary for these operations. The need for an entrainer adds a further variable to the process, thus, making optimal process design as well as operation a challenging task. Apart from the complex flowsheet design, the loss of FA is not negligible reaching a yield of about 88%. Furthermore, a steam demand of 14.5 kg kg<sub>TRI</sub><sup>−1</sup> [69] is economically and ecologically disadvantageous. Due to the high complexity, high steam demand and rather low yield of the conventional trioxane production process, Grützner et al. [97] developed a novel process, in which separation is based on distillation only. The distillation regions of the ternary system FA, trioxane, and water are pressure dependent, which makes pressure swing distillation (PSD) a possible technology for trioxane separation. Only three columns at different pressure levels, one falling film evaporator for concentrating the aqueous FA solution, and one reactor is necessary in order to produce trioxane with a negligible loss of FA (Figure 3.3). Thus, it is less complex, no entrainer is necessary, and a yield of almost 100% can be reached. These advantageous process characteristics make the concept

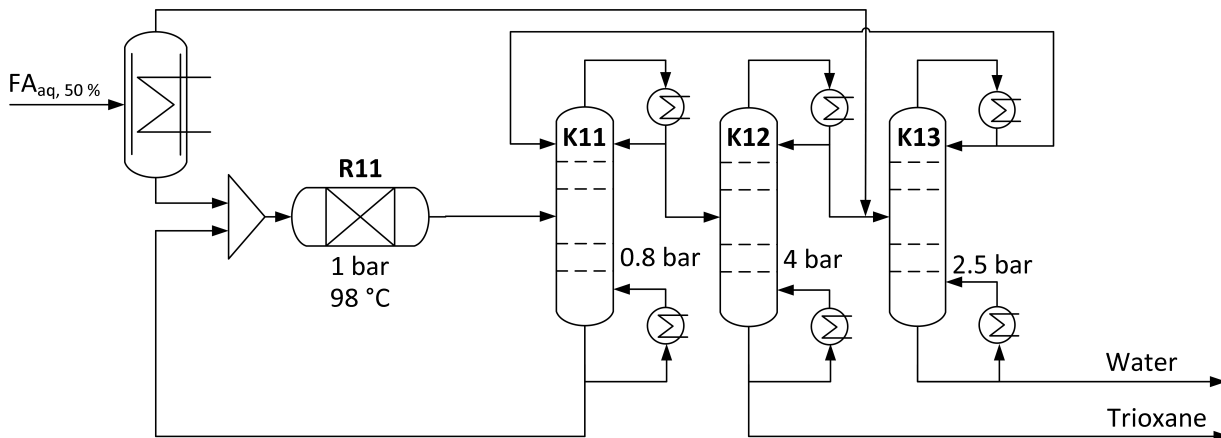


**Figure 3.3.:** Distillation-based trioxane production with three columns at different pressure levels, one falling film evaporator, and one reactor at the conditions given by Grützner [98].

highly interesting to be considered in a heat integrated process chain. However, no detailed information about its energy demand of the final process is reported in literature.

The process specifications (Table 3.1) used in this work are based on the process given in Grützner et al. [97] and Grützner [98]. They are not optimized but chosen in such a way that technical feasibility is ensured and product purity is met. The flowsheet structure has been derived by an inf/inf-analysis [103]. Aqueous FA of approximately 50 wt.-% is fed into a falling film evaporator, where the solution is concentrated to up to 70 wt.-% FA, limited by precipitation. The concentrated solution is fed together with the bottom product of the first column K11, mainly consisting of water and unreacted FA, into reactor R11, in which the reaction to trioxane takes place using a sulfuric acid catalyst. The process model proposed by Grützner et al. [97] assumes the catalyst to either stay in the reactor or to be recycled with the bottom product of column K11. The reactor effluent, i.e., trioxane, FA, and water, is fed into column K11 and its overhead product into the next stage of the PSD sequence, i.e., column K12. Due to the pressure shift from 0.8 bar to 4 bar, technical trioxane can be withdrawn as the bottom product with a purity of at least 99.9 wt.-%. The overhead product is mixed with the aqueous FA solution from the overhead product of the concentration unit, from which pure water is separated in the third stage of the PSD, i.e., column K13, at 2.5 bar. The overhead product is finally recycled to the first column K11. The process specifications are summarized in Table 3.1. Precipitation and crystallization of trioxane is not an issue since the process temperatures are higher than the melting point of trioxane, i.e., 62 °C, for all process streams. The good solubility of trioxane in water [104] as well as in ethers [85] makes the solid appearance of trioxane at ambient conditions not being obstructive for the process.

### 3.2.2.2. OME<sub>3-5</sub> Production Process

For OME<sub>3-5</sub> production from trioxane and DMM, the variety of process alternatives is small. Most of current research dealing with this synthesis route is about optimizing the catalytic reaction of trioxane and DMM to OME<sub>3-5</sub> in order to increase selectivity and conversion [91–94, 96, 105–107]. Process-related literature is only known for the heterogeneously acidic catalyzed synthesis and a subsequent separation via distillation considered herein, as well as a homogeneously catalyzed synthesis. A series of patents, e.g., [105, 106]

**Table 3.1.:** Process specifications for the trioxane production process given by Grützner. [98]

Variable	Value				
	Overall feed	R11	K11	K12	K13
Concentration	50 wt.-% FA	N/A	N/A	N/A	N/A
Pressure	1 bar	1 bar	0.8 bar	4 bar	2.5 bar
Temperature	N/A	98 °C	N/A	N/A	N/A
Top	N/A	N/A	85 °C	130 °C	115 °C
Bottom	N/A	N/A	93 °C	165 °C	127 °C
Stages	N/A	N/A	15	21	18
Feed stage	N/A	N/A	9	5	12
Mass reflux ratio	N/A	N/A	2.21	0.12	1.20
Mass distillate to feed ratio	N/A	N/A	0.045	0.905	0.900
Vapor fraction	N/A	0	N/A	N/A	N/A

, investigates the homogeneously catalyzed production process consisting of three rectification columns, one reaction unit, and an extraction column. The catalyst, i.e., an ionic liquid, along with the extraction unit make this process more complex compared to the heterogeneously catalyzed one, which was developed by Burger [87] in an industrial-academic cooperation [108] and is shown in Figure 3.4. In this process, a mixture of trioxane and DMM is fed into reactor R21 together with a recycle stream coming from the bottom of column K22 and K23. The reaction in R21 takes place under moderate conditions and the reaction mixture consisting of unreacted trioxane, DMM, OME<sub>n>1</sub>, and undesired byproducts is fed into a sequence of columns. First, in column K21 unreacted educts, OME<sub>n=2</sub>, and byproducts are separated from all OME<sub>n</sub> with a chain length higher than two FA groups. Byproducts are separated from unreacted educts and purged through the distillate of column K22, while the bottom product is recycled into reactor R21. In column K23 the desired product OME<sub>3-5</sub> is isolated from OME<sub>n</sub> with a chain length of higher than five FA groups.

Burger et al. [90] derived the structure of the flowsheet using the inf/inf-method [103] and optimized the unit specifications by a two-stage optimization procedure: First, the continuous variables, i.e., overall feed concentration and reflux ratios, were fixed and the discrete variables, i.e., number of stages and feed stage of each column, were varied in order to minimize each reboilers energy duty. Subsequently, the discrete variables were fixed and the continuous variables optimized w.r.t. minimal total reboiler duty using a gradient based method. Both steps were performed iteratively until the optimal unit specifications given in Table 3.2 were found. We increased the number of stages in all columns in order to reach the reboiler duties given by Burger et al. [90].

### 3.2.3. Model Description

All process simulations performed in this section are built on thermodynamic and chemical reaction models from literature, which are implemented in Aspen Plus®. The models of the first three process steps, i.e., methanol, formaldehyde, and DMM production, are covered

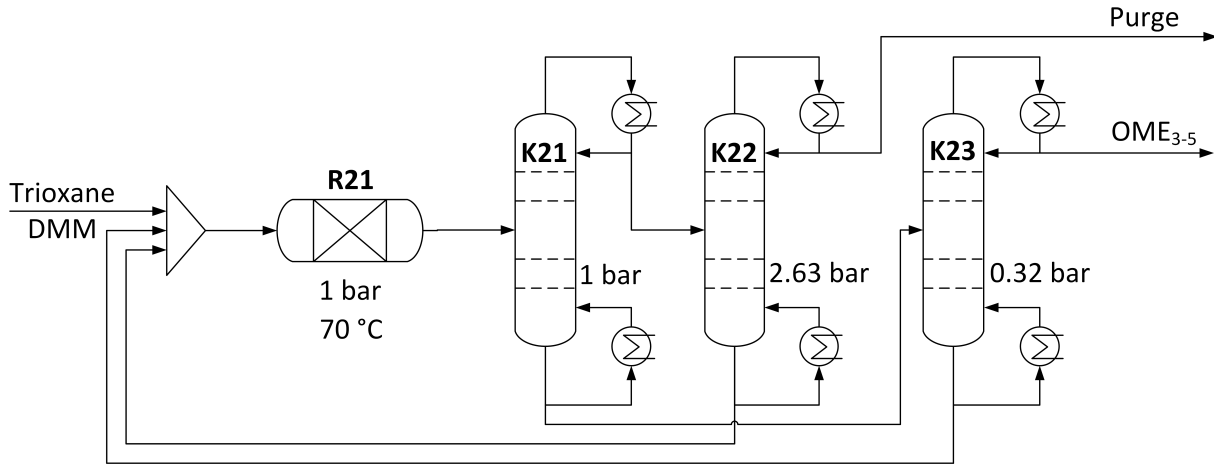


**Figure 3.4.:** Distillation-based OME<sub>3-5</sub> production with three columns at different pressure levels and one reactor at moderate conditions given by Burger et al. [90].

**Table 3.2.:** Process specifications for the OME<sub>3-5</sub> production process given by Burger et al. [90] The stage specifications have been adjusted in order to meet product specifications.

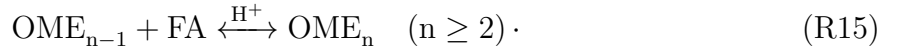
Variable	Value				
	Overall feed	R21	K21	K22	K23
Concentration	51.6 wt.-% Trioxane	N/A	N/A	N/A	N/A
Pressure	1 bar	1 bar	1 bar	2.63 bar	0.32 bar
Temperature	N/A	70 °C	N/A	N/A	N/A
Top	N/A	N/A	50 °C	18 °C	134 °C
Bottom	N/A	N/A	186 °C	83 °C	250 °C
Stages	N/A	N/A	30	30	15
Feed stage	N/A	N/A	3	31	4
Mass reflux ratio	N/A	N/A	0.048	9.700	0.215
Mass distillate to feed ratio	N/A	N/A	0.535	0.00066	0.683
Vapor fraction	N/A	0	N/A	N/A	N/A



in part one of our two-part article [16]. Overlapping models are not repeated hereinafter. Instead, Section 3.2.3 complements part one of the two-part article by providing all additional information about the thermodynamic and chemical reaction models relevant for the trioxane and OME<sub>3-5</sub> processes only. For modeling the trioxane process, the thermodynamic system of a mixture containing water and FA coupled with its oligomerization reactions to polyoxymethylene glycols (MG) are essential. In this regard, we extend the model described in part one with parameters for trioxane and OME<sub>n</sub> with a chain length of up to 20 FA groups in order to account for all relevant phenomena happening within trioxane and OME<sub>3-5</sub> production. We collected these extensions from literature, combined them with the model used in Bongartz et al. [16], and describe them in the following.

### 3.2.3.1. Chemical Reaction Model

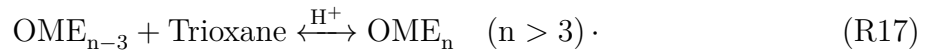
The commonly assumed chain growth mechanism for OME<sub>n</sub> synthesis is its reaction with one FA molecule [109]:



This reaction only takes place under acidic conditions [75] and if monomeric FA is present. In the considered process chain, FA is provided by trioxane, which decomposes over an acidic catalyst to three FA molecules via the overall (not elementary) reaction

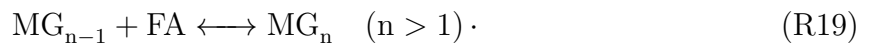


It may also be possible that the cyclic structure of trioxane brakes only at one point, such that a chain of three FA groups are incorporated directly in one OME<sub>n</sub> molecule [86]:



However, experiments did not show any evidence for this mechanism [86], so that the mechanism involving Reactions (R15) and (R16) is used in this work.

Trioxane itself is produced in a previous step, often described as the reverse of Reaction (R16), where FA is present in an aqueous solution. The presence of water makes the reaction system highly complex as FA and water instantaneously react to polyoxymethylene glycols even without the presence of any catalyst [110]:



Therefore, monomeric FA is present in the system only at very low concentration, but is rather embedded and provided via MG. This makes trioxane formation according



much more probable [111, 112]. The oligomerization reactions also play a governing role

in the synthesis of FA within this process chain, which is discussed in further detail in Bongartz et al. [16].

In addition to the desired Reactions (R15) and (R16) for OME<sub>3-5</sub> production, some side reactions may occur under specific conditions. FA can react to methyl formate (MF) via the Tischenko reaction (R21) [113]. This reaction also takes place under acidic conditions and favorably at temperatures above 90 °C when using Amberlyst 46 as a catalyst [88]. The same holds for the decomposition of DMM to DME and FA according to Reaction (R22).



How these reactions were accounted for in the simulations and how they were implemented in Aspen Plus® is described in Section 3.2.3.1 and 3.2.3.1 for the trioxane and OME<sub>3-5</sub> production, respectively. The model implementations in Aspen Plus® are available via our homepage [55].

#### Conversion-based Model for Trioxane Production

Whereas the oligomerization reactions of water and FA to MG are investigated extensively in literature [114–118], comparably little information is available about the formation of trioxane from aqueous FA. Grützner [98] performed several experiments in order to derive temperature dependent correlations for the equilibrium and reaction rate constants of Reactions (R20) and (R21). However, corresponding parameter sets are not given. Therefore, the simulation for the trioxane production process in this work is based on the reaction mechanism according to Reaction (R20) with a once-through conversion of 5% trioxane, which is a typical value for industrial trioxane production [97]. Side reactions are neglected as the concentrations of relevant components are low [97].

In contrast to the desired formation of trioxane, which takes place only within the catalytic region of the reactor, the oligomerization reactions of FA and water to MG take place in all units. Therefore, the corresponding equilibrium model [115] is implemented in each stage of the columns, all mixers and splitters, as well as in the reactor. The adaption and implementation of this model in Aspen Plus® is described in Bongartz et al. [16].

#### Reaction Kinetic Model for OME<sub>3-5</sub> Production

The OME<sub>3-5</sub> production process is based on the model developed by Burger et al. [88]. All parameters have been derived for the reaction system consisting of Reactions (R15) and (R16), which are catalyzed heterogeneously by the catalyst Amberlyst 46. In contrast to the oligomerization reactions (R18) and (R19), OME<sub>n</sub> formation only takes place in the presence of a catalyst. Therefore, these reactions are accounted for only in the reactor. As the byproduct methyl formate is formed in small amounts in Reaction (R21) and influences process design, an equation describing this reaction formally was added to the chemical reaction model (cf., Burger et al. [90]). Burger et al. [88] suggest a reaction model using a modified Langmuir-Hinshelwood-Hougen-Watson (LHHW) approach, as the sorption processes were found to be rate limiting. However, the simulation software Aspen Plus® does not allow the application of such a model, so that the pseudohomogeneous kinetic

model discussed in Burger et al. [88] is used in a slightly modified way in this work. Burger et al. [88] show that this model is not able to produce consistent results for a varying feed composition. The adaption of the reaction rate parameters for Reaction (R16), however, makes the model applicable for the optimal operating point found by Burger et al. [90] only. The set of parameters for the mole fraction-based equilibrium constants used in this work is given in Appendix Tab. A.1 and only applicable for this operating point using Amberlyst 46 as the catalyst. Corresponding parameter sets for the rate constants are given in Appendix Tab. A.2. Parameters for the formation of methyl formate are estimated in order to reach a formation rate of  $0.02 \text{ kg (h kg}_{\text{cat}})^{-1}$  [90]. All constants for OME<sub>n</sub> with different chain lengths are assumed to be equal and for trioxane decomposition the kinetic parameters were adjusted in order to fit the results given at the optimal operating point stated in Burger et al. [90]. This adjustment is necessary as the pseudohomogeneous kinetic model is not applicable for arbitrary feed compositions [88].

### 3.2.3.2. Thermodynamic Model

The thermodynamic model for OME<sub>3-5</sub> production corresponds to the one given in the work of Burger et al. [90] and is presented for pure and mixture properties hereinafter. Property models for FA and trioxane containing aqueous solutions used herein are taken from Albert [115] and Ott [119].

#### Pure Component Properties

Correlations for the pure component properties were implemented for MG and OME<sub>n>1</sub>. For the rest of the pure components, i.e., water, methanol, FA, trioxane, MF, and DMM, correlations were used from the APV88 Pure32 Aspen database. They constitute liquid molar density  $\rho_{L,i}$ , ideal heat capacity  $c_p^{\text{ig}}$ , vapor pressure  $p_i^{\text{s}}$ , and heat of vaporization  $\Delta h_{v,i}$ .

#### Mixture Properties

In order to account for nonideal interactions between all species, the UNIFAC group contribution method [120] is used as the basis for estimating all activity coefficients. For the trioxane production process, the UNIFAC approach is applied directly using corresponding UNIFAC-groups defined by Albert et al. [114], whereas the OME<sub>3-5</sub> production process uses the NRTL [121] approach based on data produced by the UNIFAC method. Burger et al. [90] fitted NRTL coefficients to the UNIFAC estimations for the binary systems constituting FA, trioxane, DMM, OME<sub>n>1</sub>, and MF. For the binary system OME<sub>2</sub> and trioxane, the activity coefficients were fitted to experimental data given by Burger et al. [90] using the global parameter estimation tool BOARPET [122–124].

### 3.2.3.3. Process Models

In order to reach high accuracy, detailed unit operation models are used within the Aspen Plus® model implementations. For the distillation columns, this is particularly important as oligomerization reactions need to be taken into account explicitly. Therefore, both process models, i.e., trioxane and OME<sub>3-5</sub> production, constitute rigorous RadFrac models for separation operations only. The Newton solution algorithm has shown best results in terms of convergence and is used for all RadFrac models. As packing specifications, column

dimensions, and pressure drop specifications are given for the distillation columns of the OME<sub>3-5</sub> production process in the work of Burger et al. [90], those have been considered in this work as well. Due to limited information about the distillation columns in the trioxane production process, they are modeled using an equilibrium calculation type. The conversion-based reaction of aqueous FA to trioxane is modeled using a RStoic reactor. Due to the given kinetics for the OME<sub>3-5</sub> process, reactions take place in a RPlug reactor with specifications given in the work of Burger et al. [90]. Compressors are isentropic and all unit operations consider oligomerization reactions given in Equation (R18) and (R19). Flowsheet tear streams are calculated using the Wegstein convergence method with a default relative tolerance of  $1 \times 10^{-4}$ .

#### 3.2.4. Results and Discussion

Detailed mass balances for the trioxane and OME<sub>3-5</sub> production process steps can be found in the work of Grützner [98] and Burger et al. [90], respectively. We address herein the overall material (Section 3.2.4.1) and utility demand (Section 3.2.4.2) of each intermediate process step, as well as the entire production chain. Special attention is given to the integrability of the distillation-based trioxane process, as its conventional stand-alone production is known to be energy-intensive and expensive. This enables a holistic and rational evaluation of the anhydrous OME<sub>3-5</sub> production and provides a further basis for fair process comparisons.

##### 3.2.4.1. Material Demand for OME<sub>3-5</sub> Production

Following the process chain for DMM production presented by Bongartz et al. [16], which is part of the process chain in this section, H<sub>2</sub> and CO<sub>2</sub> is consumed solely by the methanol production plant. For 1 kg OME<sub>3-5</sub>, 0.25 kg H<sub>2</sub> and 1.83 kg CO<sub>2</sub> is needed to produce 1.28 kg methanol as illustrated in Figure 3.5. In accordance with the simulations conducted by Burger et al. [90], the composition of OME<sub>3-5</sub> is assumed to be 43 wt.-% OME<sub>3</sub>, 34 wt.-% OME<sub>4</sub>, 22 wt.-% OME<sub>5</sub>, and 1 wt.-% OME<sub>6</sub> in this study. As depicted in Figure 3.5, more than 50% of the consumed raw materials constitute air for the combustion in the methanol and FA production processes. In the FA production process, this corresponds to a high amount of inert gases and keeps its operation beyond explosive limits. Apart from 2.14 kg air and 0.86 kg methanol about 0.40 kg water is fed into the FA process in order to absorb the FA molecules from the gaseous reactor effluent. This way 1.45 kg aqueous formaldehyde solution with 50 wt.-% FA is produced and 1.95 kg exhaust gas released to the atmosphere. In the subsequent steps more than 73% of the FA solution is used for trioxane production and the remaining 27% for DMM production. In both processes, water needs to be separated from both products, which are present in about the same quantity. In the last process the chain growth of DMM to OME<sub>3-5</sub> takes place with an overall carbon-based yield of almost 100%: 0.48 kg DMM reacts with 0.52 kg trioxane to 1 kg OME<sub>3-5</sub>. Only 0.001 kg of an equimolar mixture containing FA and MF need to be purged in order to prevent MF accumulation. However, as the corresponding material stream is comparably small, it is neglected in the diagram in Figure 3.5.

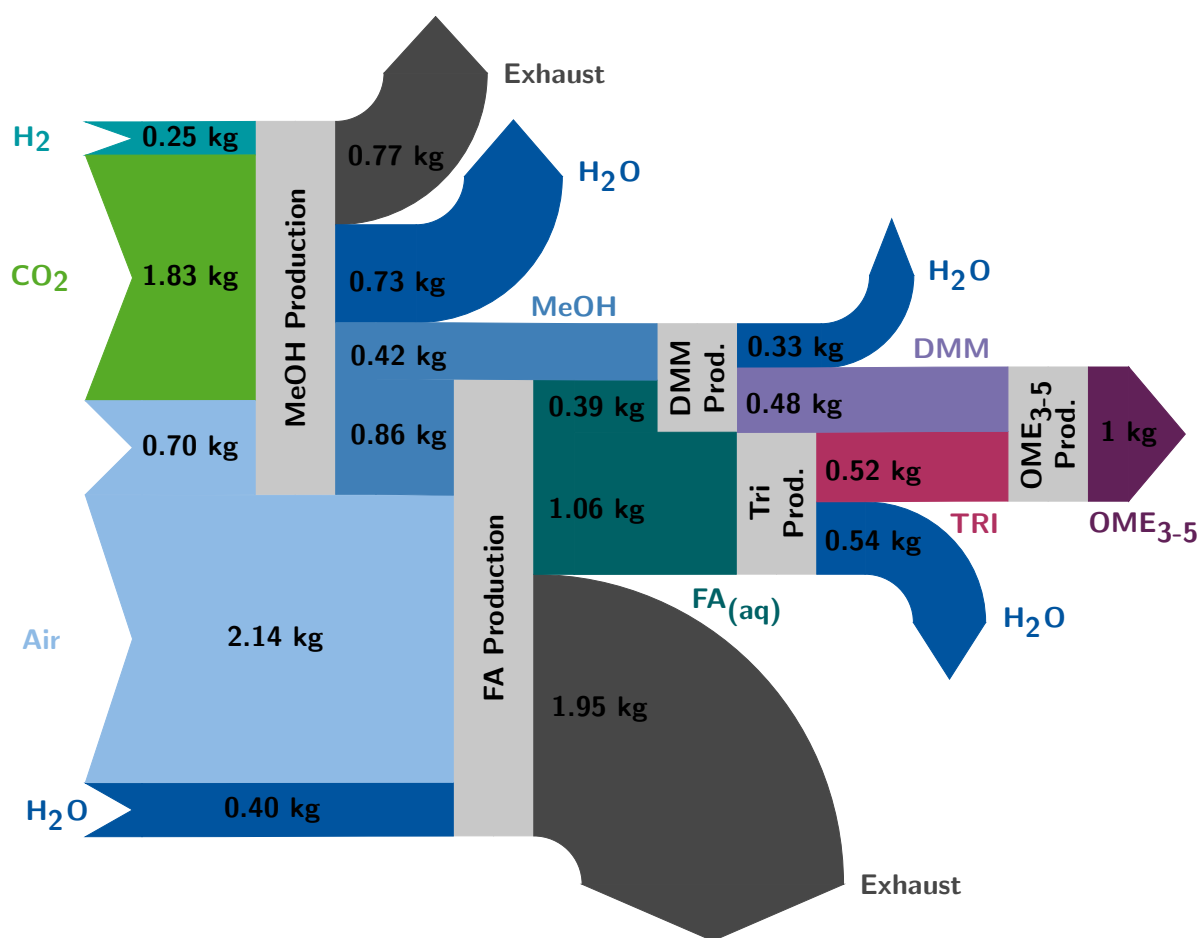


**Figure 3.5.:** Material flows within the reference process chain for the production of 1 kg OME<sub>3-5</sub>.

The *chemical conversion efficiency* (cf., e.g., König et al. [125])

$$\eta_{\text{CCE}} = \frac{\dot{m}_{\text{OME}_{3-5}} \cdot \text{LHV}_{\text{OME}_{3-5}}}{\dot{m}_{\text{H}_2} \cdot \text{LHV}_{\text{H}_2}}, \quad (3.2)$$

of this process chain is 63%, considering a lower heating value (LHV) of  $121.84 \text{ MJ kg}_{\text{H}_2}^{-1}$  and  $19.16 \text{ MJ kg}_{\text{OME}_{3-5}}^{-1}$  for  $\text{H}_2$  and  $\text{OME}_{3-5}$ , respectively. Concerning the amount of  $\text{CO}_2$  required for producing 1 kg  $\text{OME}_{3-5}$ , an overall carbon-based yield of 87% is reached.

#### 3.2.4.2. Energy Demand for $\text{OME}_{3-5}$ Production Considering Heat Integration

The main objective in this section is the evaluation of an entirely heat integrated process chain for the anhydrous production of  $\text{OME}_{3-5}$  from  $\text{H}_2$  and  $\text{CO}_2$  utilizing a novel trioxane process. In this regard, two different cases for heat integration are distinguished: In the first case, heat integration is considered for each intermediate process separately from the other processes and only remaining excess heat, i.e., steam that is commonly generated in methanol and FA production, is assumed to be used in the other process steps. In the second case, heat integration is conducted considering all heat sources and sinks within the process chain simultaneously. In both cases a targeting approach using pinch analysis is conducted. This way, an energetically best case process chain with respect to energy integration is found, which, however, does not necessarily represent the economic optimum as no rigorous heat exchanger network is developed. In order to estimate the influence of the process performance of trioxane production on the overall one, a sensitivity analysis is performed. Regarding this, FA conversion towards trioxane is varied and the heat demand of the heat integrated process calculated. This reveals potential improvements of the anhydrous  $\text{OME}_{3-5}$  production, if the catalytic trioxane reaction can be further optimized.

We assume that  $\text{H}_2$  is provided by a proton exchange membrane (PEM) electrolysis operated at 30 bar.  $\text{CO}_2$  may be captured from biogas plants, from flue gas of power plants, or directly from air and is fed into the methanol production plant at ambient conditions. As for the direct conversion of methanol from  $\text{H}_2$  and  $\text{CO}_2$  an operating pressure of about 70 bar is necessary [126], the energy demand for the compression of both educts are considered. For  $\text{CO}_2$ , a four stage compression including intercooling is applied and for  $\text{H}_2$  only one stage. This way a total electricity consumption of  $1.33 \text{ MJ kg}_{\text{OME}_{3-5}}^{-1}$  for pumping and compression need to be provided for the methanol plant (Figure 3.6). The heat demand for heat exchanger and distillation columns is entirely covered by the heat of reaction and combustion within the process itself. The same holds for the FA production process, so that excess heat of  $1.76 \text{ MJ kg}_{\text{OME}_{3-5}}^{-1}$  at about  $220^\circ\text{C}$  and  $5.01 \text{ MJ kg}_{\text{OME}_{3-5}}^{-1}$  at about  $150^\circ\text{C}$  is available for subsequent processes. About  $0.16 \text{ MJ kg}_{\text{OME}_{3-5}}^{-1}$  for compression is necessary in the FA production process to maintain a steady flow of materials. For DMM production, the energy demand for pumping and compression can be neglected as only comparably low pressure levels are necessary and the streams are comparatively small and liquid. Therefore,  $4.25 \text{ MJ kg}_{\text{OME}_{3-5}}^{-1}$  heat needs to be provided for separating DMM from methanol and water, that may be taken from either the excess heat of the FA process entirely, or partly from the methanol and FA process. If the second option is chosen, the remaining heat of the FA process may be used for trioxane production.

The trioxane production process consumes in total  $22.5 \text{ MJ kg}_{\text{OME}_{3-5}}^{-1}$  considering

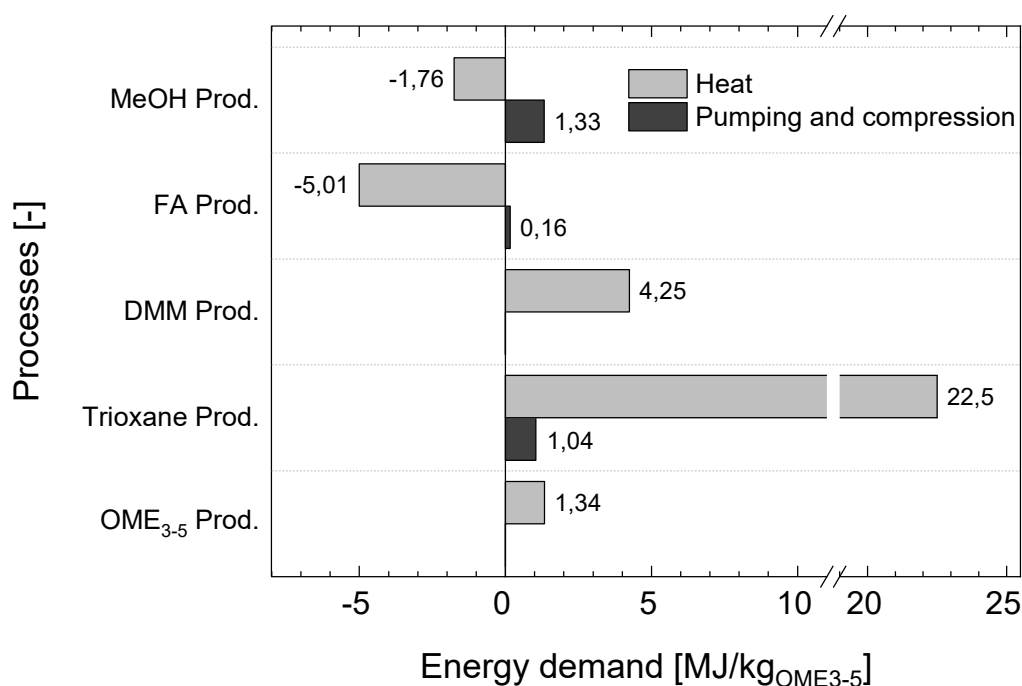


**Figure 3.6.:** Energy demand for heating as well as pumping and compression of the processes within the reference OME<sub>3-5</sub> production chain. Heat integration is considered within each individual process.

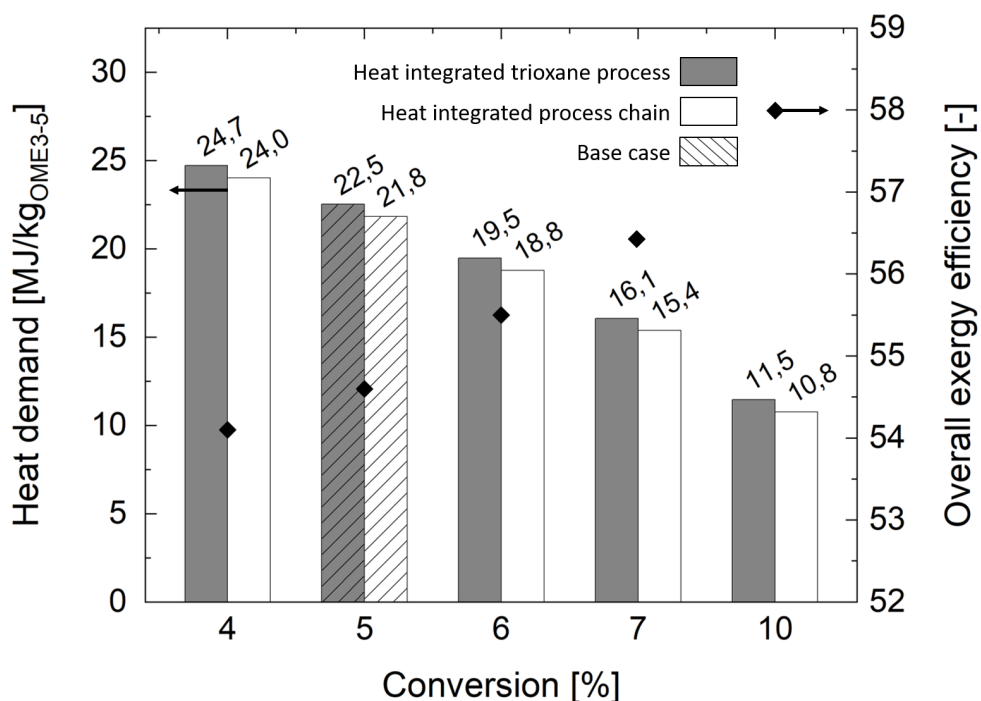


**Figure 3.7.:** Influence of the conversion of FA to trioxane on the energy demand of the separately heat integrated trioxane production process, as well as on the overall energy demand of the entire process chain. Additionally, the exergy efficiency of the overall process chain starting from H<sub>2</sub> and CO<sub>2</sub> is shown.

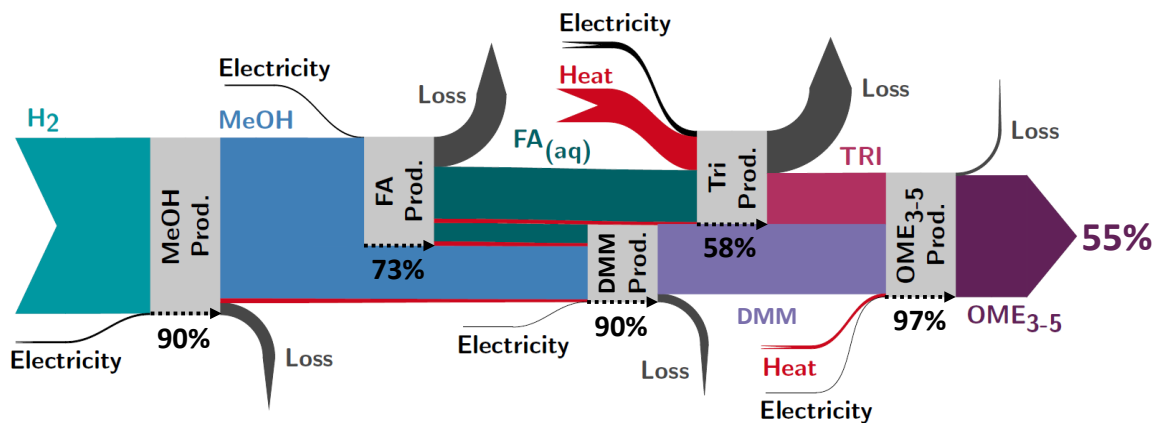


**Figure 3.8.:** Sankey diagram of exergy flows within the reference process chain for the production of 1 kg OME<sub>3-5</sub>. The gray boxes denote the different process steps and the percentages are the exergy efficiencies of these separate steps. The overall exergy efficiency from H<sub>2</sub> to OME<sub>3-5</sub> is 55%.

internal heat integration, which is about  $15 \text{ kg kg}_{\text{TRI}}^{-1}$  steam and in accordance with the steam demand of the conventional trioxane production process given in the work of Mahieux [69]. Grützner [98] reports a heat demand for the distillation-based trioxane production process of about  $65 \text{ MJ kg}_{\text{TRI}}^{-1}$ , which is about  $33.70 \text{ MJ kg}_{\text{OME}_{3-5}}^{-1}$ . This is considerably higher than found in this work as no heat integration is considered in his work. The high demand of heat is mainly caused by a small conversion of 5% of FA to trioxane in the reactor, which results in a high recycle stream leaving the bottom of column K11 and, thus, in a high energy demand for its reboiler. As a conversion of 5% is only a reference value for conventional industrial applications [97], its influence on the energy demand of the separately heat integrated trioxane production process and on the process chain's one is illustrated in Figure 3.7. The diagram shows a strong relation between FA conversion and the heat demand of the trioxane production process: Heat demand for trioxane production halves by considering a FA conversion of 10% instead of 5%. The energy demand of the overall process chain is smaller than that of the separately heat integrated trioxane process, because excess steam from formaldehyde production is utilized. In addition to heat,  $1.04 \text{ MJ kg}_{\text{OME}_{3-5}}^{-1}$  electricity for compression need to be provided, as the gaseous overhead product of column K11 need to be fed into the second column K12 operated at 4 bar. However, this way heat for internal heat integration is produced. As the energy demand for trioxane production exceeds the energy demand of the other processes within the process chain by a large amount, the overall energy efficiency is highly dependent on this process step. However, the process for trioxane production investigated in this study was not optimized rigorously and, thus, still offers potential for improvements.

The energy demand for the heat integrated OME<sub>3-5</sub> production process from trioxane and DMM is rather low with  $1.34 \text{ MJ kg}_{\text{OME}_{3-5}}^{-1}$  at  $200^\circ\text{C}$  to  $260^\circ\text{C}$  for separating the product from OME<sub>n<3</sub>, methyl formate, unreacted trioxane, and OME<sub>n>5</sub>. Energy for pumping and compression can be neglected, as it is much lower than the electricity demand of the aforementioned processes. These results are in agreement with those from Burger et al. [90].



Given all material streams entering and leaving each process together with the processes energy demand and temperature levels, all exergy fluxes within the process chain for OME<sub>3-5</sub> production were calculated (cf., part one of our two-part article [16]) and are illustrated in the Sankey diagram in Figure 3.8. As CO<sub>2</sub> is provided at 1 bar and its chemical exergy is neglected, it does not bring any exergy into the system. Only a large exergy stream associated with the stream of H<sub>2</sub> at 30 bar and some electricity enter the process as input streams of the methanol production plant. Its exergy efficiency is calculated to be about 90%. If raw material compression is not considered as part of the methanol process, for example in case H<sub>2</sub> and CO<sub>2</sub> are provided from high-pressure storage sites, its exergetic efficiency increases to 91%. For the FA and DMM production plant, only electricity need to be provided externally as excess heat is assumed to be exchanged between the processes within the production chain. The exergy efficiency for these processes is 73% and 90%, respectively. The low efficiency of the FA production process is caused by irreversibilities during methanol combustion and the residual heat of exhaust gases (cf., Bongartz et al. [16]). As already mentioned above, the trioxane production process consumes most of the energy within the reference process chain, of which most is consumed in the reboiler of column K11. This makes the exergy efficiency of this step drop to about 58%. Considering the conversion of FA towards trioxane to be 10% instead of 5% its efficiency increases to 67% and the overall process chain efficiency to more than 58% (cf., Figure 3.7). The most exergy efficient process for OME<sub>3-5</sub> production is its last step, i.e., the chain growth of DMM to OME<sub>3-5</sub>. As just little heat and electricity need to be provided to the process, its exergy efficiency reaches almost 97%. All in all, considering a system boundary around the entire reference process chain, the overall exergy efficiency for OME<sub>3-5</sub> production from renewable H<sub>2</sub> and green CO<sub>2</sub> is 55%. Considering 10% FA conversion the efficiency increases to 58%.

For the case where all process steps are at the same site, a more efficient combination of heat streams is possible and the overall exergy efficiency increases to 57%. The overall heat demand reduces by about 16% from 21.40 MJ kg<sub>OME<sub>3-5</sub></sub><sup>-1</sup> to 17.94 MJ kg<sub>OME<sub>3-5</sub></sub><sup>-1</sup>. Assuming 4.5 kWh (Nm)<sup>-3</sup>, i.e., 180 MJ kg<sub>H<sub>2</sub></sub><sup>-1</sup>, for an alkaline electrolyzer with an HHV-based efficiency of about 80% and a maximum operating pressure of 32 bar [127], 45 MJ kg<sub>OME<sub>3-5</sub></sub><sup>-1</sup> need to be provided only for hydrogen supply. The resulting overall exergy efficiency including H<sub>2</sub> supply via electrolysis is about 41%. Using PEM electrolyzers the overall efficiency is comparable as their specific energy consumption is about the same [128]. Including also a thermal energy demand of 2.20 MJ kg<sub>OME<sub>3-5</sub></sub><sup>-1</sup> for carbon capture from flue gas with a typical carbon dioxide mole fraction of 13% [129] reduces the overall efficiency to 38%. This efficiency is rather low compared to DMM production and other e-fuels. Even the best possible heat integration of the trioxane process within the entire process chain increases the total efficiency including electrolysis and carbon capture by only less than 1%. Finally, a potential optimization of the catalytic reaction of FA towards trioxane has a significant effect on the overall process performance. However, such improvements are also limited, e.g., doubling the FA conversion corresponds to an increase in overall process efficiency of only 2% starting from electricity. Despite an effective heat integration of the novel trioxane process in the entire process chain and a highly attractive final process step (i.e., OME<sub>3-5</sub> formation), from an energy point of view it is not expedient to further improve the synthesis of OME<sub>3-5</sub> via DMM and trioxane. Due to only small improvements for the entire process chain, even for a significantly improved catalytic trioxane reaction, the focus of future OME<sub>3-5</sub> research should be placed to alternative trioxane production

processes or routes avoiding trioxane production.

## 3.3. Conclusion

Key for a successful development of a resource efficient DMM and OME<sub>3-5</sub> production process is the identification of bottlenecks established process concepts suffer from. In this section, such an analysis has been conducted for both the established pathway for DMM production and the anhydrous synthesis pathway for OME<sub>3-5</sub> production starting from H<sub>2</sub> and CO<sub>2</sub>. For all process steps, simulations in Aspen Plus® have been performed using detailed process models with validated thermodynamic and chemical reaction models embedded. They were analyzed with respect to their material and energy demand, and ultimately evaluated using exergy efficiencies.

For DMM production, an exergy efficiency of 73 % was reported considering heat integration for each individual process step and subsequent steam export between processes. If heat integration for the entire process chain is considered, an exergy efficiency of 74 % can be reached. For the production of 1 kg OME<sub>3-5</sub> with 43 wt.-% OME<sub>3</sub>, 34 wt.-% OME<sub>4</sub>, 22 wt.-% OME<sub>5</sub>, and 1 wt.-% OME<sub>6</sub> 0.25 kg H<sub>2</sub> and 1.83 kg CO<sub>2</sub> need to be provided. This corresponds to an overall carbon-based yield of 87% and a *chemical conversion efficiency* of 63%. The exergy efficiency of a heat integrated process chain considering the exchange of steam adds up to 55% starting from H<sub>2</sub> and CO<sub>2</sub>. Including electricity and thermal energy demand for electrolysis and carbon capture it drops to 38%. This efficiency is comparable to that of Fischer-Tropsch diesel or methanol-to-gasoline concepts based on renewable resources which have an overall efficiency of about 45% and 39% [130], respectively, (assuming 80% efficiency for electrolysis). Taking into account that the trioxane production process is responsible for major exergy losses, the possibility for novel process concepts of avoiding this energy intensive process step, e.g., by the direct conversion of methanol and formaldehyde to OME<sub>3-5</sub>, points towards the important areas for process improvements for OME<sub>3-5</sub> production. This is the focus of current research, e.g., [61, 77], and need to be investigated in further detail in order to expand our analyses to such process concepts.

---

## 4. Optimal Process Design of Dimethoxymethane Production

The sole replacement of raw materials is due to the high  $H_2$  demand not sufficient for making DMM production suitable as a Power-to-X process (cf. Chapter 3), such that fundamentally new processes need to be developed. As process candidates are on a very different stage of development, we first develop a hierarchical process development and evaluation methodology incorporating optimization-based methods in Section 4.1. Its application to the reaction pathways introduced in Chapter 2 identifies the most suitable one for sustainable DMM production. Based on these results, in Section 4.2, we develop process models suitable for global deterministic optimization to optimize a corresponding process. The globally optimal process is then used to evaluate its potential within the entire process chain for both DMM and OME<sub>3-5</sub> production from  $H_2$  and  $CO_2$  in Section 4.3.

### 4.1. Hierarchical Comparison of Reaction Pathways

Commercial DMM production takes place via the condensation reaction of methanol and aqueous FA (cf. Chapter 2) [46]. The major drawback of the underlying reaction pathway is the reaction of  $H_2$  to water during upstream FA production increasing  $H_2$  demand considerably. Moreover, the more water is present in the system, the more undesired side products are formed [131].

To overcome the limitations of commercial DMM production, promising process alternatives have been proposed. A few authors suggest DMM purification via extractive [132, 133] and pressure swing distillation [134] intending to increase energy efficiency. Other studies propose reactive distillation to shift FA conversion towards DMM [135] and combine this approach with pressure swing distillation [45]. This combined process concept has been used to develop and analyze the entire process chain for DMM production from renewable  $H_2$  and  $CO_2$  (Section 3.1) [16]. In all of these processes, aqueous FA production still represents a key process step. Although FA production is a highly established and simple process step [25], its exergy efficiency is rather low (73 %) [16].

The inherent weaknesses of the reaction pathway containing FA production have spurred research activity toward pathways avoiding FA production. Significant improvements in catalyst performance have been achieved [31] and novel DMM synthesis pathways proposed (cf. Chapter 2). However, no process concepts have been developed and analyzed so far. Instead, the similar thermodynamic properties of the multi-component system within a novel pathway (the direct reduction of  $CO_2$  [38]) to those within an established one have been used to estimate the process performance and the impact on climate change of DMM production avoiding FA formation. An increased exergy efficiency of 86 % for DMM production from renewable  $H_2$  and  $CO_2$  and the possibility of significant cradle-to-grave

CO<sub>2</sub>-equivalent emission reductions compared to fossil diesel was reported [19]. Given the environmental benefits of DMM and the promising estimates on process performance, the use of more detailed process models in a comparative process analysis alongside the development of novel reaction pathways is essential for sustainable DMM production in the short- to medium-term.

Section 4.1 has the major goal to evaluate all reaction pathways from methanol towards DMM in order to provide feedback on the current and prospective process performance for catalyst development. Given the different maturities of the reaction pathways, we introduce a hierarchical process development and evaluation methodology to ensure a fair comparison across these pathways. We perform TEA and LCA on each level to determine the key performance indicators (KPIs) relevant for sustainable e-fuel production. As several pathways are still at an early stage of development, we identify their bottlenecks and derive performance goals that are necessary for process sustainability in the near future.

In Chapter 2, we summarized all reaction pathways and corresponding key characteristics for DMM production from methanol. Section 4.1.1 provides the methodology for process development and evaluation that enables a fair comparison of these pathways. On the basis of the methodology, Section 4.1.2 presents the results of the comparison and discusses perspective improvement potential. In Section 4.1.3, we conclude our findings.

### 4.1.1. Process Design and Evaluation Accounting for TRL

The TRLs of the DMM reaction pathways differ significantly, and so does the data availability for process design and evaluation: Whereas the established pathway has been investigated extensively over the last three decades (cf. Section 2.1), the majority of direct DMM pathways has been discovered during the last years (cf. Section 2.2-2.5). To still ensure a fair comparison despite the different stages of development and to ultimately lead the way towards sustainable DMM production, we introduce a hierarchical process development and evaluation methodology (Fig. 4.1). Within this methodology, process development (Section 4.1.1.1) and evaluation (Section 4.1.1.2) take place on up to three hierarchy levels depending on the data availability for each considered pathway. On Level 1, only reaction equations are required for calculating the maximum pathway potential. On Level 2, thermodynamic data and at least experimental data on reactions showing a sufficiently high performance need to be available to develop first process concepts. On Level 3, more detailed models are required for process optimization. On each level, three KPIs are calculated: process efficiency, production cost, and impact on climate change. We use these performance indicators to derive pathway-specific feedback for catalyst development to effectively benefit from both process and catalyst development (Section 4.1.2.4).

By applying the methodology to each pathway, we attain two important achievements: First, the pathways become comparable up to their highest common level despite their discrepancies in maturity. A fair comparison is ensured by using the same boundary conditions, model detail, and input data. Second, the gradual refinement of models and input data throughout the levels reveals information about the most relevant parameters and the gap between current and highest possible process performance. This information is not only essential for process optimization but also for catalyst optimization.

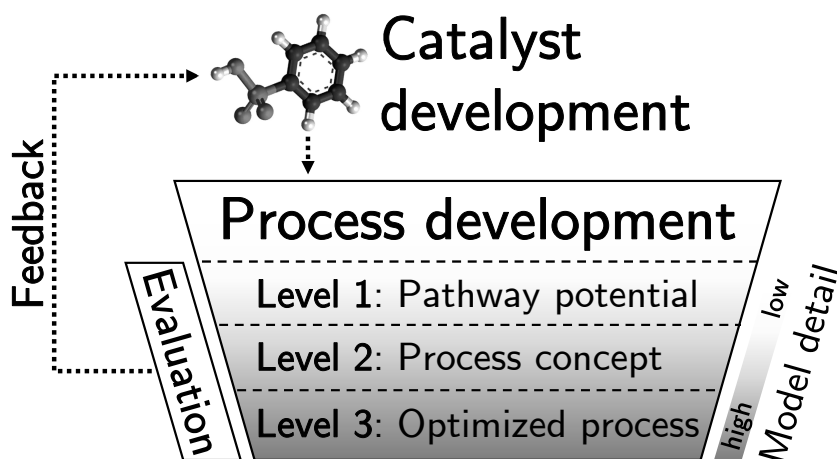


**Figure 4.1.:** Hierarchical process development and evaluation methodology.

#### 4.1.1.1. Process Development

We develop the process for each pathway sequentially from Level 1, containing only the most essential pathway characteristics, up to Level 3, containing enough information about the process for process optimization using rigorous models. In this section, we explicitly distinguish between levels, because the models and methods used for process development differ significantly between levels. Each level addresses an individual question:

- Level 1: What is the maximum potential of the pathway?
- Level 2: Which performance can we expect from a corresponding process?
- Level 3: What is the actual performance of an optimized process?

##### Level 1: Pathway potential

On Level 1, we model the process as a black-box containing only the stoichiometric coefficients of the desired reaction, thus assuming perfect selectivity. To calculate the maximum potential of the pathway, we further assume ideal separation and the recycling of unreacted educts, valuable intermediates, and side products. The result and key input for pathway evaluation on this level is the DMM-specific minimum raw material consumption.

##### Level 2: Process concept

On Level 2, we develop the separation system and the recycle structure with the reactor as the central unit of the process, as it is typically proposed for process development [136]. To determine the distillation sequence, we follow a process synthesis framework for the design of distillation processes from the literature [137]. Herein, we generate multiple variants which we then evaluate based on the Rectification Body Method (RBM) [138]. Heat integration by a subsequent pinch-analysis of the entire process finally enables finding the least energy-intensive process for each pathway. On this level, we consider experimental

data on reaction performance (Appendix Tab. B.1) or, if already available, reaction kinetics, and nonideal thermodynamics for all pathways (Appendix Tab. B.2-B.4). We use the process simulator Aspen Plus v11 to calculate mass balances and the energy demand for feed compression, and the in-house tool EE-ToolBox [139] (incorporates the RBM) to calculate the minimum energy demand (MED) of each distillation task.

### Level 3: Optimized process

On Level 3, we extend the model of the process with the lowest MED from Level 2 with additional compressors and pumps, and replace the RBM with detailed tray-to-tray distillation models [140]. This does not only increase accuracy, but also enables a more detailed process design and column sizing. We optimize the process in such a way that operational expenditure (OPEX) and capital expenditure (CAPEX) are minimized simultaneously. This results in a complex mixed-integer nonlinear programming (MINLP) problem. As currently global solution seems intractable, we follow a successive initialization procedure, reformulate the MINLP problem into a sequence of nonlinear programming (NLP) problems, and handle the flash calculations hidden from the numerical solver [140]. During optimization, only the purity constraints of streams leaving the process are considered. This prevents decisions on the sharpness of intermediate separation splits (particularly relevant for azeotropic distillation) and thus preliminary heuristic decisions. We perform the optimization with the algebraic modeling system GAMS using SNOPT as numerical solver and external functions for thermodynamic calculations [137].

#### 4.1.1.2. Pathway Evaluation

The results obtained on each level in process development (cf. Section 4.1.1.1) are inputs for the pathway evaluation. In accordance with the levels considered for process development, we evaluate each pathway up to their highest level always considering the three KPIs: process efficiency, production cost, and impact on climate change. The analyses between levels are dependent from one another only in such a way that the optimized process on Level 3 results from the least energy-intensive process concept on Level 2. The evaluation models and methods are the same for each level and differ only in their input data (cf. Appendix Tab. B.5).

### Efficiency model for DMM processes

Since renewable electricity dedicated to e-production (nonconventional production of commodities, fuels, or heat using processes that predominantly utilize renewable electricity [141]) will remain limited in the short- to medium-term, process efficiency is one of the KPIs for e-fuel production. In the present work, we consider exergy efficiency to restrict the energy output of the system to energy that is actually usable. Exergy efficiency is the maximum amount of useful energy that leaves the process (through the product, side products, and excess heat) relative to the amount of useful energy that enters the process (through  $H_2$ ,  $CO_2$ , heat demand, and electricity). Process exergy efficiency  $\eta_{P,1}$  is

calculated by

$$\eta_{P,l} = \frac{\dot{E}_{\text{DMM}} + \dot{E}_{\text{side}} + \dot{E}_{\dot{Q}_{\text{out}}}}{\dot{E}_{\text{H}_2} + \dot{E}_{\text{CO}_2} + \dot{E}_{\dot{Q}_{\text{in}}} + P_{\text{feed}} + P_{\text{misc}}} \quad l \in \{\text{L1, L2, L3}\}, \quad (4.1)$$

where  $\dot{E}_{\text{DMM}}$ ,  $\dot{E}_{\text{side}}$ ,  $\dot{E}_{\text{H}_2}$ , and  $\dot{E}_{\text{CO}_2}$  is the DMM-specific thermomechanical and chemical (based on higher heating value (HHV)) exergy content of DMM, side products,  $\text{H}_2$ , and  $\text{CO}_2$ , respectively;  $\dot{E}_{\dot{Q}_{\text{out}}}$  and  $\dot{E}_{\dot{Q}_{\text{in}}}$  is the DMM-specific exergy of excess heat and heat demand of the process, respectively ( $T_{\text{ambient}} = 298.15\text{K}$ ); and  $P_{\text{feed}}$  and  $P_{\text{misc}}$  is the DMM-specific electricity demand for feed compression and miscellaneous compression and pumping within the entire process, respectively. We distinguish between two types of exergy efficiency: process exergy efficiency (cf. Eq. (4.1)) and system exergy efficiency (cf. Appendix Eq. (B.2)). Process exergy efficiency refers only to the process for DMM production from  $\text{H}_2$  and  $\text{CO}_2$ , thus decoupling the provision of raw materials from the process. In contrast, system exergy efficiency refers to the entire system including the provision of raw materials. For the provision of raw materials, we consider a best and a worst case scenario (Tab. 4.1). In the best case scenario,  $\text{H}_2$  is provided by a solid oxide electrolyzer cell (SOEC) and  $\text{CO}_2$  is provided by a high purity ( $\sim 100\%$ ) industrial point source. In the worst case scenario,  $\text{H}_2$  is provided by a polymer electrolyte membrane (PEM) electrolysis and  $\text{CO}_2$  is provided by direct air capture (DAC). The parameters for the best and worst case scenario are summarized in ESI Tab. S8 of the original publication [142].

### Economic evaluation method for DMM processes

For an economic evaluation, we consider both OPEX and CAPEX. OPEX constitutes costs for raw materials ( $\text{H}_2$  and  $\text{CO}_2$ ), steam, coolants, and electricity. CAPEX constitutes investment costs for distillation columns (shell, trays, condensers, reboilers), reactors, pumps, and compressors. Costs for catalysts and heat exchangers are excluded as the catalysts for the direct pathways are not commercially available yet and no heat exchanger network is developed. On the most detailed level, we further calculate cost of manufacturing (COM) to get a clearer representation of a possible market price for DMM. The type and amount of output data on each level define the costs to include in the economic evaluation on each level (Appendix Tab. B.5). Production cost is measured in  $\$ \text{L}_{\text{diesel-eq.}}^{-1}$ . For the economic evaluation, we analyze the influence of the most relevant parameters by a sensitivity analysis. All equations and parameters are summarized in Appendix Section B.

### LCA method for DMM processes

LCA is a standardized method (ISO 14040/14044 [143, 144]) for evaluating potential environmental impacts of product systems. It considers the entire life cycle of a product system from raw material extraction until waste disposal ('cradle-to-grave') [145]. All environmental impacts of the material and energy flows that are exchanged with the environment are characterized in LCA.

The goal of this study is to compare DMM pathways from a climate point of view. As DMM intends to substitute fossil fuels particularly in long-distance and heavy-duty transportation, we also include fossil diesel to this comparison. Due to the different com-

bustion characteristics of these two fuels, we consider their combustion at the end-of-life to cover the cradle-to-grave perspective. The functional unit “the provision of 1 MJ of enthalpy of combustion” for both DMM and fossil diesel enables a consistent comparison between the investigated product systems. To ensure consistency also with the TEA, we do not consider environmental credits (so-called avoided burdens, i.e., an environmental credit to account for the avoided burden of the conventional production) for co-produced side products (MF and dimethyl ether (DME)) and heat. The influence of these avoided burdens on the climate impact of DMM is however investigated in ESI Section S6 of the original publication [142]. We focus on the impact category climate change (heat radiation absorption of the atmosphere caused by anthropogenic emissions, measured in kg of CO<sub>2</sub>-equivalents [146]) as e-fuels mainly aim at reducing the climate impact of transportation. For a holistic assessment of DMM, further impact categories are also important but beyond the scope of this work. The same best and worst case scenarios as for the exergy efficiency analyses are used and extended according to Tab. 4.1. All assumptions and datasets are summarized in ESI Section S3.3 of the original publication [142].

**Table 4.1.:** Selected technologies for the best and worst case scenario for the evaluation of DMM pathways. Parameters, references, and datasets are summarized in ESI Tab. S8-S10 of the original publication [142].

	Best case scenario	Worst case scenario
H <sub>2</sub> provision	SOEC	PEM electrolysis
CO <sub>2</sub> provision	Ideal point source	DAC
Electricity	Onshore wind park (Germany)	Power grid mix today (Germany)
Heat (T<90 °C)	Heat pump	Steam
Heat (90 °C<T<250 °C)	Electrode boiler	Steam
Heat (T>250 °C)	Electrode boiler	Natural gas boiler
Cooling	Vapor compression refrigeration system	

#### 4.1.2. Results on Key Performance Indicators for DMM Production

On the basis of the models and assumptions presented in Section 4.1.1, each pathway is analyzed up to a certain level given their data availability. Thermodynamic data is available for all considered pathways in open literature (cf. Section 4.1.1.1). In contrast, reaction data differs significantly between pathways. For the established pathway, reaction kinetics are available [43, 57] and enable the propagation of the pathway through all three levels. For the oxidative pathway, a comprehensive experimental data base on reaction performance has been accumulated [31], yet a kinetic model has not been derived. Notwithstanding, the vast amount of data makes the propagation through all three levels possible. For the reductive pathway, considerable achievements in catalyst optimization [38, 40] and the successful application of an alternative catalytic system [39] make process development and evaluation on Level 2 possible. For process optimization on Level 3, however, a more extensive data base or (ideally) reaction kinetics are required. For the dehydrogenative pathway, only little experimental data has been reported [41]. Nevertheless, the achieved reaction performance is high enough to develop a first process concept on Level 2. For the transfer-hydrogenative pathway, turnover numbers (TON) of the same magnitude as



for the reductive pathway have been reported [42]. A low catalyst loading compared to the reductive pathway however results in lower DMM single-pass yields with respect to methanol. Thus, the evaluation of a process concept for the transfer-hydrogenative pathway on Level 2 would systematically underestimate its performance.

On the basis of these classifications, we developed process concepts for the reductive and dehydrogenative pathway (Fig. 4.2) following the procedure presented in Section 4.1.1.1. For the established and oxidative pathway, we adapted processes from the literature [16, 147] and calculated corresponding mass and energy balances (Appendix Tab. B.8-B.10) for the analyses on both Level 2 and 3.

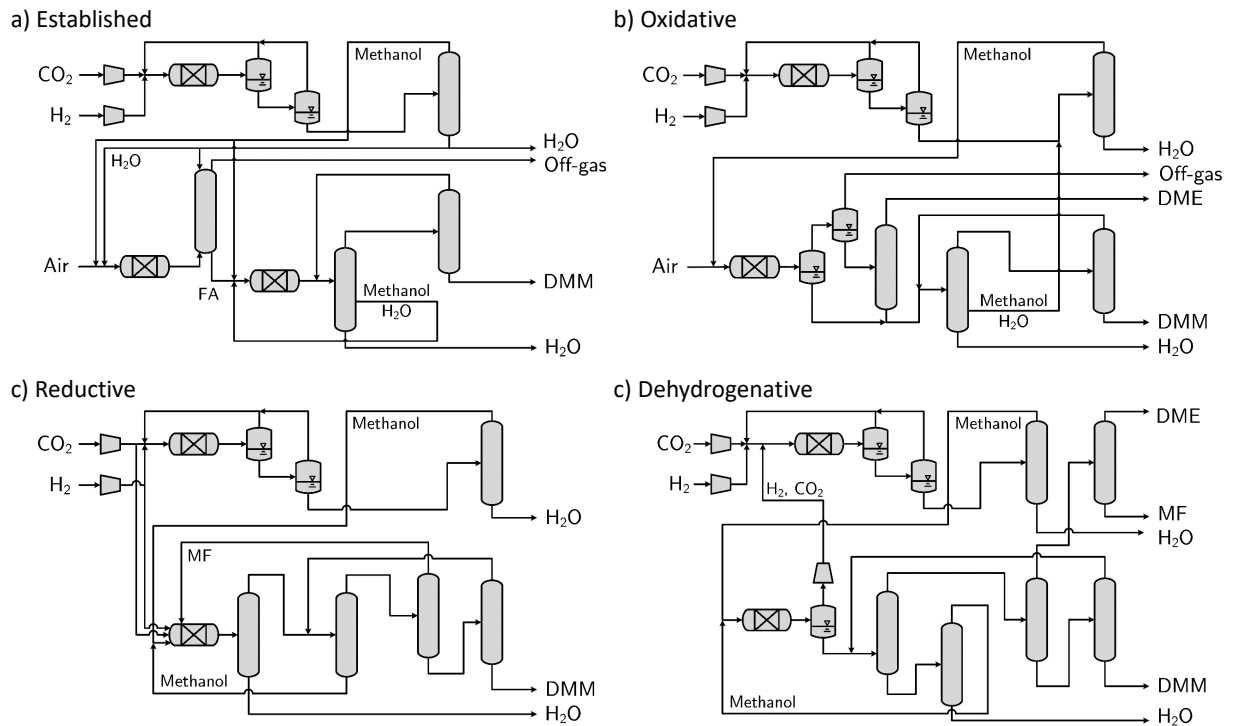


**Figure 4.2.:** Process concepts for all considered pathways on Level 2. All possible distillation sequences have been screened and the least energy-intensive sequence has been chosen.

In the following, we present the results of the analyses structured by KPI to highlight both how they differ between pathways and how they evolve through the levels for each pathway.

#### 4.1.2.1. Exergy Efficiency

On Level 1, we show that the benefit of the lower stoichiometric H<sub>2</sub> consumption for the reductive, dehydrogenative, and transfer-hydrogenative pathway corresponds to an increase in process exergy efficiency of 11 % (Fig. 4.3). These non-oxidative pathways consume 8 mol H<sub>2</sub> per 1 mol DMM formed instead of 9 mol H<sub>2</sub> (established and oxidative pathway). The benefit of saving 1 mol H<sub>2</sub> per 1 mol DMM produced enables a maximum process exergy efficiency of almost 97 %. A comparison with the maximum process exergy efficiency of other e-fuels (ethanol: 90 %; methanol: 95 %; methane: 83 %; DME: 97 %; all based on HHV) and their higher stoichiometric H<sub>2</sub> consumption relative to their heating

values (Appendix Tab. B.11) demonstrate the great potential of the non-oxidative DMM reaction pathways. Considering the experimental selectivities of the entire value chain on Level 1 instead of perfect selectivity, the gap between experimental exergy efficiencies and their theoretical limit become clear (Fig. 4.3). The negative effects caused by a low reaction conversion, however, is captured only by Level 2 and 3 evaluations.

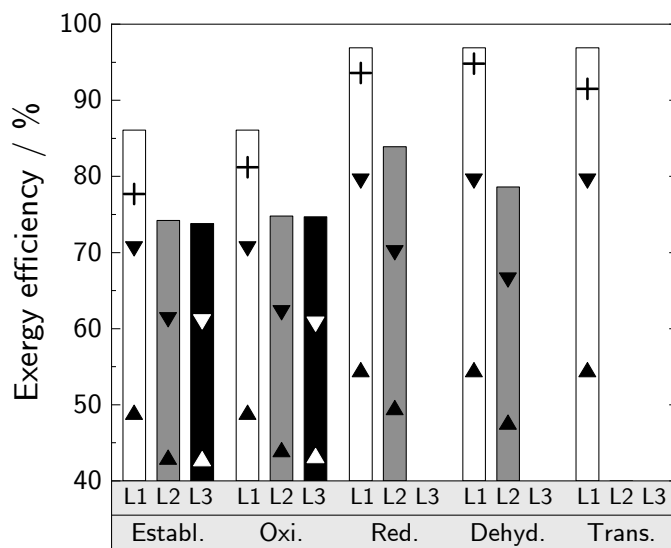


**Figure 4.3.:** Exergy efficiencies for all evaluated levels and pathways. The bars correspond to the process exergy efficiency (DMM production starting from  $H_2$  and  $CO_2$ ), whereas the triangles correspond to the best ( $\blacktriangledown$ ) and worst ( $\blacktriangle$ ) case scenario for the system exergy efficiency (DMM production starting from electricity, water, and a  $CO_2$  source). The two scenarios are specified in Table 4.1. The crosses correspond to Level 1 evaluations considering the experimental selectivities of the entire value chain instead of perfect selectivity.

On Level 2, by considering the actual reaction performance from lab-scale experiments or pilot plants (Appendix Tab. B.1) and process concepts (cf. Fig. 4.2), the exergy efficiency decreases significantly for all pathways. One common reason for this decrease is that up to 6 % of the exergy content of DMM is required for  $H_2$  and  $CO_2$  feed compression to maximum operating pressures of 70–80 bar. Furthermore, main exergy losses in the established pathway are due to methanol combustion in the FA process step [16] and a comparably low overall carbon-based DMM yield (90 %). The overall carbon-based DMM yield of the oxidative pathway (94 %) is considerably higher and only little external heating is required (cf. Appendix Tab. B.10). Yet, exergy efficiency is only about the same as that of the established pathway, because the product removal from a highly diluted gaseous reactor effluent requires more than 5 % of the DMM exergy. The overall carbon-based DMM yield of the reductive pathway (97 %) is even higher than that of the oxidative pathway as the only reported side product is the intermediate MF and assumed to be recycled back into the reactor. However, a relatively low methanol conversion of 10 % results in high recycle streams and a high heat demand for separation (8 % of the DMM exergy). This bottleneck—the most relevant one of the reductive pathway—has not been captured by the process estimations in preceding studies, where process efficiency has

been overestimated (86 %) [19]. The methanol conversion of the dehydrogenative pathway is only 3.6 %, thus resulting in a six times higher methanol recycle stream compared to the reductive pathway and in a heat demand for product separation of 16 % of the DMM exergy. This increased heat demand reduces exergy efficiency considerably. Also the overall carbon-based DMM yield of the associated process is significantly lower (77 %) as MF and small amounts of DME are formed as side products. In contrast to the reductive pathway, MF can not be converted further to DMM in the dehydrogenative pathway. As MF and DME are valuable side products, the comparatively low DMM selectivity has only negligible effect on exergy efficiency.

On Level 3, the exergy efficiency of both the established and oxidative pathway do not differ significantly from those of Level 2. Performance gains due to optimization are balanced by accounting for more detailed models (e.g., tray-to-tray distillation models) and the power demand for additional process units (e.g., pumps and compressors for recycle streams). However, we still benefit from the analyses on Level 3 in two ways: First, we obtain information on equipment sizing, which enables costing. Second, we gain more reliability on the results as more rigorous models are used. These two outcomes are highly relevant for industrial implementation.

#### 4.1.2.2. Production Cost

As is typical for e-fuels, the  $H_2$  price dominates DMM production cost for all pathways and levels (Fig. 4.4).

On Level 1, the analyses reveal that the  $H_2$  savings of the non-oxidative pathways correspond to cost reductions of 11 % of total raw material costs. As transportation is highly price sensitive, these savings in  $H_2$  consumption are paramount for DMM production.

On Level 2, an imperfect selectivity toward DMM results in additional costs. These are most pronounced for the dehydrogenative pathway due to the significant co-production of MF and DME, for which we do not consider a monetary credit given the lack of reliable data. For this pathway, also the costs for steam are the highest among the pathways due to its low methanol conversion (cf. Appendix Tab. B.1) and thus high recycle streams. Whereas conversion improvements by catalyst modifications (cf. Section 4.1.2.4) are limited by the chemical equilibrium of the dehydrogenative pathway, process modifications have potential to elevate equilibrium conversion. For instance, membrane reactors with molecular-sieves can be used for selective and in-situ  $H_2$  removal [154]. This might increase methanol conversion and reduce DMM production cost significantly. With the currently achievable reaction performance, however, the burdens of the dehydrogenative pathway result in considerably higher DMM production cost compared to other e-fuels (methane, methanol, and DME), which were evaluated on Level 2 using the same boundary conditions and model depth [21]. In contrast, production cost via the reductive pathway are in the same range as that of other e-fuels already with the current catalyst and can be further reduced by an optimized reactor design and/or co-solvent facilitating the dissolution of  $H_2$  and  $CO_2$  into the reaction phase. For the oxidative pathway, the product removal from the gaseous reactor effluent by a refrigeration machine causes the highest electricity costs among the pathways and should be avoided in an industrial application. Therefore, the application of a less energy-intensive unit operation for product removal (e.g., adsorption) need to be investigated in future work to further reduce DMM production cost. Beyond that, the product dilution in the reactor effluent can be reduced by using pure oxygen from

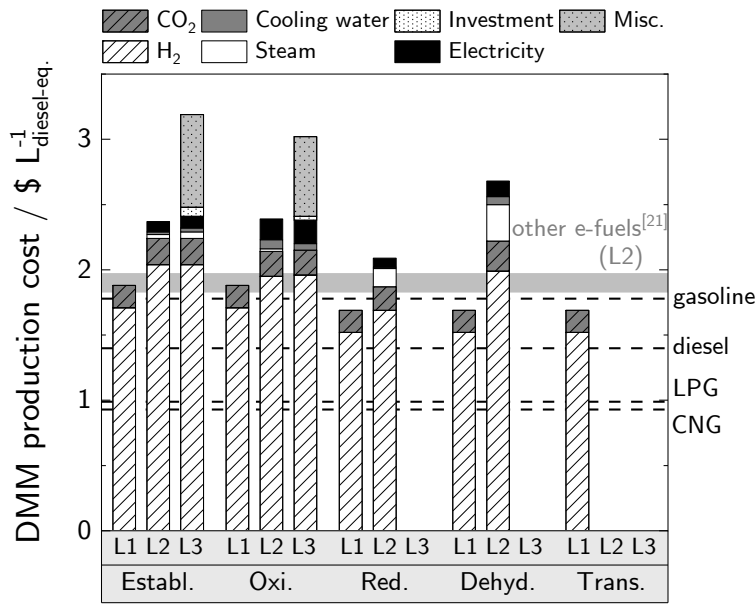


**Figure 4.4.:** Production cost for each synthesis route for all evaluated levels. Perspective H<sub>2</sub> and CO<sub>2</sub> prices of 5 \$ kg<sup>-1</sup> [148] and 70 \$ t<sup>-1</sup> [149] are considered for PEM electrolysis and CO<sub>2</sub> capture from post-combustion, respectively. A price of 7.78 \$ GJ<sup>-1</sup> for steam at 160 °C [150]; 0.02 \$ t<sup>-1</sup> and 1.2 \$ t<sup>-1</sup> for cooling water at 25 °C and 5 °C, respectively [151]; and 2.40 \$ t<sup>-1</sup> for refrigeration at -35 °C [151] are considered. Investment cost and all miscellaneous costs are calculated after Guthrie [152] and Turton et al. [153], respectively. Corresponding cost parameters can be found in Appendix Section B. The production cost of other e-fuels refer to methane, methanol, and DME and correspond to the assumptions and model detail on Level 2 [21]. The consumer prices of the conventional fossil fuels gasoline, diesel, LPG, and CNG include all taxes.

the electrolyzer instead of air for the oxidation reaction. An increased product concentration in the reactor effluent would directly reduce energy demand for product purification.

On Level 3, the economic evaluation for the established and oxidative pathway shows that investment cost for the DMM plant can be neglected (less than 1 %) considering a plant life time of 10 years. It is important to note, however, that investment cost for the electrolyzer are considered in the H<sub>2</sub> price already. The consideration of miscellaneous costs on Level 3 results in an increase of production cost of about 20 % compared to Level 2 for the established and oxidative pathway. As these costs mainly constitute general manufacturing expenses (cf. Turton et al. [153]), a similar increase is expected for the non-oxidative pathways.

The H<sub>2</sub> price is the largest cost driver for DMM production having a major influence on whether an e-fuel like DMM will become a relevant contributor in a future mobility concept or not. Unfortunately, it is also one of the most uncertain ones, which makes an analysis of its influence on DMM production cost indispensable.

Fig. 4.5 reveals clearly: Only at low H<sub>2</sub> prices (below 3.7 \$ kg<sup>-1</sup>), DMM has the chance to become cost competitive with its main competitor fossil diesel. For the extensive application of DMM in individual transportation, where fuel acceptance is driven by fuel cost [155], a competitiveness with cheap fossil diesel and thus low H<sub>2</sub> prices might be an

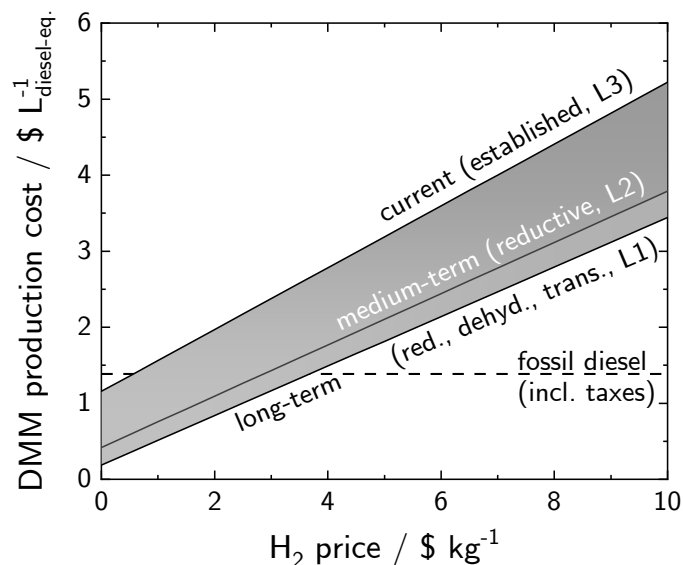


**Figure 4.5.:** DMM production cost dependence on  $H_2$  price. The base case  $CO_2$  price is  $70 \$ t^{-1}$  [149].

essential precondition. The target consumer price of DMM should therefore lie within the region of the consumer price of fossil diesel ( $1.4 \$ L^{-1}$ ). Without the non-oxidative pathways, DMM production cost will hardly fall below this target price as  $H_2$  prices would need to fall below  $0.5 \$ kg^{-1}$  for the established pathway.

In terms of  $CO_2$  supply, the technology for  $CO_2$  provision determines whether  $CO_2$  contributes significantly to DMM production cost or not. Considering industrial point sources for  $CO_2$  provision ( $0\text{--}200 \$ t^{-1}$  [149], Appendix Fig. B.1), the share of  $CO_2$  on total DMM production cost is comparably low. Technologies with a higher cost for  $CO_2$  capture (e.g.,  $600 \$ t^{-1}$  for DAC [156]) may however become a limiting factor for a successful implementation of DMM in a future mobility concept.

#### 4.1.2.3. Impact on Climate Change

The results of the LCA for the best case scenario show clearly: If renewable electricity for DMM production is used exclusively (according to the power-to-X concept [141]), the cradle-to-grave impact on climate change of DMM does not differ significantly between pathways and levels (Fig. 4.6). Compared to that of fossil diesel ( $86 g_{CO_2-eq.} MJ^{-1}$ ), all pathways for DMM production enable considerable  $CO_2$ -eq. emission reductions.

For the worst case scenario, the impact on climate change of the different routes is in the range of  $350\text{--}550 g_{CO_2-eq.} MJ^{-1}$  and, by this, exceeds that of fossil diesel considerably. With the current German electricity mix [157], it is therefore not climate friendly to produce and use DMM as an alternative to fossil diesel. The different impacts on climate change between the pathways and levels are caused by the same reasons as those for the differences in exergy efficiencies (cf. Sec. 4.1.2.1). A detailed contribution analysis for both the best and worst case scenario are presented in ESI Fig. S2 and S3 of the original publication [142], respectively.

From the analyses of the worst and best case scenario regarding the impact on climate change of DMM, we can draw two main conclusions: First, the carbon footprint of elec-

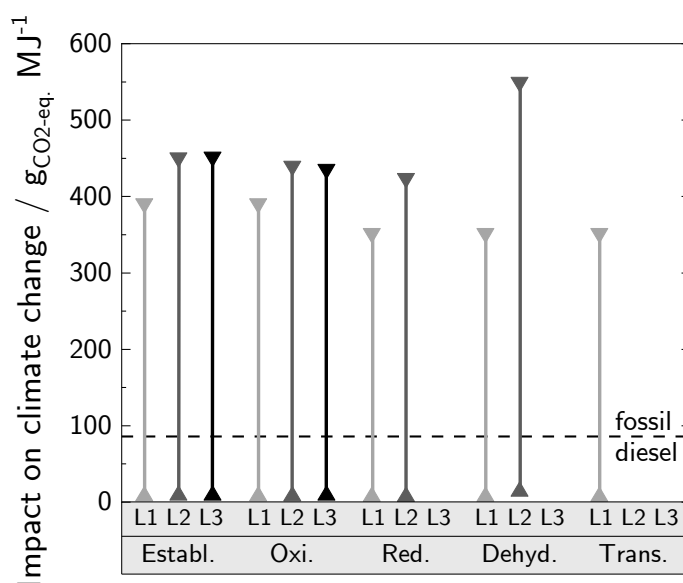


**Figure 4.6.:** Ranges of cradle-to-grave impact on climate change of different DMM synthesis routes. The routes are evaluated on different levels for both the best (▲) and worst (▼) case scenario and are compared to fossil diesel. The functional unit is “the provision of 1 MJ of enthalpy of combustion”. The combustion of the co-products MF and DME at their end-of-life is included for the dehydrogenation and oxidative route on Level 2 and 3 to cover the cradle-to-grave perspective. The two scenarios are specified in Table 4.1.

tricity supply needs to be low as cradle-to-grave CO<sub>2</sub>-eq. emissions of DMM exceed those of fossil diesel considerably if the current German electricity mix is utilized. Second, the higher the carbon footprint of the electricity mix is, the more important becomes the choice for the pathway in order to yield a low impact on climate change of DMM.

Fig. 4.7 therefore shows the impact on climate change of DMM for the different pathways on Level 2 as a function of the impact on climate change of electricity supply. The intersections of the graphs with the solid black line are the break-even points, where the CO<sub>2</sub>-eq. emissions of DMM fall below those of fossil diesel. The impact on climate change of the reductive DMM pathway depends the least on that of the electricity supply. Below the break-even point of 190 gCO<sub>2</sub>-eq. kWh<sup>-1</sup>, DMM produced by the reductive pathway is more favorable compared to fossil diesel. This break-even point has a rigorous bound at about 225 gCO<sub>2</sub>-eq. kWh<sup>-1</sup> (ESI Fig. S4 of the original publication [142]). At this bound, only stoichiometric H<sub>2</sub> and CO<sub>2</sub> consumption is considered (Level 1) such that no process can exceed this bound. The established and oxidative pathways have a break-even point of 170 gCO<sub>2</sub>-eq. kWh<sup>-1</sup> and are thus less favorable compared to the reductive pathway. For these three pathways, the grid mixes of Norway, France, and in contrast to DMM/fossil diesel blends with 35 vol% DMM [19], also of Switzerland and Finland, are sufficient for producing and using neat DMM with less impact on climate change than fossil diesel already today. In this range, it does matter which pathway is used for DMM production from a climate impact perspective. The carbon footprint of the dehydrogenative pathway depends most strongly on the impact on climate change of electricity supply as the selectivity towards DMM is the lowest. The co-production of MF and DME requires additional electricity and the low methanol conversion results in a high heat demand for product sep-

aration (cf. Appendix Tab. B.8-B.10). The impacts on climate change evaluated on Level 1 and 3 are presented in ESI Fig. S4 and S5 of the original publication [142], respectively.

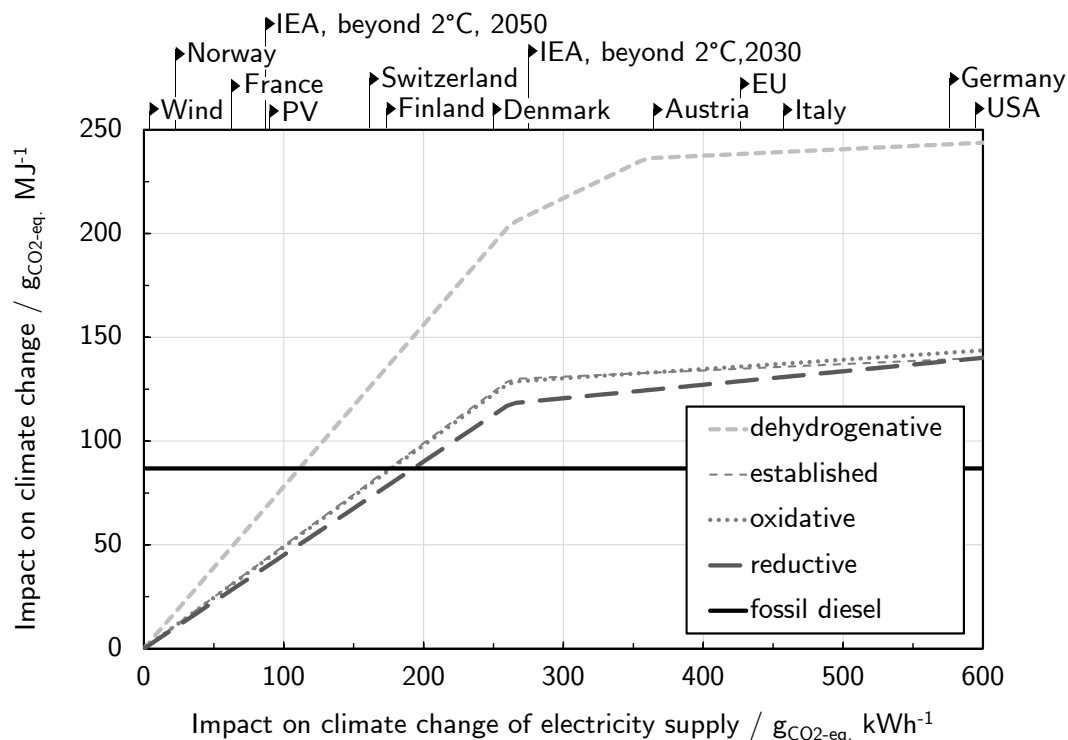


**Figure 4.7.:** Sensitivity of the cradle-to-grave impact on climate change of DMM with respect to the impact on climate change of electricity supply for different DMM synthesis pathways on Level 2 and fossil diesel. The impact on climate change is calculated using the current catalyst performance of each pathway. Avoided burdens for co-produced MF, DME, and excess heat are not considered. Below  $360 \text{ gCO}_2\text{-eq. kWh}^{-1}$ , heat between  $90\text{--}250^\circ\text{C}$  is provided by electrode boilers instead of steam production (relevant only for the dehydrogenative pathway).  $\text{H}_2$  is supplied by SOEC instead of conventional steam methane reforming below  $260 \text{ gCO}_2\text{-eq. kWh}^{-1}$ . At lower carbon-intensities of electricity supply, both the electrode boilers and the SOEC allow for lower climate change impacts compared to their conventional counterparts. The solid black lines at the top of the graph represent the impact on climate change of country-specific grid mixes and two forecasts for the global grid mix of 2030 and 2050 that are based on the “beyond  $2^\circ\text{C}$  scenario” of the International Energy Agency [158].

#### 4.1.2.4. Catalyst Improvement Potential

The non-oxidative pathways have been proposed just recently and may offer catalyst improvement potential that has not been captured with the analyses on Level 2 so far. To consider this improvement potential, we analyze the theoretically achievable reaction performance of the reductive, dehydrogenative, and transfer-hydrogenative pathway by assuming restricted equilibrium conversion. Restricted equilibrium considers only the desired reaction (perfect DMM selectivity) [159]. We calculate the equilibrium DMM yield

using the stoichiometric chemical and phase equilibrium (REquil reactor model in Aspen Plus v11) and evaluate the current gap to this performance. We then use these theoretical reaction conditions to evaluate the maximum process efficiency, minimum production cost, and minimum impact on climate change on Level 2 for all non-oxidative pathways.

### Reductive pathway

Reaction equilibrium calculations show that DMM yield increases strongly with decreasing temperature due to the exothermic nature of Reaction (R6) (Fig. 4.8a). Experimental DMM yields confirm this trend in the temperature range of 80–120 °C, but they are well below equilibrium yield due to catalyst deactivation during the course of reaction. In the temperature range below 80 °C, experimentally observed DMM yields decrease significantly since the used catalyst requires a certain activation energy to convert CO<sub>2</sub> and H<sub>2</sub>. To exploit the increased DMM equilibrium yield at temperatures below 80 °C, catalysts requiring even lower temperatures and thus lower activation energies for CO<sub>2</sub> activation are necessary. In terms of reactor pressure, the DMM equilibrium yield increases linearly with increasing pressure (Appendix Fig. B.2). Experiments do not confirm this linear trend so far, which could be caused by limitations of the experimental set-up. Due to the minimum temperature of 80 °C required for catalyst activity and the independence of experimental DMM yield on pressure, we choose an optimal operating point of 80 °C and 80 bar for evaluating the maximum performance of the reductive pathway on Level 2. This corresponds to an equilibrium yield of 15.7 % and an improvement of 7.4 percentage points compared to the current state of the catalyst.

At equilibrium yield, the heat demand required for product separation is reduced by 81 % compared to the current state of the catalyst (Appendix Tab. B.14 and Fig. B.3). As the heat demand of the reductive pathway causes the main exergy losses, this reduction is highly beneficial and increases exergy efficiency by 5 percentage points to an overall process efficiency of 89 %. Production costs are reduced by only 0.1 \$ L<sub>diesel-eq.</sub><sup>-1</sup> as fossil-based heating is cheap compared to renewable H<sub>2</sub>. A major benefit in reducing fossil-based heating rather lies in associated CO<sub>2</sub>-eq. emission reductions, which are about 10 % (44 gCO<sub>2</sub>-eq. MJ<sup>-1</sup>) in the worst case scenario. The best case scenario utilizes almost CO<sub>2</sub>-neutral heating sources, such that a reduced heat demand has only a negligible effect on climate impact (ESI Fig. S10 of the original publication [142]).

### Dehydrogenative pathway

The experimental data on the dehydrogenative pathway demonstrates that the maximum experimentally achieved DMM yield (4.1 %) is 10<sup>4</sup> times higher than that if no side reactions would be suppressed [41]. This corresponds to 48 % of the DMM equilibrium yield at 240 °C (Fig. 4.8b). At higher temperatures, equilibrium DMM yield increases, but DMM selectivity decreases due to elevated FA and MF co-production [41]. However, co-produced FA and unreacted methanol can be converted to DMM (cf. Sec. 3.1) in an additional reactive distillation section [45], such that the overall DMM yield does not necessarily decrease with increasing temperature. To still benefit from rather mild reaction conditions and maintain high yields, we chose an equilibrium DMM yield at 300 °C (9.8 %) for analyzing potential process improvements by further catalyst development. Reaction pressure does not have a significant influence on DMM yield and is kept constant at 1 bar.



Similar to the reductive pathway, heat demand decreases by about 80 % at equilibrium yield at 300 °C and exergy efficiency increases by 6 percentage points to an overall process efficiency of 85 % (Appendix Tab. B.14 and Fig. B.4). The maximum cost reduction potential is  $0.6 \$ L_{\text{diesel-eq.}}^{-1}$  or 22 % of the production costs considering the current state of the catalyst. This reduction is enabled mainly by the assumed perfect selectivity ( $0.3 \$ L_{\text{diesel-eq.}}^{-1}$ ) and by the lower heat demand ( $0.2 \$ L_{\text{diesel-eq.}}^{-1}$ ). As the absolute reduction in heat demand is even higher than that of the reductive pathway, the associated reduction in CO<sub>2</sub>-eq. emissions in the worst case scenario is higher as well (26 % or  $140 \text{ g}_{\text{CO}_2\text{-eq.}} \text{ MJ}^{-1}$ ). Although the best case scenario utilizes almost CO<sub>2</sub>-neutral heating sources, significant CO<sub>2</sub>-eq. emission reductions can be achieved there as well due to the higher selectivity (cf. ESI Fig. S10 of the original publication [142]).

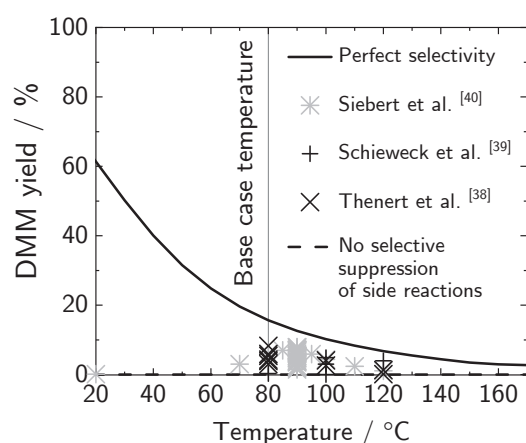
### Transfer-hydrogenative pathway

For the transfer-hydrogenative pathway, no process concept has been developed on Level 2, because reported DMM yields are still low (Appendix Tab. B.1 and Fig. 4.8c). The low DMM yields are mainly caused by comparatively low catalyst concentrations used in the experiments, which makes the direct comparison between the pathways difficult. The maximum potential calculations can overcome these difficulties and allow also for the transfer-hydrogenative pathway a fair comparison with its alternatives from a process perspective.

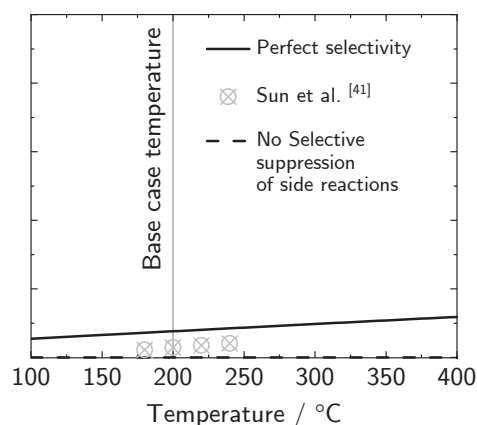
The equilibrium reaction calculations reveal that experimentally achieved DMM yields (up to 2.1 %) are well below restricted equilibrium conditions (92.1 %) at 100 °C assuming the concurrent transfer-hydrogenation reaction of styrene to ethylbenzene (EB) (Fig. 4.8c). Whereas the experimentally achieved maximum selectivity is almost perfect (98.2 %), methanol conversion is still low (0.9 %). Without the H<sub>2</sub> removal by the transfer-hydrogenative reaction ('no trans.-hydr.' in Fig. 4.8c), equilibrium yield would be limited to only 0.3 %, which is about one third of the experimentally achieved yield. The strong effect of in-situ H<sub>2</sub> removal on DMM yield for the transfer-hydrogenative pathway indicates similar benefits for the dehydrogenative pathway and should therefore be investigated in future research. Irrespective of a concurrent transfer-hydrogenation reaction, if the catalyst would not suppress MF and DME formation selectively, no DMM would be formed but exclusively MF and DME with selectivities of 83.1 % and 16.9 %, respectively.

To evaluate the maximum potential of the transfer-hydrogenative pathway, we assume equilibrium yield at 100 °C (92.1 %) and the concurrent transfer-hydrogenation of styrene to EB. In contrast to the other non-oxidative pathways, the evaluated process concept for the transfer-hydrogenative pathway contains the following additional steps: the transfer-hydrogenation of styrene, the subsequent removal of its hydrogenated molecule EB, the dehydrogenation back to styrene and H<sub>2</sub>, and the recycling of styrene into the reactor. The resulting process concept and model assumptions are given in Appendix Fig. B.6.

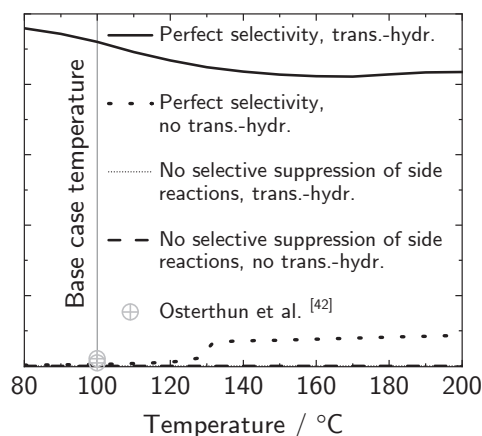
If EB dehydrogenation and H<sub>2</sub> recycling is considered at no cost (decoupling the pathway evaluation from the choice of the model hydrogen carrier substance), a maximum process exergy efficiency of 91 % can be achieved (Appendix Fig. B.5a). This is slightly higher than that of the reductive pathway (89 %) and significantly higher than that of the dehydrogenative pathway (85 %) due to a higher equilibrium conversion and, in turn, a lower heat demand. Considering commercial EB dehydrogenation and H<sub>2</sub> recycling, the efficiency drops to 72 % due to its massive heat demand at high temperature (cf. Appendix



**(a)** For the reductive pathway, the base case pressure is 80 bar. 'No selective suppression of side reactions' considers additional DME and carbon monoxide (CO) formation.



**(b)** For the dehydrogenative pathway, the base case pressure is 1 bar. 'No selective suppression of side reactions' considers additional MF and DME formation.



**(c)** For the transfer-hydrogenative pathway, the base case pressure is 20 bar. 'No selective suppression of side reactions' considers additional MF and DME formation.

**Figure 4.8.:** DMM yield dependence on reactor temperature for the reductive pathway (Fig. 4.8a), the dehydrogenative pathway (Fig. 4.8b), and the transfer-hydrogenative pathway (Fig. 4.8c). Restricted equilibrium conversion (considering perfect DMM selectivity) has been considered throughout the entire temperature range and was calculated with an REquil reactor model in Aspen Plus v11.

Tab. B.14). It should be noted that the use of styrene as a hydrogen acceptor is not industrially viable, since styrene itself is produced industrially by EB dehydrogenation. The hydrogen carrier couple styrene-EB was nevertheless selected for the experiments due to its ease of hydrogenation and analytical simplifications in the experimental development of a transition-metal catalyst that could catalyze the conversion of methanol to DMM. For industrial applications, a hydrogen carrier couple allowing for a more energy efficient  $H_2$  recycling has to be found, which is subject to ongoing research. Alternatively, the

co-production of a high value hydrogenated by-product could be envisioned as well.

The minimum production cost for the transfer-hydrogenative pathway is identical to that of the reductive pathway ( $2.0 \$L_{\text{diesel-eq.}}^{-1}$ ) (Appendix Fig. B.5b). The same amount of  $H_2$  and  $CO_2$  is consumed as well as compressed to operating pressure. DMM production cost by the dehydrogenative pathway is slightly more expensive ( $2.1 \$L_{\text{diesel-eq.}}^{-1}$ ) as a considerable amount of external heat is required for product separation despite equilibrium conversion.

In terms of impact on climate change, the transfer-hydrogenation pathway has the lowest climate impact among the alternative pathways in the worst case scenario ( $370 \text{ g}_{CO_2\text{-eq.}} \text{ MJ}^{-1}$ ) if EB dehydrogenation and  $H_2$  recycling at no cost is considered (ESI Fig. S12c of the original publication [142]). In the other cases, the climate impact slightly exceeds that of the dehydrogenative pathway. For the best case scenario, the impact on climate change is below  $10 \text{ g}_{CO_2\text{-eq.}} \text{ MJ}^{-1}$  and thus, similar to the alternative pathways, well below that of fossil diesel ( $86 \text{ g}_{CO_2\text{-eq.}} \text{ MJ}^{-1}$ ) (cf. ESI Fig. S10 of the original publication [142]).

In total, methanol transfer-hydrogenation toward DMM can represent a promising pathway alternative if two prerequisites can be satisfied: significant catalyst improvements allowing a higher single-pass DMM yield and a more promising  $H_2$  carrier substance. Such a substance can be more promising either in terms of a higher efficiency regarding  $H_2$  management, or in terms of value as a final by-product.

A summary of the existing bottlenecks connected to each reaction pathway is given in Tab. 4.2. To support future research in DMM synthesis, we therein estimate the significance of each bottleneck’s impact on KPIs and propose improvement measures correspondingly.

### 4.1.3. Conclusion

Extensive effort in catalyst development for dimethoxymethane (DMM) production during the last years have resulted in remarkably improved reaction performances and completely new reaction pathways. Yet, the achievements in catalyst development have not been assessed from a process perspective such that their actual performance and sustainability for industrial applications still remain unknown. In this section, we demonstrate that DMM produced via different reaction pathways offers considerable benefits compared to fossil diesel if requirements on cost and carbon footprint of raw material provision are met. However, for each individual pathway special aspects for their further development need to be addressed if those requirements can not be fulfilled to an arbitrary large extent.

Our hierarchical process evaluation shows that comparable process efficiencies to other e-fuels (e.g., dimethyl ether (DME)) can only be achieved if  $H_2$  consumption is low. The non-oxidative pathways (reductive, dehydrogenative, and transfer-hydrogenative pathway) have a maximum exergy efficiency of 97 % (Level 1), which is significantly higher than that of the established and oxidative pathway and most other e-fuels. More detailed process analyses (Level 2 and 3) of all pathways reveal that exergy losses mainly result from an energy-intensive product separation and a low DMM single-pass yield of current catalysts. Although these losses are more pronounced for the non-oxidative reaction pathways, their exergy efficiency is higher than that of the established and oxidative one. Their comparably low  $H_2$  consumption is key for efficient DMM production—especially in a world with limited renewable electricity.

**Table 4.2.:** Bottlenecks of each reaction pathway, their impact on key performance indicators, and potential measures for improvements.

Reaction Pathways	Bottlenecks	Impact on KPIs	Improvement measures
Established	High H <sub>2</sub> consumption due to oxidative FA production	High	FA prod. via methanol dehydrogenation
	Three process steps	Low	none <sup>a</sup>
Oxidative	High H <sub>2</sub> consumption due to oxidative in-situ FA formation	High	none <sup>a</sup>
	High DMM dilution in reactor effluent	Medium	Pure oxygen as oxidant and methanol excess
	High cooling demand	Medium	Application of an alternative gas separation
Reductive	Gap to chemical equilibrium	Medium	Further catalyst optimization to suppress catalyst deactivation
Dehydrogenative	Low equilibrium conversion	High	In-situ H <sub>2</sub> removal (e.g., by membrane reactor)
	Comparatively low DMM selectivity	Medium	Further catalyst optimization to suppress side reactions
	Gas separation for H <sub>2</sub> recycling necessary	Medium	none <sup>a</sup>
Transfer-hydrogenative	Gap to chemical equilibrium	High	Further catalyst optimization to suppress catalyst deactivation
	Currently only model substrate as hydrogen carrier	High	Extending the reaction to use industrially viable hydrogen acceptors

<sup>a</sup> Intrinsically given by reaction pathway.

The production cost for DMM may fall below the price of fossil diesel only if H<sub>2</sub> can be produced for less than 4 \$ kg<sup>-1</sup> and if a low H<sub>2</sub> consumption can be ensured. Cost competitiveness with fossil diesel is most likely achievable for the reductive pathway already for the current catalyst performance. It is also the only pathway that is currently cost-competitive with the production of other e-fuels.

In terms of the impact on climate change of DMM, the pathways do not differ significantly from one another if exclusively renewable electricity is utilized. In this case, DMM has the potential to reduce its climate impact by up to 92 % compared to fossil diesel. In contrast, if the impact on climate change of electricity supply increases to that of Finland or Switzerland (up to 190 gCO<sub>2</sub>-eq. kWh<sup>-1</sup>), it does matter which pathway is used for DMM production from a climate impact perspective. In this range, the currently high heat demand and co-production of side products make the impact on climate change of the dehydrogenative pathway being most dependent on the impact on climate change of electricity supply. The climate impact of the reductive pathway is least dependent on the electricity carbon-intensity and is lower than that of fossil diesel below 190 gCO<sub>2</sub>-eq. kWh<sup>-1</sup>. For an even higher carbon-intensity of electricity supply, DMM should not be considered as

an alternative fuel since its impacts on climate change would exceed those of fossil diesel.

In contrast to the established and oxidative pathway, the non-oxidative pathways have been proposed just recently such that their catalyst performances are expected to still improve significantly. For exploiting the full potential of these pathways and ultimately deciding which one is suited most for sustainable DMM production, more research need to be conducted. For the dehydrogenative pathway, future catalyst development need to aim at suppressing side reactions even more effectively. Alternatively, a systematic exploitation of the co-products in a multi-product plant for producing different e-fuels (e.g., DMM, DME, and methyl formate) should be evaluated. For the transfer-hydrogenative pathway, future experimental studies should aim not exclusively at increasing turnover numbers, but also increasing single-pass DMM yield. Together with the identification of an industrially viable hydrogen carrier substance, comparable performance indicators to those of the reductive pathway can be achieved. The reductive pathway is the most developed one among the non-oxidative pathways. We have shown that already with a catalyst at its current state, an efficient DMM production at competitive cost and low climate impact is possible in some countries.

## 4.2. Optimal Process Design for Reductive DMM Production

The existing publications on process development, including our own [142], rely on intermediate-fidelity models incorporating activity coefficient thermodynamic models. Activity coefficient models are however usually not accurate at high pressures [160] and for systems containing significant amounts of quadrupolar components (e.g.,  $\text{CO}_2$ ). For such systems, to which the reductive synthesis of DMM belongs to, equations of state (EOS) should be preferred. In this regard, the perturbed-chain polar statistical associating fluid theory (PCP-SAFT) EOS [161, 162] has been successfully applied to various systems [163]. The necessity of a complicated thermodynamic model in combination with typically non-linear process unit models for such chemical processes results in a nonconvex optimization problem, which makes deterministic process optimization for the direct  $\text{CO}_2$  reduction challenging. Especially deterministic global optimization, which is required to guarantee optimal solutions for nonconvex problems, is often computationally not tractable.

In this section, we measure liquid equilibrium densities and use data from the open literature to fit missing binary parameters of the PCP-SAFT EOS for the underlying system of components. We then use the PCP-SAFT EOS to develop data-driven models to make global optimization for reductive DMM production tractable while keeping model accuracy high. More specifically, we use a data-driven model for the reactor to predict the solubility of  $\text{H}_2$  and  $\text{CO}_2$  in the liquid reaction mixture at high pressure and their conversion with methanol to DMM. Additionally, a data-driven model is developed for the flash downstream the reactor unit that recycles unreacted gaseous components. To also account for DMM purification and identify the least energy-intensive separation process, we consider two alternative distillation column sequences formulated as a simple superstructure.

Section 4.2.1 introduces the process concept that is used for process optimization and the underlying chemical reaction. In Section 4.2.2 and 4.2.3, we fit binary PCP-SAFT parameters and develop data-driven models for the reactor and the flash unit, as well

as the superstructure model for distillation column sequencing. On the basis of these models, Section 4.2.4 describes how the optimization problem is solved using our open-source deterministic global solver MAiNGO [164], before the results are discussed in Section 4.2.5. In Section 4.2.6, we conclude our findings.

### 4.2.1. Process Flowsheet for Reductive DMM Production

The production of DMM via the direct reduction of  $\text{CO}_2$  is based on the reaction



which is catalyzed by a ruthenium-based catalyst [38, 40]. In this reaction,  $\text{CO}_2$  and  $\text{H}_2$  are dissolved under high pressure in methanol, where the formation of the intermediate product methyl formate (MF) takes place, before it is finally converted to DMM.

In Section 4.1, we developed a hierarchical process development and comparison methodology that we applied to several reaction pathways for DMM production. Using intermediate-fidelity models, the reaction pathway according to Reaction (R23) was found to be the most suitable one for sustainable DMM production at its current state of development. As the goal of this section is to refine the process and optimize its design and operating conditions using a more accurate thermodynamic model, some process modifications are required (Fig. 4.9). First, the unreacted gases dissolved in the liquid reactor effluent are separated by a flash and a low-temperature distillation column. Second, as the amount of MF at reaction equilibrium is negligible (based on our own calculations considering the two-step reaction [38] with MF as an intermediate) and its recycling together with  $\text{H}_2$  and  $\text{CO}_2$  is simple, we do not consider MF formation in this study. Third, we do not consider a fixed distillation column sequence for the purification of DMM as it is dependent on the upstream reaction performance. Instead, we use a superstructure model to incorporate the choice for the optimal sequence into the optimization resulting in a mixed-integer nonlinear program (MINLP). As the mixture contains an azeotrope between methanol and DMM, a pressure swing distillation (column D1 and D2) is considered (Fig. 4.9). Finally, we only consider DMM synthesis from methanol,  $\text{CO}_2$ , and  $\text{H}_2$ . Thus, we do not optimize the upstream process for methanol production via  $\text{CO}_2$  hydrogenation.

For the exothermic vapor-liquid reaction (R23), a temperature of  $80^\circ\text{C}$  has been found experimentally to be ideal for the ruthenium-based catalyst at its current state due to its required minimum activation energy [38]. In contrast, the ideal reactor pressure still remains unknown. Experiments have shown that a high pressure enhances the solubility of gases into methanol and may increase conversion [38–40]. However, a high reactor pressure results in high compression cost. The use of co-solvents with an enhanced solubility for  $\text{H}_2$  and  $\text{CO}_2$  has high potential to counteract corresponding mass transfer limitations within the reactor. However, these co-solvents also have an influence on the catalytic reaction [165], which has not been investigated sufficiently so far. Therefore, we do not consider the use of co-solvents within this section. The combination of a high pressure and the presence of components with a quadrupole moment ( $\text{CO}_2$ ) that might influence fluid properties significantly makes the consideration of an accurate thermodynamic model inevitable.

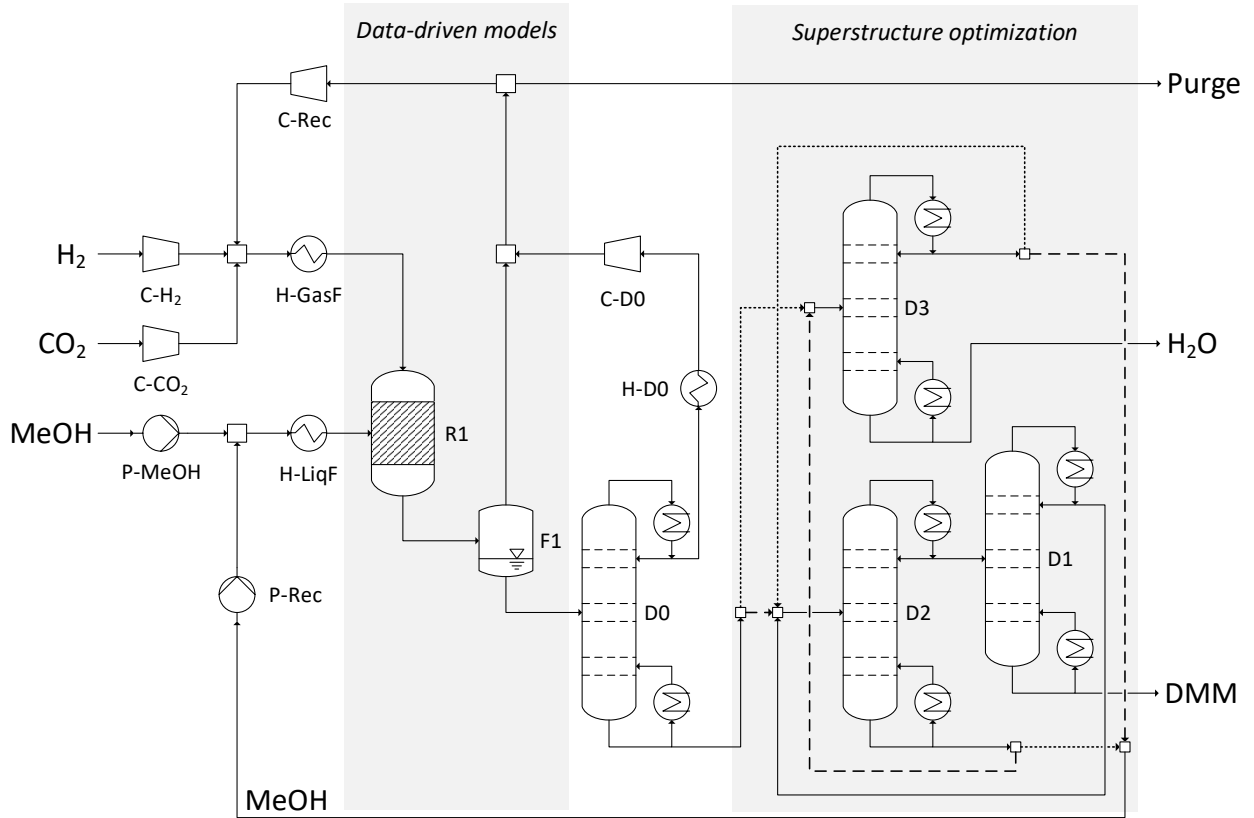


**Figure 4.9.:** Process flowsheet for the reductive production of DMM. The corresponding process model includes a data-driven model for the reactor, where the vapor-liquid reaction (R23) takes place at high pressure, and a data-driven model for a flash unit, where unreacted  $\text{H}_2$  and  $\text{CO}_2$  is separated and recycled. Downstream the distillation column D0, which separates remaining  $\text{CO}_2$ , a superstructure model for the purification of DMM using pressure swing distillation (column D1 and D2) is used for column sequencing. The different line types correspond to the different column configurations.

#### 4.2.2. Thermodynamic Modeling

Since the reactor is the central unit of the process and has a significant influence on the downstream process units, we place a firm focus on the accuracy of the reactor model. As the reaction according to Equation (R23) requires high pressures (based on our own experiments and those from literature [38–40], a reactor pressure of 50 bar is sufficient to ensure a reasonable solubility of  $\text{H}_2$  and  $\text{CO}_2$  in the liquid), the reactor is modeled with the PCP-SAFT EOS. As the subsequent flash unit recycles unreacted gaseous educts potentially at high pressures (to avoid recycling of gaseous DMM), it has a direct influence on the reaction and is therefore also modeled with the PCP-SAFT EOS. For the downstream process at moderate pressures, the system is approximated as an ideal system (with the azeotrope between DMM and methanol being considered as a pseudo-component, cf. Section 4.2.3) to maintain optimization tractability while still obtaining estimates on the exergy demand for DMM purification. As the exergy demand for DMM purification makes up only a smaller part of the total energy demand [142] (cf. Section 4.1), the resulting

inaccuracies are expected to affect overall process performance only moderately.

#### 4.2.2.1. PCP-SAft Equation of State

PCP-SAFT EOS is based on PC-SAFT EOS [166] with additional polar terms for dipole-dipole [162] and quadrupole-quadrupole [161] interactions. For further information on the used model, we refer to Aigner et al. [167].

Phase equilibrium calculations using only pure component parameters (Appendix Tab. C.1) often deliver results with significant deviations to experimental data [160]. To gain reliable phase equilibria for multicomponent systems, conventional combining rules usually require the adjustment of interaction parameters to the binary subsystems. We consider two cases: For non associating systems, the binary interaction parameter  $k_{ij}$  is used for the correction of dispersive interactions [168]. In case of cross-associating systems, polar interactions occur involving a molecule that is either a hydrogen bond acceptor or a hydrogen bond donor. This effect is modeled by the binary association strength  $\epsilon^{A_i B_j}$  and binary association volume  $\kappa^{A_i B_j}$  [167]. These corrections lead to a significant improvement of phase equilibrium calculations.

In our case, the solubility of the gaseous educts  $\text{H}_2$  and  $\text{CO}_2$  is of utter importance because of its significant influence on the chemical equilibrium and thus on the total process performance. Therefore, binary parameters are used for all binary subsystems including  $\text{H}_2$  or  $\text{CO}_2$ . Parameters are either taken directly from literature or adjusted to vapor-liquid equilibria from literature. Since there is no experimental VLE-data for  $\text{H}_2$  or  $\text{CO}_2$  with DMM available in the open literature, we measured liquid equilibrium densities (ESI Section 2 of the original publication [169]), which we used to calculate the binary interaction parameters  $k_{\text{CO}_2, \text{DMM}}$  and  $k_{\text{H}_2, \text{DMM}}$  (Tab. 4.3). For parameter fitting, the deviation between the experimental results and those generated by the PCP-SAFT EOS are evaluated by the weighted root-mean-square deviation RMSDw

$$\text{RMSDw}(\rho) = \sqrt{\frac{1}{N} \sum_n \left( \frac{\rho_{\text{eq},n}^{\text{calc}} - \rho_{\text{eq},n}^{\text{exp}}}{u_c(\rho)_{i,n}} \right)^2} \quad (4.2)$$

taking the uncertainties  $u_c(\rho)_{i,n}$  of the experimental liquid equilibrium densities  $\rho_{\text{eq}}^{\text{exp}}$  into account. It is noticeable that all gas solubilities were significantly underestimated without the use of binary parameters.

**Table 4.3.:** Binary parameters for the PCP-SAFT EOS.

Parameter source	Component $i$	Component $j$	$k_{ij} / -$	$\epsilon^{A_i B_j} / \text{K}$	$\kappa^{A_i B_j} / -$	Data Ref.
Literature	$\text{CO}_2$	Water	-	2882.3	$5.72967 \times 10^{-4}$	Aigner et al. [167]
Regression	$\text{CO}_2$	Methanol	-	3127.43	$6.06313 \times 10^{-4}$	Leu et al. [170]
	$\text{H}_2$	Water	-0.4622	-	-	Gillespie and Wilson [171], Kling and Maurer [172], DeVaney et al. [173]
	$\text{H}_2$	Methanol	-0.5132	-	-	Brunner et al. [174]
Experiments	$\text{CO}_2$	DMM	-0.0875	-	-	this work
	$\text{H}_2$	DMM	-0.127	-	-	this work



#### 4.2.2.2. Data-driven Thermodynamic Model

Given the complicated form of the PCP-SAFT EOS, it is not straightforward to consider this thermodynamic model directly in deterministic global process optimization. It is not available in most commercial process simulation tools and complicated to rigorously implement in process models. The multitude of terms required to describe the complex interactions between different types of molecules and phases introduces many variables and makes the solution of the corresponding system of equations challenging. Only few standalone model implementations are available in the open literature [175], which can however not be integrated into commercial process simulation tools. To still benefit from the high accuracy of the PCP-SAFT EOS for process optimization, we develop data-driven models for the reactor and the flash unit for gas recycling, which can efficiently be used for deterministic process optimization [176, 177]. The presence of both data-driven and mechanistic models results in a hybrid process model. With this hybrid modeling approach, we enable the integration of models that are too complicated for deterministic global optimization while exploiting the large validity range of mechanistic models for the remaining process units.

#### Flash Model

In accordance to the reported suitability of artificial neural networks [178] (ANNs) for approximating phase equilibrium calculations for systems described by the PC-SAFT EOS [179], we use an ANN to model the vapor-liquid equilibrium (VLE) within the flash unit F1 considering the PCP-SAFT EOS. The input variables of this model are the operating conditions of the flash ( $T_{F1}$  and  $P_{F1}$ ) and the component mole fractions of the liquid reactor effluent ( $x_{Prod,i}$ ). The bounds for  $x_{Prod,i}$  correspond to the attainable region of the reaction effluent and are summarized in Tab. 4.4. In order to yield a linear process model for the flash unit and keep the output dimension as small as possible, the output variables are chosen to be the split factors  $\xi_i$  of each component  $i$ . As the consideration of 6 input variables requires a large set of samples, we generate 10,000 data points using a mechanistic flash model implemented in Matlab incorporating the PCP-SAFT EOS.

**Table 4.4.:** Input variables and their bounds for the training of the ANN flash model.

Input variable	Description	Bounds
$T_{F1}$ / °C	Temperature of flash F1	[25;100]
$P_{F1}$ / bar	Pressure of flash F1	[4;40]
$x_{Prod,H_2}$ / -	Liquid mole fraction of component $H_2$ in reactor effluent	[0.01;0.03]
$x_{Prod,CO_2}$ / -	Liquid mole fraction of $CO_2$ in reactor effluent	[0.05;0.11]
$x_{Prod,DMM}$ / -	Liquid mole fraction of DMM in reactor effluent	[0.01;0.08]
$x_{Prod,H_2O}$ / -	Liquid mole fraction of water in reactor effluent	[0.03;0.14]

For deterministic global process optimization, it is crucial to keep the problem size as small as possible and relaxations as tight as possible in order to keep the optimization tractable. At the same time, accuracy requirements need to be met. To find the optimal trade-off between model accuracy and computational performance, sophisticated methods exist (e.g., ALAMO - Automatic Learning of Algebraic MOdels [180]). Such methods

use a library of terms with a simple functional form to iteratively build a process or unit model until a desired accuracy is reached. The resulting models are tailored to fulfill the desired trade-off as good as possible. In this study, we do not intend to find the sweet spot of this trade-off, but rather show that deterministic global optimization for complex processes is also possible with off-the-shelf surrogate models. In fact, in the reduced-space problem formulation in MAiNGO (cf. Section 4.2.4), the optimization problem remains the same irrespective of the size of the surrogate model, i.e., the ANN, but it only affects the relaxation tightness and the model accuracy [176]. To ensure a reasonable accuracy, we performed a sensitivity analysis regarding the number of hidden layers and neurons per layer. The mean squared error (MSE) for all cases and all settings for the training of the ANN model are summarized in Fig. 4.10. For an acceptable maximum MSE of  $10^{-4}$ , the ANN must have at least 10 neurons in total. Numerical experiments have shown that the ANN with 3 layers and 4 neurons for each layer results in a lower solution time than ANNs with the same size but different amount of layers or those with an even smaller size. This indicates that the number of layers has a significant influence on the relaxation tightness (cf., Section 4.2.5). The prediction capabilities of the final ANN model are demonstrated in Fig. 4.11a-4.11c exemplary for the split factors of  $H_2$ ,  $CO_2$ , and DMM.

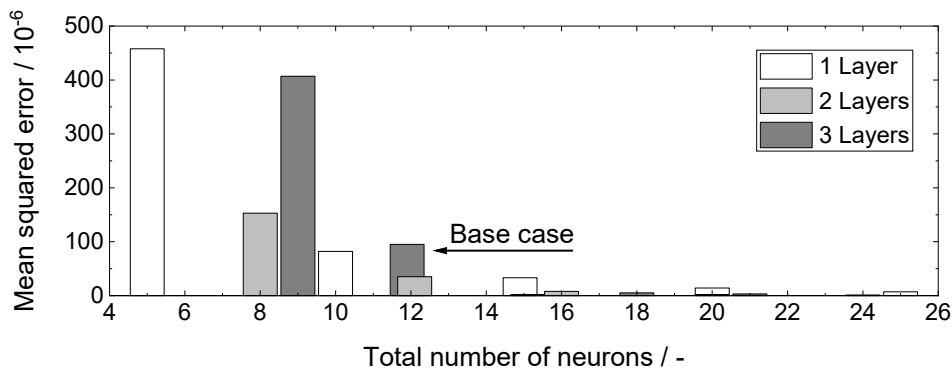


**Figure 4.10.:** MSE averaged over all test set data points for ANNs with a different total number of neurons and a different number of hidden layers. For training, the Levenberg Marquardt training function, a hyperbolic tangent transfer function, a training ratio of 70 %, a validation ratio of 15 %, and a test ratio of 15 % was used.

## Reactor Model

For the reductive synthesis of DMM from methanol,  $H_2$  and  $CO_2$ , there is no reaction kinetic model available in the open literature. As we want to find the maximum expected process performance, we consider reaction equilibrium throughout this study. Although the catalytic reaction (R23) takes place only in the liquid phase, the VLE within the reactor influences reaction equilibrium and vice versa. Therefore, the conversion of methanol is dependent on the ratio of  $H_2$  to  $CO_2$  in the gaseous reactor feed, as well as on the ratio of gas to liquid within the reactor. However, a corresponding sensitivity analysis (Appendix Fig. C.1 and C.2) has shown that their influence on reactor performance is low. As mainly the reactor performance determines how much gas need to be supplied back to the system, the two ratios do not affect process design and exergy demand significantly. Therefore, a fixed gas composition corresponding reaction stoichiometry and a molar ratio of 1:1 for the

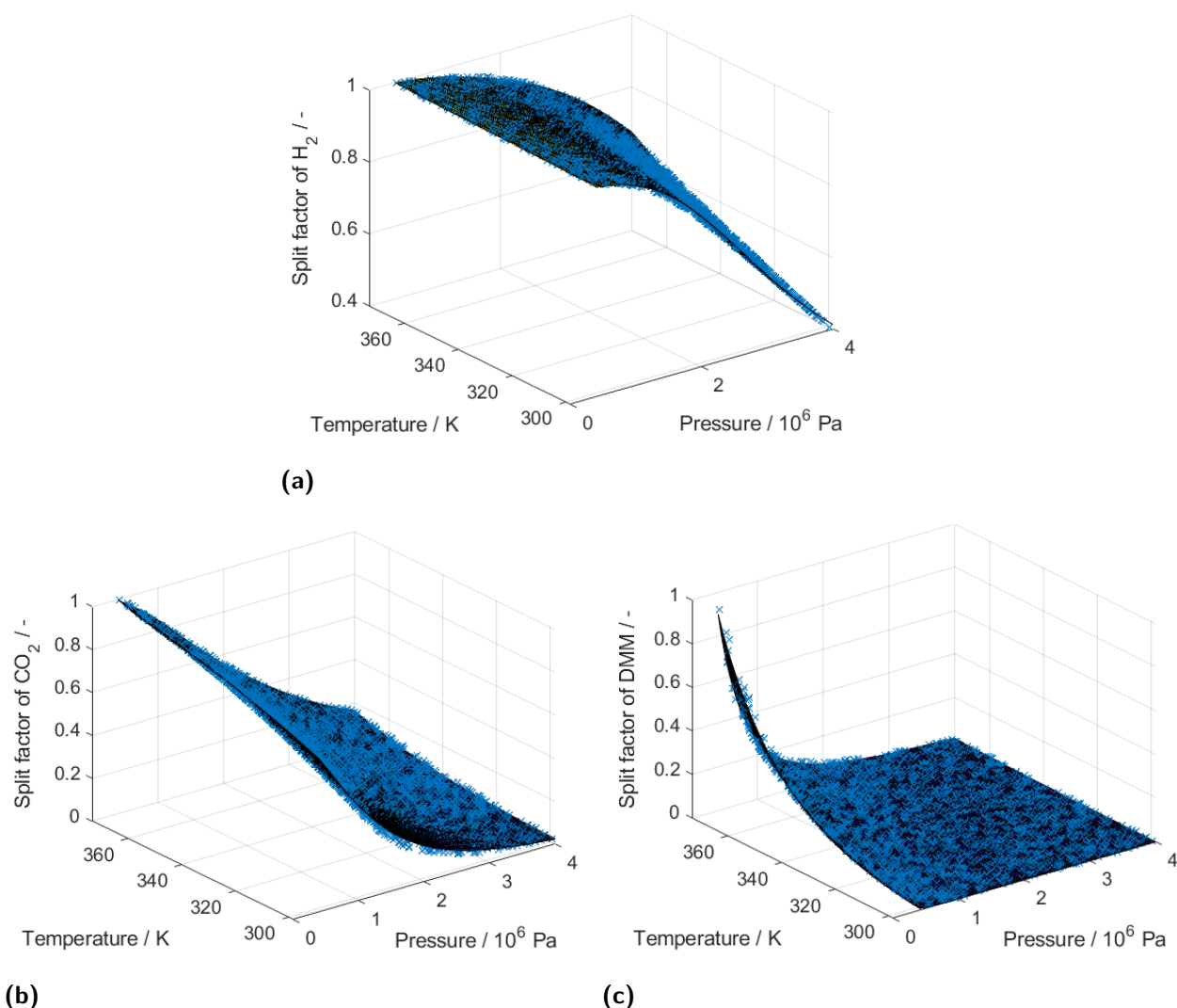


**Figure 4.11.:** ANN prediction (surface) and PCP-SAFT training data ( $\times$ ) for the split factor of  $H_2$  (Fig. 4.11a),  $CO_2$  (Fig. 4.11b), and DMM (Fig. 4.11c) within the flash unit F1 as a function of temperature and pressure. An ANN with 3 layers and 4 neurons each with the settings summarized in the description of Fig. 4.10 is used for optimization. The plotted split factors are shown for the globally optimal molar reactor outlet composition ( $H_2$ : 0.018,  $CO_2$ : 0.091, DMM: 0.070, Methanol: 0.694, Water: 0.127).

amount of gas within the reactor is used for the optimization. For industrial application, the catalyst is assumed to be immobilized and therefore not withdrawn with the liquid reactor effluent containing only DMM, water, and unreacted methanol,  $H_2$ , and  $CO_2$ . With these assumptions, only the reactor pressure needs to be considered as input variable for the data-driven reactor model. The output variable has been chosen to be methanol conversion at simultaneous phase and reaction equilibrium to yield linear equations for the reactor process model. As unreacted  $H_2$  and  $CO_2$  remain in the liquid phase at reaction equilibrium, also the  $K$ -values for these two components need to be considered as output variables.

For data generation, we use the same in-house Java implementation of the PCP-SAFT EOS as for the flash model. As it does not allow the simultaneous consideration of chemical

reactions to this date and convergence is sensitive to initial values in the first place, an iterative procedure for calculating the combined phase and chemical equilibrium is applied in Matlab. First, the phase equilibrium via the PCP-SAFT EOS determines how much gas dissolves in methanol. The resulting liquid phase composition  $\tilde{x}_{\text{Prod},i}$  (before reaction) is then used to solve the definition of the equilibrium constant

$$K(T) = \prod_{i \in C} \left( \frac{1}{\tilde{x}_{\text{Prod},i}} \frac{\tilde{f}_i}{f_i^0} x_{\text{Prod},i} \right)^{\nu_i} = \exp \left( \frac{-\Delta G_{\text{R}}^0}{RT} \right) \quad (4.3)$$

for mole fractions  $x_{\text{Prod},i}$  (after reaction). The fugacities  $\tilde{f}_i$  of each component  $i$  can be taken from the in-house Java implementation of the PCP-SAFT EOS, in which the standard state fugacity  $f_i^0$  corresponds to standard pressure. Parameter  $\nu_i$  is the stoichiometric coefficient of component  $i$  according to Reaction (R23). The standard Gibbs energy is calculated by

$$\Delta G_{\text{R}}^0 = \sum_{i \in C} \nu_i \mu_i^0 = \sum_{i \in C} \nu_i \left( \int_{T_0}^T c_{\text{p},i}^{\text{iG}} dT' - T \int_{T_0}^T \frac{c_{\text{p},i}^{\text{iG}}}{T'} dT' + \Delta_{\text{f}} H_i^{\text{iG}}(T^0) - T \Delta_{\text{f}} S_i^{\text{iG}}(T^0, p^0) \right). \quad (4.4)$$

The ideal gas heat capacities  $c_{\text{p},i}^{\text{iG}}$ , the standard enthalpies of formation  $\Delta_{\text{f}} H_i^{\text{iG}}$  and the standard molar entropies  $\Delta_{\text{f}} S_i^{\text{iG}}$  are taken from the DIPPR 801 Database. The iterations eventually terminate once a threshold for the reaction extent has been reached.

The iterative procedure makes the application of the mechanistic reactor model computationally much more demanding compared to the mechanistic flash model resulting in long computation times per data point. Therefore, data-driven modeling using ANNs is not suitable because of the high number of required samples. Instead, given the small number of attainable samples, Gaussian processes [181] (GPs) represent a suitable alternative modeling approach. As we consider only a single input for the reactor model and for each of the three output variables its own GP, only a small set of samples is required to accurately model the behavior within the reactor. Similarly to the data-driven flash model, we performed a sensitivity analysis to determine the minimum complexity of the GP models to improve optimization tractability. As the GP model complexity scales with the number of data points, the most suitable trade-off between model accuracy and computational performance could be achieved with 6 data points (cf. Section 4.2.5). The corresponding MSEs are summarized in Tab. 4.5. The prediction capabilities of the final GP models are demonstrated in Fig. 4.12a-4.12c for the equilibrium methanol conversion ( $C_{\text{MeOH}}$ ) and the  $K$ -values of  $\text{H}_2$  and  $\text{CO}_2$ . The large deviation between the simulation data calculated with the PCP-SAFT and the PC-SAFT EOS for these variables (Fig. 4.12) highlights the importance of the correct choice of the thermodynamic model for the reactor model.

### 4.2.3. Process Modeling

For the remaining process units, the consideration of a simpler thermodynamic model is justified as either only moderate operating pressures are considered or  $\text{H}_2$  and  $\text{CO}_2$  have already been separated. Furthermore, the remaining process units provide only approximate estimates for the exergy demand for compression and product purification, for which simple models are sufficient as they are expected to make up only a smaller share of the overall exergy demand [142].

**Table 4.5.:** MSE for the GP models for  $C_{\text{MeOH}}$ ,  $K_{\text{H}_2}$ , and  $K_{\text{CO}_2}$  for a different number of considered training data points and the matern kernel with parameter 3/2 as the covariance function. The MSE corresponds to the test set only. The base case model is highlighted in gray.

	GP data points				
	4	6	8	10	12
$\text{MSE}_{C_{\text{MeOH}}} / 10^{-10}$	140	6.5	1.1	0.5	0.6
$\text{MSE}_{K_{\text{H}_2}} / -$	0.707	0.039	0.029	0.019	0.010
$\text{MSE}_{K_{\text{CO}_2}} / 10^{-4}$	50	2.95	1.89	1.13	0.62

### Distillation Column Sequencing by Superstructure Optimization

As the optimal distillation column sequence is generally dependent on the upstream process, a fixed sequence could lead to a suboptimal process design and operating conditions. Therefore, we consider superstructure optimization, which calculates the optimal distillation column sequence based on the optimal operating conditions of the upstream process. We consider only distillation columns D1-D3 for superstructure optimization as  $\text{CO}_2$  should be separated first to minimize the need for low-temperature distillation (cf. Fig. 4.9). This results in only two possible sequences, which we could have simply considered as two separate nonlinear programs (NLP). We nevertheless formulate the separation process as a superstructure and demonstrate that solving the MINLP is cheaper than enumerating the two options as NLPs.

In this study, we use the state-equipment network [182] (SEN) superstructure representation, in which we assign all separation tasks that have a cut between the same components to the same distillation column (separation cut SEN) [183, 184]. In contrast to the state-task network, this representation requires the smallest number of distillation column models, while keeping model equations comparatively simple.

For the separation cut SEN, the connection between columns can be fully described by two types of binary variables. Variable  $X_d^F$  indicates whether column  $d$  is connected to the global feed (i.e., the bottom product of column D0) to the superstructure. Variable  $X_{l,j}^s$  indicates whether the output stream  $s$  (distillate or bottom) of column  $l$  is connected to column  $j$ . In this work, the following equations are used to describe the connection between the distillation columns:

$$X_{2,3}^B + X_{3,2}^D = 1 \quad (4.5)$$

$$X_3^F = X_{3,2}^D \quad (4.6)$$

$$X_2^F = X_{2,3}^B. \quad (4.7)$$

Note that the distillate stream of column 1 is always fed to column 2 and the distillate stream from column 2 is always fed to column 1, regardless of the selected sequence (Fig. 4.9). To determine the feed flow rates to a column, all flow rates that can be fed to a

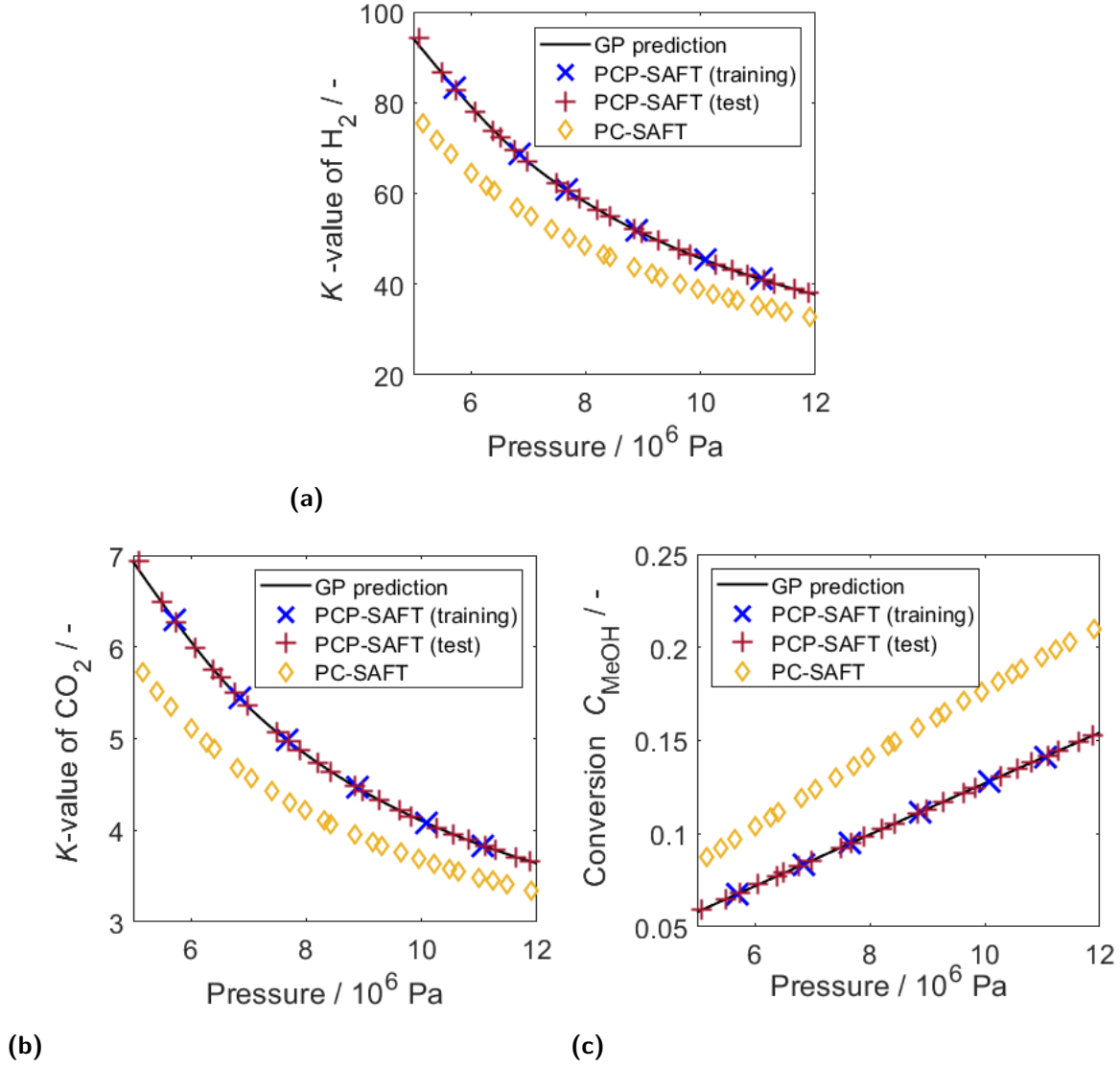


**Figure 4.12.:** GP prediction (black line) and PCP-SAFT training data ( $\times$ ) for the  $K$ -values of  $H_2$  (Fig. 4.12a) and  $CO_2$  (Fig. 4.12b), and methanol equilibrium conversion  $C_{MeOH}$  (Fig. 4.12c) for the reactor unit as a function of pressure. The red plus markers (+) represent the PCP-SAFT test data used to calculate the MSE reported in Tab. 4.5 to demonstrate the validity of the GP model between training samples. The orange diamonds ( $\diamond$ ) correspond to the PC-SAFT EOS and demonstrate the deviation between PC-SAFT and PCP-SAFT EOS for the underlying system.

column are multiplied by the corresponding binary variable to ensure that only the flow rates of the active connections are used (cf. *Direct MINLP* problem formulation in Burre et al. [185], Section 5.2.5). For example, the feed of component  $i$  to column 2 is given by

$$F_{2,i} = D_{1,i} + X_2^F F_i + X_{3,2}^D D_{3,i}, \quad (4.8)$$

where  $F_i$  is the global feed of component  $i$  and  $D_{d,i}$  is the distillate flow rate of component  $i$  in column  $d$ .

For the distillation column models, the Underwood equations [186] are used. In order to apply the Underwood method to the azeotropic mixture considered in this work, the coordinate transformation presented by Liu et al. [187] is used. In their method, the azeotropic system is divided into subsystems which behave approximately like a non-azeotropic mixture. Within this transformation, the azeotropes are treated as pseudo-components. In this work, the subsystems are modeled as ideal mixtures and the vapor pressures of the pure components are determined using the extended Antoine equation. To determine the vapor pressures of the azeotropic pseudo-components, the Antoine parameters are fitted using data from flash calculations in Aspen Plus.

### Miscellaneous Models

The remaining units are modeled using simple process models to get an estimate on exergy demand while maintaining optimization tractability. For gas compression, we use a one-stage compressor model to keep the amount of optimization variables small and consider an isentropic and mechanical efficiency of 80 % and 90 %, respectively. This provides a rather conservative estimate, as the model overestimates the actual exergy demand slightly. In Section 4.2.5, we evaluate whether this simplification is reasonable. For the pumps, an isentropic efficiency of 90 % is considered. For the heat exchanger, we use the logarithmic mean temperature difference to approximate the thermodynamic mean temperature, which we use to compute exergy demand and excess. Heat integration is only approximated in the objective function by the simple summation of exergy demand and excess within the entire system. All parameters for the pure component property models (extended Antoine for vapor pressure, DIPPR-106 for heat of vaporization, DIPPR-107 for heat capacity) are taken from the Aspen Plus DB-PURE37 data base and for the Henry’s constant correlation for  $H_2$  and  $CO_2$  from the APV110 HENRY-AP and BINARY data bases.

#### 4.2.4. Problem Formulation and Objective Function

Most process models introduced in Section 4.2.2 and 4.2.3 are nonlinear. In addition to the nonconvex terms of the pure component property models, the hyperbolic tangent activation function applied in the ANN model as well as the covariance function of the GP model introduce nonconvexities into the process model. Also the Underwood equations for modeling the distillation columns within the superstructure and the corresponding discrete decisions therein are responsible for further nonconvex terms. Irrespective of the considered process models, the structure of the process itself with its recycle streams makes the resulting optimization problem nonconvex. To find the most promising process structure and operating conditions for reductive DMM production despite its nonconvex nature, global optimization is desirable.

The application of global optimization to large optimization problems is however challenging. Particularly, problems incorporating data-driven submodels usually exhibit a large number of optimization variables, which often makes the optimization problem not tractable for state-of-the-art deterministic global solvers. To still solve such problems to global optimality, our open-source deterministic global solver MAiNGO [164] effectively exploits the smaller problem size of the so-called *reduced-space* problem formulation [188], in which the only optimization variables are the degrees of freedom and tear variables. By additionally considering tailored relaxations for the nonconvex terms of the process

model, processes incorporating hybrid models could already be solved efficiently to global optimality [176, 177].

The overall process model is implemented in the programming language C++, in which all intermediate process variables are calculated as functions of the degrees of freedom, tear variables, and a few additional optimization variables (to avoid model equations yielding weak relaxations[189]). The degrees of freedom for the DMM production process depicted in Fig. 4.9 are the reactor pressure ( $P_{R1}$ ), the temperature ( $T_{F1}$ ) and pressure ( $P_{F1}$ ) of the flash unit for gas recycling, the binary decision variable for the choice of the optimal distillation sequence ( $X_{2,3}^B$ ), as well as the recoveries of the light and heavy key component ( $\gamma_{LK,d}$  and  $\gamma_{HK,d}$ , respectively) of distillation columns D1 - D3 (Tab. 4.7). As column D0 is not part of the superstructure and separates pure CO<sub>2</sub> from the remaining liquid mixture,  $\gamma_{LK,0}$  and  $\gamma_{HK,0}$  are fixed to 1 and 0, respectively. Tear variables are introduced for each recycle stream and for process units that otherwise would need to be modeled by implicit functions [188]. The elimination of optimization variables using the model equality constraints (i.e., the reduced-space formulation in MAiNGO) results in a dramatic reduction in problem size. The resulting process model contains only 41 optimization variables, one of which is binary. It has 55 inequality and 31 equality constraints (Tab. 4.6). To facilitate the modeling procedure and benefit from tailored relaxations, we use the model libraries implemented in MAiNGO (e.g., enthalpy of vaporization, ideal gas enthalpy [190]) and MeLON [176, 177]. The model library MeLON provides several machine learning models including ANNs and GPs, which are accessed by MAiNGO via a build-in interface. Corresponding model parameters from the training in Matlab are provided by an automatically generated csv- (ANN) or json-file (GP). Relaxations of all functions and their subgradients are automatically obtained from the MC++ library [191].

The objective function of the optimization problem is the minimization of the net exergy demand

$$\begin{aligned} \dot{E}_{\text{total}} = \dot{n}_{\text{H}_2} \hat{e}_{\text{H}_2} + \dot{n}_{\text{MeOH}} \hat{e}_{\text{MeOH}} + \sum_{c \in C} W_c + \sum_{p \in P} W_p + \sum_{h \in H} \dot{E}_{Q_{\text{in},h}} + \sum_{d \in D} \dot{E}_{Q_{\text{reb},d}} \\ - \sum_{h \in H} \dot{E}_{Q_{\text{out},h}} - \sum_{d \in D} \dot{E}_{Q_{\text{cond},d}} - \dot{E}_{Q_{R1,\text{out}}}, \end{aligned} \quad (4.9)$$

where  $\dot{n}_{\text{H}_2}$  and  $\dot{n}_{\text{MeOH}}$  is the net consumption of raw materials H<sub>2</sub> and methanol, respectively,  $\hat{e}_{\text{H}_2}$  and  $\hat{e}_{\text{MeOH}}$  is their molar exergy,  $W_c$  is the power input of compressor  $c \in C$ ,  $W_p$  is the power input of pump  $p \in P$ ,  $\dot{E}_{Q_{\text{in},h}}$  and  $\dot{E}_{Q_{\text{out},h}}$  is the exergy flow of the heat demand and excess for heat exchanger  $h \in H$  and flash F1,  $\dot{E}_{Q_{\text{reb},d}}$  and  $\dot{E}_{Q_{\text{cond},d}}$  is the exergy flow of reboiler and condenser duties of distillation column  $d \in D$ , and  $\dot{E}_{Q_{R1,\text{out}}}$  is the exergy flow of excess heat from the reaction. The ambient temperature is assumed to be 25 °C to calculate the exergy flows.

#### 4.2.5. Results and Discussion

The deterministic global solver MAiNGO [164] v0.5.0.2 employs a spatial branch-and-bound algorithm with several bound tightening techniques and uses the multivariate McCormick method [192, 193] implemented in MC++ [191] to obtain relaxations. The optimization is carried out with the parallel version of MAiNGO on an Intel Xeon Platinum 8160 processor using 40 cores. Both the relative and absolute optimality tolerance is set



to  $10^{-3}$ . To improve convergence, we use the following non-default settings in MAiNGO: First, we utilize a combination of an adaptation of the *Kelley's* algorithm [194] and a  $n$ -simplex algorithm to linearize relaxations instead of utilizing a midpoint linearization. Second, we selectively consider auxiliary variables (AVs) for repeated nonlinear terms to improve the tightness of the relaxations [189]. With this, the base case optimization problem considers *Kelley's* and  $n$ -simplex relaxation linearization, 84 AVs, 6 GP data points, and 3 layers and 4 neurons each layer. All characteristics of the optimization problem are summarized in Tab. 4.6.

The consideration of a special linearization strategy for relaxations reduces the number of nodes required for convergence significantly but in turn increases solution time per node. The consideration of AVs is key for convergence in the first place (Tab. 4.6 and Fig. 4.13). As MAiNGO treats the process model in the reduced-space as one function being dependent only on the degrees of freedom, tear variables, and a few additional optimization variables (cf. Section 4.2.4), the model relaxation is constructed from a sequence of mathematical operations (cf. McCormick method [192]), which results from the procedural concatenation of explicit model equations implemented in the C++ code. Within this sequence of mathematical operations some individual terms may appear repeatedly, which could weaken model relaxations [193]. To prevent this and still yield tight relaxations for the optimization in the reduced-space, we add certain selected AVs to benefit from both the reduced problem size and potentially tight relaxations from the auxiliary variable method [195, 196] (AVM) typically employed by most state-of-the-art deterministic global solvers [197, 198].

**Table 4.6.:** Problem size and numerical results for different objective functions, solver settings, and model detail. For all considered cases, the global optimal solution was found in the root node.

Objective function Solver settings / model detail	$\min \dot{E}_{\text{total}}$					$\max \eta_{\text{Ex}}$
	Base case	Midpoint linearization	No AVs	GP w 8 data points	ANN w 5 neurons	Base case
Number of						
Continuous variables	40	40	40	40	40	40
Discrete variables	1	1	1	1	1	1
Equality constraints	31	31	31	31	31	31
Inequality constraints	55	55	55	55	55	55
B&B nodes	2715	225887	456000 <sup>a</sup>	45000 <sup>a</sup>	37200 <sup>a</sup>	38500 <sup>a</sup>
Optimal objective value / MJ kg <sup>-1</sup>	27.4	27.4	27.4 <sup>a</sup>	27.4 <sup>a</sup>	27.5 <sup>a</sup>	91.9 % <sup>a</sup>
Lower bound of root node / MJ kg <sup>-1</sup>	-16	$-2.2 \times 10^9$	$-3.5 \times 10^{11}$	-16	-61.3	$-4.1 \times 10^8$
CPU time per B&B node / s	7.7	0.4	0.6	6.4	7.7	7.5
Total CPU time / h	5.8	27.6	80 <sup>a</sup>	80 <sup>a</sup>	80 <sup>a</sup>	80 <sup>a</sup>
Rel. optimality gap / %	0	0	$9.0 \times 10^7$	0.8	0.5	1.6

<sup>a</sup> Optimization has reached the CPU limit of 80 CPUh.

The base case optimization problem is solved to global optimality in 5.8 CPUh or 2715 nodes (Tab. 4.6 and Fig. 4.13). The global solution is 2.08 MJ mol<sup>-1</sup> or 27.4 MJ kg<sup>-1</sup> net exergy demand per produced DMM, which corresponds to an exergy efficiency of 91.9 %. At the optimal operating conditions, a maximum reactor pressure of 120 bar is applied (Tab. 4.7) resulting in an equilibrium methanol conversion of 15.4 %. As the pressure variable is at its upper bound, an even higher pressure could result in an even better performance but also requires a more complex reactor design. With the one-stage compressor model, compression accounts for only 4 % of the total exergy demand, which

would decrease even further if a multi-stage compressor model would be considered. As the optimal operating pressure is already at its upper bound, a multi-stage compressor model would not influence the optimal operating conditions. For a detailed process design at a later stage of development, however, a multi-stage compressor model should be considered.

On the modeling level, the choice of the objective function also has a significant influence on the optimization. Instead of minimizing net exergy demand (cf. Equation (4.9)), maximizing exergy efficiency

$$\eta_{\text{Ex}} = \frac{\dot{n}_{\text{DMM}} \hat{e}_{\text{DMM}} + \sum_{h \in H} \dot{E}_{Q_{\text{out},h}} + \sum_{d \in D} \dot{E}_{Q_{\text{cond},d}} + \dot{E}_{Q_{\text{R1,out}}}}{\dot{n}_{\text{H}_2} \hat{e}_{\text{H}_2} + \dot{n}_{\text{MeOH}} \hat{e}_{\text{MeOH}} + \sum_{c \in C} W_c + \sum_{p \in P} W_p + \sum_{h \in H} \dot{E}_{Q_{\text{in},h}} + \sum_{d \in D} \dot{E}_{Q_{\text{reb},d}}}, \quad (4.10)$$

the optimization does not converge within 80 CPUh (optimality gap of 1.6 %, Tab. 4.6). Also the complexity of each process model must be kept moderate to yield tight relaxations. Considering 8 instead of 6 data points for the Gaussian process reactor model, an optimality gap of 0.8 % remains. Considering 5 instead of 4 neurons for each of the 3 layers for the flash model, an optimality gap of 0.5 % remains (Tab. 4.6). If the two individual NLPs are solved, the total solution time (30.1 CPUh) exceeds that of the base case MINLP problem incorporating the superstructure model for distillation column sequencing significantly. This shows that a superstructure representation (SEN, cf. Section 4.2.3) together with a problem formulation (Direct MINLP [185] in a reduced-space, Section 5.2.5) that both do not introduce many additional variables (here, only the binary variable  $X_{2,3}^{\text{B}}$ ) are promising for deterministic global optimization.

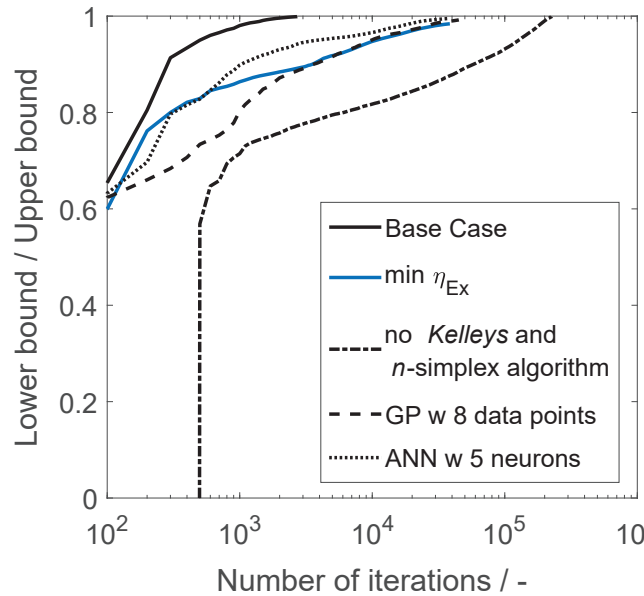


**Figure 4.13.:** Convergence indicated by the ratio of the lower bound to the upper bound during the course of optimization for all considered cases. As the lower bound for the case without the consideration of AVs is low and does not increase within the course of optimization, it is not displayed in this diagram.

The flash unit operates at 4 bar and 42.0 °C to recycle 99.6 %  $\text{H}_2$  and 77.6 %  $\text{CO}_2$ . The rest of the  $\text{CO}_2$  is separated by the low-temperature distillation column D0, before DMM can be purified in the subsequent distillation column sequence. The optimal sequence is

**Table 4.7.:** Degrees of freedom for the reductive DMM production process (Fig. 4.9), their interval bounds and optimal values.

Degree of freedom	Description	Bounds	Optimal value
$P_{R1}$ / bar	Pressure of reactor R1	[50, 120]	120
$T_{F1}$ / °C	Temperature of flash F1	[25, 90]	42.0
$P_{F1}$ / bar	Pressure of flash F1	[4, 10]	4
$X_{2,3}^B$ / -	Decision variable for connecting column D2 with D3 via the bottom product	{0, 1}	1
$\gamma_{LK,1}$ / -	Recovery of the LK component of column D1	[0, 1]	1
$\gamma_{HK,1}$ / -	Recovery of the HK component of column D1	[0, 1]	0
$\gamma_{LK,2}$ / -	Recovery of the LK component of column D2	[0, 1]	1
$\gamma_{HK,2}$ / -	Recovery of the HK component of column D2	[0, 1]	0
$\gamma_{LK,3}$ / -	Recovery of the LK component of column D3	[0, 1]	1
$\gamma_{HK,3}$ / -	Recovery of the HK component of column D3	[0, 1]	0.05

obtained for  $X_{2,3}^B = 1$ , where column D2 first separates the azeotrope between methanol and DMM from the bottom product of column D0. Then, DMM is separated from methanol in the pressure swing distillation comprising column D2 and D3 leading to a total share of exergy demand for separation of about 9.6 % of that for the entire process. This is in good agreement with values from literature (7 % [19] and 8 % [142], both decoupled from the upstream methanol process). However, the exergy demand for separation reported by Burre et al. [142] (cf. Section 4.1) corresponds to a reactor pressure of 80 bar, for which a methanol conversion of 15.7 % was estimated using the NRTL thermodynamic model—the most suitable one to this date. Our calculations with the more accurate PCP-SAFT EOS show that this conversion can only be reached at even higher pressures.

The results show that the correct choice of the thermodynamic model for the reactor is crucial for process design and evaluation. To evaluate the accuracy of the simple Underwood model for distillation, we compare corresponding results with those obtained from a tray-to-tray model and the NRTL thermodynamic model (accurate for moderate pressures) in Aspen Plus. The results show that the total exergy demand is overestimated by the Underwood model only slightly by about 10 % (Tab. 4.8). The estimates for the individual distillation columns are, however, partly inaccurate for the Underwood model for this non-ideal system. Although these inaccuracies do not have a significant influence on the overall performance of the process, it certainly has for a more detailed process design at a later stage of development. Therefore, more research should be dedicated to the development of more accurate distillation models suitable for global flowsheet optimization.

#### 4.2.6. Conclusion

The direct reduction of  $\text{CO}_2$  belongs to the most hydrogen-efficient pathways for dimethoxymethane (DMM) production given its favorable reaction stoichiometry. Its need for a high reactor pressure makes the application of thermodynamic models available in the open literature however inaccurate, which has limited process design to the development of simple process models so far.

To enable reliable process design and ultimately advance efficient DMM production,

**Table 4.8.:** Comparison of the exergy demand for distillation column D0-D3 calculated with the Underwood model and the tray-to-tray model using the NRTL thermodynamic model in Aspen Plus (RadFrac).

Distillation column	Exergy demand / MJ kg <sup>-1</sup>	
	Underwood (this study)	Tray-to-tray (Aspen Plus)
D0	0.23	0.24
D1	0.65	0.11
D2	0.23	0.25
D3	1.14	1.41
<b>Total</b>	<b>2.25</b>	<b>2.01</b>

we measured liquid equilibrium densities and fitted binary parameters for the PCP-SAFT equation of state (EOS) for the components involved in the reaction. Whereas this thermodynamic model was found to predict the vapor-liquid equilibrium of the system properly, it constitutes a major challenge for deterministic global optimization for process design. To benefit from both the high accuracy of the thermodynamic model and the potential of deterministic optimization, we developed data-driven thermodynamic models for process units that potentially operate at high pressures and contain significant amounts of H<sub>2</sub> and CO<sub>2</sub>. The equilibrium-based reactor model is therefore approximated by Gaussian processes, while the flash unit for gas recycling is approximated by an artificial neural network. In combination with a superstructure model for distillation column sequencing and several recycling streams within the process, the resulting mathematical program is nonconvex. To still find the most favorable process design and operating conditions, we used our open-source deterministic global solver MAiNGO for optimization.

The capability of MAiNGO to exploit the small problem size of the so-called *reduced-space* problem formulation makes the optimization converge to the global optimum in 5.8 CPUh. To achieve this performance, several measures had to be taken: On the algorithm level, a combination of *Kelley's* and a *n*-simplex algorithm for linearize relaxations, as well as a hybrid of the McCormick and the auxiliary variable method had to be used. On the modeling level, a suitable trade-off between model complexity (regarding the data-driven models) and computational performance for global optimization had to be found. The resulting process performance for reductive DMM production from methanol, H<sub>2</sub>, and CO<sub>2</sub> was found to be 91.9% at an optimal reactor pressure of 120 bar. As only simple Underwood models were used for the distillation columns within the superstructure, which have been found to succumb significant inaccuracies for the underlying system, future work should focus on the development of distillation models that are suitable for global optimization. To increase methanol conversion and decrease the exergy demand for separation, co-solvents could be considered to either enhance gas solubility or enable in-situ extraction of DMM from the reaction phase. In this regard, data on the phase equilibrium of reaction mixtures including different co-solvents and on their suitability for the ruthenium-catalyzed reaction would be beneficial. This data could be used to fit PCP-SAFT EOS parameters for a variety of multi-phase systems. Such parameters would then enable an optimization-based screening of co-solvents, which potentially increase reaction equilibrium and decrease energy demand for DMM purification.

### 4.3. Process Chains via Reductive DMM Production

As heat integration is key for Power-to-X processes, we can not simply multiply efficiencies to obtain the overall efficiency for DMM and OME<sub>3-5</sub> production from H<sub>2</sub> and CO<sub>2</sub>. Additionally, OME<sub>3-5</sub> production via reductive DMM synthesis has high potential to benefit even further from more resource-efficient pathways than the established ones (cf. Section 3.2). However, corresponding process concepts have not been developed so far. For a conclusive evaluation of the reductive reaction pathway for DMM production, we therefore develop simple process concepts for the OME<sub>3-5</sub> process chain and analyze the performance of the heat-integrated process chain for both DMM (Section 4.3.1) and OME<sub>3-5</sub> production (Section 4.3.2) starting from renewable H<sub>2</sub> and CO<sub>2</sub>.

#### 4.3.1. DMM Production from Renewable H<sub>2</sub> and CO<sub>2</sub>

For the process chain for reductive DMM production from H<sub>2</sub> and CO<sub>2</sub>, the same methanol process as in the process chain for established DMM production (cf. Section 3.1) is considered. Assuming a pinch-based heat integration between the two process steps, an overall process exergy efficiency of 82 % is achieved (Fig. 4.14) following Equation (3.1).

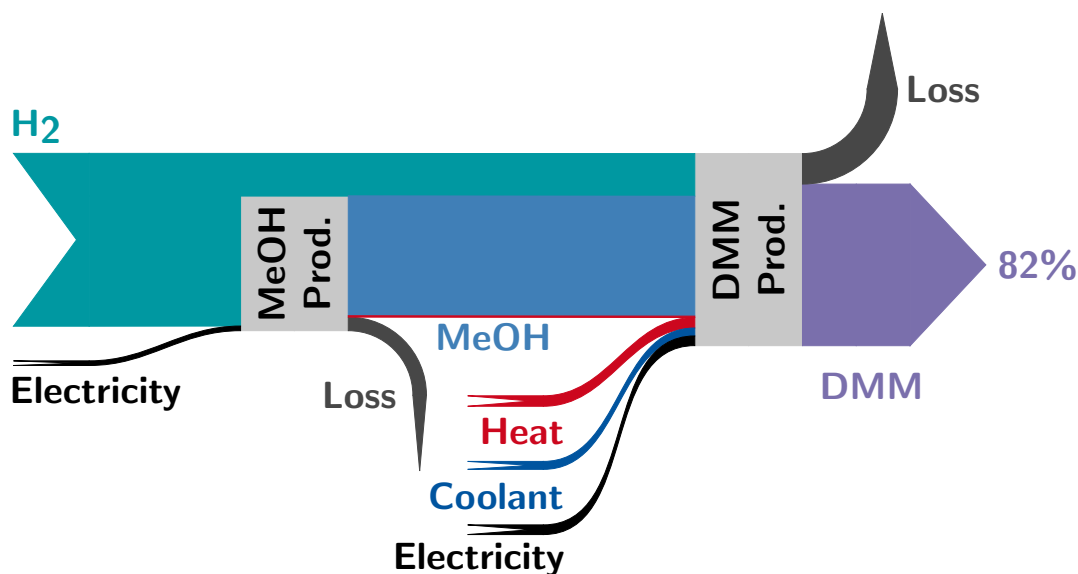


**Figure 4.14.:** Exergy flow diagram of the value chain for DMM production from H<sub>2</sub> and CO<sub>2</sub> via the reductive reaction pathway. For clarity, only the most relevant heat streams resulting from heat integration between process steps are displayed. An overall process exergy efficiency of 82 % is reached. Corresponding material and energy balances are summarized in Appendix Tab. D.1.

Given the small deviation between the total exergy demand for DMM purification derived by simple Underwood equations and tray-to-tray models (Section 4.2.5, Tab. 4.8), the process evaluation in this section corresponds to Level 3 considerations according to the hierarchical process development and evaluation methodology presented in Section 4.1.1. Thus, the process efficiency can be directly compared with the one of the established process chain reported in Section 3.1.3 (74 %) and is 8 percentage points higher. This increase in

process exergy efficiency can be mainly attributed to the lower molar  $\text{H}_2$  consumption for the reductive reaction pathway (cf. Section 4.1.2.1). Compared to the Level 2 process efficiency of the same reaction pathway at equilibrium conditions (89 %, cf. Section 4.1.2.4), the Level 3 evaluation within this section results in a significantly lower efficiency. This has mainly two reasons: First, as reported in Section 4.2.5, the conversion of methanol at equilibrium conditions was significantly overestimated by the NRTL thermodynamic model used in the approximate process calculations of Section 4.1 (15.7 % at 80 bar with NRTL vs. 15.4 % at 120 bar with PCP-SAFT EOS). This leads to an underestimation of the electricity demand required for the compression of the gaseous reactants to achieve a comparable methanol conversion. Second, the process design on Level 2 does not consider the exergy demand for the low-temperature distillation of  $\text{CO}_2$  from the reactor effluent, which is about  $0.55 \text{ MJ kg}^{-1}$  of produced DMM. Moreover, the exergy efficiency of the individual DMM process step within the process chain demonstrated in Fig. 4.14 is only 89.6 % and thus about 2 percentage points lower compared to that resulting from the global optimization in Section 4.2 (91.9 %). This decrease is caused by the more realistic but still optimistic heat integration by pinch analysis compared to the simple summation of exergy flows used for global optimization. All in all, the direct reduction of  $\text{CO}_2$  yields significant improvements for DMM production from renewable  $\text{H}_2$  and  $\text{CO}_2$  compared to the established process concept. For further improvements, a more advanced reactor concept (e.g., by in-situ product extraction) as well as an alternative to the low-temperature  $\text{CO}_2$  separation are required.

### 4.3.2. OME<sub>3-5</sub> Production from Renewable $\text{H}_2$ and $\text{CO}_2$

The main weakness of the process chain for OME<sub>3-5</sub> production from  $\text{H}_2$  and  $\text{CO}_2$  using established process concepts is the energy-intensive trioxane production process step and should be avoided for future industrial OME<sub>3-5</sub> production (cf. Section 3.2). In this regard, the currently much discussed direct synthesis of OME<sub>3-5</sub> from aqueous FA and methanol is a promising process alternative circumventing both DMM and trioxane production [18, 199]. However, the presence of water inhibits OME<sub>3-5</sub> formation and complicates product purification [200]. A reaction pathway that avoids both trioxane production and the presence of water in the OME<sub>3-5</sub> formation step is its synthesis from DMM and gaseous FA [28, 29]. Considering reductive DMM production and FA production by methanol dehydrogenation, a corresponding process chain would further benefit from two highly resource-efficient intermediate reaction pathways if  $\text{H}_2$  recycling is considered. Therefore, we have developed a process concept that exploits these advantages. As both the methanol dehydrogenation to FA and the OME<sub>3-5</sub> formation from DMM and gaseous FA are still on a very early stage of development, the resulting estimate for process efficiency can not be compared directly with that of the established process concept reported in Section 3.2.4.2, which models are more detailed.

Similarly to the process chain for reductive DMM production, the same methanol production process as in Section 3.2.4.2 is considered. For FA production via methanol dehydrogenation, we have screened several experimental results from the open literature and found the reaction catalyzed by a Cu-Zn-Se catalyst at a temperature of  $650^\circ\text{C}$  to be promising [36]. Therein, a FA yield of 62.1 % for an equimolar methanol- $\text{H}_2$  atmosphere was reached. Small amounts of carbon monoxide and methane were found as side products. Using these data, we have developed a simple process concept incorporating a reactor as

well as separators with sharp split specifications (approximating membranes potentially promising for  $\text{H}_2$  and FA purification [201, 202]) to obtain material balances and an estimate for the heat demand required for methanol dehydrogenation. For the  $\text{OME}_{3-5}$  process step, we assume the same heat demand as for  $\text{OME}_{3-5}$  production from DMM and trioxane, as a comparable reactor effluent with a similar product distribution according to the Schulz-Flory distribution [96] can be expected.

With this process concept and underlying assumptions, we calculated an estimate for the overall process efficiency of 77 % for  $\text{OME}_{3-5}$  production from  $\text{H}_2$  and  $\text{CO}_2$  via reductive DMM production. This corresponds to an improvement of 20 percentage points compared to the process chain via trioxane production. This improvement is mainly caused by two aspects: First, the circumvention of the trioxane process reduces net heat demand in terms of exergy by 44 %. Second, net  $\text{H}_2$  consumption—being responsible for the main energy demand of Power-to-X processes—is reduced by 26 % (cf. Appendix Tab. D.2). This reduction is realized by the more resource-efficient production of DMM via the direct reduction of  $\text{CO}_2$  as well as the recycling of  $\text{H}_2$  released during methanol dehydrogenation. Although the comparison between the two process chains must be seen with caution due to the simplified consideration of the FA and the  $\text{OME}_{3-5}$  process step, it demonstrates the great potential of the more resource-efficient intermediate process steps for DMM and FA production and should be therefore refined in future studies to yield sustainable  $\text{OME}_{3-5}$  production.

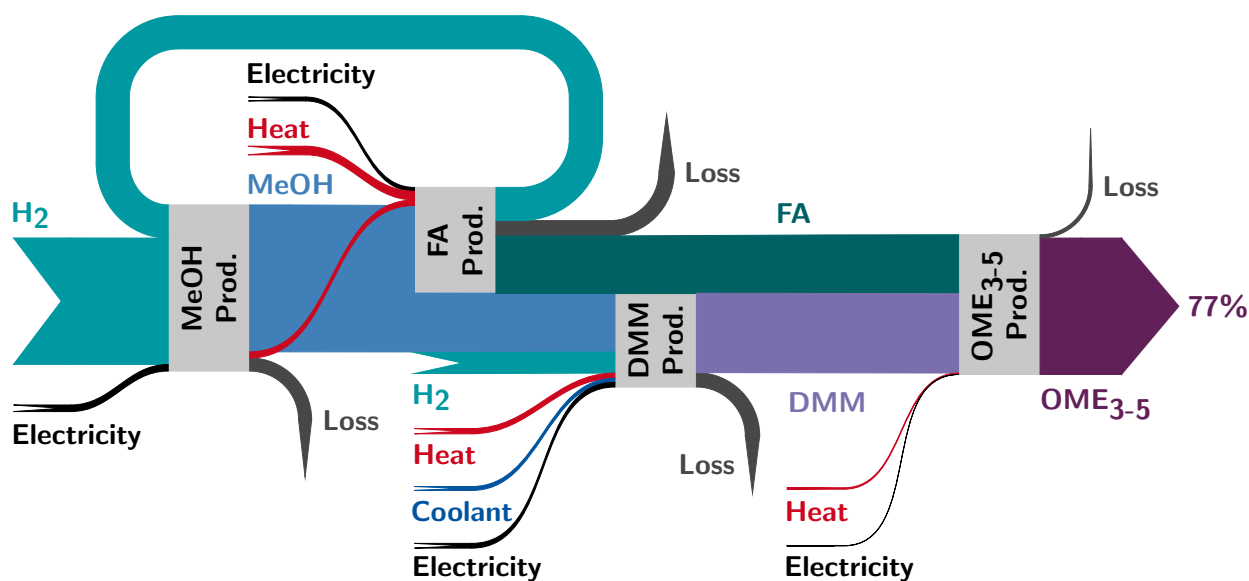


**Figure 4.15.:** Exergy flow diagram of the value chain for  $\text{OME}_{3-5}$  production from  $\text{H}_2$  and  $\text{CO}_2$  via the reductive reaction pathway for the DMM production process step. For clarity, only the most relevant heat streams resulting from heat integration between process steps are displayed. An overall process exergy efficiency of 77 % is reached. Corresponding material and energy balances are summarized in Appendix Tab. D.2.





---

## 5. MINLP Problem Formulations for Global Superstructure Optimization

Discrete decisions in design problems are not limited to the selection of column configurations (cf. Section 4.2) but can be caused by any structural alternative within the process. Even such decisions that are not caused by the selection of process units but by their operation (such as mode-switching) can be discrete. Superstructure optimization represents a suitable but computationally demanding approach to solve such problems. Typical formulations include discrete variables. However, in some cases the formulations are purely continuous (e.g., blending problem for fuels [203], process water networks [204]). Superstructures can be represented in several ways resulting in different problem formulations for which different solution algorithms exist [184, 205]. A common and intuitive modeling approach is their formulation as generalized disjunctive programming (GDP) problems consisting of algebraic constraints, disjunctions, Boolean variables, and logic propositions [206]. These GDP problems can be solved directly with dedicated solution algorithms (e.g., logic-based Outer Approximation [207] or GDP branch and bound [208]) that aim to exploit the disjunctions effectively (e.g., by directly branching on them or reducing the problem size by considering only the active disjuncts). Alternatively, they can be reformulated to mixed-integer nonlinear programming (MINLP) problems [209], in which integer variables replace Boolean variables and algebraic equations model the logic propositions.

Conventional reformulation approaches are the Big-M [210] and Convex Hull [207] method. The reformulation of GDP to MINLP problems enables the use of powerful commercial MINLP solvers and thus the possibility to solve GDP problems containing nonconvex functions [211, 212]. In contrast, existing solvers dedicated to GDP problems are restricted to GDP problems containing only convex functions. It is also possible to avoid introducing Boolean or binary variables for modeling the disjunctions by using complementarity constraints resulting in mathematical programs with equilibrium constraints (MPEC) [213]. This results in a special type of nonlinear programming (NLP) problem with only a few optimization variables. The NLP problem can be either solved directly or again reformulated (e.g., by using the Plus Function [214]), which often involves smoothing techniques. In summary, a number of modeling approaches and solution algorithms has been developed over the past decades. Their comparison has mainly been limited to the conventional approaches and problems with only linear or convex constraints representing the process models. For problems containing nonconvex functions, which require global optimization techniques, a comparative assessment of all approaches mentioned above is missing so far.

For global optimization, several techniques for improving computational tractability have been proposed. As superstructure optimization problems often have many variables and constraints, factorable reduced-space (RS) formulations can be beneficial (for an overview of these formulations, see Bongartz [215], Chapter 3). In such RS formulations, equality

constraints are used to eliminate optimization variables from the problem, while ensuring that the optimization problem remains factorable, i.e., all functions can still be expressed as compositions of simple so-called intrinsic functions (i.e., functions for which convex and concave relaxations are known). Compared to the more conventional (equation-oriented) full-space (FS) formulations of the problem, the RS formulations have fewer optimization variables and constraints. In the branch-and-bound (BaB) algorithms that are used for global optimization of nonconvex problems, RS formulations reduce the dimensionality of the space that needs to be partitioned via branching, and they reduce the size of the subproblems for computing lower and upper bounds on the optimal objective value. Depending on the method used for constructing relaxations, they may however result in weaker relaxations (see Bongartz [215], p. 64). Factorable RS formulations have been used successfully for flowsheet optimization problems [188, 216, 217], parameter estimation problems involving ordinary differential equations [218], and problems with machine learning models embedded [176, 177]. Its application to superstructure optimization problems has not been investigated yet. Even more variables and constraints can be eliminated from the problem by dropping the requirement that the functions remain factorable, and instead allowing the use of implicit functions defined by the constraints. Barton and co-workers have presented methods for handling such implicit functions in BaB algorithms [219–221]. However, these are beyond the scope of this work as corresponding implementations are not readily available yet.

In this chapter, we compare different problem formulations for superstructure optimization problems comprising nonconvex functions. Within this comparison, we investigate whether the optimization can benefit from a RS formulation. In this regard, we introduce a simple and a more complex illustrative example problem in Section 5.1. For the simple example problem, the conventional and unconventional problem formulations are developed in Section 5.2. The comparison of all problem formulations for the two example problems are presented in Section 5.3. In Section 5.4, the key results are confirmed by an optimization problem with a different structure (i.e., piecewise-defined cost function instead of unit selection), which can be modeled using the same reformulation approaches. Section 5.5 concludes our findings.

## 5.1. Problem Definition

To introduce the different problem formulations in Section 5.2, we use a simple illustrative example problem (Section 5.1.1). This example problem and a more complex one with multiple disjunctions (Section 5.1.2) are then used to analyze each problem formulation in greater detail in Section 5.3.

### 5.1.1. Simple Illustrative Example Problem

In this simple example problem, we consider only two mutually exclusive options (either Unit P or Unit S) to produce a desired amount of a product,  $\dot{n}_{\text{out}} = 1$  (considered as a parameter). This illustrative example problem is motivated by our work on power-to-X [141, 142, 222], in which decisions need to be taken on how to provide raw materials (e.g., hydrogen and carbon dioxide) and process them toward the final product (e.g., electricity-based fuels).

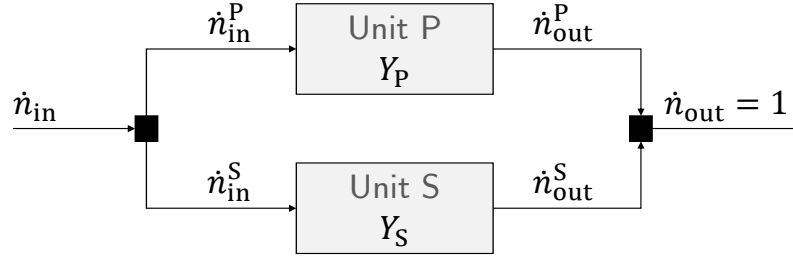


**Figure 5.1.:** Schematic of the simple example problem with the choice of producing a desired amount of a product,  $\dot{n}_{\text{out}} = 1$ , either via Unit P ( $Y_P = \text{True}$ ,  $Y_S = \text{False}$ ) or Unit S ( $Y_P = \text{False}$ ,  $Y_S = \text{True}$ ).

Each option comes with operating and investment costs, both of which are dependent on molar flow rates and unit-specific cost parameters (Tab. 5.1). Operating costs  $C_{\text{op}}$  are quadratically dependent on the molar flow rate passing through the chosen unit ( $C_{\text{op}}^j = (\dot{n}_{\text{in}}^j)^2 e_j$ ). Investment costs  $C_{\text{inv}}$  are dependent on the maximal rating given as the global feed flow rate into the superstructure,  $\dot{n}_{\text{in}}$ , and a constant cost parameter ( $C_{\text{inv}}^j = C_j + \dot{n}_{\text{in}}^{0.6}$ ). The dependency on  $\dot{n}_{\text{in}}$  (in addition to  $\dot{n}_{\text{in}}^j$  for operating costs) puts more emphasis on the nonconvexity regarding multiple variables in typical process synthesis problems. This concave term can also be moved out of the disjunction directly into the objective function. Our simple numerical experimentation showed that this does not have any effect on the optimization. Also the consideration of a constant conversion parameter for each process unit does not have an influence on the overall results. To keep the illustrative example problem simple, we do not consider such a parameter.

**Table 5.1.:** Cost parameters for the simple (GDP1) and the multiple-disjunction (GDP2) example problem.  $C_j$  are fixed investment costs and  $e_j$  are specific operating costs.

Parameter	Unit P	Unit S	Unit F1	Unit F2
$e_j$	7	3	0.1	0.3
$C_j$	4	7	0.5	0.4

The objective is to find the process with the lowest total cost  $C$  by solving the following

optimization problem formulated as a GDP problem:

$$\begin{aligned}
 \min \quad & C = C_{\text{op}} + C_{\text{inv}} \\
 \text{s.t.} \quad & \dot{n}_{\text{in}} = \dot{n}_{\text{in}}^{\text{P}} + \dot{n}_{\text{in}}^{\text{S}} \\
 & \dot{n}_{\text{out}} = \dot{n}_{\text{out}}^{\text{P}} + \dot{n}_{\text{out}}^{\text{S}} \\
 & \begin{bmatrix} Y_{\text{P}} \\ \dot{n}_{\text{in}}^{\text{S}} = \dot{n}_{\text{out}}^{\text{S}} = 0 \\ \dot{n}_{\text{out}}^{\text{P}} = \dot{n}_{\text{in}}^{\text{P}} \\ C_{\text{op}} = (\dot{n}_{\text{in}}^{\text{P}})^2 e_{\text{P}} \\ C_{\text{inv}} = C_{\text{P}} + \dot{n}_{\text{in}}^{0.6} \end{bmatrix} \vee \begin{bmatrix} Y_{\text{S}} \\ \dot{n}_{\text{in}}^{\text{P}} = \dot{n}_{\text{out}}^{\text{P}} = 0 \\ \dot{n}_{\text{out}}^{\text{S}} = \dot{n}_{\text{in}}^{\text{S}} \\ C_{\text{op}} = (\dot{n}_{\text{in}}^{\text{S}})^2 e_{\text{S}} \\ C_{\text{inv}} = C_{\text{S}} + \dot{n}_{\text{in}}^{0.6} \end{bmatrix} \quad (\text{GDP1}) \\
 & Y_{\text{P}} \vee Y_{\text{S}} \\
 & C_{\text{op}}, C_{\text{inv}}, \dot{n}_{\text{in}}, \dot{n}_{\text{in}}^{\text{P}}, \dot{n}_{\text{in}}^{\text{S}}, \dot{n}_{\text{out}}^{\text{P}}, \dot{n}_{\text{out}}^{\text{S}} \geq 0 \\
 & C_{\text{op}}, C_{\text{inv}}, \dot{n}_{\text{in}}, \dot{n}_{\text{in}}^{\text{P}}, \dot{n}_{\text{in}}^{\text{S}}, \dot{n}_{\text{out}}^{\text{P}}, \dot{n}_{\text{out}}^{\text{S}} \in \mathbb{R} \\
 & Y_{\text{P}}, Y_{\text{S}} \in \{\text{True}, \text{False}\}
 \end{aligned}$$

There are alternative ways for modeling the system, e.g., by eliminating the global (i.e., independent from disjunctions) equality constraints and modifying the disjunctive constraints correspondingly. As Problem (GDP1) is the most direct representation of the superstructure shown in Fig. 5.1, the use of these global constraints is considered throughout this work. Additionally, we explicitly restrict all illustrative example problems to the exclusive choice between units (denoted by the logic exclusive “or”-operator  $\vee$ ) to keep it as simple as possible.

### 5.1.2. Multiple-Disjunction Example Problem

As the flowsheet structure of Problem (GDP1) is minimalist, we analyze a more complex example problem with two disjunctions taken from [209], where the outlet of Unit S needs to be further processed by either Unit F1 or F2 (Fig.5.2). To make the choice for one of these units economically viable and the case study interesting, we introduce a cost factor of 0.1 for Unit F1 and F2.

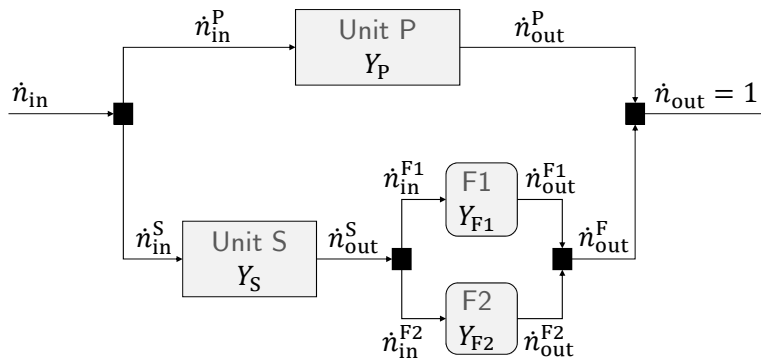


**Figure 5.2.:** Schematic of the flowsheet structure with two disjunctions and the choice of producing a desired amount of a product,  $\dot{n}_{\text{out}} = 1$ , either via Unit P ( $Y_{\text{P}} = 1, Y_{\text{S}} = 0$ ) or Unit S ( $Y_{\text{P}} = 0, Y_{\text{S}} = 1$ ). If Unit S is chosen, the product needs to be further processed by either Unit F1 ( $Y_{\text{F1}} = 1, Y_{\text{F2}} = 0$ ) or F2 ( $Y_{\text{F1}} = 0, Y_{\text{F2}} = 1$ ).

The more complex flowsheet structure results in Problem (P2) (Appendix Section E), which is further reformulated to Problem (GDP2) to remove the nested structure within the disjunction and derive corresponding problem formulations as described in Section 5.2. These are summarized in Appendix Section E.

$$\begin{aligned}
 \min \quad & C = C_{\text{op}} + C_{\text{inv}} \\
 \text{s.t.} \quad & \dot{n}_{\text{in}} = \dot{n}_{\text{in}}^{\text{P}} + \dot{n}_{\text{in}}^{\text{S}} \\
 & \dot{n}_{\text{out}}^{\text{S}} = \dot{n}_{\text{in}}^{\text{F1}} + \dot{n}_{\text{in}}^{\text{F2}} \\
 & \dot{n}_{\text{out}}^{\text{F}} = \dot{n}_{\text{out}}^{\text{F1}} + \dot{n}_{\text{out}}^{\text{F2}} \\
 & \dot{n}_{\text{out}} = \dot{n}_{\text{out}}^{\text{P}} + \dot{n}_{\text{out}}^{\text{F}} \\
 & \left[ \begin{array}{c} Y_{\text{P}} \\ \dot{n}_{\text{in}}^{\text{S}} = \dot{n}_{\text{out}}^{\text{S}} = 0 \\ \dot{n}_{\text{out}}^{\text{P}} = \dot{n}_{\text{in}}^{\text{P}} \\ C_{\text{op}} = (\dot{n}_{\text{in}}^{\text{P}})^2 e_{\text{P}} \\ C_{\text{inv}} = C_{\text{P}} + \dot{n}_{\text{in}}^{0.6} \end{array} \right] \vee \left[ \begin{array}{c} Y_{\text{S}} \\ \dot{n}_{\text{in}}^{\text{P}} = \dot{n}_{\text{out}}^{\text{P}} = 0 \\ \dot{n}_{\text{out}}^{\text{S}} = \dot{n}_{\text{in}}^{\text{S}} \\ C_{\text{op}} = (\dot{n}_{\text{in}}^{\text{S}})^2 e_{\text{S}} + C_{\text{op}}^{\text{F}} \\ C_{\text{inv}} = C_{\text{S}} + \dot{n}_{\text{in}}^{0.6} + C_{\text{inv}}^{\text{F}} \end{array} \right] \quad (\text{GDP2}) \\
 & \left[ \begin{array}{c} Y_{\text{F1}} \\ \dot{n}_{\text{in}}^{\text{F2}} = \dot{n}_{\text{out}}^{\text{F2}} = 0 \\ \dot{n}_{\text{out}}^{\text{F1}} = \dot{n}_{\text{in}}^{\text{F1}} \\ C_{\text{op}}^{\text{F}} = (\dot{n}_{\text{in}}^{\text{F1}})^2 e_{\text{F1}} \\ C_{\text{inv}}^{\text{F}} = C_{\text{F1}} + 0.1\dot{n}_{\text{in}}^{0.6} \end{array} \right] \vee \left[ \begin{array}{c} Y_{\text{F2}} \\ \dot{n}_{\text{in}}^{\text{F1}} = \dot{n}_{\text{out}}^{\text{F1}} = 0 \\ \dot{n}_{\text{out}}^{\text{F2}} = \dot{n}_{\text{in}}^{\text{F2}} \\ C_{\text{op}}^{\text{F}} = (\dot{n}_{\text{in}}^{\text{F2}})^2 e_{\text{F2}} \\ C_{\text{inv}}^{\text{F}} = C_{\text{F2}} + 0.1\dot{n}_{\text{in}}^{0.6} \end{array} \right] \vee \left[ \begin{array}{c} Y_{\text{notF}} \\ \dot{n}_{\text{in}}^{\text{F1}} = \dot{n}_{\text{in}}^{\text{F2}} = \dot{n}_{\text{out}}^{\text{F1}} = \dot{n}_{\text{out}}^{\text{F2}} = 0 \\ C_{\text{op}}^{\text{F}} = 0 \\ C_{\text{inv}}^{\text{F}} = 0 \end{array} \right] \\
 & Y_{\text{P}} \vee Y_{\text{S}} \\
 & Y_{\text{F1}} \vee Y_{\text{F2}} \vee Y_{\text{notF}} \\
 & Y_{\text{S}} \Leftrightarrow Y_{\text{F1}} \vee Y_{\text{F2}} \\
 & C_{\text{op}}, C_{\text{inv}}, C_{\text{op}}^{\text{F}}, C_{\text{inv}}^{\text{F}}, \dot{n}_{\text{in}}, \dot{n}_{\text{in}}^{\text{P}}, \dot{n}_{\text{in}}^{\text{S}}, \dot{n}_{\text{in}}^{\text{F1}}, \dot{n}_{\text{in}}^{\text{F2}}, \dot{n}_{\text{out}}^{\text{P}}, \dot{n}_{\text{out}}^{\text{S}}, \dot{n}_{\text{out}}^{\text{F1}}, \dot{n}_{\text{out}}^{\text{F2}}, \dot{n}_{\text{out}}^{\text{F}} \geq 0 \\
 & C_{\text{op}}, C_{\text{inv}}, C_{\text{op}}^{\text{F}}, C_{\text{inv}}^{\text{F}}, \dot{n}_{\text{in}}, \dot{n}_{\text{in}}^{\text{P}}, \dot{n}_{\text{in}}^{\text{S}}, \dot{n}_{\text{in}}^{\text{F1}}, \dot{n}_{\text{in}}^{\text{F2}}, \dot{n}_{\text{out}}^{\text{P}}, \dot{n}_{\text{out}}^{\text{S}}, \dot{n}_{\text{out}}^{\text{F1}}, \dot{n}_{\text{out}}^{\text{F2}}, \dot{n}_{\text{out}}^{\text{F}} \in \mathbb{R} \\
 & Y_{\text{P}}, Y_{\text{S}}, Y_{\text{F1}}, Y_{\text{F2}}, Y_{\text{notF}} \in \{\text{True}, \text{False}\}
 \end{aligned}$$

## 5.2. Problem Formulations

In this section, the most common problem formulations for superstructure optimization and less common ones are presented and applied to the simple illustrative example problem (GDP1). One of the most conventional methods to reformulate GDP into MINLP problems are the *Big-M* (Section 5.2.1, [210]) and the *Convex Hull* method (Section 5.2.2, [207]). Big-M and Convex Hull transform Boolean variables  $Y_j$  into binary variables  $y_j$  to express the relationship between and within disjunctions. In contrast, a nonsmooth reformulation approach can be used to prevent the use of any additional variables completely by introducing complementarity constraints. The resulting *MPECs* can be either solved directly (Section 5.2.3, [223]) or again reformulated using the *Plus Function* (Section 5.2.4, [214]). Another alternative problem formulation, hereafter called *Direct MINLP*, utilizes binary variables directly within the equality constraints of the process model to capture the ex-

istence or nonexistence of a unit or process stream within a disjunction (Section 5.2.5). As we also consider RS formulations for all reformulation approaches, Section 5.2.6 illustrates such a RS formulation exemplarily for the Direct MINLP reformulation approach. In addition to the aforementioned reformulation approaches, superstructures representing problems with piecewise-defined functions can also be handled by using step functions (cf. Section 5.4, [224]).

### 5.2.1. Big-M

The Big-M method introduces the parameter  $M$  (a big number potentially individual for each constraint of disjunct  $j$ ), which is used to make the constraints of unchosen choices ( $y_j = 0$ ) redundant. Several methods exist in literature that determine the optimal value for  $M$  and thus tighten relaxations (e.g., [225]). To maintain a manageable complexity, we do not consider such improved Big-M methods. Instead, we choose  $M$  to be equal to the global upper bound of the variable that is bounded by the corresponding constraint. Besides binary variables for each disjunct (the transformed Boolean variables), no additional variables need to be introduced. However, a poor choice for  $M$  can result in weak relaxations. Applied to Problem (GDP1), the Big-M method results in Problem (BM1):

$$\begin{aligned}
 \min \quad & C = C_{\text{op}} + C_{\text{inv}} \\
 \text{s.t.} \quad & \dot{n}_{\text{in}} = \dot{n}_{\text{in}}^{\text{P}} + \dot{n}_{\text{in}}^{\text{S}} \\
 & \dot{n}_{\text{out}} = \dot{n}_{\text{out}}^{\text{P}} + \dot{n}_{\text{out}}^{\text{S}} \\
 & 0 - M(1 - y_{\text{P}}) \leq \dot{n}_k^{\text{S}} \leq 0 + M(1 - y_{\text{P}}) & k \in \{\text{in}, \text{out}\} \\
 & 0 - M(1 - y_{\text{S}}) \leq \dot{n}_k^{\text{P}} \leq 0 + M(1 - y_{\text{S}}) & k \in \{\text{in}, \text{out}\} \\
 & \dot{n}_{\text{in}}^j - M(1 - y_j) \leq \dot{n}_{\text{out}}^j \leq \dot{n}_{\text{in}}^j + M(1 - y_j) & j \in \{\text{P}, \text{S}\} \\
 & (\dot{n}_{\text{in}}^j)^2 e_j - M(1 - y_j) \leq C_{\text{op}} \leq (\dot{n}_{\text{in}}^j)^2 e_j + M(1 - y_j) & j \in \{\text{P}, \text{S}\} \\
 & C_j + \dot{n}_{\text{in}}^{0.6} - M(1 - y_j) \leq C_{\text{inv}} \leq C_j + \dot{n}_{\text{in}}^{0.6} + M(1 - y_j) & j \in \{\text{P}, \text{S}\} \\
 & y_{\text{P}} + y_{\text{S}} = 1 \\
 & C_{\text{op}}, C_{\text{inv}}, \dot{n}_{\text{in}}, \dot{n}_{\text{in}}^{\text{P}}, \dot{n}_{\text{in}}^{\text{S}}, \dot{n}_{\text{out}}^{\text{P}}, \dot{n}_{\text{out}}^{\text{S}} \geq 0 \\
 & C_{\text{op}}, C_{\text{inv}}, \dot{n}_{\text{in}}, \dot{n}_{\text{in}}^{\text{P}}, \dot{n}_{\text{in}}^{\text{S}}, \dot{n}_{\text{out}}^{\text{P}}, \dot{n}_{\text{out}}^{\text{S}} \in \mathbb{R} \\
 & y_{\text{P}}, y_{\text{S}} \in \{0, 1\}
 \end{aligned} \tag{BM1}$$

### 5.2.2. Convex Hull

For the Convex Hull method, a new (disaggregated) variable,  $\nu_j$ , needs to be introduced for each variable that is affected by a disjunction and for each choice within the respective disjunction. The bounds on these disaggregated variables can be either chosen to be the global variable bounds or tightened based on the disjunct. In our illustrative example problems, we use global variable bounds (i.e.,  $0 \leq \dot{n} \leq 1$ ,  $0 \leq C \leq 20$ ). Each constraint  $r_j(\nu_j) \leq 0$  of disjunct  $j$  is expressed by the closure of the perspective function [226]:

$$y_j r_j \left( \frac{\nu_j}{y_j} \right) \leq 0 \tag{5.1}$$

To avoid singularities for  $y_j = 0$ , Lee and Grossmann [207] proposed a modification of the original perspective function, which was again modified by Sawaya [227] to improve numerical performance and accuracy:

$$((1 - \epsilon)y_j + \epsilon)r_j \left( \frac{\nu_j}{(1 - \epsilon)y_j + \epsilon} \right) \leq 0 \quad (5.2)$$

For the illustrative example problems, parameter  $\epsilon$  only needs to be nonzero as the disaggregated variables of unchosen units ( $\nu_j = 0$ ) make Constraint (5.2) being fulfilled independently from the value of  $\epsilon$ . In general,  $\epsilon$  needs to be chosen sufficiently small to maintain a high accuracy. As Constraints (5.2) represents the commonly used type of perspective function for global optimization, we use it for all Convex Hull formulations within this study where necessary. Other modifications exist and are summarized in Furman et al. [228]. In this study, they are not considered.

The introduction of disaggregated variables increases problem size but generally yields tighter relaxations compared to the Big-M formulation, even if the most suitable Big-M parameter is utilized [229]. The conversion of Problem (GDP1) with the Convex Hull method results in Problem (CH1):

$$\begin{aligned}
 \min \quad & C = C_{\text{op}} + C_{\text{inv}} \\
 \text{s.t.} \quad & \dot{n}_{\text{in}} = \dot{n}_{\text{in}}^{\text{P}} + \dot{n}_{\text{in}}^{\text{S}} \\
 & \dot{n}_{\text{out}} = \dot{n}_{\text{out}}^{\text{P}} + \dot{n}_{\text{out}}^{\text{S}} \\
 & \dot{n}_{\text{in}}^j = \dot{n}_{\text{in},\text{P}}^j + \dot{n}_{\text{in},\text{S}}^j & j \in \{\text{P}, \text{S}\} \\
 & \dot{n}_{\text{out}}^j = \dot{n}_{\text{out},\text{P}}^j + \dot{n}_{\text{out},\text{S}}^j & j \in \{\text{P}, \text{S}\} \\
 & C_{\text{op}} = C_{\text{op}}^{\text{P}} + C_{\text{op}}^{\text{S}} \\
 & C_{\text{inv}} = C_{\text{inv}}^{\text{P}} + C_{\text{inv}}^{\text{S}} \\
 & \dot{n}_{k,\text{P}}^{\text{S}}, \dot{n}_{k,\text{S}}^{\text{P}} \leq 0 & k \in \{\text{in}, \text{out}\} \\
 & C_{\text{op}}^j \geq \left( \frac{\dot{n}_{\text{in},j}^j}{(1-\epsilon)y_j + \epsilon} \right)^2 e_j((1-\epsilon)y_j + \epsilon) & j \in \{\text{P}, \text{S}\} \\
 & C_{\text{inv}}^j \geq (C_j + \dot{n}_{\text{in}}^{0.6})y_j & j \in \{\text{P}, \text{S}\} \\
 & y_{\text{P}} + y_{\text{S}} = 1 & (\text{CH1}) \\
 & 0 \leq \dot{n}_{k,\text{P}}^{\text{S}} \leq 1y_{\text{P}} & k \in \{\text{in}, \text{out}\} \\
 & 0 \leq \dot{n}_{k,\text{S}}^{\text{P}} \leq 1y_{\text{S}} & k \in \{\text{in}, \text{out}\} \\
 & 0 \leq \dot{n}_{k,j}^j \leq 1y_j & k \in \{\text{in}, \text{out}\} \quad j \in \{\text{P}, \text{S}\} \\
 & 0 \leq C_m^j \leq 20y_j & m \in \{\text{op}, \text{inv}\} \quad j \in \{\text{P}, \text{S}\} \\
 & C_{\text{op}}, C_{\text{inv}}, \dot{n}_{\text{in}}, \dot{n}_{\text{in}}^{\text{P}}, \dot{n}_{\text{in}}^{\text{S}}, \dot{n}_{\text{out}}^{\text{P}}, \dot{n}_{\text{out}}^{\text{S}} \geq 0 \\
 & C_{\text{op}}, C_{\text{inv}}, C_{\text{op}}^{\text{P}}, C_{\text{op}}^{\text{S}}, C_{\text{inv}}^{\text{P}}, C_{\text{inv}}^{\text{S}} \in \mathbb{R} \\
 & \dot{n}_{\text{in}}, \dot{n}_{\text{in}}^{\text{P}}, \dot{n}_{\text{in}}^{\text{S}}, \dot{n}_{\text{in},\text{P}}^{\text{P}}, \dot{n}_{\text{in},\text{P}}^{\text{S}}, \dot{n}_{\text{in},\text{S}}^{\text{P}}, \dot{n}_{\text{in},\text{S}}^{\text{S}} \in \mathbb{R} \\
 & \dot{n}_{\text{out},\text{P}}^{\text{P}}, \dot{n}_{\text{out},\text{P}}^{\text{S}}, \dot{n}_{\text{out},\text{S}}^{\text{P}}, \dot{n}_{\text{out},\text{S}}^{\text{S}}, \dot{n}_{\text{out}}^{\text{P}}, \dot{n}_{\text{out}}^{\text{S}} \in \mathbb{R} \\
 & y_{\text{P}}, y_{\text{S}} \in \{0, 1\}
 \end{aligned}$$

### 5.2.3. MPEC

In order to prevent the use of discrete variables and thus prevent solving a MINLP problem, superstructure optimization problems can be formulated as MPECs. This type of problem formulation introduces complementarity constraints to model the discrete choices in a process superstructure.

The MPEC problem formulation can be derived from Problem (GDP1) by considering all global constraints (to represent the part of the flowsheet that is not affected by disjunctions) and a subset of disjunctive constraints (to represent the part of the flowsheet that is affected by disjunctions). The subset of disjunctive constraints is chosen in such a way that (a) only those model equations of a disjunction are considered that correspond to the part of the flowsheet where  $Y_j = \text{True}$  ( $\dot{n}_{\text{out}}^{\text{P}} = \dot{n}_{\text{in}}^{\text{P}}$ ,  $C_{\text{op}}^{\text{P}} = (\dot{n}_{\text{in}}^{\text{P}})^2 e_{\text{P}}$ , and  $C_{\text{inv}}^{\text{P}} = C_{\text{P}} + \dot{n}_{\text{in}}^{0.6}$  for the choice  $Y_{\text{P}} = \text{True}$ ;  $\dot{n}_{\text{out}}^{\text{S}} = \dot{n}_{\text{in}}^{\text{S}}$ ,  $C_{\text{op}}^{\text{S}} = (\dot{n}_{\text{in}}^{\text{S}})^2 e_{\text{S}}$ , and  $C_{\text{inv}}^{\text{S}} = C_{\text{S}} + \dot{n}_{\text{in}}^{0.6}$  for the choice  $Y_{\text{S}} = \text{True}$ ) and (b) zero values can be realized if the choice  $j$  within the disjunction is not active. However, this is not given for all types of disjunctive problems: In the simple illustrative example problem (GDP1),  $C_{\text{inv}}^j$  contains constant investment costs  $C_j$



for unit  $j$  and therefore need to be modified by a step function that is dependent on the material stream  $\dot{n}_{\text{in}}^j$  passing through unit  $j$ . Such a step function introduces nonconvexities additionally to those that are inherently part of the modeled system into the problem. If tailored relaxations are implemented for such a step function [224], the optimization may however not be necessarily affected negatively. For all problem formulations in this work, the tanh-function is used as a smoothed step function resulting in an error below the feasibility tolerance. By adding up the cost terms  $C_{\text{op}}^j$  and  $C_{\text{inv}}^j$  for each unit  $j$ , operating costs  $C_{\text{op}}$  and investment costs  $C_{\text{inv}}$  are then retrieved, respectively. The relationship between disjunctions and choices within each disjunction is represented by complementarity constraints instead of binary variables. For Problem (MPEC1), the molar flows passing each unit are multiplied by each other and set to zero. Therefore, either  $\dot{n}_{\text{in}}^{\text{P}}$  or  $\dot{n}_{\text{in}}^{\text{S}}$  need to become zero if the other one is nonzero. Due to the absence of any discrete variables, global NLP solvers can be used to find the global optimum. This can however be challenging. Although a considerably smaller problem size can be achieved in comparison to the other approaches, the introduced complementarity constraints can result in the problem violating constraint qualifications and hence cause problems for the local solvers used for upper bounding. Often, a regularization parameter (a small number  $\mu$ ) need to be added to make the constraint qualifications hold again. The solution of the original problem is then obtained by sequentially reducing  $\mu$  to zero [230]. Such a regularization is however not required for the problems analyzed in this work, as the global solvers used herein do in practice not depend heavily on the performance of the NLP solver for upper bounding, for which the constraint qualifications need to hold. To improve performance, BARON detects complementary constraints automatically and treats them accordingly. In MAiNGO, there is no special algorithm to detect and treat complementarity constraints implemented yet.

The MPEC formulation of Problem (GDP1) using complementarity constraints results in Problem (MPEC1), in which parameter  $P$  (a big number) is used to approximate the step function more accurately.

$$\begin{aligned}
 \min \quad & C = C_{\text{op}} + C_{\text{inv}} \\
 \text{s.t.} \quad & \dot{n}_{\text{in}} = \dot{n}_{\text{in}}^{\text{P}} + \dot{n}_{\text{in}}^{\text{S}} \\
 & \dot{n}_{\text{out}}^j = \dot{n}_{\text{in}}^j \quad j \in \{\text{P}, \text{S}\} \\
 & \dot{n}_{\text{out}} = \dot{n}_{\text{out}}^{\text{P}} + \dot{n}_{\text{out}}^{\text{S}} \\
 & C_{\text{op}} = \sum_{j \in J} (\dot{n}_{\text{in}}^j)^2 e_j \\
 & C_{\text{inv}} = \sum_{j \in J} \left[ \tanh(P \dot{n}_{\text{in}}^j) (C_j + \dot{n}_{\text{in}}^{0.6}) \right] \\
 & 0 = \dot{n}_{\text{in}}^{\text{P}} \dot{n}_{\text{in}}^{\text{S}} \\
 & C_{\text{op}}, C_{\text{inv}}, \dot{n}_{\text{in}}, \dot{n}_{\text{in}}^{\text{P}}, \dot{n}_{\text{in}}^{\text{S}}, \dot{n}_{\text{out}}^{\text{P}}, \dot{n}_{\text{out}}^{\text{S}} \geq 0 \\
 & C_{\text{op}}, C_{\text{inv}}, \dot{n}_{\text{in}}, \dot{n}_{\text{in}}^{\text{P}}, \dot{n}_{\text{in}}^{\text{S}}, \dot{n}_{\text{out}}^{\text{P}}, \dot{n}_{\text{out}}^{\text{S}} \in \mathbb{R}
 \end{aligned} \tag{MPEC1}$$

### 5.2.4. Plus Function

An alternative representation of the complementarity constraint ( $0 = \dot{n}_{\text{in}}^{\text{P}} \dot{n}_{\text{in}}^{\text{S}}$ ) in Problem (MPEC1) can be achieved by using the Plus Function [214]:

$$0 = \dot{n}_{\text{in}}^{\text{P}} - \max(0, \dot{n}_{\text{in}}^{\text{P}} - \dot{n}_{\text{in}}^{\text{S}}). \quad (5.3)$$

This function is commonly used for modeling the nonsmooth behavior of flash units for vapor-liquid(-liquid) equilibrium calculations with vanishing phases [231, 232], for which it has shown a promising computational performance. We refer to the resulting problem formulation as Problem (PLUS1) (Appendix Section E).

### 5.2.5. Direct MINLP

A problem formulation for superstructure optimization that is only barely used is the direct multiplication of binary variables with the continuous variables being present in the disjunctions. Similarly to the aforementioned problem formulations, it can be derived from GDP problem (GDP1). Boolean variables  $Y_j$  of the GDP problem transform to binary variables  $y_j$  and are (in contrast to the Big-M and Convex Hull method) multiplied with the continuous model variables ( $\dot{n}_{\text{in}}^j = y_j \dot{n}_{\text{in}}$  and  $C_{\text{inv}} = \sum_{j \in J} y_j (C_j + \dot{n}_{\text{in}}^{0.6})$ ) to represent the existence or nonexistence of option  $j$  within the process flowsheet. Instead of introducing additional inequality constraints modeling the disjunctions, the Direct MINLP formulation incorporates the disjunctions directly into the algebraic equality constraints of the model. Doing this, potential redundant global constraints may need to be disregarded ( $\dot{n}_{\text{in}} = \dot{n}_{\text{in}}^{\text{P}} + \dot{n}_{\text{in}}^{\text{S}}$ ) and the variables in the objective function for each choice in the disjunction added up ( $C_{\text{op}} = \sum_{j \in J} (\dot{n}_{\text{in}}^j)^2 e_j$  and  $C_{\text{inv}} = \sum_{j \in J} y_j (C_j + \dot{n}_{\text{in}}^{0.6})$ ). The model formulation results in:

$$\begin{aligned} \min \quad & C = C_{\text{op}} + C_{\text{inv}} \\ \text{s.t.} \quad & C_{\text{op}} = \sum_{j \in J} (\dot{n}_{\text{in}}^j)^2 e_j \\ & C_{\text{inv}} = \sum_{j \in J} y_j (C_j + \dot{n}_{\text{in}}^{0.6}) \\ & \dot{n}_{\text{in}}^j = y_j \dot{n}_{\text{in}} \quad j \in \{\text{P}, \text{S}\} \\ & \dot{n}_{\text{out}}^j = \dot{n}_{\text{in}}^j \quad j \in \{\text{P}, \text{S}\} \\ & \dot{n}_{\text{out}} = \dot{n}_{\text{out}}^{\text{P}} + \dot{n}_{\text{out}}^{\text{S}} \\ & y_{\text{P}} + y_{\text{S}} = 1 \\ & C_{\text{op}}, C_{\text{inv}}, \dot{n}_{\text{in}}, \dot{n}_{\text{in}}^{\text{P}}, \dot{n}_{\text{in}}^{\text{S}}, \dot{n}_{\text{out}}^{\text{P}}, \dot{n}_{\text{out}}^{\text{S}} \geq 0 \\ & C_{\text{op}}, C_{\text{inv}}, \dot{n}_{\text{in}}, \dot{n}_{\text{in}}^{\text{P}}, \dot{n}_{\text{in}}^{\text{S}}, \dot{n}_{\text{out}}^{\text{P}}, \dot{n}_{\text{out}}^{\text{S}} \in \mathbb{R} \\ & y_j \in \{0, 1\} \quad j \in \{\text{P}, \text{S}\} \end{aligned} \quad (\text{MINLP1})$$

In contrast to the conventional problem formulations, the Direct MINLP formulation introduces nonlinearities by the multiplication of the binary variables  $y_j$  with expressions of the continuous variable  $\dot{n}_{\text{in}}$  as part of the algebraic equality constraints in the model. If the remaining model is linear or convex, the reformulation using the Big-M (cf. Section

5.2.1) or Convex Hull (cf. Section 5.2.2) method results in a mixed-integer linear programming (MILP) or convex MINLP problem, respectively, which can be efficiently solved with general-purpose solvers. Thus, for MILP and convex MINLP problems, the conventional reformulation approaches are typically superior to alternative approaches. If the remaining model is nonconvex anyway, e.g., in more detailed process engineering, where nonconvexities are usually inherently part of the (mechanistic) process model, it is not clear whether it is beneficial to reformulate it with the conventional approaches, as it does not result in a MILP or convex MINLP problem [233]. Keeping bilinear terms according to the Direct MINLP formulation can result in smaller subproblems, which can be directly given to MINLP solvers.

From a modeling perspective, we may also view Problem (MINLP1) instead of Problem (GDP1) as a starting formulation, which may again be reformulated using the Big-M or Convex Hull approach. This results in slightly larger problems compared to Problem (BM1) and (CH1) and was therefore found to be less computationally efficient than the direct reformulation of Problem (GDP1).

### 5.2.6. Reduced-Space Formulation

The problem formulations stated in the preceding sections are given in their conventional FS formulation. As we also consider RS formulations (i.e., eliminating optimization variables and constraints), we exemplarily introduce the RS formulation of Problem (MINLP1) in such a way that variables  $y$  that depend on other model variables  $x$  are written as factorable functions  $\tilde{y}(x)$ . By doing so, the objective function becomes an explicit function of the degrees of freedom  $x$  only. This can be done for all problem formulations. The RS formulation for Problem (MINLP1) is

$$\begin{aligned}
 \min_{y_P, \dot{n}_{in}} \quad & \tilde{C}(y_P, \dot{n}_{in}) \\
 \text{s.t.} \quad & \dot{n}_{out} - \dot{n}_{out}^P(y_P, \dot{n}_{in}) - \dot{n}_{out}^S(y_P, \dot{n}_{in}) = 0, \\
 & \dot{n}_{in} \geq 0 \\
 & \dot{n}_{in} \in \mathbb{R} \\
 & y_P \in \{0, 1\},
 \end{aligned} \tag{MINLP1 RS}$$

which has only two variables  $(y_P, \dot{n}_{in})$  and contains the following functions:

$$\begin{aligned}
 \tilde{C}(y_P, \dot{n}_{in}) &:= \tilde{C}_{op}(y_P, \dot{n}_{in}) + \tilde{C}_{inv}(y_P, \dot{n}_{in}) \\
 \tilde{C}_{op}(y_P, \dot{n}_{in}) &:= (\dot{n}_{in}^P(y_P, \dot{n}_{in}))^2 \cdot e_P + (\dot{n}_{in}^S(y_P, \dot{n}_{in}))^2 \cdot e_S \\
 \tilde{C}_{inv}(y_P, \dot{n}_{in}) &:= y_P \cdot (C_P + \dot{n}_{in}^{0.6}) + \tilde{y}_S(y_P) \cdot (C_S + \dot{n}_{in}^{0.6}) \\
 \dot{n}_{in}^P(y_P, \dot{n}_{in}) &:= y_P \cdot \dot{n}_{in} \\
 \dot{n}_{in}^S(y_P, \dot{n}_{in}) &:= \tilde{y}_S(y_P) \cdot \dot{n}_{in} \\
 \tilde{y}_S(y_P) &:= 1 - y_P \\
 \dot{n}_{out}^P(y_P, \dot{n}_{in}) &:= \dot{n}_{in}^P(y_P, \dot{n}_{in}) \\
 \dot{n}_{out}^S(y_P, \dot{n}_{in}) &:= \dot{n}_{in}^S(y_P, \dot{n}_{in}).
 \end{aligned}$$

Such a RS formulation with intermediate variables computed as a function of other variables can easily be implemented in procedural modeling environments, e.g., via the C++ or Python APIs of MAiNGO, which then uses the MC++ library [191] to obtain relaxations of these functions. The elimination of variables in such procedural modeling environments corresponds to the construction of a sequence of mathematical operations, for which a relaxation and their subgradients are constructed. This procedure can be considered as propagating the relaxations through the algorithm [218].

### 5.3. Results for the Example Problems

As we focus on superstructure optimization problems containing nonconvex functions, we do not consider dedicated solvers for GDP problems but rather reformulate the optimization problem either into a MINLP or a (nonsmooth) NLP problem (cf. Section 5.2). The resulting nonconvex optimization problems generally exhibit multiple suboptimal minima, such that a global solver needs to be used. We use our open-source deterministic global solver MAiNGO v0.5.0.2 [164], which employs a standard BaB algorithm with several bound tightening techniques and the multivariate McCormick method [192, 193] implemented in MC++ [191] to obtain relaxations. For a comparison with state-of-the-art deterministic global solvers, we perform each optimization also with the commercial solver BARON v19.3.24 [234] in the modeling system GAMS 27.0.0 using the automated generation of GAMS files by MAiNGO. In contrast to MAiNGO, BARON uses the auxiliary variable method (AVM) [195, 196], which replaces each nonlinear term by an auxiliary variable (AV) and a constraint. For such constraints, known relaxations are constructed. This method is also used by other state-of-the-art deterministic global solvers such as ANTIGONE [197] and SCIP [198], the analysis of which is however beyond the scope of this work. All calculations are conducted on an Intel® Core™i3-6100 CPU with 3.7 GHz running Windows 10 and no other applications. For both global solvers, default settings are selected. The optimality and feasibility tolerance is  $10^{-3}$  and  $10^{-6}$ , respectively. Each optimization has been performed 100 times to reduce the variations in solution time for small problems caused by system background processes. For all problems, the arithmetic mean solution time is reported in this study.

#### 5.3.1. Simple Illustrative Example Problem

For the simple illustrative example problem (GDP1), the problem size and numerical results of each problem formulation are summarized in Tab. 5.2. FS formulations treat all model variables as optimization variables, whereas RS formulations use model equality constraints to eliminate as many optimization variables as possible. One of the remaining equality constraints in the RS formulations makes sure that the sum of streams  $\dot{n}_{\text{out}}^{\text{P}}$  and  $\dot{n}_{\text{out}}^{\text{S}}$  (i.e., the exiting stream  $\dot{n}_{\text{out}}$ ) equals 1. The second remaining equality constraint in Problem (MPEC1) and (PLUS1) is the complementarity constraint modeling the logic proposition of Problem (GDP1). As the complementarity equality constraint does not eliminate a degree of freedom, the problem still has one degree of freedom despite having the same number of variables and equality constraints. The remaining inequality constraints in the RS formulations for Problem (BM1) and (CH1) result from the remaining disjunctive optimization variables. In the FS formulation, the Convex Hull formulation leads to much

larger problems than its alternatives, whereas in the RS formulation, the corresponding problem is the same size as that resulting from the Big-M formulation. The unconventional reformulation approaches however still lead to smaller problem sizes, which gets more pronounced for more complex problems (cf. Section 5.3.2 and 5.4).

In overall, the RS formulations in MAiNGO yield significantly lower overall solution times than corresponding FS formulations and are the lowest for the unconventional reformulation approaches. The higher number of BaB nodes and the lower lower bound (LB) in the root node for Problem (BM1) compared to those of Problem (MPEC1), (PLUS1), and (MINLP1) in the FS formulation indicate weaker relaxations despite the additional nonconvexities introduced by the unconventional approaches. For Problem (CH1), the optimization in FS suffers from the high number of optimization variables (21, cf. Tab. 5.2). The RS formulation accelerates the optimization by about one third of the solution time in the FS formulation (0.20 s vs. 0.28 s) given its smaller problem size. Compared to the alternative problem formulations, the optimization still takes longer.

The solution time for Problem (MPEC1) in FS is similar to that of Problem (MINLP1) in FS. In RS, solution time reductions are again possible despite weaker relaxations. The same findings also apply to Problem (MINLP1). The Plus Function formulation of the complementarity constraints in Problem (PLUS1) seems to reduce computational effort even further.

**Table 5.2.:** Problem size and numerical results for the problem formulations of Problem (GDP1) presented in Section 5.2. The optimization has been executed 100 times, of which the arithmetic mean value is shown. The optimal value is 11.

	Big-M (BM1)		Convex Hull (CH1)		MPEC (MPEC1)		Plus Function (PLUS1)		Direct MINLP (MINLP1)	
	FS	RS	FS	RS	FS	RS	FS	RS	FS	RS
Number of										
Continuous variables	7	2	19	2	7	2	7	2	7	1
Discrete variables	2	1	2	1	0	0	0	0	2	1
Equality constraints	3	1	9	1	7	2	7	2	8	1
Inequality constraints	20	4	34	4	0	0	0	0	0	0
BaB nodes	3	3	3	3	1	5	1	5	1	3
Lower bound of root node	0	5.75	5	4.5	11	2.12	11	2.12	11	8.5
CPU time per BaB node / s	0.058	0.053	0.094	0.068	0.094	0.005	0.04	0.005	0.097	0.022
Solution time / s	0.174	0.16	0.282	0.204	0.094	0.027	0.04	0.026	0.097	0.066

Compared to the commercial global solver BARON, optimization with MAiNGO for the unconventional problem formulations (MPEC1) and (MINLP1) is comparably fast for the FS formulations and even faster for the RS formulations, whereas BARON can handle the conventional problem formulations (BM1) and (CH1) better (especially for the FS formulations). This tendency was expected, as MAiNGO explicitly exploits the benefits of a smaller problem size in the lower bounding problem by using McCormick relaxations [193] opposed to the AVM used in BARON.

If linear instead of the nonlinear cost functions are considered, the Big-M and Convex Hull method results in MILP problems (cf. Problem (BM1lin) and (CH1lin), respectively, Appendix Section E), which can be solved using CPLEX for both the FS and RS formulation. In contrast, the alternative reformulation approaches (yielding Problem (MPEC1lin), (PLUS1lin), and (MINLP1lin), Appendix Section E) still result in MINLP problems with nonconvex functions, which need to be solved using a global solver. However, the overall

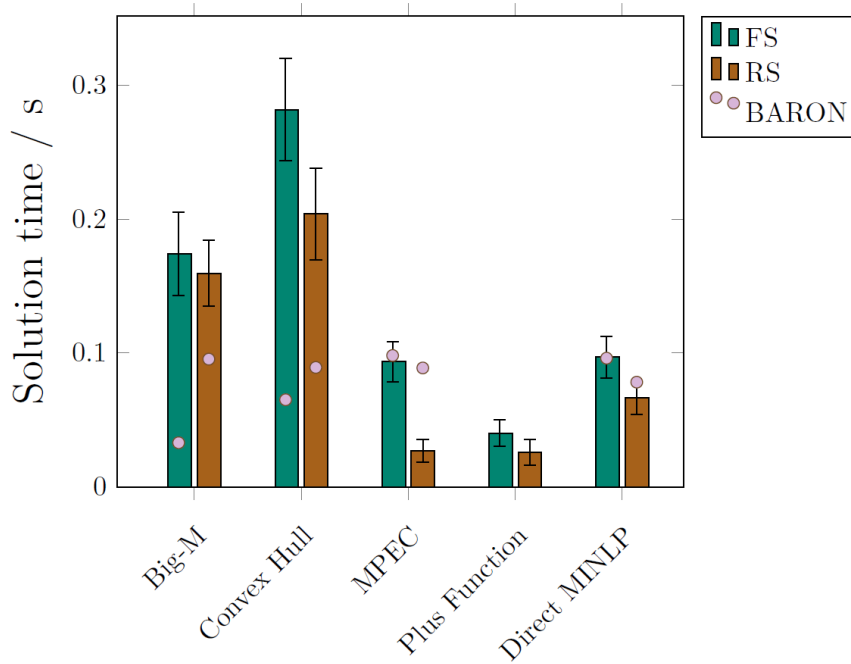


**Figure 5.3.:** Solution time for Problem (GDP1) using the problem formulations presented in Section 5.2. As BARON can not handle *max*-functions, there are no results for the Plus Function formulation. The error bars represent the standard deviation from the arithmetic mean value of the solution time from 100 optimization runs using MAiNGO.

results for these three problems considering linear cost functions (cf. Appendix Tab. E.1 and Appendix Fig. E.1) do not differ from those with nonconvex cost functions. This indicates that the nonconvexity of model equations seem to have only minor influence on the optimization of this simple illustrative example problem.

### 5.3.2. Multiple-Disjunction Example Problem

Tab. 5.3 summarizes the problem size and numerical results of each problem formulation for Problem (GDP2) (each problem formulation is given in Appendix Section E). The newly introduced inequality constraint in the RS formulation of Problem (MINLP2) makes sure that the binary variable  $y_{F2}$  can not become negative. Beyond the equality constraint for the leaving stream  $\dot{n}_{out}$ , Problem (BM2) and (CH2) require an additional equality constraint for the RS formulation to ensure that exactly one choice is being made for the second disjunction (choice for either F1, F2, or none). Problem (MINLP2) does not need a binary for this third choice (neither F1 nor F2) as the algebraic equations for representing the disjunctions differ from those that result directly from reformulating Problem (GDP2) using the Big-M and Convex Hull approach (cf. Appendix Problem (BM2) and (CH2)). As a result, no additional equality constraint is required. Similarly to the simple illustrative example problem (cf. Section 5.3.1), the RS formulations of Problem (MPEC2), (PLUS2), and (MINLP2) lead to the smallest problems.

As for the simple illustrative example problem (cf. Section 5.3.1), the RS formulations in MAiNGO always yield lower overall solution times than corresponding FS formulations. However, the differences between the conventional and unconventional reformulation ap-

proaches are for the RS formulations not as pronounced as in the previous example problem. In contrast, they are still well-marked for the FS formulations. In the FS formulation, Problem (MPEC2) and (PLUS2) perform similarly due to their same size and similar relaxation tightness (cf. Tab. 5.3). Despite Problem (MINLP2) having four additional binary variables, its solution time is similar to that of the aforementioned problem formulations. Problem (BM2) and (MINLP2) benefit from a significantly smaller problem size compared to Problem (CH2), such that their time consumed per BaB node is also significantly smaller. The complementarity-constrained problems (MPEC2) and (PLUS2) do not exploit their small problem size so effectively. The prominent advantage of the Convex Hull method—achieving tight relaxations—does not seem to be significant here: The relaxations of the complementarity-constrained problem formulations (MPEC2) and (PLUS2) in FS seem to be even tighter (higher LB in root node) and the optimization requires fewer BaB nodes than Problem (CH2) (cf. Tab. 5.3). For Problem (BM2), MAiNGO seems to have considerable problems in the FS formulation. The solution time exceeds 30 minutes, which is most likely caused by the simplistic handling of integer variables in MAiNGO. There are no sophisticated heuristics for generating integer-feasible points implemented yet, which can result in poor performance. In RS formulations, this becomes less likely because of the much lower number of possible branches. However, relaxations generally tend to become weaker in the RS formulation, which is confirmed by the lower LB in the root node for RS compared to the FS formulations. The effect of the reduction in problem size on overall solution time is however bigger than that of the relaxation tightness, which is impressively demonstrated for Problem (CH2). All in all, the much simpler and potentially more intuitive problem formulations (MPEC2), (PLUS2), and (MINLP2) seem to benefit from their comparably small problem sizes both in the FS and RS formulation while maintaining comparatively tight relaxations. They always yield solution times as low as or lower than that of the more complex formulations (BM2) and (CH2).

The comparison of the results obtained by MAiNGO with those obtained by BARON confirms the findings from the simple illustrative example problem (cf. Section 5.3.1), yet to a smaller extent: BARON performs better than MAiNGO for FS formulations with only few nonconvex terms (Problem (BM2) and (CH2)), whereas it performs slightly worse for problems in the RS formulation with a higher number of nonconvex terms (Problem (MPEC2) and (MINLP2)).

**Table 5.3.:** Problem size and numerical results for the problem formulations of Problem (GDP2) presented in Section 5.2. The optimization has been executed 100 times, of which the arithmetic mean value is shown. The optimal value is 11.7.

	Big-M (BM2)		Convex Hull (CH2)		MPEC (MPEC2)		Plus Function (PLUS2)		Direct MINLP (MINLP2)	
	FS	RS	FS	RS	FS	RS	FS	RS	FS	RS
Number of										
Continuous variables	14	3	44	3	12	3	12	3	12	1
Discrete variables	5	2	5	2	0	0	0	0	4	2
Equality constraints	8	2	20	2	11	2	11	2	14	1
Inequality constraints	54	12	86	29	0	0	0	0	0	1
BaB nodes	706,798	13	3	7	1	25	1	7	7	7
Lower bound of root node	0	5.8	11.36	5.75	11.7	1.52	11.7	1.52	6.19	3.65
CPU time per BaB node / s	0.003	0.009	0.238	0.017	0.195	0.003	0.135	0.009	0.035	0.012
Solution time / s	2,193	0.112	0.714	0.119	0.195	0.079	0.135	0.064	0.248	0.087

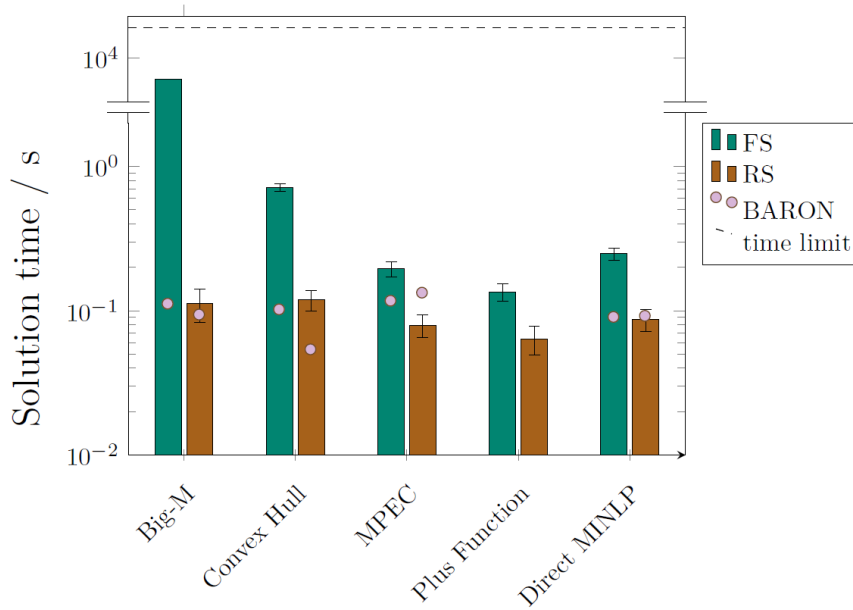


**Figure 5.4.:** Solution time for Problem (GDP2) using the problem formulations presented in Section 5.2. As BARON can not handle *max*-functions, there are no results for the Plus Function formulation. The error bars represent the standard deviation from the arithmetic mean value of the solution time from 100 optimization runs using MAiNGO.

### 5.3.3. Selective Branching for FS Formulations

As an alternative to reducing the problem size on the modeling level, the problem size can also be reduced on the algorithm level in the means of *selective branching* [235–237]. The crucial difference between operating in a *reduced space* on the modeling level (RS formulation in MAiNGO) and on the algorithm level (selective branching) is that selective branching only reduces the dimensionality of the space that needs to be partitioned via branching, whereas the RS formulation in MAiNGO additionally reduces the dimension of subproblems to be solved in both the lower and upper bounding problem. In selective branching, the same (significant) reductions in the number of BaB nodes required to solve the optimization problem and the overall solution time have been reported [235]. This does however apply only to problems with a specific structure and if constraint propagation is used to remain a high convergence order [238].

Irrespective of the approach for reformulating the GDP, the RS formulation in MAiNGO always results in lower solution times than the corresponding FS formulation for both the simple and more complex flowsheet structure (Fig. 5.3 and 5.4, respectively). In contrast, the LB in the root node is always lower and the number of BaB nodes required for global optimality is always larger for the RS formulation than for the FS formulation or they are equal, which indicates weaker relaxations for the RS formulations caused by the propagation of relaxations through the algorithm.

For comparison and to isolate the effect of a smaller problem size from that of the branching behavior, we perform selective branching on the RS optimization variables in the FS formulations. This selective branching should result in similar BaB trees between the FS and RS formulations in terms of selection of branching variables and points, while it still exploits the potentially tighter relaxations of the FS formulations. This investigation



**Table 5.4.:** Problem size and numerical results for the FS formulation of Problem (GDP2) if selective branching is applied. The optimization has been executed 100 times, of which the arithmetic mean value is shown. The optimal value is 11.7. For the FS formulation of Problem (BM2), the maximum solution time of 86,400 s has been reached.

	Big-M (BM2)	Convex Hull (CH2)	MPEC (MPEC2)	Plus Function (PLUS2)	Direct MINLP (MINLP2)
Number of					
Continuous variables	14	44	12	12	12
Discrete variables	5	5	0	0	4
Equality constraints	8	20	11	11	14
Inequality constraints	54	86	0	0	0
BaB nodes	8,138,810	3	1	1	5
Lower bound of root node	0	11.36	11.7	11.7	6.19
CPU time per BaB node / s	0.011	0.241	0.197	0.136	0.048
Solution time / s	86,400	0.723	0.197	0.136	0.24

is performed for the more complex flowsheet structure (Problem (GDP2)) as the differences in solution times for the FS and RS formulations are most pronounced for this problem and their branching variables differ from each other.

Except for Problem (BM2), which seems to have an anomaly in the FS formulation, the results in Tab. 5.4 and Fig. 5.5 show that the solution time remains about the same if selective branching is applied to the FS formulations. This shows that the reduction in solution time is exclusively due to the smaller size of the subproblems. For Problem (MINLP2), the selective branching results in a lower number of BaB nodes compared to its FS formulation without selective branching. This has however only a negligible effect on the overall solution time compared to the solution times for RS formulations as the time consumed per BaB node for the RS formulation is considerably smaller. Selective branching in BARON via the specification of branching priorities has also only negligible influence on the solution time and the number of BaB nodes.

## 5.4. Application to Problems with Piecewise-Defined Functions

A commonly used case study for testing problem formulations with piecewise-defined functions is the solution of a heat exchanger network design problem, which can be formulated as a superstructure optimization problem. This is a special case of superstructure optimization problems as the alternative units can be described as one single unit with a piecewise-defined function, in this case, of the heat exchanger area  $A_i$ . Thus, the disjuncts do not represent different units but rather different regions within the piecewise-defined cost function of each unit (heat exchanger). The case study is taken from Türkay and Grossmann [239] and is depicted in Fig. 5.6 with parameters given in Tab. 5.5. The corresponding formulation of Problem (HEXGDP) can be found in Appendix Section E.

For the RS formulations, model equations had to be rearranged (e.g., for the elimination of  $T_1$ , by a partial fraction decomposition) in order to tighten relaxations and prevent singularities. Since in this example the alternative units can also be described as a single unit containing a piecewise-defined (potentially discontinuous) function, we introduce a new

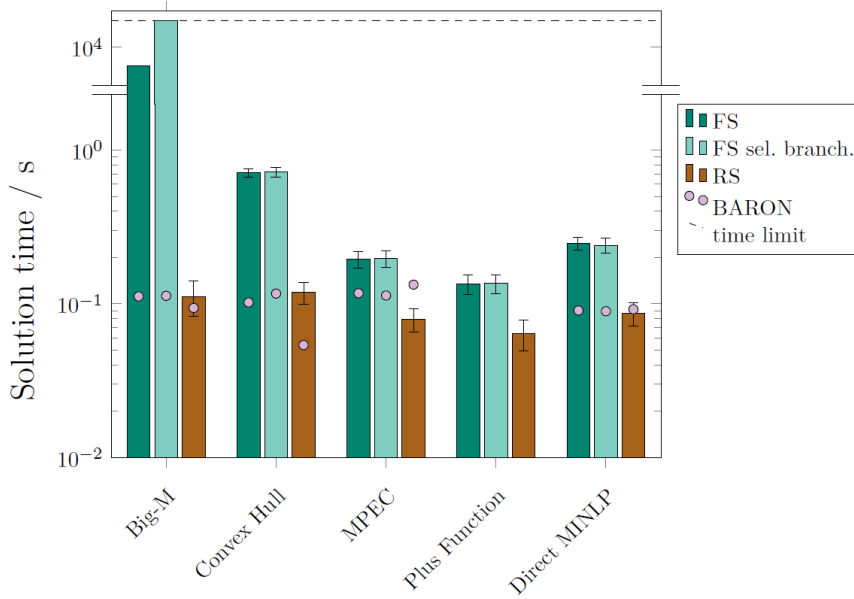


**Figure 5.5.:** Solution time for the FS formulation of Problem (GDP2) if selective branching is applied compared to both the FS formulation without selective branching and the RS formulation. As BARON can not handle *max*-functions, there are no results for the Plus Function formulation. The error bars represent the standard deviation from the arithmetic mean value of the solution time from 100 optimization runs using MAiNGO.

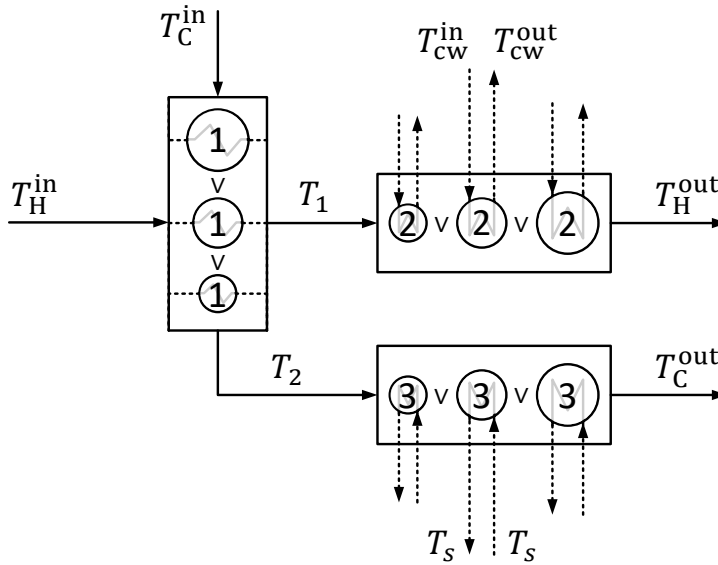


**Figure 5.6.:** Heat exchanger network based on the work of Türkay and Grossmann [239] with the choice between three different sizes for each heat exchanger 1-3.

problem formulation (Problem (HEXStepF), Appendix Section E), hereafter called *Step Formulation*. This formulation involves step functions, for which McCormick relaxations

**Table 5.5.:** Parameters for the heat exchanger network design problem taken from Trkay and Grossmann [239].

Stream	$FCP_i$ / kW K <sup>-1</sup>	$T^{\text{in}}$ / K	$T^{\text{out}}$ / K	$C$ / \$ kW <sup>-1</sup> yr <sup>-1</sup>
H	10.0	500	340	N/A
C	7.5	350	560	N/A
cw	N/A	300	320	20
s	N/A	600	600	80
Heat exchanger	Overall heat transfer / kW m <sup>-2</sup> K <sup>-1</sup>			
1	1.5			
2	0.5			
3	1			
Heat exchanger	Area / m <sup>2</sup>	Costs / \$yr <sup>-1</sup>		
1,2, and 3	$0 < A \leq 10$	$2750A^{0.6} + 3000$		
	$10 \leq A \leq 25$	$1500A^{0.6} + 15000$		
	$25 \leq A \leq 50$	$600A^{0.6} + 46500$		

can be constructed [224]. The piecewise-defined function

$$\phi(x) = \begin{cases} \phi_1(x) & \text{if } x \leq x_1 \\ \phi_2(x) & \text{otherwise} \end{cases} \quad (5.4)$$

is reformulated as follows:

$$\phi(x) = \pi(x - x_1)\phi_2(x) + [1 - \pi(x - x_1)]\phi_1(x), \quad (5.5)$$

where

$$\pi(x) = \begin{cases} 0 & \text{if } x \leq 0 \\ 1 & \text{otherwise.} \end{cases} \quad (5.6)$$

The problem size and numerical results for each problem formulation (see Appendix Section E for each formulation) are summarized in Tab. 5.6. For both global solvers, default settings are used.

The key findings from the previous case studies are confirmed by this discontinuous optimization problem. The RS formulations always result in shorter overall optimization times mainly resulting from the reduced problem size. The negative effect of the elimination of optimization variables on the tightness of the root node relaxation is particularly pronounced for this case study. However, for Problem (HEXBM), (HEXCH), and (HEXMINLP), this has only a minor negative influence on the number of BaB nodes required. For the other problems, the number of BaB nodes does even decrease much likely due to a more directed branching. Despite the lowest LB in the root node of Problem (HEXMINLP), it requires the fewest BaB nodes and thus outperforms the Big-M and Convex Hull formulation for the RS formulation in this case study.

Reformulation approaches avoiding the introduction of binary variables and thus leading to NLP problems (Problem (HEXMPEC), (HEXPLUSF), and (HEXStepF)) do not benefit

**Table 5.6.:** Problem size and numerical results for Problem (HEXGDP) with problems formulations presented in Section 5.2 and the Step Formulation. The optimization has been executed 100 times, of which the arithmetic mean value is shown. The optimal value is 114,385. No results are given for the RS (AVM/McCormick hybrid) Step Formulation, as it does not contain repeated nonlinear terms that could be replaced by AVs.

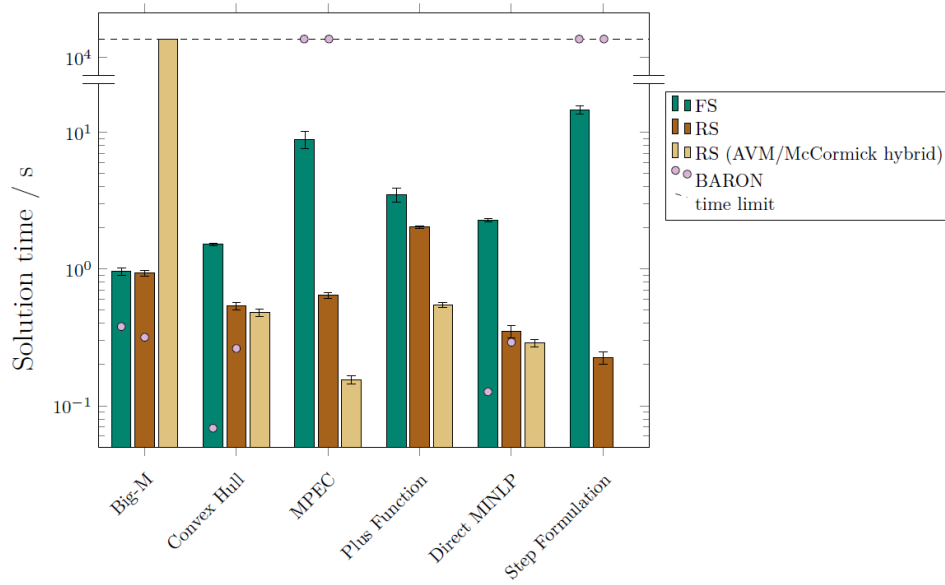
	Big-M (HEXBM)			Convex Hull (HEXCH)			MPEC (HEXMPEC)		
	FS	RS	RS (hybrid)	FS	RS	RS (hybrid)	FS	RS	RS (hybrid)
Number of									
Continuous variables	14	9	9	50	9	9	14	9	9
Discrete variables	9	6	6	9	6	6	0	0	0
Equality constraints	7	2	2	19	2	2	10	5	5
Inequality constraints	72	58	58	72	25	25	0	0	0
BaB nodes	47	138	32,000,000	63	87	47	5,728	593	111
Lower bound of root node	500	-221,505	-120,625	15,952	-230,505	-130,549	19,534	-230,505	-230,505
CPU time per BaB node / s	0.02	0.007	0.003	0.024	0.006	0.012	0.002	0.001	0.001
Solution time / s	0.958	0.931	86,400	1.513	0.535	0.48	8.896	0.643	0.156

	Plus Function (HEXPLUSF)			Direct MINLP (HEXMINLP)			Step Formulation (HEXStepF)	
	FS	RS	RS (hybrid)	FS	RS	RS (hybrid)	FS	RS
Number of								
Continuous variables	14	9	9	14	9	9	8	3
Discrete variables	0	0	0	9	6	6	0	0
Equality constraints	10	5	5	10	2	2	7	2
Inequality constraints	0	0	0	0	3	3	0	0
BaB nodes	1,838	1,721	271	19	61	27	11,774	187
Lower bound of root node	19,534	-230,505	-230,505	2,388	-300,115	-83,131	1,404	-189,277
CPU time per BaB node / s	0.002	0.001	0.002	0.12	0.006	0.011	0.001	0.001
Solution time / s	3.51	2.024	0.55	2.281	0.35	0.287	14.643	0.224

in the FS formulation from their smaller problem size. Their subproblems are solved quickly, but a high number of BaB nodes is required despite yielding the tightest relaxations in the root node among all formulations. Moving to RS formulations reduces solution time considerably as significantly fewer BaB nodes are required. Since relaxations can never be tighter in RS than corresponding FS formulations, the reduced number of BaB nodes can mainly be attributed to a more directed branching. The combination of a more directed branching with a small problem size resulting from RS formulations for the reformulation approaches introducing additional nonconvexities yield the lowest computational effort. Also the overall trend, BARON performing better than MAiNGO for the conventional reformulations approaches and MAiNGO generally performing better than BARON for the unconventional approaches in the RS formulations (except for the MINLP formulation), is confirmed by this heat exchanger network design problem.

We have demonstrated that RS formulations have the big advantage of a smaller problem size and a more directed branching, while they suffer from weaker relaxations than FS formulations. To combine the advantage of a small problem size from the RS formulations with the relaxation tightness of the FS formulations, we can selectively consider AVs for repeated nonlinear terms, thus achieving a hybrid [189] between McCormick relaxations and the AVM. Such a hybrid can be easily considered by MAiNGO using its automated identification and replacement of repeated nonlinear terms with AVs. In general, it is



**Figure 5.7.:** Solution time for Problem (HEXGDP) using the problem formulations presented in Section 5.2 and the Step Formulation. As BARON can not handle *max*-functions, there are no results for the Plus Function formulation. The solution times of the optimization with BARON and the MPEC and Step Formulation exceed the maximum solution time of 86400 s. No results are given for the RS (AVM/McCormick hybrid) Step Formulation, as it does not contain repeated nonlinear terms that could be replaced by AVs. The error bars represent the standard deviation from the arithmetic mean value of the solution time from 100 optimization runs using MAiNGO.

much more likely for RS than FS formulations to contain these repeated nonlinear terms (see Bongartz [215], p.64ff.). In fact, for the heat exchanger network design problem, only the RS formulations contain repeated nonlinear terms. As illustrated in Tab. 5.6 and Fig. 5.7, the selected addition of AVs is beneficial especially for the complementarity-constrained problems (HEXMPEC) and (HEXPLUSF) despite an unchanged LB in the root node. However, the number of BaB nodes reduces considerably while the CPU time per BaB node remains about the same. In contrast, for the other problem formulations (except Problem (HEXBM)) the subproblems seem to become more difficult to solve, such that the benefit of the tighter relaxations resulting from adding selected AVs is almost outweighed. Problem (HEXStepF) does not exhibit repeated nonlinear terms in both the FS and RS formulations. The analysis shows: The consideration of selected AVs within the RS formulations has the potential to improve computational effort even further.

## 5.5. Conclusion

Superstructure optimization problems for process synthesis often contain nonconvex functions resulting in nonconvex MINLP problems, for which global solvers need to be used. Although the same problem formulations as those developed for superstructure optimization problems with only convex functions can be used, it remains unclear whether these are always the most computationally efficient ones for problems with nonconvex functions. In particular, for problems with only convex functions, preference is usually given to formulations such as Big-M or Convex Hull that avoid introducing nonconvexities, thus resulting in a convex MINLP or even MILP. We conjectured that for problems that contain nonconvex functions anyway, alternative formulations that do introduce additional nonconvexities but may result in smaller problems or allow tighter relaxations could be promising.

Our analysis shows that for problems containing nonconvex functions anyway, these additional nonconvexities do not necessarily have a considerable negative influence on the optimization. The resulting relaxations often seem to remain comparably tight despite these additional nonconvexities and the corresponding problem formulations contain fewer variables than the conventional formulations. Accordingly, the alternative formulations result in similar or even lower computational time than the conventional ones for most considered examples. As an additional approach to reduce problem size, we exploited reduced-space (RS) formulations, where we eliminate as many optimization variables as possible using the model equations. Despite weaker relaxations, the smaller problem size of RS formulations is beneficial for all problem formulations for the considered case studies.

The comparison of the results obtained with our open-source solver MAiNGO with those obtained with the state-of-the-art commercial solver BARON shows that neither the auxiliary variable method (AVM) employed in BARON, nor the propagation of McCormick relaxations employed in MAiNGO suffers significantly from the additional nonconvex terms resulting from the unconventional problem reformulation approaches. Yet, the reduction of the problem size in the RS formulations can be exploited more effectively by MAiNGO, resulting in the lowest overall solution times observed for the illustrative example problems. For the conventional reformulation approaches, BARON generally outperforms MAiNGO.

We have extended the comparison of model formulations by also considering a problem with piecewise-defined functions instead of unit selections, which can be formulated as a superstructure optimization problem. For this problem, the RS formulation for all refor-

mulation approaches was again computationally more efficient than the FS formulation. A formulation that directly treated the discontinuous function with the help of step functions was particularly advantageous.

In summary, the unconventional reformulation approaches, which introduce nonconvex terms, are promising for nonconvex superstructure optimization problems, especially when combined with RS formulations. Bearing in mind that modeling using these approaches is rather intuitive and the resulting models simple, they represent an interesting alternative to established approaches such as the Big-M and Convex Hull method. To further validate this claim, a benchmark library with more complex superstructure optimization problems is required for such comparative analyses in future studies. In this work, only a few simple flowsheet optimization problems have been considered, as each problem formulation needed to be implemented manually for all reformulation approaches and for both the FS and RS formulation individually. To overcome the considerable manual effort and benefit from a flexible application of different reformulation approaches given specific problem characteristics, the automated generation of problem formulations (in the vein of, e.g., the open-source Python package for component-oriented modeling and optimization for nonlinear design and operation of integrated energy systems COMANDO [240], the Pyomo.GDP package [241] that allows automated reformulation and solution of GDPs, or the Pyosyn framework [242] for superstructure modeling) based on a GDP problem would be beneficial.





---

## 6. Conclusion and Outlook

The urgent need to introduce renewable energy sources into all sectors requires processes that efficiently convert renewable electricity into liquid energy carriers. In this thesis, optimization-based methods were proposed that enable the systematic identification and design of these *Power-to-X* processes with the goal of maximizing their resource-efficiency. To demonstrate the capabilities of these methods, they were applied to the production of dimethoxymethane (DMM)—a promising synthetic fuel candidate and intermediate for oxymethylene ether (OME<sub>3-5</sub>) production.

Power-to-X processes are processes that either need to be operated flexibly (*demand side management*), need to temporarily store renewable electricity in a flexible but efficient way (*e-storage*), or need to be able to utilize raw materials that fundamentally differ from fossil-based ones to produce certain products (*e-production*). For e-production, we have shown that the sole replacement of fossil-based raw materials with those from renewable sources is not useful. Although many industrial processes are optimized to a high degree regarding energy efficiency (in terms of utility demand), they often rely on reactions that do not enable a resource-efficient conversion of their raw materials.

Established process concepts for both DMM and OME<sub>3-5</sub> production are rather resource-inefficient. The replacement of fossil-based methanol with such produced from renewable sources requires great amounts of hydrogen (H<sub>2</sub>), which is produced from renewable electricity following the Power-to-X concept. Our analysis with detailed process models showed that major exergy losses are caused by the unfavorable reaction pathway for FA production. The underlying partial oxidation of methanol converts valuable H<sub>2</sub> to water, which increases net H<sub>2</sub> demand for DMM production. Also the established pathway for DMM production itself causes unavoidable exergy losses due to significant amounts of water produced as a by-product. As these two processes constitute intermediate process steps for OME<sub>3-5</sub> production using established process concepts, the same significant exergy losses are present therein. Even more significant are exergy losses caused by the enormous heat demand for trioxane purification, which can not be reduced significantly by a more efficient heat integration. These inherent process inefficiencies make both DMM and OME<sub>3-5</sub> production by simply replacing fossil-based raw materials with renewable ones not being suitable for Power-to-X processes. Therefore, fundamentally new processes based on more resource-efficient reaction pathways need to be developed. As corresponding pathways from the open literature are on a very different stage of development and therefore difficult to compare in a fair way, we developed a hierarchical process development and evaluation methodology. The integration of optimization-based methods geared to the level of detail of the hierarchy levels enables a systematic design of process candidates. In this regard, five different reaction pathways for DMM production were considered, of which three were found to be potentially more resource-efficient than the established pathway. Intermediate-fidelity models and rigorous process models were used for optimization-based process design to obtain a more realistic estimate for their performance. Process evaluation on each level regarding production costs, exergy efficiency, and global warming impact

identified the direct reduction of carbon dioxide ( $\text{CO}_2$ ) to be most suitable for sustainable DMM production at its current state.

For a more reliable process design—which constitutes a fundamental part in the development and successful implementation of Power-to-X processes—more detailed process models need to be developed. In case of DMM production via the reductive pathway, the reactor model needed to be refined as the thermodynamic model (NRTL) used for preceding analyses allows only approximate calculations. The high reactor pressure required for a sufficient solubility of  $\text{H}_2$  and  $\text{CO}_2$  in methanol and their complex molecular interactions make the application of the perturbed-chain polar statistical associating fluid theory equation of state (PCP-SAFT EOS) indispensable. As a corresponding process model contains nonconvex functions—as most models for Power-to-X processes do—deterministic global optimization is required to find the most promising process design. However, complicated thermodynamic models often make optimization computationally intractable and so does the PCP-SAFT EOS for the reductive DMM production process. To still benefit from both the high accuracy of the model and the great potential of optimization-based methods, we developed a hybrid process model. Gaussian processes and artificial neural networks sufficiently approximate such mechanistic process models that are otherwise too complicated for deterministic global optimization. As these data-driven models introduce many additional optimization variables, optimization with state-of-the-art deterministic global solvers is challenging—and often not possible in the first place. The reduced-space problem formulation of our open-source deterministic global solver MAiNGO reduces the size of the optimization problem significantly. In combination with a hybrid of the McCormick and the auxiliary variable method, global process optimization for reductive DMM production eventually converged to its global optimum.

As process synthesis problems often contain discrete decisions, such as the choice of the least energy-intensive distillation column sequence in reductive DMM production, mixed-integer nonlinear programming (MINLP) problem formulations suitable for global optimization are required. Whereas the Big-M and the Convex Hull method are the most powerful ones for mixed-integer linear programming (MILP) problems and MINLP problems containing only convex functions, they are not necessarily the most powerful options for those MINLP problems that contain nonconvex functions. In this regard, we have shown for a few simple example problems that problem formulations with a small number of optimization variables can be computationally more efficient than conventional approaches. Although these unconventional approaches introduce nonconvex terms additionally to those that are inherently part of the process model (e.g., by the multiplication of binary and continuous variables, complementarity constraints, step functions), relaxations remain comparably tight. Although their combination with the reduced-space formulation in MAiNGO weakens relaxations significantly, solution time was most often smaller due to their much smaller problem size. The potential of these unconventional problem formulations were confirmed by the process optimization for reductive DMM production. The multiplication of binary with continuous variables to enable the choice between two distillation configurations was found to be computationally less demanding than the solution of the two separate nonlinear programming (NLP) problems.

The integration of the globally optimal process for reductive DMM production in its entire process chain from renewable  $\text{H}_2$  and  $\text{CO}_2$  has demonstrated its potential as a Power-to-X process to increase resource-efficiency significantly. Especially for  $\text{OME}_{3-5}$  production, improvements of up to 20 percentage points can be expected. However, before

---

these advanced process concepts can be considered for large-scale DMM and OME<sub>3-5</sub> production, further actions need to be taken.

For the evaluation of the OME<sub>3-5</sub> process chain incorporating reductive DMM production, both the intermediate process step for gaseous FA production and the final process step for OME<sub>3-5</sub> production from gaseous FA and DMM are on a very early stage of development, for which only simplified process models have been developed in this work. The improvement potential of 20 percentage points for OME<sub>3-5</sub> production need to be therefore seen with caution as the models used for evaluating the process chain incorporating established process concepts only are more detailed. For FA production via methanol dehydrogenation, a special focus should be placed on incorporating the effects of catalyst deactivation into the respective process model as this was found to be a fundamental issue in lab-scale experiments. Also the gas separation for FA purification and H<sub>2</sub> recycling—the key advantage of this process concept—need to be considered in further detail. Regarding the process step for OME<sub>3-5</sub> production from gaseous FA and DMM, a special focus should be placed on the reactor model as a liquid-liquid-phase reaction system was used for corresponding experiments [29]. However, the separation of the two phases was reported to be simple without a significant solubility between phases. In contrast, the process model developed in this work for reductive DMM production for a system with an immobilized catalyst is detailed enough to predict process performance rather accurately. The calculated reaction equilibrium is in good agreement with experimental results from the open literature, even if only for a homogeneously catalyzed system. The ruthenium-based catalyst has not been immobilized so far, which should be investigated in future work. A major weakness of the reductive pathway for DMM production is the rather low equilibrium conversion at high pressures resulting in a comparably high energy demand for DMM purification. To shift equilibrium to the products' side, a multi-phase reaction system for in-situ product removal from the reaction phase as well as for an increased solubility of the gaseous educts is being investigated in ongoing research.

In addition to further improvement potential on the application side, some further improvements on the methods side were identified. To obtain an even more holistic comparison of different process candidates, additional evaluation metrics such as operational safety and environmental aspects other than carbon footprint can be incorporated into the hierarchical process development and evaluation methodology. This may be realized by embedding further optimization-based methods into the methodology. However, computational tractability must be ensured. To obtain computational tractability for the deterministic global optimization of the overall process for reductive DMM production, simple Underwood equations had to be used to estimate the minimum energy demand of distillation columns. Although the final total exergy demand does not differ much from that derived from detailed tray-to-tray models, the heat demand of some individual columns differs significantly. For nonideal systems, a more accurate distillation model suitable for deterministic global optimization is therefore desirable. In this regard, pinch-based methods offer an attractive trade-off between accuracy, general validity, and computational effort [243]. However, their implicit character potentially incorporating complicated algorithms (e.g., homotopy continuation approach [244]) make their application for deterministic optimization challenging. A related weakness identified by the global optimization of the DMM production process was the approximate consideration of heat integration by a simple summation of the processes' exergy flows. As shown by the subsequent pinch-

based heat integration (representing an optimistic estimate for heat integration) within the entire process for DMM production from  $\text{H}_2$  and  $\text{CO}_2$ , a simple summation of exergy flows can lead to an overestimated potential for heat integration. Instead, an integrated pinch-analysis or a simple matching of heat streams respecting a predefined minimum temperature difference should be considered. The latter could be realized by superstructure optimization using the MINLP problem formulations identified as suitable for global superstructure optimization in this work. Although the high computational performance of those MINLP problem formulations that reduce the number of optimization variables but introduce nonconvex terms could be confirmed by three example problems, a generally valid conclusion can not be drawn from this study. For a more conclusive statement, the different MINLP problem formulations should be tested on a large set of benchmark problems with different complexity. For this, an automated generation of the different problem formulations would be necessary. An even more fundamental question that has not been answered so far is for which cases it is worth to consider superstructure optimization over simple enumeration in the first place. This question might be relatively simple to answer for MILP problems that are so large that they rely on the fathoming of branching trees. For large MINLP problems incorporating nonconvex functions, the answer to this question is not obvious as the deterministic global optimization of their separate NLPs is already challenging. However, if the process model and the solution algorithm are geared to each other, the MINLP program can be computationally less demanding than the separate NLPs, as demonstrated by the global process optimization for reductive DMM production in this work. For deriving generally valid statements, each superstructure problem formulation need to be analyzed in even greater detail, or they need to be applied to a larger set of benchmark problems—ideally both.

If these open questions, both on the application as well as on the methods side, can be addressed adequately, highly resource-efficient Power-to-X processes can be designed and in turn more energy from renewable sources can be made accessible for sectors that can not be electrified directly.

---

## Appendix A.

# Reaction Kinetic Parameters for OME<sub>3-5</sub> Formation

For the simulations of the OME<sub>3-5</sub> process step, the pseudohomogeneous model developed by Burger et al. [88] is used. Corresponding parameters for the temperature dependent bulk equilibrium constants are given in Table A.1 and rate constants are given in Table A.2. The latter have been adjusted in such a way that they meet the unit requirements of Aspen Plus<sup>®</sup> using a catalyst capacity for Amberlyst46 of 0.43 mol H<sup>+</sup>/kg<sub>cat</sub> given by Rohm and Haas Company [245]. Additionally, a kinetic factor of 1366 is added to the reaction rate of Reaction (R2) in order to fit the model to the optimal operating point found by Burger et al. [90]. The original parameters derived for the pseudohomogeneous model are only valid for the operating point of the experiment, but not applicable to arbitrary feed compositions (cf., Burger et al. [88]). The Aspen Plus<sup>®</sup> models are available via our homepage[55].

**Table A.1.:** Mole fraction-based parameters for the equilibrium constant  $\ln(K_j) = a_j + b_j/T$  of the reaction system of OME<sub>n</sub> production after Burger et al. [88]

Reaction j	$a_j$ [-]	$b_j$ [K]
(R15)	0.3221	1292
(R16)	-1.7759	-2986

**Table A.2.:** Mole fraction-based parameters for the forward reaction rate constant  $\ln(k_j^f/(\text{kmol}/\text{kg}_{\text{cat}}\text{s})) = a_j^f + b_j^f/T$  of the reaction system of OME<sub>n</sub> production based on the work of Burger et al. [88]

Reaction j	$a_j^f$ [-]	$b_j^f$ [K]
(R15)	10.6683	0
(R16)	-9.0417	-1871.1
(R21)	7.5	-4916

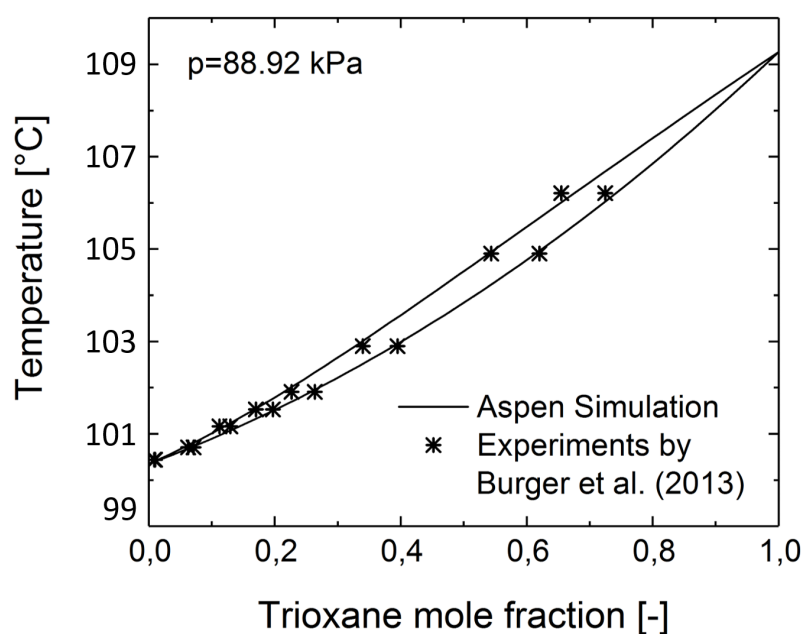


**Figure A.1.:** VLE of a system containing trioxane and  $\text{OME}_2$  at 88.92 kPa using NRTL parameters  $b_{ij} = -154.08$ ,  $b_{ji} = 332.95$ , and  $a_{ij} = a_{ji} = 0.3$ . Experimental data were taken from the work of Burger et al. [90]

# Appendix B.

## DMM Pathway Comparison

### Experimental Reaction Parameters

**Table B.1.:** Reaction parameters of the experiments with the highest reported yields for DMM synthesis via different routes. Abbreviations: VTiSi = silica-modified and titanium-oxide-supported vanadium oxide, Ru(triphos)(tmm) = triphos-based ruthenium catalyst, Cu/HB = HB zeolite with copper nanoparticles, Ir(DPEphos)(cod) = Bis[(2-diphenylphosphino)phenyl]ether-based iridium catalyst, Het. = Heterogeneous, Hom. = Homogeneous, conc. = concentration.

Parameter	Established [16, 45] (Reaction (R1))	Oxidative [31, 37] (Reaction (R5))	Reductive [38] (Reaction (R6))	Dehydrogenative [41] (Reaction (R8))	Transfer-hydrogenative [42] (Reaction (R9))
Catalyst [-]	Amberlyst 15	VTiSi	Ru(triphos)(tmm)	Cu/HB	Ir(DPEphos)(cod)
Phase [-]	Het.	Het.	Hom.	Het.	Hom.
Temperature [°C]	60	140	80	200	100
Pressure [bar]	2	1	80	1	20
Residence time [h]	0.2	N/A	18	N/A	18
GHSV [mL h <sup>-1</sup> g <sub>cat</sub> <sup>-1</sup> ]	N/A	12,000	N/A	14,549	N/A
Catalyst conc. [mmol L <sup>-1</sup> ]	N/A	N/A	12.5	N/A	0.25
Methanol conversion [%]	12.8	51.0	10.1	3.6	0.9
DMM selectivity [%]	99.9	99.0	81.8	80.3	98.2

## Thermodynamic Model Parameters

Pure component property data is taken from the Aspen Plus v11 databank APV110 PURE37. Parameters for the UNIFAC model for the established pathway are taken from Fredenslund et al. [47], Maurer [48], Hasse et al. [49], Hahnenstein et al. [50], Albert et al. [51, 52, 246], and Kuhnert et al. [131]. Parameters for the NRTL model for the direct pathways are given in Appendix Tab. B.2-B.4.

**Table B.2.:** NRTL parameter  $a_{ij}$  (Aspen Plus notation) for nonideal interactions within the multi-component system of the direct pathways. The remaining interactions are assumed to be ideal.

Component i	Component j					
	Water	DMM	MeOH	MF	DME	CO <sub>2</sub>
Water	N/A	0 <sup>a</sup>	2.7322 <sup>a</sup>	−91.5425 <sup>d</sup>	0.825228 <sup>b</sup>	10.064 <sup>e</sup>
DMM	0 <sup>a</sup>	N/A	0 <sup>a</sup>	−0.359076 <sup>d</sup>	0 <sup>c</sup>	0
MeOH	−0.693 <sup>a</sup>	0 <sup>a</sup>	N/A	0 <sup>a</sup>	8.0627 <sup>b</sup>	0
MF	−86.3908 <sup>d</sup>	0.224382 <sup>d</sup>	0 <sup>a</sup>	N/A	0.224382 <sup>g</sup>	0
DME	0.96683 <sup>b</sup>	0 <sup>c</sup>	−15.0667 <sup>b</sup>	−0.359076 <sup>g</sup>	N/A	0.394439 <sup>f</sup>
CO <sub>2</sub>	10.064 <sup>e</sup>	0	0	0	−0.44005 <sup>f</sup>	N/A

<sup>a</sup> From AspenPlus APV110 VLE-IG databank.

<sup>b</sup> From Dirk-Faitakis et al. [247].

<sup>c</sup> From Breitzkreuz et al. [248].

<sup>d</sup> From Deutz et al. [19].

<sup>e</sup> From AspenPlus APV110 ENRTL-RK databank.

<sup>f</sup> From NISTV84 NIST-HOC databank.

<sup>g</sup> In accordance to the assumptions in Breitzkreuz et al. [248].



**Table B.3.:** NRTL parameter  $b_{ij}$  (Aspen Plus notation) for nonideal interactions within the multi-component system of the direct pathways. The remaining interactions are assumed to be ideal.

Component i	Component j					
	Water	DMM	MeOH	MF	DME	CO <sub>2</sub>
Water	N/A	618.9311 <sup>a</sup>	-617.2687 <sup>a</sup>	13650 <sup>d</sup>	65.5774 <sup>b</sup>	-3268.135 <sup>e</sup>
DMM	491.2114 <sup>a</sup>	N/A	175.4218 <sup>a</sup>	100 <sup>d</sup>	0 <sup>c</sup>	0
MeOH	172.9871 <sup>a</sup>	303.1328 <sup>a</sup>	N/A	199.0137 <sup>a</sup>	-1659.63 <sup>b</sup>	0
MF	15500 <sup>d</sup>	0 <sup>d</sup>	217.046 <sup>a</sup>	N/A	0 <sup>g</sup>	0
DME	-39.5507 <sup>b</sup>	0 <sup>c</sup>	3836.09 <sup>b</sup>	100 <sup>g</sup>	N/A	0 <sup>f</sup>
CO <sub>2</sub>	-3268.135 <sup>e</sup>	0	0	0	0 <sup>f</sup>	N/A

<sup>a</sup> From AspenPlus APV110 VLE-IG databank.

<sup>b</sup> From Dirk-Faitakis et al. [247].

<sup>c</sup> From Breitzkreuz et al. [248].

<sup>d</sup> From Deutz et al. [19].

<sup>e</sup> From AspenPlus APV110 ENRTL-RK databank.

<sup>f</sup> From NISTV84 NIST-HOC databank.

<sup>g</sup> In accordance to the assumptions in Breitzkreuz et al. [248].

**Table B.4.:** NRTL parameter  $c_{ij}$  (Aspen Plus notation) for nonideal interactions within the multi-component system of the direct pathways. The remaining interactions are assumed to be ideal.

Component i	Component j					
	Water	DMM	MeOH	MF	DME	CO <sub>2</sub>
Water	N/A	0.3 <sup>a</sup>	0.3 <sup>a</sup>	0.383 <sup>d</sup>	-0.77735 <sup>b</sup>	0.2 <sup>e</sup>
DMM	0.3 <sup>a</sup>	N/A	0.3 <sup>a</sup>	0.3 <sup>d</sup>	0 <sup>c</sup>	0
MeOH	0.3 <sup>a</sup>	0.3 <sup>a</sup>	N/A	0.3 <sup>a</sup>	-0.12748 <sup>b</sup>	0
MF	0.383 <sup>d</sup>	0.3 <sup>d</sup>	0.3 <sup>a</sup>	N/A	0.3 <sup>g</sup>	0
DME	-0.77735 <sup>b</sup>	0 <sup>c</sup>	-0.12748 <sup>b</sup>	0.3 <sup>g</sup>	N/A	0.5 <sup>f</sup>
CO <sub>2</sub>	0.2 <sup>e</sup>	0	0	0	0.5 <sup>f</sup>	N/A

<sup>a</sup> From AspenPlus APV110 VLE-IG databank.

<sup>b</sup> From Dirk-Faitakis et al. [247].

<sup>c</sup> From Breitzkreuz et al. [248].

<sup>d</sup> Additionally,  $f_{\text{H}_2\text{O},\text{MF}} = 0.1613$  and  $f_{\text{MF},\text{H}_2\text{O}} = 0.1219$  need to be provided. From Deutz et al. [19].

<sup>e</sup> From AspenPlus APV110 ENRTL-RK databank.

<sup>f</sup> From NISTV84 NIST-HOC databank.

<sup>g</sup> In accordance to the assumptions in Breitzkreuz et al. [248].

# Model Equations and Assumptions for Pathway Evaluation

**Table B.5.:** Level-specific input data for DMM pathway evaluation.  $\dot{E}_{H_2}$ ,  $\dot{E}_{CO_2}$ ,  $\dot{E}_{DMM}$ , and  $\dot{E}_{side}$  is the DMM-specific thermomechanical and chemical (based on higher heating value) exergy content of  $H_2$ ,  $CO_2$ , DMM, and side products respectively;  $\dot{E}_Q$  is the DMM-specific exergy demand of the process ( $T_{ambient} = 298.15K$ );  $P_{feed}$  and  $P_{misc}$  is the DMM-specific electricity demand for feed compression and miscellaneous compression and pumping within the entire process, respectively;  $I_{H_2}$ ,  $I_{CO_2}$ ,  $I_{comb}$ ,  $I_{side}$ ,  $I_{steam}$ ,  $I_{coolant}$ ,  $I_{P,feed}$ , and  $I_{P,misc}$  is the impact on climate change contribution resulting from  $H_2$  supply,  $CO_2$  supply, fuel combustion, side product treatment, steam demand, cooling demand, feed compression, and miscellaneous compression and pumping, respectively;  $C_{H_2}$ ,  $C_{CO_2}$ ,  $C_{steam}$ ,  $C_{coolant}$ ,  $C_{P,feed}$ ,  $C_{P,misc}$ , and  $C_{inv}$  is the production cost contribution resulting from  $H_2$  supply,  $CO_2$  supply, steam demand, cooling demand, feed compression, miscellaneous compression and pumping, investment cost, and miscellaneous costs, respectively.

Level	Input variables															
	Efficiency								Impact on climate change				Cost			
	$E_{H_2}$	$E_{CO_2}$	$E_{DMM}$	$E_{side}$	$E_Q$	$P_{feed}$	$P_{misc}$	$I_{H_2}$	$I_{CO_2}$	$I_{comb}$	$I_{side}$	$I_{steam}$	$I_{coolant}$	$I_{P,feed}$	$I_{P,misc}$	$C_{H_2}$
1	X	X	X	X	X	X	X	X	X	X	X	X	X	X	X	X
2	X	X	X	X	X	X	X	X	X	X	X	X	X	X	X	X
3	X	X	X	X	X	X	X	X	X	X	X	X	X	X	X	X

The DMM-specific minimum raw material consumption  $m_{L1,i}$  on Level 1 is calculated according to Appendix Equation (B.1):

$$m_{L1,i} = \frac{|\nu_i|}{\nu_{DMM}} \frac{M_i}{M_{DMM}} \quad i \in \{H_2, CO_2\}, \quad (B.1)$$

with the stoichiometric coefficients of the overall reaction equation towards DMM,  $\nu_i$  and  $\nu_{DMM}$ , and the molar mass of component i and DMM,  $M_i$  and  $M_{DMM}$ , respectively.

## Exergy Efficiency

System exergy efficiency  $\eta_{S,l}$  is calculated by

$$\eta_{S,l} = \frac{\dot{E}_{\text{DMM}} + \dot{E}_{\text{side}} + \dot{E}_{\dot{Q}_{\text{out}}}}{m_{l,\text{H}_2} B_{\text{H}_2} + m_{l,\text{CO}_2} B_{\text{CO}_2} + \dot{E}_{\dot{Q}_{\text{in}}} + P_{\text{feed}} + P_{\text{misc}}} \quad l \in \{\text{L1}, \text{L2}, \text{L3}\}, \quad (\text{B.2})$$

where  $\dot{E}_{\text{DMM}}$  and  $\dot{E}_{\text{side}}$  is the DMM-specific thermomechanical and chemical (based on higher heating value) exergy content of DMM and side products, respectively;  $\dot{E}_{\dot{Q}_{\text{out}}}$  and  $\dot{E}_{\dot{Q}_{\text{in}}}$  is the DMM-specific exergy of excess heat and heat demand of the process, respectively ( $T_{\text{ambient}} = 298.15\text{K}$ );  $B_{\text{H}_2}$  and  $B_{\text{CO}_2}$  is the  $\text{H}_2$ - and  $\text{CO}_2$ -specific exergy demand for producing  $\text{H}_2$  and capturing  $\text{CO}_2$ , respectively;  $P_{\text{feed}}$  and  $P_{\text{misc}}$  is the DMM-specific electricity demand for feed compression and miscellaneous compression and pumping within the entire process, respectively.

## Sizing and Costing

The column diameter  $D_{\text{col}}$  is determined by the molar vapor flow  $\dot{V}$  such that tray flooding is prevented in the highest loaded column section. The column diameter  $D_{\text{col}}$  is calculated according to Appendix Equation (B.3):

$$D_{\text{col}} = \sqrt{\frac{1}{F_v(1-\phi)} \frac{4}{\pi} \frac{\dot{V}}{n_{\text{col}}} \sqrt{\frac{RT_{\text{top}}\bar{M}}{100p}}}, \quad (\text{B.3})$$

with F-factor  $F_v$ , relative free area on a tray  $\phi$ , number of parallel columns  $n_{\text{col}}$ , ideal gas constant  $R$ , column top temperature  $T_{\text{top}}$ , molar mass of the gaseous mixture  $\bar{M}$ , and column pressure  $p$ . The values for  $F_v$  and  $\phi$  are given in Appendix Tab. B.6.

The column height  $H_{\text{col}}$  is determined by the number of trays  $N_{\text{col}}$  found by deterministic optimization (simultaneous minimization of OPEX and CAPEX) according to Kossack et al. [140] and Kraemer et al. [137]. The column height  $H_{\text{col}}$  is calculated according to Appendix Equation (B.4):

$$H_{\text{col}} = N_{\text{col}} H_{\text{tray}} + \Delta H, \quad (\text{B.4})$$

with tray spacing  $H_{\text{tray}}$  and extra space  $\Delta H$  for the top and bottom of the column. The values for  $H_{\text{tray}}$  and  $\Delta H$  are given in Appendix Tab. B.6.

The size of reboiler/condenser heat exchange area  $A_{\text{R/C}}$  is calculated according to Appendix Equation (B.5):

$$A_{\text{R/C}} = \frac{\dot{Q}_{\text{R/C}}}{k_{\text{R/C}} T_{\text{log}}}, \quad (\text{B.5})$$

with heat demand  $\dot{Q}_{\text{R/C}}$  of the reboiler or condenser of the column, heat exchange coefficient  $k_{\text{R/C}}$ , and logarithmic mean temperature difference  $T_{\text{log}}$ . The values for  $k_{\text{R/C}}$  are given in Appendix Tab. B.6.

The reactor length  $L_{\text{reac}}$  and the diameter  $D_{\text{reac}}$  are determined by the volume flow  $\dot{V}_{\text{reac}}$  through a cylindrical reactor with volume  $V_{\text{reac}}$  and residence time  $\tau_{\text{reac}}$ . The Volume  $V_{\text{reac}}$  is calculated through the first equality in Appendix Equation (B.6) and the reactor length  $L_{\text{reac}}$  and the diameter  $D_{\text{reac}}$  through the second equality in Appendix Equation (B.6) and

Appendix Equation (B.7):

$$V_{\text{reac}} = \frac{\dot{V}_{\text{reac}} \tau_{\text{reac}}}{\epsilon} = \frac{\pi}{4} D_{\text{reac}}^2 L_{\text{reac}} \quad (\text{B.6})$$

$$\frac{L_{\text{reac}}}{D_{\text{reac}}} = 4, \quad (\text{B.7})$$

with bed voidage  $\epsilon$  given in Appendix Tab. B.6.

Investment costs for compressors and pumps are directly determined by their shaft power. [152]

**Table B.6.:** Parameters for column and reactor sizing.

Parameter	Unit	Value	Reference
$F_v$	$\text{kg}^{0.5} \text{m}^{-0.5} \text{s}^{-1}$	1.4	Peters and Timmerhaus [249]
$\phi$	—	0.15	Peters and Timmerhaus [249]
$H_{\text{tray}}$	m	0.5	Peters and Timmerhaus [249]
$\Delta H$	m	4	Peters and Timmerhaus [249]
$\epsilon$	—	0.5	
$k_R$	$\text{kW K}^{-1} \text{m}^{-2}$	0.568	Luyben [150]
$k_C$	$\text{kW K}^{-1} \text{m}^{-2}$	0.852	Luyben [150]

The costing of distillation columns, reactors, compressors, and pumps was performed according to the models provided by Guthrie [152]. All column, tray, and heat exchanger cost parameters are taken from the original model. A M&S Index value of 1473.3 (2010) is used. Economic parameters for CAPEX calculations are given in Appendix Tab. B.7.

Cost of Manufacturing (COM) is calculated according to the procedure given in Turton et al. [153] and can be estimated with Appendix Equation (B.8) [153]:

$$\text{COM} = 0.280\text{FCI} + 2.73C_{\text{OL}} + 1.23(C_{\text{UT}} + C_{\text{WT}} + C_{\text{RM}}), \quad (\text{B.8})$$

with fixed capital investment FCI, cost of operating labor  $C_{\text{OL}}$ , cost of utilities  $C_{\text{UT}}$ , cost of waste treatment  $C_{\text{WT}}$ , and cost of raw materials  $C_{\text{RM}}$ . Appendix Equation (B.8) is a summation of several cost positions with individual cost parameters listed in Turton et al. [153].

**Table B.7.:** Economic parameters for CAPEX calculations.

Parameter	Unit	Value
Plant capacity (w.r.t. DMM)	$\text{t a}^{-1}$	200000
Interest rate	%	6
Plant life time	a	10
Operating hours	$\text{hr a}^{-1}$	8000

---

## Mass and Energy Balances

**Table B.8.:** DMM-specific material input for each pathway and level.

Pathway	Mass [kg kg <sup>-1</sup> ]					
	H <sub>2</sub>			CO <sub>2</sub>		
	L1	L2	L3	L1	L2	L3
Established	0.238	0.264	0.265	1.735	1.923	1.925
Oxidative	0.238	0.253	0.254	1.735	1.840	1.851
Reductive	0.212	0.219		1.735	1.791	
Dehydrogenative	0.212	0.258		1.735	2.251	
Transfer-hydrogenative	0.212			1.735		

**Table B.9.:** DMM-specific material output for each pathway and level.

Pathway	Mass [kg kg <sup>-1</sup> ]								
	MF			DME			CO <sub>2</sub>		
	L1	L2	L3	L1	L2	L3	L1	L2	L3
Established	0.000	0.000	0.000	0.000	0.000	0.000	0.000	0.176	0.176
Oxidative	0.000	0.000	0.000	0.000	0.005	0.007	0.000	0.057	0.058
Reductive	0.000	0.000		0.000	0.000		0.000	0.042	
Dehydrogenative	0.000	0.255		0.000	0.025		0.000	0.078	
Transfer-hydrogenative	0.000			0.000			0.000		

**Table B.10.:** DMM-specific energy streams for each pathway and level. Negative values denote outgoing energy streams. Heat integration was performed via pinch analysis.

Pathway	Energy [MJ kg <sup>-1</sup> ]					
	Heat			Electricity		
	L1	L2	L3	L1	L2	L3
Established	0.000	2.101 (90 °C)	1.465 (80 °C)	0.000	1.148	1.421
Oxidative	0.000	1.545 (58 °C) −0.351 (−25 °C)	−0.161 (1 000 °C) −0.206 (−20 °C)	0.000	2.422	2.640
Reductive	0.000	10.949 (86 °C) 1.111 (64 °C)		0.000	1.079	
Dehydrogenative	0.000	23.590 (100 °C)		0.000	1.739	
Transfer-hydrogenative	0.000			0.000		

**Table B.11.:** Stoichiometric H<sub>2</sub> consumption for the synthesis of various e-fuels from H<sub>2</sub> and CO<sub>2</sub> relative to their heating values (both LHV and HHV). For DMM synthesis, the non-oxidative pathways are considered. The specific LHV and HHV of fossil diesel is 42.6 MJ kg<sup>-1</sup> and 45.6 MJ kg<sup>-1</sup>, respectively.

	Unit	DMM	Ethanol	Methanol	DME	Methane
Molar H <sub>2</sub> consumption	[mol mol <sup>-1</sup> ]	8	6	3	6	4
Molar mass	[g mol <sup>-1</sup> ]	76.1	46.1	32.0	46.1	16.0
Specific LHV	[MJ kg <sup>-1</sup> ]	23.3	26.7	19.9	28.9	50
Specific HHV	[MJ kg <sup>-1</sup> ]	25.7	29.7	23.0	31.7	55.5
Molar LHV	[MJ mol <sup>-1</sup> ]	1.77	1.23	0.64	1.33	0.80
Molar HHV	[MJ mol <sup>-1</sup> ]	1.96	1.37	0.74	1.46	0.89
H <sub>2</sub> consumption/LHV	[mol MJ <sup>-1</sup> ]	4.5	4.9	4.7	4.5	5.0
H <sub>2</sub> consumption/HHV	[mol MJ <sup>-1</sup> ]	4.1	4.4	4.1	4.1	4.5

## Production Cost

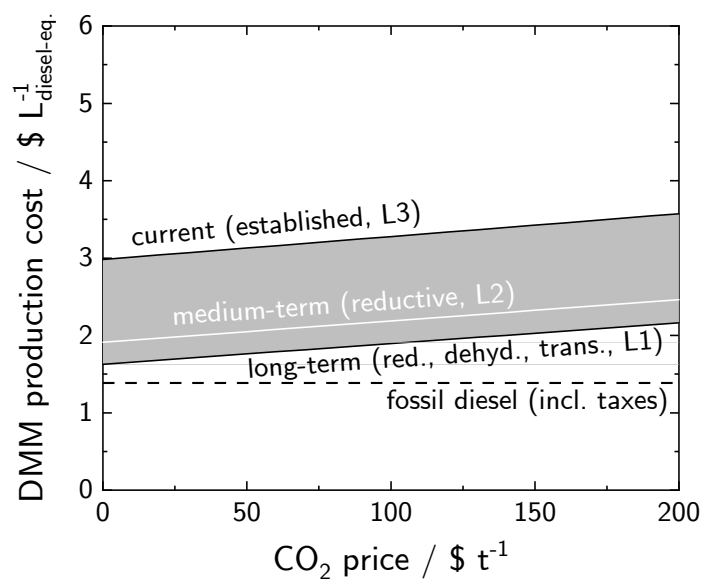


**Figure B.1.:** DMM production cost dependence on CO<sub>2</sub> price. The base case H<sub>2</sub> price is 5 \$ kg<sup>-1</sup>. [148]



**Table B.12.:** Operating (OPEX) and investment (CAPEX) cost for each pathway and level.

Category	Cost [M\$ a <sup>-1</sup> ]											
	Established			Oxidative			Reductive			Dehydrogenative		
	L1	L2	L3	L1	L2	L3	L1	L2	L3	L1	L2	L3
<b>OPEX</b>												
H <sub>2</sub>	262.23	296.62	314.06	262.23	310.02	307.31	235.67	273.34	235.67	349.06	235.67	235.67
CO <sub>2</sub>	239.04	264.97	265.34	239.04	253.54	253.57	212.48	219.92	212.48	259.06	212.48	212.48
Heating	23.19	25.71	25.75	23.19	24.60	24.61	23.19	23.94	23.19	30.10	23.19	23.19
Cooling		3.27	6.60		2.40	0		18.77		36.71		
Electricity		2.66	4.30		9.03	6.16		1.17		7.82		
<b>CAPEX</b>		10.15	12.08		21.42	22.98		9.54		15.38		
Columns			9.26			4.08						
Reactors			7.16			2.80						
Pumps			0.11			0.06						
Compressors			0.01			0.02						
			1.99			1.21						

**Table B.13.:** Cost of Manufacturing (COM) for the established and oxidative pathway on Level 3.

Category	Cost [M\$ a <sup>-1</sup> ]	
	Established pathway	Oxidative pathway
<b>Direct Manufacturing Costs (DMC)</b>	333.19	322.08
Raw materials ( $C_{RM}$ )	291.09	278.18
Waste treatment ( $C_{WT}$ )	0	0
Utilities ( $C_{UT}$ )	22.98	29.14
Operating labor ( $C_{OL}$ )	1.60	0.78
Direct supervisory and clerical labor	0.29	0.14
Maintenance and repairs	4.09	1.80
Operating supplies	0.61	0.27
Laboratory charges	0.24	0.17
Patents and royalties	12.29	11.66
<b>Fixed Manufacturing Costs (FMC)</b>	15.04	6.68
Depreciation	9.26	4.08
Local taxes and insurances	2.18	0.96
Plant overhead costs	3.59	1.63
<b>General Manufacturing Costs (GM)</b>	66.46	62.57
Administration costs	0.90	0.41
Distribution and selling costs	45.07	42.74
Research and development	20.49	19.43
<b>Total costs</b>	414.69	391.33
Total costs in [ $\$ L_{\text{diesel-eq.}}^{-1}$ ]	3.19	3.02

## Pathway Potential at Equilibrium Conditions

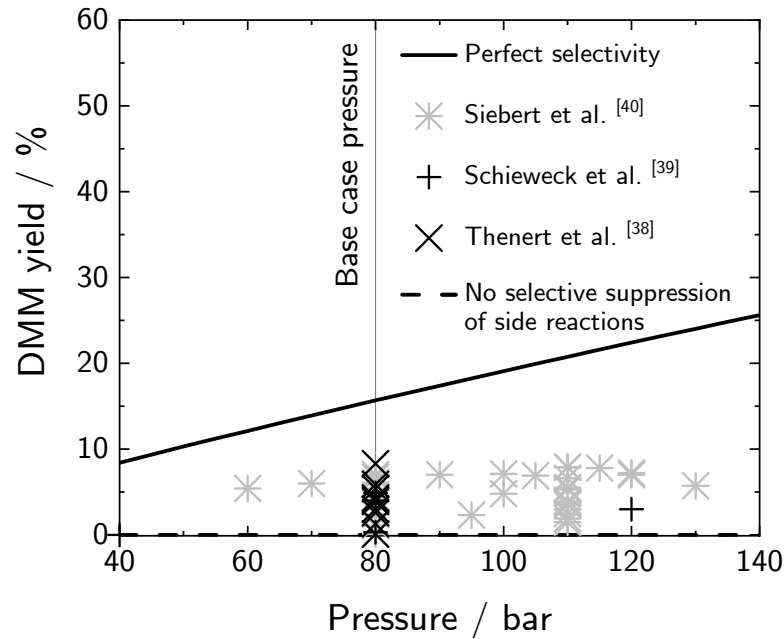


**Figure B.2.:** DMM yield dependence on reactor pressure for the reductive pathway (cf. Reaction (R6)). Restricted equilibrium conversion (considering perfect DMM selectivity) has been considered throughout the entire pressure range. Equilibrium conversion was calculated with an REquil reactor model in Aspen Plus v11. For the 'No selective suppression of side reactions' case additional DME and carbon monoxide (CO) formation was considered.

**Table B.14.:** DMM-specific material and energy balances for each pathway at equilibrium conversion and perfect selectivity on Level 2. Negative values denote outgoing energy streams. Heat integration was performed via pinch analysis.

Pathway	Mass [kg kg <sup>-1</sup> ]						Energy [MJ kg <sup>-1</sup> ]	
	Input			Output				
	H <sub>2</sub>	CO <sub>2</sub>	MF	DME	CO <sub>2</sub>	H <sub>2</sub> O	Heat	Electricity
Reductive	0.218	1.780	0.000	0.000	0.039	0.953	1.491 (100 °C) 0.802 (58 °C)	1.072
Dehydrogenative	0.223	1.819	0.001	0.000	0.057	0.968	5.823 (100 °C)	1.327
Transfer-hydrogenative without H <sub>2</sub> recycling	0.248	1.804	0.000	0.000	0.056	0.945	−1.256 (230 °C)	1.076
Transfer-hydrogenative with H <sub>2</sub> recycling	0.221	1.804	0.000	0.000	0.056	0.945	0.476 (78 °C) 9.764 (630 °C)	1.268
Transfer-hydrogenative with H <sub>2</sub> recycling at no cost	0.221	1.804	0.000	0.000	0.056	0.945	−1.256 (230 °C)	1.268

## Potential Pathway Improvements

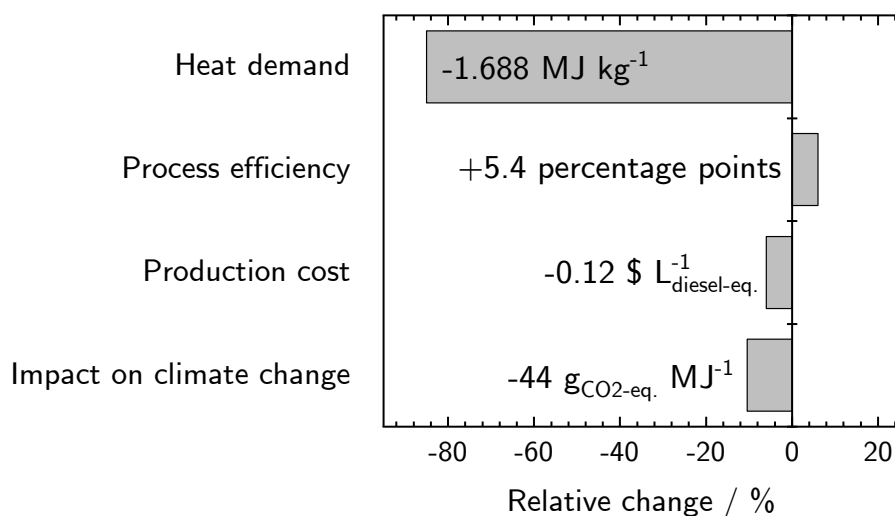


**Figure B.3.:** Potential improvements of the reductive pathway if restricted equilibrium methanol conversion (15.7 %) instead of experimental conversion (10.1 %) and perfect DMM selectivity instead of experimental selectivity (81.8 %) at a reaction temperature of 80 °C is assumed. The results on impact on climate change are given for the worst case scenario.

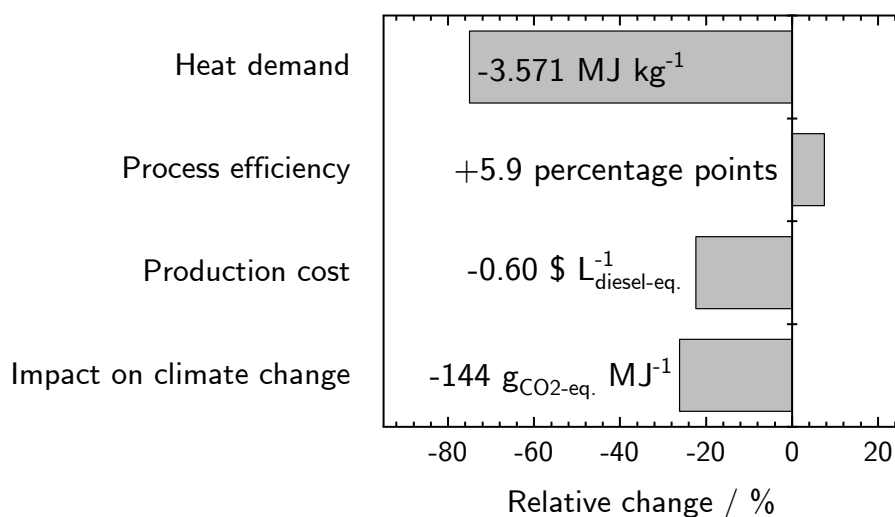
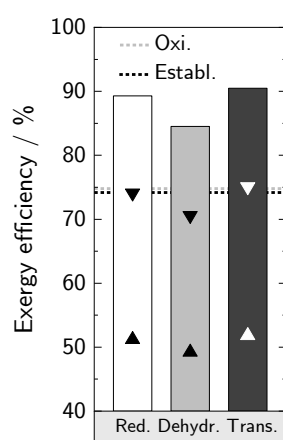
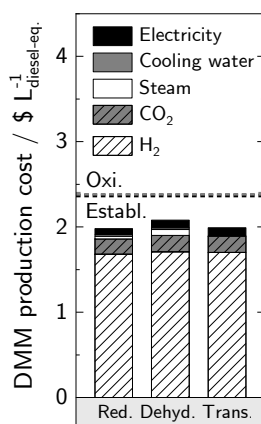


**Figure B.4.:** Potential improvements of the dehydrogenative pathway if restricted equilibrium methanol conversion (9.8 %) at 300 °C instead of the experimental conversion (3.6 %) at 200 °C and perfect DMM selectivity instead of experimental selectivity (80.3 %) is assumed. The results on impact on climate change are given for the worst case scenario.

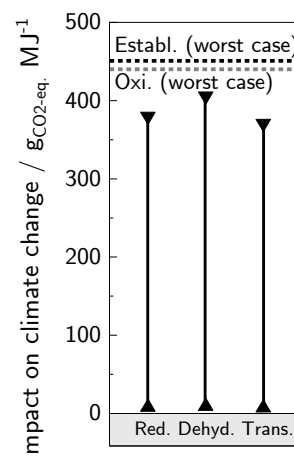
## Maximum Potential of Non-oxidative Pathways



**(a)** Exergy efficiency of the DMM synthesis routes from  $H_2$  and  $CO_2$  (bars) and for the entire system for the worst (▲) and best (▼) case scenario. The dashed lines correspond to the established and oxidative pathway evaluated on Level 2 considering actual reaction performance.



**(b)** Cost of DMM production. The dashed lines correspond to the established and oxidative pathway evaluated on Level 2 considering actual reaction performance.



**(c)** Impact of DMM on climate change for the worst (▼) and best (▲) case scenario. The dashed lines correspond to the worst case scenario for the established and oxidative pathway evaluated on Level 2 considering actual reaction performance.

**Figure B.5.:** Exergy efficiency (Appendix Fig. B.5a), production cost (Appendix Fig. B.5b), and impact on climate change (Appendix Fig. B.5c) for DMM production via the reductive, dehydrogenative, and transfer-hydrogenative synthesis route considering perfect selectivity and equilibrium conversion evaluated on Level 2. For the transfer-hydrogenation, EB dehydrogenation at no cost has been considered.

## Process Flowsheets

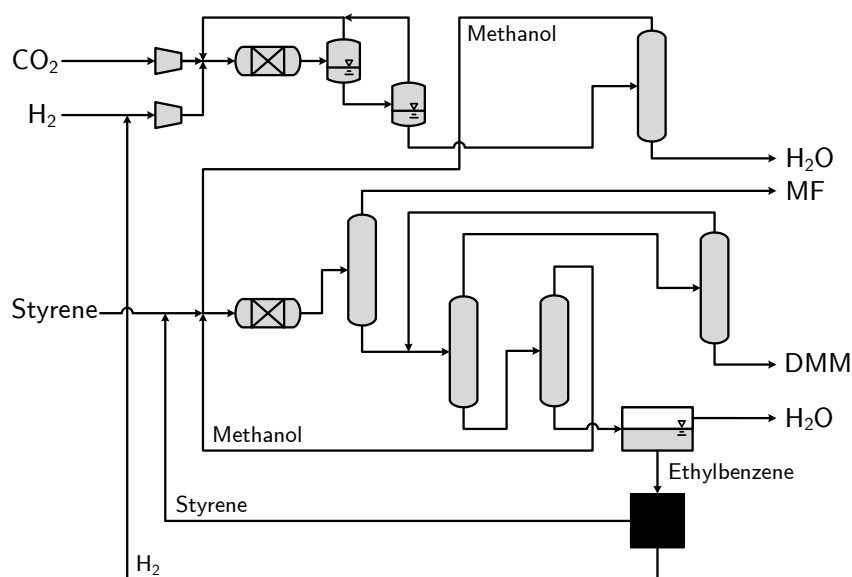


**Figure B.6.:** Process concept for the transfer-hydrogenative pathway on Level 2. All possible distillation sequences have been screened and the least energy-intensive sequence has been chosen. Styrene is added to the reactor in such a way that it is completely converted to EB and simultaneously consumes co-produced  $\text{H}_2$  completely. Modeling detail is identical to that of the alternative non-oxidative pathways with the process step for EB dehydrogenation as an exception. Ethylbenzene dehydrogenation is modeled as a black box with process parameters at equilibrium conditions from the literature [250].

---

## Appendix C.

# PCP-SAFT EOS Parameters and Sensitivity Analysis

### Pure Component Parameters

**Table C.1.:** Pure component parameters for the PCP-SAFT EOS.

	CO <sub>2</sub>	H <sub>2</sub>	Methanol	DMM	Water
$\epsilon/k$ / K	163.33	19.2775	161.9	231.26	366.51
$\sigma$ / Å	3.1869	2.986	2.456	3.3631	3.0007
$m$ / –	1.5131	1	3.4447	2.9218	1.0656
$\mu$ / D	0	0	1.6906	1.74	0
$Q$ / DÅ	4.4	0	0	0	0
$\epsilon^{A_i B_i}/k$ / K	-	-	1684.5	-	2500.7
$\kappa^{A_i B_i}$ / –	-	-	0.18195	-	0.034868
Number of H <sub>2</sub> bond acceptors	2	0	1	0	1
Number of H <sub>2</sub> bond donors	0	0	1	0	1
Reference	Gross [161]	Ghosh et al. [251]	Kozłowska et al. [252]	Pokorný et al. [253]	Gross and Sadowski [254]

### Sensitivity Analysis

In order to keep the optimization tractable, the molar gas-to-liquid ratio in the reactor and the ratio of H<sub>2</sub> to CO<sub>2</sub> in the gaseous reactor feed are kept constant. As demonstrated in Fig. C.1 and C.2, the two variables have only a minor impact on the reactor performance compared to the reactor pressure.

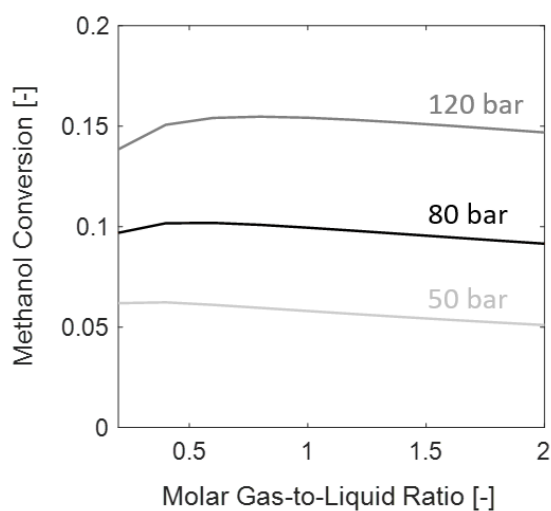


**Figure C.1.:** Methanol conversion in dependence on the molar gas-to-liquid ratio in the reactor.

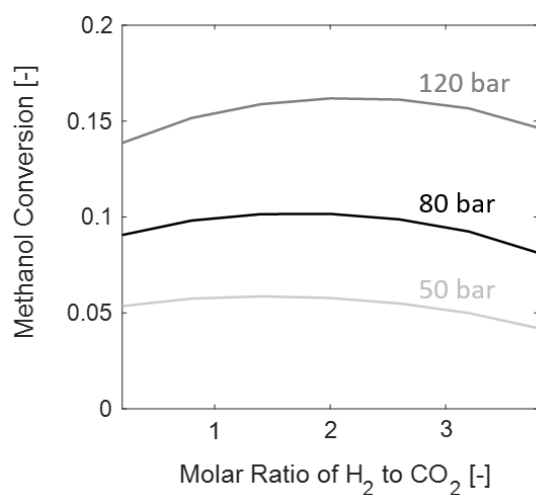


**Figure C.2.:** Methanol conversion in dependence on the molar ratio of  $H_2$  to  $CO_2$  in the gaseous reactor feed.



---

## Appendix D.

# Material Balances and Energy Demand of Process Chains via Reductive DMM Production

## DMM Production from H<sub>2</sub> and CO<sub>2</sub>

**Table D.1.:** DMM-specific material and energy balances for each process step within the process chain for DMM production from H<sub>2</sub> and CO<sub>2</sub>. Negative values denote outgoing streams. Heat integration was performed via pinch analysis. Only net heat demand is considered here.

Process step	Mass [kg kg <sup>-1</sup> ]					Energy [MJ kg <sup>-1</sup> ]		
	H <sub>2</sub>	CO <sub>2</sub>	MeOH	H <sub>2</sub> O	DMM	Heat	Coolant	Electricity
Methanol production	0.166	1.209	−0.850	−0.483	0	0	0	0.836
DMM production	0.054	0.800	0.850	−0.450	−1	0.189 (136 °C) 5.305 (84 °C) 1.034 (80 °C)	0.993 (−81 °C)	1.108

## OME<sub>3-5</sub> Production from H<sub>2</sub> and CO<sub>2</sub>

**Table D.2.:** OME<sub>3-5</sub>-specific material and energy balances for each process step within the process chain for OME<sub>3-5</sub> production from H<sub>2</sub> and CO<sub>2</sub> via the reductive production of DMM. Negative values denote outgoing streams. Heat integration was performed via pinch analysis. Only net heat demand is considered here. The small amounts of the side product carbon monoxide in the FA process step is not listed here.

Process step	Mass [kg kg <sup>-1</sup> ]							Energy [MJ kg <sup>-1</sup> ]		
	H <sub>2</sub>	CO <sub>2</sub>	MeOH	H <sub>2</sub> O	DMM	FA	OME <sub>3-5</sub>	Heat	Coolant	Electricity
MeOH production	0.201	1.465	-1.030	-0.586	0	0	0	0	0	1.014
DMM production	0.026	0.390	0.414	-0.219	-0.487	0	0	0.523 (136 °C) 1.550 (86 °C)	0.484 (-81 °C)	0.540
FA production	-0.042	-0.054	0.616	-0.004	0	-0.513	0	1.002 (80 °C) 1.944 (650 °C)	0	0.604
OME <sub>3-5</sub> production	0	0	0	0	0.487	0.513	-1	0.519 (250 °C)	0	0.001

---

## Appendix E.

# MINLP Problem Formulations for Superstructure Optimization

### Illustrative Example Problem with Linear Cost Functions

#### GDP

$$\begin{aligned} \min \quad & C = C_{\text{op}} + C_{\text{inv}} \\ \text{s.t.} \quad & \dot{n}_{\text{in}} = \dot{n}_{\text{in}}^{\text{P}} + \dot{n}_{\text{in}}^{\text{S}} \\ & \dot{n}_{\text{out}} = \dot{n}_{\text{out}}^{\text{P}} + \dot{n}_{\text{out}}^{\text{S}} \\ & \begin{bmatrix} Y_{\text{P}} \\ \dot{n}_{\text{in}}^{\text{S}} = \dot{n}_{\text{out}}^{\text{S}} = 0 \\ \dot{n}_{\text{out}}^{\text{P}} = \dot{n}_{\text{in}}^{\text{P}} \\ C_{\text{op}} = \dot{n}_{\text{in}}^{\text{P}} e_{\text{P}} \\ C_{\text{inv}} = C_{\text{P}} \end{bmatrix} \vee \begin{bmatrix} Y_{\text{S}} \\ \dot{n}_{\text{in}}^{\text{P}} = \dot{n}_{\text{out}}^{\text{P}} = 0 \\ \dot{n}_{\text{out}}^{\text{S}} = \dot{n}_{\text{in}}^{\text{S}} \\ C_{\text{op}} = \dot{n}_{\text{in}}^{\text{S}} e_{\text{S}} \\ C_{\text{inv}} = C_{\text{S}} \end{bmatrix} \quad (\text{GDP1lin}) \\ & Y_{\text{P}} \vee Y_{\text{S}} \\ & C_{\text{op}}, C_{\text{inv}}, \dot{n}_{\text{in}}, \dot{n}_{\text{in}}^{\text{P}}, \dot{n}_{\text{in}}^{\text{S}}, \dot{n}_{\text{out}}^{\text{P}}, \dot{n}_{\text{out}}^{\text{S}} \geq 0 \\ & C_{\text{op}}, C_{\text{inv}}, \dot{n}_{\text{in}}, \dot{n}_{\text{in}}^{\text{P}}, \dot{n}_{\text{in}}^{\text{S}}, \dot{n}_{\text{out}}^{\text{P}}, \dot{n}_{\text{out}}^{\text{S}} \in \mathbb{R} \\ & Y_{\text{P}}, Y_{\text{S}} \in \{\text{True}, \text{False}\} \end{aligned}$$

## BigM

$$\begin{aligned}
 \min \quad & C = C_{\text{op}} + C_{\text{inv}} \\
 \text{s.t.} \quad & \dot{n}_{\text{in}} = \dot{n}_{\text{in}}^{\text{P}} + \dot{n}_{\text{in}}^{\text{S}} \\
 & \dot{n}_{\text{out}} = \dot{n}_{\text{out}}^{\text{P}} + \dot{n}_{\text{out}}^{\text{S}} \\
 & 0 - M^{\text{P}}(1 - y_{\text{P}}) \leq \dot{n}_{\text{in}}^{\text{S}} \leq 0 + M^{\text{P}}(1 - y_{\text{P}}) \\
 & 0 - M^{\text{P}}(1 - y_{\text{P}}) \leq \dot{n}_{\text{out}}^{\text{S}} \leq 0 + M^{\text{P}}(1 - y_{\text{P}}) \\
 & \dot{n}_{\text{in}}^{\text{P}} - M^{\text{P}}(1 - y_{\text{P}}) \leq \dot{n}_{\text{out}}^{\text{P}} \leq \dot{n}_{\text{in}}^{\text{P}} + M^{\text{P}}(1 - y_{\text{P}}) \\
 & \dot{n}_{\text{in}}^{\text{P}} e_{\text{P}} - M^{\text{P}}(1 - y_{\text{P}}) \leq C_{\text{op}} \leq \dot{n}_{\text{in}}^{\text{P}} e_{\text{P}} + M^{\text{P}}(1 - y_{\text{P}}) \\
 & C_{\text{P}} - M^{\text{P}}(1 - y_{\text{P}}) \leq C_{\text{inv}} \leq C_{\text{P}} + M^{\text{P}}(1 - y_{\text{P}}) \\
 & 0 - M^{\text{S}}(1 - y_{\text{S}}) \leq \dot{n}_{\text{in}}^{\text{P}} \leq 0 + M^{\text{S}}(1 - y_{\text{S}}) \\
 & 0 - M^{\text{S}}(1 - y_{\text{S}}) \leq \dot{n}_{\text{out}}^{\text{P}} \leq 0 + M^{\text{S}}(1 - y_{\text{S}}) \\
 & \dot{n}_{\text{in}}^{\text{S}} - M^{\text{S}}(1 - y_{\text{S}}) \leq \dot{n}_{\text{out}}^{\text{S}} \leq \dot{n}_{\text{in}}^{\text{S}} + M^{\text{S}}(1 - y_{\text{S}}) \\
 & \dot{n}_{\text{in}}^{\text{S}} e_{\text{S}} - M^{\text{S}}(1 - y_{\text{S}}) \leq C_{\text{op}} \leq \dot{n}_{\text{in}}^{\text{S}} e_{\text{S}} + M^{\text{S}}(1 - y_{\text{S}}) \\
 & C_{\text{S}} - M^{\text{S}}(1 - y_{\text{S}}) \leq C_{\text{inv}} \leq C_{\text{S}} + M^{\text{S}}(1 - y_{\text{S}}) \\
 & y_{\text{P}} + y_{\text{S}} = 1 \\
 & C_{\text{op}}, C_{\text{inv}}, \dot{n}_{\text{in}}, \dot{n}_{\text{in}}^{\text{P}}, \dot{n}_{\text{in}}^{\text{S}}, \dot{n}_{\text{out}}^{\text{P}}, \dot{n}_{\text{out}}^{\text{S}} \geq 0 \\
 & C_{\text{op}}, C_{\text{inv}}, \dot{n}_{\text{in}}, \dot{n}_{\text{in}}^{\text{P}}, \dot{n}_{\text{in}}^{\text{S}}, \dot{n}_{\text{out}}^{\text{P}}, \dot{n}_{\text{out}}^{\text{S}} \in \mathbb{R} \\
 & y_{\text{P}}, y_{\text{S}} \in \{0, 1\}
 \end{aligned} \tag{BM1lin}$$

## Convex Hull

$$\begin{aligned}
\min \quad & C = C_{\text{op}} + C_{\text{inv}} \\
\text{s.t.} \quad & \dot{n}_{\text{in}} = \dot{n}_{\text{in}}^{\text{P}} + \dot{n}_{\text{in}}^{\text{S}} \\
& \dot{n}_{\text{out}} = \dot{n}_{\text{out}}^{\text{P}} + \dot{n}_{\text{out}}^{\text{S}} \\
& \dot{n}_{\text{in}}^j = \dot{n}_{\text{in},\text{P}}^j + \dot{n}_{\text{in},\text{S}}^j \quad j \in \{\text{P}, \text{S}\} \\
& \dot{n}_{\text{out}}^j = \dot{n}_{\text{out},\text{P}}^j + \dot{n}_{\text{out},\text{S}}^j \quad j \in \{\text{P}, \text{S}\} \\
& C_{\text{op}} = C_{\text{op}}^{\text{P}} + C_{\text{op}}^{\text{S}} \\
& C_{\text{inv}} = C_{\text{inv}}^{\text{P}} + C_{\text{inv}}^{\text{S}} \\
& \dot{n}_{\text{in},\text{P}}^{\text{S}} \leq 0 \\
& \dot{n}_{\text{out},\text{P}}^{\text{S}} \leq 0 \\
& \dot{n}_{\text{out},\text{P}}^{\text{P}} \leq \dot{n}_{\text{in},\text{P}}^{\text{P}} \\
& C_{\text{op}}^{\text{P}} \geq \dot{n}_{\text{in},\text{P}}^{\text{P}} e_{\text{P}} \\
& C_{\text{inv}}^{\text{P}} \geq C_{\text{P}} y_{\text{P}} \\
& \dot{n}_{\text{in},\text{S}}^{\text{P}} \leq 0 \\
& \dot{n}_{\text{out},\text{S}}^{\text{P}} \leq 0 \\
& \dot{n}_{\text{out},\text{S}}^{\text{S}} \leq \dot{n}_{\text{in},\text{S}}^{\text{S}} \\
& C_{\text{op}}^{\text{S}} \geq \dot{n}_{\text{in},\text{S}}^{\text{S}} e_{\text{S}} \\
& C_{\text{inv}}^{\text{S}} \geq C_{\text{S}} y_{\text{S}} \\
& y_{\text{P}} + y_{\text{S}} = 1 \tag{CH1lin} \\
& 0 \leq \dot{n}_{\text{in},\text{P}}^{\text{P}} \leq 1 y_{\text{P}} \\
& 0 \leq \dot{n}_{\text{in},\text{P}}^{\text{S}} \leq 1 y_{\text{P}} \\
& 0 \leq \dot{n}_{\text{out},\text{P}}^{\text{P}} \leq 1 y_{\text{P}} \\
& 0 \leq \dot{n}_{\text{out},\text{P}}^{\text{S}} \leq 1 y_{\text{P}} \\
& 0 \leq C_{\text{op}}^{\text{P}} \leq 20 y_{\text{P}} \\
& 0 \leq C_{\text{inv}}^{\text{P}} \leq 20 y_{\text{P}} \\
& 0 \leq \dot{n}_{\text{in},\text{S}}^{\text{P}} \leq 1 y_{\text{S}} \\
& 0 \leq \dot{n}_{\text{in},\text{S}}^{\text{S}} \leq 1 y_{\text{S}} \\
& 0 \leq \dot{n}_{\text{out},\text{S}}^{\text{P}} \leq 1 y_{\text{S}} \\
& 0 \leq \dot{n}_{\text{out},\text{S}}^{\text{S}} \leq 1 y_{\text{S}} \\
& 0 \leq C_{\text{op}}^{\text{S}} \leq 20 y_{\text{S}} \\
& 0 \leq C_{\text{inv}}^{\text{S}} \leq 20 y_{\text{S}} \\
& C_{\text{op}}, C_{\text{inv}}, \dot{n}_{\text{in}}, \dot{n}_{\text{in}}^{\text{P}}, \dot{n}_{\text{in}}^{\text{S}}, \dot{n}_{\text{out}}^{\text{P}}, \dot{n}_{\text{out}}^{\text{S}} \geq 0 \\
& C_{\text{op}}, C_{\text{inv}}, C_{\text{op}}^{\text{P}}, C_{\text{op}}^{\text{S}}, C_{\text{inv}}^{\text{P}}, C_{\text{inv}}^{\text{S}}, \dot{n}_{\text{in}}, \dot{n}_{\text{in}}^{\text{P}}, \dot{n}_{\text{in}}^{\text{S}}, \dot{n}_{\text{in},\text{P}}^{\text{P}}, \dot{n}_{\text{in},\text{P}}^{\text{S}}, \dot{n}_{\text{in},\text{S}}^{\text{P}}, \dot{n}_{\text{in},\text{S}}^{\text{S}} \in \mathbb{R} \\
& \dot{n}_{\text{out},\text{P}}^{\text{P}}, \dot{n}_{\text{out},\text{P}}^{\text{S}}, \dot{n}_{\text{out},\text{S}}^{\text{P}}, \dot{n}_{\text{out},\text{S}}^{\text{S}}, \dot{n}_{\text{out}}^{\text{P}}, \dot{n}_{\text{out}}^{\text{S}} \in \mathbb{R} \\
& y_{\text{P}}, y_{\text{S}} \in \{0, 1\}
\end{aligned}$$

## MPEC

$$\begin{aligned}
 \min \quad & C = C_{\text{op}} + C_{\text{inv}} \\
 \text{s.t.} \quad & \dot{n}_{\text{in}} = \dot{n}_{\text{in}}^{\text{P}} + \dot{n}_{\text{in}}^{\text{S}} \\
 & \dot{n}_{\text{out}}^j = \dot{n}_{\text{in}}^j \quad j \in \{\text{P}, \text{S}\} \\
 & \dot{n}_{\text{out}} = \dot{n}_{\text{out}}^{\text{P}} + \dot{n}_{\text{out}}^{\text{S}} \\
 & C_{\text{op}} = \sum_j \dot{n}_{\text{in}}^j e_j \\
 & C_{\text{inv}} = \sum_j \tanh(P \dot{n}_{\text{in}}^j) C_j \\
 & 0 = \dot{n}_{\text{in}}^{\text{P}} \dot{n}_{\text{in}}^{\text{S}} \\
 & C_{\text{op}}, C_{\text{inv}}, \dot{n}_{\text{in}}, \dot{n}_{\text{in}}^{\text{P}}, \dot{n}_{\text{in}}^{\text{S}}, \dot{n}_{\text{out}}^{\text{P}}, \dot{n}_{\text{out}}^{\text{S}} \geq 0 \\
 & C_{\text{op}}, C_{\text{inv}}, \dot{n}_{\text{in}}, \dot{n}_{\text{in}}^{\text{P}}, \dot{n}_{\text{in}}^{\text{S}}, \dot{n}_{\text{out}}^{\text{P}}, \dot{n}_{\text{out}}^{\text{S}} \in \mathbb{R}
 \end{aligned} \tag{MPEC1lin}$$

## Plus Function

$$\begin{aligned}
 \min \quad & C = C_{\text{op}} + C_{\text{inv}} \\
 \text{s.t.} \quad & \dot{n}_{\text{in}} = \dot{n}_{\text{in}}^{\text{P}} + \dot{n}_{\text{in}}^{\text{S}} \\
 & \dot{n}_{\text{out}}^j = \dot{n}_{\text{in}}^j \quad j \in \{\text{P}, \text{S}\} \\
 & \dot{n}_{\text{out}} = \dot{n}_{\text{out}}^{\text{P}} + \dot{n}_{\text{out}}^{\text{S}} \\
 & C_{\text{op}} = \sum_j \dot{n}_{\text{in}}^j e_j \\
 & C_{\text{inv}} = \sum_j \tanh(P \dot{n}_{\text{in}}^j) C_j \\
 & 0 = \dot{n}_{\text{in}}^{\text{P}} - \max(0, \dot{n}_{\text{in}}^{\text{P}} - \dot{n}_{\text{in}}^{\text{S}}) \\
 & C_{\text{op}}, C_{\text{inv}}, \dot{n}_{\text{in}}, \dot{n}_{\text{in}}^{\text{P}}, \dot{n}_{\text{in}}^{\text{S}}, \dot{n}_{\text{out}}^{\text{P}}, \dot{n}_{\text{out}}^{\text{S}} \geq 0 \\
 & C_{\text{op}}, C_{\text{inv}}, \dot{n}_{\text{in}}, \dot{n}_{\text{in}}^{\text{P}}, \dot{n}_{\text{in}}^{\text{S}}, \dot{n}_{\text{out}}^{\text{P}}, \dot{n}_{\text{out}}^{\text{S}} \in \mathbb{R}
 \end{aligned} \tag{PLUS1lin}$$

## Direct MINLP

$$\begin{aligned}
\min \quad & C = C_{\text{op}} + C_{\text{inv}} \\
\text{s.t.} \quad & C_{\text{op}} = \sum_j \dot{n}_{\text{in}}^j e_j \\
& C_{\text{inv}} = \sum_j y_j C_j \\
& \dot{n}_{\text{in}}^j = y_j \dot{n}_{\text{in}} \quad j \in \{P, S\} \\
& \dot{n}_{\text{out}}^j = \dot{n}_{\text{in}}^j \quad j \in \{P, S\} \\
& \dot{n}_{\text{out}} = \dot{n}_{\text{out}}^P + \dot{n}_{\text{out}}^S \\
& y_P + y_S = 1 \\
& C_{\text{op}}, C_{\text{inv}}, \dot{n}_{\text{in}}, \dot{n}_{\text{in}}^P, \dot{n}_{\text{in}}^S, \dot{n}_{\text{out}}^P, \dot{n}_{\text{out}}^S \geq 0 \\
& C_{\text{op}}, C_{\text{inv}}, \dot{n}_{\text{in}}, \dot{n}_{\text{in}}^P, \dot{n}_{\text{in}}^S, \dot{n}_{\text{out}}^P, \dot{n}_{\text{out}}^S \in \mathbb{R} \\
& y_j \in \{0, 1\} \quad j \in \{P, S\}
\end{aligned} \tag{MINLP1lin}$$

## Results

The optimal objective value is 10 ( $C_{\text{op}} = 3$ ,  $C_{\text{inv}} = 7$ ). In this case, Unit S is chosen. The numerical results for each problem formulation are summarized in Tab. E.1. Only for Problem (MINLP1lin), (PLUS1lin), and (MPEC1lin), nonlinear terms are present such that the global solver needs to be called. In these cases, the optimization for the RS formulations benefits from the reduced problem size, which is reflected by the decreased solution time. The consumed time per iteration is reduced and only a moderate increase in number of iterations (Problem (MPEC1lin) and (PLUS1lin)) observed. The reformulation with the Big-M and Convex Hull approaches yield MILP problems (Problems (BM1lin) and (CH1lin)), which can be solved with CPLEX immediately.

**Table E.1.:** Numerical results for the problem formulations of Problem (GDP1lin) presented in Section 5.2 for linear cost functions. The optimization has been executed 100 times, of which the arithmetic mean value is shown. For Problem (BM1lin) and (CH1lin), no BaB iterations are required as only CPLEX is called.

	BigM (BM1lin)		Convex Hull (CH1lin)		MPEC (MPEC1lin)		Plus Function (PLUS1lin)		Direct MINLP (MINLP1lin)	
	FS	RS	FS	RS	FS	RS	FS	RS	FS	RS
Number of										
Continuous variables	7	2	19	2	7	2	7	2	7	1
Discrete variables	2	1	2	1	0	0	0	0	2	1
Equality constraints	3	1	9	1	7	2	7	2	8	1
Inequality constraints	20	4	34	4	0	0	0	0	0	0
BaB nodes	0	0	0	0	1	3	1	3	1	1
CPU time per BaB node / s	NaN	NaN	NaN	NaN	0.108	0.007	0.035	0.008	0.103	0.045
Solution time / s	0	0	0	0	0.108	0.022	0.035	0.023	0.103	0.045

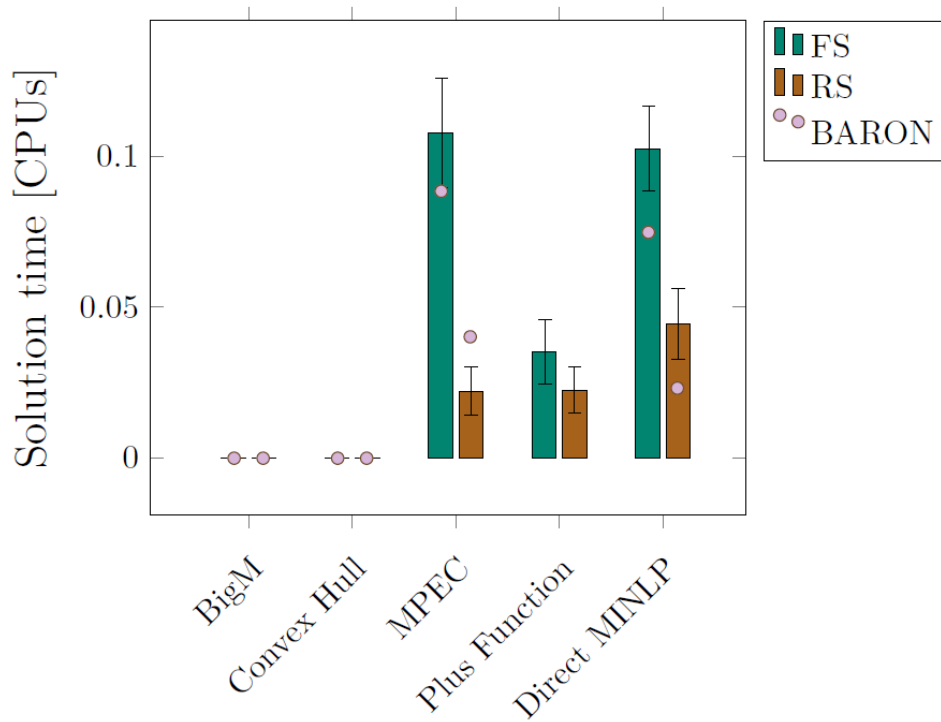


**Figure E.1.:** Solution time for Problem (GDP1lin) using the problem formulations presented in Section 5.2 for linear cost functions. As BARON can not handle *max*-functions, there are no results for the Plus Function formulation. The error bars represent the standard deviation from the arithmetic mean value of the solution time from 100 optimization runs using MAiNGO.



---

## Plus Function Problem Formulation for the Simple Example Problem

$$\begin{aligned}
\min \quad & C = C_{\text{op}} + C_{\text{inv}} \\
\text{s.t.} \quad & \dot{n}_{\text{in}} = \dot{n}_{\text{in}}^{\text{P}} + \dot{n}_{\text{in}}^{\text{S}} \\
& \dot{n}_{\text{out}}^j = \dot{n}_{\text{in}}^j \quad j \in \{\text{P}, \text{S}\} \\
& \dot{n}_{\text{out}} = \dot{n}_{\text{out}}^{\text{P}} + \dot{n}_{\text{out}}^{\text{S}} \\
& C_{\text{op}} = \sum_{j \in J} (\dot{n}_{\text{in}}^j)^2 e_j \\
& C_{\text{inv}} = \sum_{j \in J} \left[ \tanh(P \dot{n}_{\text{in}}^j) (C_j + \dot{n}_{\text{in}}^{0.6}) \right] \\
& 0 = \dot{n}_{\text{in}}^{\text{P}} - \max(0, \dot{n}_{\text{in}}^{\text{P}} - \dot{n}_{\text{in}}^{\text{S}}) \\
& C_{\text{op}}, C_{\text{inv}}, \dot{n}_{\text{in}}, \dot{n}_{\text{in}}^{\text{P}}, \dot{n}_{\text{in}}^{\text{S}}, \dot{n}_{\text{out}}^{\text{P}}, \dot{n}_{\text{out}}^{\text{S}} \geq 0 \\
& C_{\text{op}}, C_{\text{inv}}, \dot{n}_{\text{in}}, \dot{n}_{\text{in}}^{\text{P}}, \dot{n}_{\text{in}}^{\text{S}}, \dot{n}_{\text{out}}^{\text{P}}, \dot{n}_{\text{out}}^{\text{S}} \in \mathbb{R}
\end{aligned} \tag{PLUS1}$$

## Problem Formulations for the Multiple-Disjunction Example Problem

### Nested GDP problem

$$\begin{aligned}
 \min \quad & C = C_{\text{op}} + C_{\text{inv}} \\
 \text{s.t.} \quad & \dot{n}_{\text{in}} = \dot{n}_{\text{in}}^{\text{P}} + \dot{n}_{\text{in}}^{\text{S}} \\
 & \dot{n}_{\text{out}}^{\text{S}} = \dot{n}_{\text{in}}^{\text{F1}} + \dot{n}_{\text{in}}^{\text{F2}} \\
 & \dot{n}_{\text{out}}^{\text{F}} = \dot{n}_{\text{out}}^{\text{F1}} + \dot{n}_{\text{out}}^{\text{F2}} \\
 & \dot{n}_{\text{out}} = \dot{n}_{\text{out}}^{\text{P}} + \dot{n}_{\text{out}}^{\text{F}}
 \end{aligned} \tag{P2}$$

$$\left[ \begin{array}{c} Y_{\text{P}} \\ \dot{n}_{\text{in}}^{\text{S}} = \dot{n}_{\text{out}}^{\text{S}} = 0 \\ \dot{n}_{\text{out}}^{\text{P}} = \dot{n}_{\text{in}}^{\text{P}} \\ C_{\text{op}} = (\dot{n}_{\text{in}}^{\text{P}})^2 e_{\text{P}} \\ C_{\text{inv}} = C_{\text{P}} + \dot{n}_{\text{in}}^{0.6} \\ \dot{n}_{\text{in},\text{out}}^{\text{F1,F2}} = 0 \\ C_{\text{op}}^{\text{F}} = 0 \\ C_{\text{inv}}^{\text{F}} = 0 \end{array} \right] \vee \left[ \begin{array}{c} Y_{\text{S}} \\ \dot{n}_{\text{in}}^{\text{P}} = \dot{n}_{\text{out}}^{\text{P}} = 0 \\ \dot{n}_{\text{out}}^{\text{S}} = \dot{n}_{\text{in}}^{\text{S}} \\ C_{\text{op}} = (\dot{n}_{\text{in}}^{\text{S}})^2 e_{\text{S}} + C_{\text{op}}^{\text{F}} \\ C_{\text{inv}} = C_{\text{S}} + \dot{n}_{\text{in}}^{0.6} + C_{\text{inv}}^{\text{F}} \end{array} \right] \vee \left[ \begin{array}{c} Y_{\text{F1}} \\ \dot{n}_{\text{in}}^{\text{F2}} = \dot{n}_{\text{out}}^{\text{F2}} = 0 \\ \dot{n}_{\text{out}}^{\text{F1}} = \dot{n}_{\text{in}}^{\text{F1}} \\ C_{\text{op}}^{\text{F}} = (\dot{n}_{\text{in}}^{\text{F1}})^2 e_{\text{F1}} \\ C_{\text{inv}}^{\text{F}} = C_{\text{F1}} + 0.1 \dot{n}_{\text{in}}^{0.6} \end{array} \right] \vee \left[ \begin{array}{c} Y_{\text{F2}} \\ \dot{n}_{\text{in}}^{\text{F1}} = \dot{n}_{\text{out}}^{\text{F1}} = 0 \\ \dot{n}_{\text{out}}^{\text{F2}} = \dot{n}_{\text{in}}^{\text{F2}} \\ C_{\text{op}}^{\text{F}} = (\dot{n}_{\text{in}}^{\text{F2}})^2 e_{\text{F2}} \\ C_{\text{inv}}^{\text{F}} = C_{\text{F2}} + 0.1 \dot{n}_{\text{in}}^{0.6} \end{array} \right]$$

$$Y_{\text{P}} \vee Y_{\text{S}}$$

$$Y_{\text{S}} \Leftrightarrow Y_{\text{F1}} \vee Y_{\text{F2}}$$

$$C_{\text{op}}, C_{\text{inv}}, C_{\text{op}}^{\text{F}}, C_{\text{inv}}^{\text{F}}, \dot{n}_{\text{in}}, \dot{n}_{\text{in}}^{\text{P}}, \dot{n}_{\text{in}}^{\text{S}}, \dot{n}_{\text{in}}^{\text{F1}}, \dot{n}_{\text{in}}^{\text{F2}}, \dot{n}_{\text{out}}^{\text{P}}, \dot{n}_{\text{out}}^{\text{S}}, \dot{n}_{\text{out}}^{\text{F1}}, \dot{n}_{\text{out}}^{\text{F2}}, \dot{n}_{\text{out}}^{\text{F}} \geq 0$$

$$C_{\text{op}}, C_{\text{inv}}, C_{\text{op}}^{\text{F}}, C_{\text{inv}}^{\text{F}}, \dot{n}_{\text{in}}, \dot{n}_{\text{in}}^{\text{P}}, \dot{n}_{\text{in}}^{\text{S}}, \dot{n}_{\text{in}}^{\text{F1}}, \dot{n}_{\text{in}}^{\text{F2}}, \dot{n}_{\text{out}}^{\text{P}}, \dot{n}_{\text{out}}^{\text{S}}, \dot{n}_{\text{out}}^{\text{F1}}, \dot{n}_{\text{out}}^{\text{F2}}, \dot{n}_{\text{out}}^{\text{F}} \in \mathbb{R}$$

$$Y_{\text{P}}, Y_{\text{S}}, Y_{\text{F1}}, Y_{\text{F2}} \in \{\text{True}, \text{False}\}$$

## BigM

$$\begin{aligned}
\min \quad & C = C_{\text{op}} + C_{\text{inv}} \\
\text{s.t.} \quad & \dot{n}_{\text{in}} = \dot{n}_{\text{in}}^{\text{P}} + \dot{n}_{\text{in}}^{\text{S}} \\
& \dot{n}_{\text{out}}^{\text{S}} = \dot{n}_{\text{in}}^{\text{F1}} + \dot{n}_{\text{in}}^{\text{F2}} \\
& \dot{n}_{\text{out}}^{\text{F}} = \dot{n}_{\text{out}}^{\text{F1}} + \dot{n}_{\text{out}}^{\text{F2}} \\
& \dot{n}_{\text{out}} = \dot{n}_{\text{out}}^{\text{P}} + \dot{n}_{\text{out}}^{\text{F}} \\
& 0 - M^{\text{P}}(1 - y_{\text{P}}) \leq \dot{n}_{\text{in}}^{\text{S}} \leq 0 + M^{\text{P}}(1 - y_{\text{P}}) \\
& 0 - M^{\text{P}}(1 - y_{\text{P}}) \leq \dot{n}_{\text{out}}^{\text{S}} \leq 0 + M^{\text{P}}(1 - y_{\text{P}}) \\
& \dot{n}_{\text{in}}^{\text{P}} - M^{\text{P}}(1 - y_{\text{P}}) \leq \dot{n}_{\text{out}}^{\text{P}} \leq \dot{n}_{\text{in}}^{\text{P}} + M^{\text{P}}(1 - y_{\text{P}}) \\
& (\dot{n}_{\text{in}}^{\text{P}})^2 e_{\text{P}} - M^{\text{P}}(1 - y_{\text{P}}) \leq C_{\text{op}} \leq (\dot{n}_{\text{in}}^{\text{P}})^2 e_{\text{P}} + M^{\text{P}}(1 - y_{\text{P}}) \\
& C_{\text{P}} + \dot{n}_{\text{in}}^{0.6} - M^{\text{P}}(1 - y_{\text{P}}) \leq C_{\text{inv}} \leq C_{\text{P}} + \dot{n}_{\text{in}}^{0.6} + M^{\text{P}}(1 - y_{\text{P}}) \quad (\text{BM2}) \\
& 0 - M^{\text{S}}(1 - y_{\text{S}}) \leq \dot{n}_{\text{in}}^{\text{P}} \leq 0 + M^{\text{S}}(1 - y_{\text{S}}) \\
& 0 - M^{\text{S}}(1 - y_{\text{S}}) \leq \dot{n}_{\text{out}}^{\text{P}} \leq 0 + M^{\text{S}}(1 - y_{\text{S}}) \\
& \dot{n}_{\text{in}}^{\text{S}} - M^{\text{S}}(1 - y_{\text{S}}) \leq \dot{n}_{\text{out}}^{\text{S}} \leq \dot{n}_{\text{in}}^{\text{S}} + M^{\text{S}}(1 - y_{\text{S}}) \\
& (\dot{n}_{\text{in}}^{\text{S}})^2 e_{\text{S}} + C_{\text{op}}^{\text{F}} - M^{\text{S}}(1 - y_{\text{S}}) \leq C_{\text{op}} \leq (\dot{n}_{\text{in}}^{\text{S}})^2 e_{\text{S}} + C_{\text{op}}^{\text{F}} + M^{\text{S}}(1 - y_{\text{S}}) \\
& C_{\text{S}} + \dot{n}_{\text{in}}^{0.6} + C_{\text{inv}}^{\text{F}} - M^{\text{S}}(1 - y_{\text{S}}) \leq C_{\text{inv}} \leq C_{\text{S}} + \dot{n}_{\text{in}}^{0.6} + C_{\text{inv}}^{\text{F}} + M^{\text{S}}(1 - y_{\text{S}}) \\
& 0 - M^{\text{F1}}(1 - y_{\text{F1}}) \leq \dot{n}_{\text{in}}^{\text{F2}} \leq 0 + M^{\text{F1}}(1 - y_{\text{F1}}) \\
& 0 - M^{\text{F1}}(1 - y_{\text{F1}}) \leq \dot{n}_{\text{out}}^{\text{F2}} \leq 0 + M^{\text{F1}}(1 - y_{\text{F1}}) \\
& \dot{n}_{\text{in}}^{\text{F1}} - M^{\text{F1}}(1 - y_{\text{F1}}) \leq \dot{n}_{\text{out}}^{\text{F1}} \leq \dot{n}_{\text{in}}^{\text{F1}} + M^{\text{F1}}(1 - y_{\text{F1}}) \\
& (\dot{n}_{\text{in}}^{\text{F1}})^2 e_{\text{F1}} - M^{\text{F1}}(1 - y_{\text{F1}}) \leq C_{\text{op}}^{\text{F}} \leq (\dot{n}_{\text{in}}^{\text{F1}})^2 e_{\text{F1}} + M^{\text{F1}}(1 - y_{\text{F1}}) \\
& C_{\text{F1}} + 0.1\dot{n}_{\text{in}}^{0.6} - M^{\text{F1}}(1 - y_{\text{F1}}) \leq C_{\text{inv}}^{\text{F}} \leq C_{\text{F1}} + 0.1\dot{n}_{\text{in}}^{0.6} + M^{\text{F1}}(1 - y_{\text{F1}}) \\
& 0 - M^{\text{F2}}(1 - y_{\text{F2}}) \leq \dot{n}_{\text{in}}^{\text{F1}} \leq 0 + M^{\text{F2}}(1 - y_{\text{F2}}) \\
& 0 - M^{\text{F2}}(1 - y_{\text{F2}}) \leq \dot{n}_{\text{out}}^{\text{F1}} \leq 0 + M^{\text{F2}}(1 - y_{\text{F2}}) \\
& \dot{n}_{\text{in}}^{\text{F2}} - M^{\text{F2}}(1 - y_{\text{F2}}) \leq \dot{n}_{\text{out}}^{\text{F2}} \leq \dot{n}_{\text{in}}^{\text{F2}} + M^{\text{F2}}(1 - y_{\text{F2}}) \\
& (\dot{n}_{\text{in}}^{\text{F2}})^2 e_{\text{F2}} - M^{\text{F2}}(1 - y_{\text{F2}}) \leq C_{\text{op}}^{\text{F}} \leq (\dot{n}_{\text{in}}^{\text{F2}})^2 e_{\text{F2}} + M^{\text{F2}}(1 - y_{\text{F2}}) \\
& C_{\text{F2}} + 0.1\dot{n}_{\text{in}}^{0.6} - M^{\text{F2}}(1 - y_{\text{F2}}) \leq C_{\text{inv}}^{\text{F}} \leq C_{\text{F2}} + 0.1\dot{n}_{\text{in}}^{0.6} + M^{\text{F2}}(1 - y_{\text{F2}}) \\
& \dot{n}_{\text{in}}^j \leq 0 + M^{\text{notF}}(1 - y_{\text{notF}}) \quad j \in \{\text{F1}, \text{F2}\} \\
& \dot{n}_{\text{out}}^j \leq 0 + M^{\text{notF}}(1 - y_{\text{notF}}) \quad j \in \{\text{F}, \text{F1}, \text{F2}\} \\
& C_m^{\text{F}} \leq 0 + M^{\text{notF}}(1 - y_{\text{notF}}) \quad m \in \{\text{op}, \text{inv}\} \\
& y_{\text{P}} + y_{\text{S}} = 1 \\
& y_{\text{F1}} + y_{\text{F2}} + y_{\text{notF}} = 1 \\
& y_{\text{P}} = y_{\text{notF}} \\
& y_{\text{S}} = y_{\text{F1}} + y_{\text{F2}}
\end{aligned}$$

$$\begin{aligned}
 &C_{\text{op}}, C_{\text{inv}}, C_{\text{op}}^{\text{F}}, C_{\text{inv}}^{\text{F}}, \dot{n}_{\text{in}}, \dot{n}_{\text{in}}^{\text{P}}, \dot{n}_{\text{in}}^{\text{S}}, \dot{n}_{\text{in}}^{\text{F1}}, \dot{n}_{\text{in}}^{\text{F2}}, \dot{n}_{\text{out}}^{\text{P}}, \dot{n}_{\text{out}}^{\text{S}}, \dot{n}_{\text{out}}^{\text{F1}}, \dot{n}_{\text{out}}^{\text{F2}}, \dot{n}_{\text{out}}^{\text{F}} \geq 0 \\
 &C_{\text{op}}, C_{\text{inv}}, C_{\text{op}}^{\text{F}}, C_{\text{inv}}^{\text{F}}, \dot{n}_{\text{in}}, \dot{n}_{\text{in}}^{\text{P}}, \dot{n}_{\text{in}}^{\text{S}}, \dot{n}_{\text{in}}^{\text{F1}}, \dot{n}_{\text{in}}^{\text{F2}}, \dot{n}_{\text{out}}^{\text{P}}, \dot{n}_{\text{out}}^{\text{S}}, \dot{n}_{\text{out}}^{\text{F1}}, \dot{n}_{\text{out}}^{\text{F2}}, \dot{n}_{\text{out}}^{\text{F}} \in \mathbb{R} \\
 &y_{\text{P}}, y_{\text{S}}, y_{\text{F1}}, y_{\text{F2}}, y_{\text{notF}} \in \{0, 1\}
 \end{aligned}$$

## Convex Hull

$$\begin{aligned}
\min \quad & C = C_{\text{op}} + C_{\text{inv}} \\
\text{s.t.} \quad & \dot{n}_{\text{in}} = \dot{n}_{\text{in}}^{\text{P}} + \dot{n}_{\text{in}}^{\text{S}} \\
& \dot{n}_{\text{out}}^{\text{S}} = \dot{n}_{\text{in}}^{\text{F1}} + \dot{n}_{\text{in}}^{\text{F2}} \\
& \dot{n}_{\text{out}}^{\text{F}} = \dot{n}_{\text{out}}^{\text{F1}} + \dot{n}_{\text{out}}^{\text{F2}} \\
& \dot{n}_{\text{out}} = \dot{n}_{\text{out}}^{\text{P}} + \dot{n}_{\text{out}}^{\text{F}} \\
& \dot{n}_{\text{in}}^j = \dot{n}_{\text{in,P}}^j + \dot{n}_{\text{in,S}}^j & j \in \{\text{P}, \text{S}\} \\
& \dot{n}_{\text{out}}^j = \dot{n}_{\text{out,P}}^j + \dot{n}_{\text{out,S}}^j & j \in \{\text{P}, \text{S}\} \\
& \dot{n}_{\text{in}}^j = \dot{n}_{\text{in,F1}}^j + \dot{n}_{\text{in,F2}}^j + \dot{n}_{\text{in,notF}}^j & j \in \{\text{F1}, \text{F2}\} \\
& \dot{n}_{\text{out}}^j = \dot{n}_{\text{out,F1}}^j + \dot{n}_{\text{out,F2}}^j + \dot{n}_{\text{out,notF}}^j & j \in \{\text{F1}, \text{F2}\} \\
& C_{\text{op}} = C_{\text{op}}^{\text{P}} + C_{\text{op}}^{\text{S}} \\
& C_{\text{inv}} = C_{\text{inv}}^{\text{P}} + C_{\text{inv}}^{\text{S}} \\
& C_{\text{op}}^{\text{F}} = C_{\text{op,F1}}^{\text{F}} + C_{\text{op,F2}}^{\text{F}} + C_{\text{op,notF}}^{\text{F}} \\
& C_{\text{inv}}^{\text{F}} = C_{\text{inv,F1}}^{\text{F}} + C_{\text{inv,F2}}^{\text{F}} + C_{\text{inv,notF}}^{\text{F}} \\
& \dot{n}_{\text{in,P}}^{\text{S}} \leq 0 \\
& \dot{n}_{\text{out,P}}^{\text{S}} \leq 0 \\
& \dot{n}_{\text{out,P}}^{\text{P}} \leq \dot{n}_{\text{in,P}}^{\text{P}} \\
& C_{\text{op}}^{\text{P}} \geq \left( \dot{n}_{\text{in,P}}^{\text{P}} \right)^2 \frac{1}{(1-\epsilon)y_{\text{P}} + \epsilon} e_{\text{P}} \\
& C_{\text{inv}}^{\text{P}} \geq (C_{\text{P}} + \dot{n}_{\text{in}}^{0.6}) y_{\text{P}} \\
& \dot{n}_{\text{in,S}}^{\text{P}} \leq 0 \\
& \dot{n}_{\text{out,S}}^{\text{P}} \leq 0 \\
& \dot{n}_{\text{out,S}}^{\text{S}} \leq \dot{n}_{\text{in,S}}^{\text{S}} \\
& C_{\text{op}}^{\text{S}} \geq \left( \dot{n}_{\text{in,S}}^{\text{S}} \right)^2 \frac{1}{((1-\epsilon)y_{\text{S}} + \epsilon)} e_{\text{S}} + C_{\text{op}}^{\text{F}}((1-\epsilon)y_{\text{S}} + \epsilon) \\
& C_{\text{inv}}^{\text{S}} \geq (C_{\text{S}} + \dot{n}_{\text{in}}^{0.6} + C_{\text{inv}}^{\text{F}}) y_{\text{S}} \\
& \dot{n}_{\text{in,F1}}^{\text{F2}} \leq 0 \\
& \dot{n}_{\text{out,F1}}^{\text{F2}} \leq 0 \\
& \dot{n}_{\text{out,F1}}^{\text{F1}} \leq \dot{n}_{\text{in,F1}}^{\text{F1}} \\
& C_{\text{op}}^{\text{F1}} \geq \left( \dot{n}_{\text{in,F1}}^{\text{F1}} \right)^2 \frac{1}{(1-\epsilon)y_{\text{F1}} + \epsilon} e_{\text{F1}} \\
& C_{\text{inv,F1}}^{\text{F}} \geq (C_{\text{F1}} + 0.1\dot{n}_{\text{in}}^{0.6}) y_{\text{F1}} \\
& \dot{n}_{\text{in,F2}}^{\text{F1}} \leq 0 \\
& \dot{n}_{\text{out,F2}}^{\text{F1}} \leq 0
\end{aligned} \tag{CH2}$$

$$\begin{aligned}
\dot{n}_{\text{out},\text{F2}}^{\text{F2}} &\leq \dot{n}_{\text{in},\text{F2}}^{\text{F2}} \\
C_{\text{op}}^{\text{F2}} &\geq \left(\dot{n}_{\text{in},\text{F2}}^{\text{F2}}\right)^2 \frac{1}{(1-\epsilon)y_{\text{F2}} + \epsilon} e_{\text{F2}} \\
C_{\text{inv},\text{F2}}^{\text{F}} &\geq (C_{\text{F2}} + 0.1\dot{n}_{\text{in}}^{0.6})y_{\text{F2}} \\
\dot{n}_{\text{in},\text{notF}}^j &\leq 0 & j \in \{\text{F1}, \text{F2}\} \\
\dot{n}_{\text{out},\text{notF}}^j &\leq 0 & j \in \{\text{F}, \text{F1}, \text{F2}\} \\
C_{\text{op},\text{notF}}^{\text{F}} &\leq 0 \\
C_{\text{inv},\text{notF}}^{\text{F}} &\leq 0 \\
y_{\text{P}} + y_{\text{S}} &= 1 \\
y_{\text{F1}} + y_{\text{F2}} + y_{\text{notF}} &= 1 \\
y_{\text{P}} &= y_{\text{notF}} \\
y_{\text{S}} &= y_{\text{F1}} + y_{\text{F2}} \\
0 \leq \dot{n}_{\text{in},\text{P}}^{\text{P}} &\leq 1y_{\text{P}} \\
0 \leq \dot{n}_{\text{in},\text{P}}^{\text{S}} &\leq 1y_{\text{P}} \\
0 \leq \dot{n}_{\text{out},\text{P}}^{\text{P}} &\leq 1y_{\text{P}} \\
0 \leq \dot{n}_{\text{out},\text{P}}^{\text{S}} &\leq 1y_{\text{P}} \\
0 \leq C_{\text{op}}^{\text{P}} &\leq 20y_{\text{P}} \\
0 \leq C_{\text{inv}}^{\text{P}} &\leq 20y_{\text{P}} \\
0 \leq \dot{n}_{\text{in},\text{S}}^{\text{P}} &\leq 1y_{\text{S}} \\
0 \leq \dot{n}_{\text{in},\text{S}}^{\text{S}} &\leq 1y_{\text{S}} \\
0 \leq \dot{n}_{\text{out},\text{S}}^{\text{P}} &\leq 1y_{\text{S}} \\
0 \leq \dot{n}_{\text{out},\text{S}}^{\text{S}} &\leq 1y_{\text{S}} \\
0 \leq C_{\text{op}}^{\text{S}} &\leq 20y_{\text{S}} \\
0 \leq C_{\text{inv}}^{\text{S}} &\leq 20y_{\text{S}} \\
0 \leq \dot{n}_{\text{in},\text{F1}}^{\text{F1}} &\leq 1y_{\text{F1}} \\
0 \leq \dot{n}_{\text{in},\text{F1}}^{\text{F2}} &\leq 1y_{\text{F1}} \\
0 \leq \dot{n}_{\text{out},\text{F1}}^{\text{F1}} &\leq 1y_{\text{F1}} \\
0 \leq \dot{n}_{\text{out},\text{F1}}^{\text{F2}} &\leq 1y_{\text{F1}} \\
0 \leq C_{\text{op},\text{F1}}^{\text{F}} &\leq 20y_{\text{F1}} \\
0 \leq C_{\text{inv},\text{F1}}^{\text{F}} &\leq 20y_{\text{F1}} \\
0 \leq \dot{n}_{\text{in},\text{F2}}^{\text{F1}} &\leq 1y_{\text{F2}} \\
0 \leq \dot{n}_{\text{in},\text{F2}}^{\text{F2}} &\leq 1y_{\text{F2}} \\
0 \leq \dot{n}_{\text{out},\text{F2}}^{\text{F1}} &\leq 1y_{\text{F2}} \\
0 \leq \dot{n}_{\text{out},\text{F2}}^{\text{F2}} &\leq 1y_{\text{F2}}
\end{aligned}$$

---


$$\begin{aligned}
0 &\leq C_{\text{op},\text{F2}}^{\text{F}} \leq 20y_{\text{F2}} \\
0 &\leq C_{\text{inv},\text{F2}}^{\text{F}} \leq 20y_{\text{F2}} \\
0 &\leq \dot{n}_{\text{in},\text{notF}}^{\text{F1}} \leq 1y_{\text{notF}} \\
0 &\leq \dot{n}_{\text{in},\text{notF}}^{\text{F2}} \leq 1y_{\text{notF}} \\
0 &\leq \dot{n}_{\text{out},\text{notF}}^{\text{F1}} \leq 1y_{\text{notF}} \\
0 &\leq \dot{n}_{\text{out},\text{notF}}^{\text{F2}} \leq 1y_{\text{notF}} \\
0 &\leq C_{\text{op},\text{notF}}^{\text{F}} \leq 20y_{\text{notF}} \\
0 &\leq C_{\text{inv},\text{notF}}^{\text{F}} \leq 20y_{\text{notF}} \\
C_{\text{op}}, C_{\text{inv}}, C_{\text{op}}^{\text{F}}, C_{\text{inv}}^{\text{F}}, \dot{n}_{\text{in}}, \dot{n}_{\text{in}}^{\text{P}}, \dot{n}_{\text{in}}^{\text{S}}, \dot{n}_{\text{in}}^{\text{F1}}, \dot{n}_{\text{in}}^{\text{F2}}, \dot{n}_{\text{out}}^{\text{P}}, \dot{n}_{\text{out}}^{\text{S}}, \dot{n}_{\text{out}}^{\text{F}}, \dot{n}_{\text{out}}^{\text{F1}}, \dot{n}_{\text{out}}^{\text{F2}} &\geq 0 \\
C_{\text{op}}, C_{\text{inv}}, C_{\text{op}}^{\text{F}}, C_{\text{inv}}^{\text{F}}, C_{\text{op}}^{\text{P}}, C_{\text{op}}^{\text{S}}, C_{\text{inv}}^{\text{P}}, C_{\text{inv}}^{\text{S}}, C_{\text{op},\text{F1}}^{\text{F}}, C_{\text{inv},\text{F1}}^{\text{F}}, C_{\text{op},\text{F2}}^{\text{F}}, C_{\text{inv},\text{F2}}^{\text{F}} &\in \mathbb{R} \\
C_{\text{op},\text{notF}}^{\text{F}}, C_{\text{inv},\text{notF}}^{\text{F}}, \dot{n}_{\text{in}}, \dot{n}_{\text{in}}^{\text{P}}, \dot{n}_{\text{in}}^{\text{S}}, \dot{n}_{\text{in},\text{P}}^{\text{P}}, \dot{n}_{\text{in},\text{P}}^{\text{S}}, \dot{n}_{\text{in},\text{S}}^{\text{P}}, \dot{n}_{\text{in},\text{S}}^{\text{S}}, \dot{n}_{\text{out},\text{P}}^{\text{P}}, \dot{n}_{\text{out},\text{P}}^{\text{S}}, \dot{n}_{\text{out},\text{S}}^{\text{P}}, \dot{n}_{\text{out},\text{S}}^{\text{S}}, \dot{n}_{\text{out}}^{\text{P}}, \dot{n}_{\text{out}}^{\text{S}} &\in \mathbb{R} \\
\dot{n}_{\text{in}}^{\text{F1}}, \dot{n}_{\text{in}}^{\text{F2}}, \dot{n}_{\text{in},\text{F1}}^{\text{F1}}, \dot{n}_{\text{in},\text{F1}}^{\text{F2}}, \dot{n}_{\text{in},\text{F2}}^{\text{F1}}, \dot{n}_{\text{in},\text{F2}}^{\text{F2}}, \dot{n}_{\text{in},\text{notF}}^{\text{F1}}, \dot{n}_{\text{in},\text{notF}}^{\text{F2}}, \dot{n}_{\text{out}}^{\text{F}}, \dot{n}_{\text{out}}^{\text{F1}}, \dot{n}_{\text{out}}^{\text{F2}}, \dot{n}_{\text{out},\text{F1}}^{\text{F1}}, \dot{n}_{\text{out},\text{F1}}^{\text{F2}} &\in \mathbb{R} \\
\dot{n}_{\text{out},\text{F2}}^{\text{F1}}, \dot{n}_{\text{out},\text{F2}}^{\text{F2}}, \dot{n}_{\text{out},\text{notF}}^{\text{F1}}, \dot{n}_{\text{out},\text{notF}}^{\text{F2}} &\in \mathbb{R} \\
y_{\text{P}}, y_{\text{S}}, y_{\text{F1}}, y_{\text{F2}}, y_{\text{notF}} &\in \{0, 1\}
\end{aligned}$$

## MPEC

$$\begin{aligned}
\min \quad & C = C_{\text{op}} + C_{\text{inv}} \\
\text{s.t.} \quad & \dot{n}_{\text{in}} = \dot{n}_{\text{in}}^{\text{P}} + \dot{n}_{\text{in}}^{\text{S}} \\
& \dot{n}_{\text{out}}^j = \dot{n}_{\text{in}}^j \quad j \in \{\text{P}, \text{S}, \text{F1}, \text{F2}\} \\
& \dot{n}_{\text{out}}^{\text{S}} = \dot{n}_{\text{in}}^{\text{F1}} + \dot{n}_{\text{in}}^{\text{F2}} \\
& \dot{n}_{\text{out}}^{\text{F}} = \dot{n}_{\text{out}}^{\text{F1}} + \dot{n}_{\text{out}}^{\text{F2}} \\
& \dot{n}_{\text{out}} = \dot{n}_{\text{out}}^{\text{P}} + \dot{n}_{\text{out}}^{\text{F}} \quad (\text{MPEC2}) \\
& C_{\text{op}} = \sum_j (\dot{n}_{\text{in}}^j)^2 e_j \\
& C_{\text{inv}} = \sum_{j \in \{\text{P}, \text{S}\}} \left[ \tanh(P\dot{n}_{\text{in}}^j)(C_j + \dot{n}_{\text{in}}^{0.6}) \right] + \sum_{j \in \{\text{F1}, \text{F2}\}} \left[ \tanh(P\dot{n}_{\text{in}}^j)(C_j + 0.1\dot{n}_{\text{in}}^{0.6}) \right] \\
& 0 = \dot{n}_{\text{in}}^{\text{P}} \dot{n}_{\text{in}}^{\text{S}} + \dot{n}_{\text{in}}^{\text{F1}} \dot{n}_{\text{in}}^{\text{F2}} \\
& C_{\text{op}}, C_{\text{inv}}, \dot{n}_{\text{in}}, \dot{n}_{\text{in}}^{\text{P}}, \dot{n}_{\text{in}}^{\text{S}}, \dot{n}_{\text{in}}^{\text{F1}}, \dot{n}_{\text{in}}^{\text{F2}}, \dot{n}_{\text{out}}^{\text{P}}, \dot{n}_{\text{out}}^{\text{S}}, \dot{n}_{\text{out}}^{\text{F1}}, \dot{n}_{\text{out}}^{\text{F2}}, \dot{n}_{\text{out}}^{\text{F}} \geq 0 \\
& C_{\text{op}}, C_{\text{inv}}, \dot{n}_{\text{in}}, \dot{n}_{\text{in}}^{\text{P}}, \dot{n}_{\text{in}}^{\text{S}}, \dot{n}_{\text{in}}^{\text{F1}}, \dot{n}_{\text{in}}^{\text{F2}}, \dot{n}_{\text{out}}^{\text{P}}, \dot{n}_{\text{out}}^{\text{S}}, \dot{n}_{\text{out}}^{\text{F1}}, \dot{n}_{\text{out}}^{\text{F2}}, \dot{n}_{\text{out}}^{\text{F}} \in \mathbb{R}
\end{aligned}$$

## Plus Function

$$\begin{aligned}
 \min \quad & C = C_{\text{op}} + C_{\text{inv}} \\
 \text{s.t.} \quad & \dot{n}_{\text{in}} = \dot{n}_{\text{in}}^{\text{P}} + \dot{n}_{\text{in}}^{\text{S}} \\
 & \dot{n}_{\text{out}}^j = \dot{n}_{\text{in}}^j \quad j \in \{\text{P}, \text{S}, \text{F1}, \text{F2}\} \\
 & \dot{n}_{\text{out}}^{\text{S}} = \dot{n}_{\text{in}}^{\text{F1}} + \dot{n}_{\text{in}}^{\text{F2}} \\
 & \dot{n}_{\text{out}}^{\text{F}} = \dot{n}_{\text{out}}^{\text{F1}} + \dot{n}_{\text{out}}^{\text{F2}} \\
 & \dot{n}_{\text{out}} = \dot{n}_{\text{out}}^{\text{P}} + \dot{n}_{\text{out}}^{\text{F}} \quad (\text{PLUS2}) \\
 & C_{\text{op}} = \sum_j (\dot{n}_{\text{in}}^j)^2 e_j \\
 & C_{\text{inv}} = \sum_{j \in \{\text{P}, \text{S}\}} \left[ \tanh(P \dot{n}_{\text{in}}^j) (C_j + \dot{n}_{\text{in}}^{0.6}) \right] + \sum_{j \in \{\text{F1}, \text{F2}\}} \left[ \tanh(P \dot{n}_{\text{in}}^j) (C_j + 0.1 \dot{n}_{\text{in}}^{0.6}) \right] \\
 & 0 = \dot{n}_{\text{in}}^{\text{P}} - \max(0, \dot{n}_{\text{in}}^{\text{P}} - \dot{n}_{\text{in}}^{\text{S}}) + \dot{n}_{\text{in}}^{\text{F1}} - \max(0, \dot{n}_{\text{in}}^{\text{F1}} - \dot{n}_{\text{in}}^{\text{F2}}) \\
 & C_{\text{op}}, C_{\text{inv}}, \dot{n}_{\text{in}}, \dot{n}_{\text{in}}^{\text{P}}, \dot{n}_{\text{in}}^{\text{S}}, \dot{n}_{\text{in}}^{\text{F1}}, \dot{n}_{\text{in}}^{\text{F2}}, \dot{n}_{\text{out}}^{\text{P}}, \dot{n}_{\text{out}}^{\text{S}}, \dot{n}_{\text{out}}^{\text{F1}}, \dot{n}_{\text{out}}^{\text{F2}}, \dot{n}_{\text{out}}^{\text{F}} \geq 0 \\
 & C_{\text{op}}, C_{\text{inv}}, \dot{n}_{\text{in}}, \dot{n}_{\text{in}}^{\text{P}}, \dot{n}_{\text{in}}^{\text{S}}, \dot{n}_{\text{in}}^{\text{F1}}, \dot{n}_{\text{in}}^{\text{F2}}, \dot{n}_{\text{out}}^{\text{P}}, \dot{n}_{\text{out}}^{\text{S}}, \dot{n}_{\text{out}}^{\text{F1}}, \dot{n}_{\text{out}}^{\text{F2}}, \dot{n}_{\text{out}}^{\text{F}} \in \mathbb{R}
 \end{aligned}$$

## Direct MINLP

$$\begin{aligned}
 \min \quad & C = C_{\text{op}} + C_{\text{inv}} \\
 \text{s.t.} \quad & C_{\text{op}} = \sum_j (\dot{n}_{\text{in}}^j)^2 e_j \\
 & C_{\text{inv}} = \sum_j y_j (C_j + \dot{n}_{\text{in}}^{0.6}) \\
 & \dot{n}_{\text{in}}^j = y_j \dot{n}_{\text{in}} \quad j \in \{\text{P}, \text{S}\} \quad (\text{MINLP2}) \\
 & \dot{n}_{\text{in}}^j = y_j \dot{n}_{\text{out}}^{\text{S}} \quad j \in \{\text{F1}, \text{F2}\} \\
 & \dot{n}_{\text{out}}^j = \dot{n}_{\text{in}}^j \quad j \in \{\text{P}, \text{S}, \text{F1}, \text{F2}\} \\
 & \dot{n}_{\text{out}}^{\text{F}} = \dot{n}_{\text{out}}^{\text{F1}} + \dot{n}_{\text{out}}^{\text{F2}} \\
 & \dot{n}_{\text{out}} = \dot{n}_{\text{out}}^{\text{P}} + \dot{n}_{\text{out}}^{\text{F}} \\
 & y_{\text{P}} + y_{\text{S}} = 1 \\
 & y_{\text{F1}} + y_{\text{F2}} - y_{\text{S}} = 0 \\
 & C_{\text{op}}, C_{\text{inv}}, \dot{n}_{\text{in}}, \dot{n}_{\text{in}}^{\text{P}}, \dot{n}_{\text{in}}^{\text{S}}, \dot{n}_{\text{in}}^{\text{F1}}, \dot{n}_{\text{in}}^{\text{F2}}, \dot{n}_{\text{out}}^{\text{P}}, \dot{n}_{\text{out}}^{\text{S}}, \dot{n}_{\text{out}}^{\text{F1}}, \dot{n}_{\text{out}}^{\text{F2}}, \dot{n}_{\text{out}}^{\text{F}} \geq 0 \\
 & C_{\text{op}}, C_{\text{inv}}, \dot{n}_{\text{in}}, \dot{n}_{\text{in}}^{\text{P}}, \dot{n}_{\text{in}}^{\text{S}}, \dot{n}_{\text{in}}^{\text{F1}}, \dot{n}_{\text{in}}^{\text{F2}}, \dot{n}_{\text{out}}^{\text{P}}, \dot{n}_{\text{out}}^{\text{S}}, \dot{n}_{\text{out}}^{\text{F1}}, \dot{n}_{\text{out}}^{\text{F2}}, \dot{n}_{\text{out}}^{\text{F}} \in \mathbb{R} \\
 & y_j \in \{0, 1\} \quad j \in \{\text{P}, \text{S}, \text{F1}, \text{F2}\}
 \end{aligned}$$



# Heat Exchanger Network Design Problem

## GDP

$$\begin{aligned}
 \min \quad & C = \sum_i CP_i + FCP_H(T_1 - T_H^{\text{out}})C_{\text{cw}} + FCP_C(T_C^{\text{out}} - T_2)C_s \\
 \text{s.t.} \quad & FCP_H(T_H^{\text{in}} - T_1) = A_1 U_1 \frac{(T_H^{\text{in}} - T_2) + (T_1 - T_C^{\text{in}})}{2} \\
 & FCP_H(T_1 - T_H^{\text{out}}) = A_2 U_2 \frac{(-T_{\text{cw}}^{\text{in}} + T_H^{\text{out}}) + (T_1 - T_{\text{cw}}^{\text{out}})}{2} \\
 & FCP_C(T_C^{\text{out}} - T_2) = A_3 U_3 \frac{(T_s - T_2) + (T_s - T_C^{\text{out}})}{2} \\
 & FCP_H(T_H^{\text{in}} - T_1) = FCP_C(T_2 - T_C^{\text{in}}) \\
 & \left[ \begin{array}{c} Y_{i,1} \\ CP_i = 2750A_i^{0.6} + 3000 \\ 0 \leq A_i \leq 10 \end{array} \right] \vee \left[ \begin{array}{c} Y_{i,2} \\ CP_i = 1500A_i^{0.6} + 15000 \\ 10 \leq A_i \leq 25 \end{array} \right] \\
 & \vee \left[ \begin{array}{c} Y_{i,3} \\ CP_i = 600A_i^{0.6} + 46500 \\ 25 \leq A_i \leq 50 \end{array} \right] \quad i = 1, 2, 3 \\
 & T_1^{\text{lo}} \leq T_1 \leq T_1^{\text{up}} \\
 & T_2^{\text{lo}} \leq T_2 \leq T_2^{\text{up}} \\
 & T_l \in \mathbb{R} \quad l = 1, 2 \\
 & Y_{i,1} \vee Y_{i,2} \vee Y_{i,3} \quad i = 1, 2, 3 \\
 & Y_{i,j} \in \{\text{True}, \text{False}\} \quad i = 1, 2, 3 \quad j = 1, 2, 3 \\
 & A_i \in \mathbb{R} \quad i = 1, 2, 3
 \end{aligned} \tag{HEXGDP}$$

## BigM

$$\begin{aligned}
 \min \quad & C = \sum_i CP_i + FCP_H(T_1 - T_H^{\text{out}})C_{\text{cw}} + FCP_C(T_C^{\text{out}} - T_2)C_s \\
 \text{s.t.} \quad & FCP_H(T_H^{\text{in}} - T_1) = (A_{1,1} + A_{1,2} + A_{1,3})U_1 \frac{(T_H^{\text{in}} - T_2) + (T_1 - T_C^{\text{in}})}{2} \\
 & FCP_H(T_1 - T_H^{\text{out}}) = (A_{2,1} + A_{2,2} + A_{2,3})U_2 \frac{(-T_{\text{cw}}^{\text{in}} + T_H^{\text{out}}) + (T_1 - T_{\text{cw}}^{\text{out}})}{2} \\
 & FCP_C(T_C^{\text{out}} - T_2) = (A_{3,1} + A_{3,2} + A_{3,3})U_3 \frac{(T_s - T_2) + (T_s - T_C^{\text{out}})}{2} \\
 & FCP_H(T_H^{\text{in}} - T_1) = FCP_C(T_2 - T_C^{\text{in}}) \\
 & 0 - M_{1,1}(1 - y_{1,1}) \leq A_{1,1} \leq 10 + M_{1,1}(1 - y_{1,1}) \quad (\text{HEXBM}) \\
 & 0 - M_{1,1}(1 - y_{1,1}) \leq A_{1,2} \leq 0 + M_{1,1}(1 - y_{1,1}) \\
 & 0 - M_{1,1}(1 - y_{1,1}) \leq A_{1,3} \leq 0 + M_{1,1}(1 - y_{1,1}) \\
 & (2750A_{1,1}^{0.6} + 3000) - M_{1,1}(1 - y_{1,1}) \leq CP_1 \leq (2750A_{1,1}^{0.6} + 3000) + M_{1,1}(1 - y_{1,1}) \\
 & 0 - M_{1,2}(1 - y_{1,2}) \leq A_{1,1} \leq 0 + M_{1,2}(1 - y_{1,2}) \\
 & 10 - M_{1,2}(1 - y_{1,2}) \leq A_{1,2} \leq 25 + M_{1,2}(1 - y_{1,2}) \\
 & 0 - M_{1,2}(1 - y_{1,2}) \leq A_{1,3} \leq 0 + M_{1,2}(1 - y_{1,2}) \\
 & (1500A_{1,2}^{0.6} + 15000) - M_{1,2}(1 - y_{1,2}) \leq CP_1 \leq (1500A_{1,2}^{0.6} + 15000) + M_{1,2}(1 - y_{1,2}) \\
 & 0 - M_{1,3}(1 - y_{1,3}) \leq A_{1,1} \leq 0 + M_{1,3}(1 - y_{1,3}) \\
 & 0 - M_{1,3}(1 - y_{1,3}) \leq A_{1,2} \leq 0 + M_{1,3}(1 - y_{1,3}) \\
 & 25 - M_{1,3}(1 - y_{1,3}) \leq A_{1,3} \leq 50 + M_{1,3}(1 - y_{1,3}) \\
 & (600A_{1,3}^{0.6} + 46500) - M_{1,3}(1 - y_{1,3}) \leq CP_1 \leq (600A_{1,3}^{0.6} + 46500) + M_{1,3}(1 - y_{1,3}) \\
 & 0 - M_{2,1}(1 - y_{2,1}) \leq A_{2,1} \leq 10 + M_{2,1}(1 - y_{2,1}) \\
 & 0 - M_{2,1}(1 - y_{2,1}) \leq A_{2,2} \leq 0 + M_{2,1}(1 - y_{2,1}) \\
 & 0 - M_{2,1}(1 - y_{2,1}) \leq A_{2,3} \leq 0 + M_{2,1}(1 - y_{2,1}) \\
 & (2750A_{2,1}^{0.6} + 3000) - M_{2,1}(1 - y_{2,1}) \leq CP_2 \leq (2750A_{2,1}^{0.6} + 3000) + M_{2,1}(1 - y_{2,1}) \\
 & 0 - M_{2,2}(1 - y_{2,2}) \leq A_{2,1} \leq 0 + M_{2,2}(1 - y_{2,2}) \\
 & 10 - M_{2,2}(1 - y_{2,2}) \leq A_{2,2} \leq 25 + M_{2,2}(1 - y_{2,2}) \\
 & 0 - M_{2,2}(1 - y_{2,2}) \leq A_{2,3} \leq 0 + M_{2,2}(1 - y_{2,2}) \\
 & (1500A_{2,2}^{0.6} + 15000) - M_{2,2}(1 - y_{2,2}) \leq CP_2 \leq (1500A_{2,2}^{0.6} + 15000) + M_{2,2}(1 - y_{2,2}) \\
 & 0 - M_{2,3}(1 - y_{2,3}) \leq A_{2,1} \leq 0 + M_{2,3}(1 - y_{2,3}) \\
 & 0 - M_{2,3}(1 - y_{2,3}) \leq A_{2,2} \leq 0 + M_{2,3}(1 - y_{2,3}) \\
 & 25 - M_{2,3}(1 - y_{2,3}) \leq A_{2,3} \leq 50 + M_{2,3}(1 - y_{2,3}) \\
 & (600A_{2,3}^{0.6} + 46500) - M_{2,3}(1 - y_{2,3}) \leq CP_2 \leq (600A_{2,3}^{0.6} + 46500) + M_{2,3}(1 - y_{2,3}) \\
 & 0 - M_{3,1}(1 - y_{3,1}) \leq A_{3,1} \leq 10 + M_{3,1}(1 - y_{3,1}) \\
 & 0 - M_{3,1}(1 - y_{3,1}) \leq A_{3,2} \leq 0 + M_{3,1}(1 - y_{3,1}) \\
 & 0 - M_{3,1}(1 - y_{3,1}) \leq A_{3,3} \leq 0 + M_{3,1}(1 - y_{3,1})
 \end{aligned}$$

---


$$\begin{aligned}
(2750A_{3,1}^{0.6} + 3000) - M_{3,1}(1 - y_{3,1}) &\leq CP_3 \leq (2750A_{3,1}^{0.6} + 3000) + M_{3,1}(1 - y_{3,1}) \\
0 - M_{3,2}(1 - y_{3,2}) &\leq A_{3,1} \leq 0 + M_{3,2}(1 - y_{3,2}) \\
10 - M_{3,2}(1 - y_{3,2}) &\leq A_{3,2} \leq 25 + M_{3,2}(1 - y_{3,2}) \\
0 - M_{3,2}(1 - y_{3,2}) &\leq A_{3,3} \leq 0 + M_{3,2}(1 - y_{3,2}) \\
(1500A_{3,2}^{0.6} + 15000) - M_{3,2}(1 - y_{3,2}) &\leq CP_3 \leq (1500A_{3,2}^{0.6} + 15000) + M_{3,2}(1 - y_{3,2}) \\
0 - M_{3,3}(1 - y_{3,3}) &\leq A_{3,1} \leq 0 + M_{3,3}(1 - y_{3,3}) \\
0 - M_{3,3}(1 - y_{3,3}) &\leq A_{3,2} \leq 0 + M_{3,3}(1 - y_{3,3}) \\
25 - M_{3,3}(1 - y_{3,3}) &\leq A_{3,3} \leq 50 + M_{3,3}(1 - y_{3,3}) \\
(600A_{3,3}^{0.6} + 46500) - M_{3,3}(1 - y_{3,3}) &\leq CP_3 \leq (600A_{3,3}^{0.6} + 46500) + M_{3,3}(1 - y_{3,3}) \\
y_{1,1} + y_{1,2} + y_{1,3} &= 1 \\
y_{2,1} + y_{2,2} + y_{2,3} &= 1 \\
y_{3,1} + y_{3,2} + y_{3,3} &= 1 \\
T_1^{lo} &\leq T_1 \leq T_1^{up} \\
T_2^{lo} &\leq T_2 \leq T_2^{up} \\
T_l &\in \mathbb{R} & l = 1, 2 \\
CP_i &\in \mathbb{R} & i = 1, 2, 3 \\
A_{i,j} &\in \mathbb{R} & i = 1, 2, 3 \quad j = 1, 2, 3 \\
y_{i,j} &\in \{0, 1\} & i = 1, 2, 3 \quad j = 1, 2, 3
\end{aligned}$$

## Convex Hull

$$\begin{aligned}
 \min \quad & C = \sum_i CP_i + FCP_H(T_1 - T_H^{\text{out}})C_{\text{cw}} + FCP_C(T_C^{\text{out}} - T_2)C_s \\
 \text{s.t.} \quad & FCP_H(T_H^{\text{in}} - T_1) = (A_{1,1} + A_{1,2} + A_{1,3})U_1 \frac{(T_H^{\text{in}} - T_2) + (T_1 - T_C^{\text{in}})}{2} \\
 & FCP_H(T_1 - T_H^{\text{out}}) = (A_{2,1} + A_{2,2} + A_{2,3})U_2 \frac{(-T_{\text{cw}}^{\text{in}} + T_H^{\text{out}}) + (T_1 - T_{\text{cw}}^{\text{out}})}{2} \\
 & FCP_C(T_C^{\text{out}} - T_2) = (A_{3,1} + A_{3,2} + A_{3,3})U_3 \frac{(T_s - T_2) + (T_s - T_C^{\text{out}})}{2} \\
 & FCP_H(T_H^{\text{in}} - T_1) = FCP_C(T_2 - T_C^{\text{in}}) \\
 & CP_1 = CP_{1,1} + CP_{1,2} + CP_{1,3} \\
 & CP_2 = CP_{2,1} + CP_{2,2} + CP_{2,3} \\
 & CP_3 = CP_{3,1} + CP_{3,2} + CP_{3,3} \\
 & A_{1,1} = A_{1,11} + A_{1,12} + A_{1,13} \\
 & A_{1,2} = A_{1,21} + A_{1,22} + A_{1,23} \\
 & A_{1,3} = A_{1,31} + A_{1,32} + A_{1,33} \\
 & A_{2,1} = A_{2,11} + A_{2,12} + A_{2,13} \\
 & A_{2,2} = A_{2,21} + A_{2,22} + A_{2,23} \\
 & A_{2,3} = A_{2,31} + A_{2,32} + A_{2,33} \\
 & A_{3,1} = A_{3,11} + A_{3,12} + A_{3,13} \\
 & A_{3,2} = A_{3,21} + A_{3,22} + A_{3,23} \\
 & A_{3,3} = A_{3,31} + A_{3,32} + A_{3,33} \\
 & A_{i,12}, A_{i,13} \leq 0 \quad i = 1, 2, 3 \\
 & A_{i,21}, A_{i,23} \leq 0 \quad i = 1, 2, 3 \\
 & A_{i,31}, A_{i,32} \leq 0 \quad i = 1, 2, 3 \\
 & CP_{i,1} \geq \left( 2750 \left( \frac{A_{i,11}}{(1-\epsilon)y_{i,1} + \epsilon} \right)^{0.6} + 3000 \right) ((1-\epsilon)y_{i,1} + \epsilon) \quad i = 1, 2, 3 \\
 & CP_{i,2} \geq \left( 1500 \left( \frac{A_{i,22}}{(1-\epsilon)y_{i,2} + \epsilon} \right)^{0.6} + 15000 \right) ((1-\epsilon)y_{i,2} + \epsilon) \quad i = 1, 2, 3 \\
 & CP_{i,3} \geq \left( 600 \left( \frac{A_{i,33}}{(1-\epsilon)y_{i,3} + \epsilon} \right)^{0.6} + 46500 \right) ((1-\epsilon)y_{i,3} + \epsilon) \quad i = 1, 2, 3 \\
 & 1 = y_{1,1} + y_{1,2} + y_{1,3} \\
 & 1 = y_{2,1} + y_{2,2} + y_{2,3} \\
 & 1 = y_{3,1} + y_{3,2} + y_{3,3}
 \end{aligned} \tag{HEXCH}$$

---

$0 \leq A_{i,1} \leq 10y_{i,1}$	$i = 1, 2, 3$		
$0 \leq A_{i,11} \leq 10y_{i,1}$	$i = 1, 2, 3$		
$0 \leq A_{i,12} \leq 10y_{i,1}$	$i = 1, 2, 3$		
$0 \leq A_{i,13} \leq 10y_{i,1}$	$i = 1, 2, 3$		
$0 \leq A_{i,2} \leq 25y_{i,2}$	$i = 1, 2, 3$		
$0 \leq A_{i,21} \leq 25y_{i,2}$	$i = 1, 2, 3$		
$0 \leq A_{i,22} \leq 25y_{i,2}$	$i = 1, 2, 3$		
$0 \leq A_{i,23} \leq 25y_{i,2}$	$i = 1, 2, 3$		
$0 \leq A_{i,3} \leq 50y_{i,3}$	$i = 1, 2, 3$		
$0 \leq A_{i,31} \leq 50y_{i,3}$	$i = 1, 2, 3$		
$0 \leq A_{i,32} \leq 50y_{i,3}$	$i = 1, 2, 3$		
$0 \leq A_{i,33} \leq 50y_{i,3}$	$i = 1, 2, 3$		
$0 \leq CP_{i,1} \leq 53000y_{i,1}$	$i = 1, 2, 3$		
$0 \leq CP_{i,2} \leq 53000y_{i,2}$	$i = 1, 2, 3$		
$0 \leq CP_{i,3} \leq 53000y_{i,3}$	$i = 1, 2, 3$		
$T_1^{lo} \leq T_1 \leq T_1^{up}$			
$T_2^{lo} \leq T_2 \leq T_2^{up}$			
$T_l \in \mathbb{R}$	$l = 1, 2$		
$CP_{i,j} \in \mathbb{R}$	$i = 1, 2, 3$	$j = 1, 2, 3$	
$A_{i,j} \in \mathbb{R}$	$i = 1, 2, 3$	$j = 1, 2, 3$	
$A_{i,jk} \in \mathbb{R}$	$i = 1, 2, 3$	$j = 1, 2, 3$	$k = 1, 2, 3$
$y_{i,j} \in \{0, 1\}$	$i = 1, 2, 3$	$j = 1, 2, 3$	

## MPEC

$$\begin{aligned}
 \min \quad & C = \sum_i CP_i + FCP_H(T_1 - T_H^{\text{out}})C_{\text{cw}} + FCP_C(T_C^{\text{out}} - T_2)C_s \\
 \text{s.t.} \quad & FCP_H(T_H^{\text{in}} - T_1) = (A_{1,1} + A_{1,2} + A_{1,3})U_1 \frac{(T_H^{\text{in}} - T_2) + (T_1 - T_C^{\text{in}})}{2} \\
 & FCP_H(T_1 - T_H^{\text{out}}) = (A_{2,1} + A_{2,2} + A_{2,3})U_2 \frac{(-T_{\text{cw}}^{\text{in}} + T_H^{\text{out}}) + (T_1 - T_{\text{cw}}^{\text{out}})}{2} \\
 & FCP_C(T_C^{\text{out}} - T_2) = (A_{3,1} + A_{3,2} + A_{3,3})U_3 \frac{(T_s - T_2) + (T_s - T_C^{\text{out}})}{2} \\
 & FCP_H(T_H^{\text{in}} - T_1) = FCP_C(T_2 - T_C^{\text{in}}) \\
 & CP_1 = (2750A_{1,1}^{0.6} + \tanh(PA_{1,1})3000) + (1500A_{1,2}^{0.6} + \tanh(PA_{1,2})15000) \\
 & \quad + (600A_{1,3}^{0.6} + \tanh(PA_{1,3})46500) \\
 & CP_2 = (2750A_{2,1}^{0.6} + \tanh(PA_{2,1})3000) + (1500A_{2,2}^{0.6} + \tanh(PA_{2,2})15000) \\
 & \quad + (600A_{2,3}^{0.6} + \tanh(PA_{2,3})46500) \\
 & CP_3 = (2750A_{3,1}^{0.6} + \tanh(PA_{3,1})3000) + (1500A_{3,2}^{0.6} + \tanh(PA_{3,2})15000) \\
 & \quad + (600A_{3,3}^{0.6} + \tanh(PA_{3,3})46500) \\
 & 0 = A_{1,1}A_{1,2} + A_{1,1}A_{1,3} + A_{1,2}A_{1,3} \\
 & 0 = A_{2,1}A_{2,2} + A_{2,1}A_{2,3} + A_{2,2}A_{2,3} \\
 & 0 = A_{3,1}A_{3,2} + A_{3,1}A_{3,3} + A_{3,2}A_{3,3} \\
 & T_1^{\text{lo}} \leq T_1 \leq T_1^{\text{up}} \quad \quad \quad (\text{HEXMPEC}) \\
 & T_2^{\text{lo}} \leq T_2 \leq T_2^{\text{up}} \\
 & T_l \in \mathbb{R} \quad \quad \quad l = 1, 2 \\
 & CP_i^{\text{lo}} \leq CP_i \leq CP_i^{\text{up}} \quad \quad \quad i = 1, 2, 3 \\
 & CP_i \in \mathbb{R} \quad \quad \quad i = 1, 2, 3 \\
 & A_{i,j} \in \mathbb{R} \quad \quad \quad i = 1, 2, 3 \quad \quad j = 1, 2, 3
 \end{aligned}$$

---

## Plus Function

$$\begin{aligned}
\min \quad & C = \sum_i CP_i + FCP_H(T_1 - T_H^{\text{out}})C_{\text{cw}} + FCP_C(T_C^{\text{out}} - T_2)C_s \\
\text{s.t.} \quad & FCP_H(T_H^{\text{in}} - T_1) = (A_{1,1} + A_{1,2} + A_{1,3})U_1 \frac{(T_H^{\text{in}} - T_2) + (T_1 - T_C^{\text{in}})}{2} \\
& FCP_H(T_1 - T_H^{\text{out}}) = (A_{2,1} + A_{2,2} + A_{2,3})U_2 \frac{(-T_{\text{cw}}^{\text{in}} + T_H^{\text{out}}) + (T_1 - T_{\text{cw}}^{\text{out}})}{2} \\
& FCP_C(T_C^{\text{out}} - T_2) = (A_{3,1} + A_{3,2} + A_{3,3})U_3 \frac{(T_s - T_2) + (T_s - T_C^{\text{out}})}{2} \\
& FCP_H(T_H^{\text{in}} - T_1) = FCP_C(T_2 - T_C^{\text{in}}) \\
& CP_1 = (2750A_{1,1}^{0.6} + \tanh(PA_{1,1})3000) + (1500A_{1,2}^{0.6} + \tanh(PA_{1,2})15000) \\
& \quad + (600A_{1,3}^{0.6} + \tanh(PA_{1,3})46500) \\
& CP_2 = (2750A_{2,1}^{0.6} + \tanh(PA_{2,1})3000) + (1500A_{2,2}^{0.6} + \tanh(PA_{2,2})15000) \\
& \quad + (600A_{2,3}^{0.6} + \tanh(PA_{2,3})46500) \\
& CP_3 = (2750A_{3,1}^{0.6} + \tanh(PA_{3,1})3000) + (1500A_{3,2}^{0.6} + \tanh(PA_{3,2})15000) \\
& \quad + (600A_{3,3}^{0.6} + \tanh(PA_{3,3})46500) \\
& 0 = A_{1,1} - \max(0, A_{1,1} - A_{1,2}) + A_{1,1} - \max(0, A_{1,1} - A_{1,3}) + A_{1,2} \\
& \quad - \max(0, A_{1,2} - A_{1,3}) \\
& 0 = A_{2,1} - \max(0, A_{2,1} - A_{2,2}) + A_{2,1} - \max(0, A_{2,1} - A_{2,3}) + A_{2,2} \\
& \quad - \max(0, A_{2,2} - A_{2,3}) \\
& 0 = A_{3,1} - \max(0, A_{3,1} - A_{3,2}) + A_{3,1} - \max(0, A_{3,1} - A_{3,3}) + A_{3,2} \\
& \quad - \max(0, A_{3,2} - A_{3,3}) \\
& T_1^{\text{lo}} \leq T_1 \leq T_1^{\text{up}} \\
& T_2^{\text{lo}} \leq T_2 \leq T_2^{\text{up}} \quad \text{(HEXPLUSF)} \\
& T_l \in \mathbb{R} \quad l = 1, 2 \\
& CP_i^{\text{lo}} \leq CP_i \leq CP_i^{\text{up}} \quad i = 1, 2, 3 \\
& CP_i \in \mathbb{R} \quad i = 1, 2, 3 \\
& A_{i,j} \in \mathbb{R} \quad i = 1, 2, 3 \quad j = 1, 2, 3
\end{aligned}$$

## Direct MINLP

$$\begin{aligned}
 \min \quad & C = \sum_i CP_i + FCP_H(T_1 - T_H^{\text{out}})C_{\text{cw}} + FCP_C(T_C^{\text{out}} - T_2)C_s \\
 \text{s.t.} \quad & FCP_H(T_H^{\text{in}} - T_1) = (y_{1,1}A_{1,1} + y_{1,2}A_{1,2} + y_{1,3}A_{1,3})U_1 \frac{(T_H^{\text{in}} - T_2) + (T_1 - T_C^{\text{in}})}{2} \\
 & FCP_H(T_1 - T_H^{\text{out}}) = (y_{2,1}A_{2,1} + y_{2,2}A_{2,2} + y_{2,3}A_{2,3})U_2 \frac{(-T_{\text{cw}}^{\text{in}} + T_H^{\text{out}}) + (T_1 - T_{\text{cw}}^{\text{out}})}{2} \\
 & FCP_C(T_C^{\text{out}} - T_2) = (y_{3,1}A_{3,1} + y_{3,2}A_{3,2} + y_{3,3}A_{3,3})U_3 \frac{(T_s - T_2) + (T_s - T_C^{\text{out}})}{2} \\
 & FCP_H(T_H^{\text{in}} - T_1) = FCP_C(T_2 - T_C^{\text{in}}) \\
 & CP_1 = y_{1,1}(2750A_{1,1}^{0.6} + 3000) + y_{1,2}(1500A_{1,2}^{0.6} + 15000) + y_{1,3}(600A_{1,3}^{0.6} + 46500) \\
 & CP_2 = y_{2,1}(2750A_{2,1}^{0.6} + 3000) + y_{2,2}(1500A_{2,2}^{0.6} + 15000) + y_{2,3}(600A_{2,3}^{0.6} + 46500) \\
 & CP_3 = y_{3,1}(2750A_{3,1}^{0.6} + 3000) + y_{3,2}(1500A_{3,2}^{0.6} + 15000) + y_{3,3}(600A_{3,3}^{0.6} + 46500) \\
 & 1 = y_{1,1} + y_{1,2} + y_{1,3} \\
 & 1 = y_{2,1} + y_{2,2} + y_{2,3} \\
 & 1 = y_{3,1} + y_{3,2} + y_{3,3} \quad (\text{HEXMINLP}) \\
 & T_1^{\text{lo}} \leq T_1 \leq T_1^{\text{up}} \\
 & T_2^{\text{lo}} \leq T_2 \leq T_2^{\text{up}} \\
 & T_l \in \mathbb{R} \quad l = 1, 2 \\
 & CP_i^{\text{lo}} \leq CP_i \leq CP_i^{\text{up}} \quad i = 1, 2, 3 \\
 & CP_i \in \mathbb{R} \quad i = 1, 2, 3 \\
 & A_{i,j} \in \mathbb{R} \quad i = 1, 2, 3 \quad j = 1, 2, 3 \\
 & y_{i,j} \in \{0, 1\} \quad i = 1, 2, 3 \quad j = 1, 2, 3
 \end{aligned}$$



## Step Function

$$\begin{aligned}
\min \quad & C = \sum_i CP_i + FCP_H(T_1 - T_H^{\text{out}})C_{\text{cw}} + FCP_C(T_C^{\text{out}} - T_2)C_s \\
\text{s.t.} \quad & FCP_H(T_H^{\text{in}} - T_1) = A_1 U_1 \frac{(T_H^{\text{in}} - T_2) + (T_1 - T_C^{\text{in}})}{2} \\
& FCP_H(T_1 - T_H^{\text{out}}) = A_2 U_2 \frac{(-T_{\text{cw}}^{\text{in}} + T_H^{\text{out}}) + (T_1 - T_{\text{cw}}^{\text{out}})}{2} \quad (\text{HEXStepF}) \\
& FCP_C(T_C^{\text{out}} - T_2) = A_3 U_3 \frac{(T_s - T_2) + (T_s - T_C^{\text{out}})}{2} \\
& FCP_H(T_H^{\text{in}} - T_1) = FCP_C(T_2 - T_C^{\text{in}}) \\
& CP_1 = (0.5 \tanh(P(25 - A_1)) + 0.5)((0.5 \tanh(P(A_1 - 10)) + 0.5) \\
& \quad (1500A_1^{0.6} + 15000) + (0.5 \tanh(P(10 - A_1)) + 0.5)(2750A_1^{0.6} + 3000) \\
& \quad - (600A_1^{0.6} + 46500)) + (600A_1^{0.6} + 46500) \\
& CP_2 = (0.5 \tanh(P(25 - A_2)) + 0.5)((0.5 \tanh(P(A_2 - 10)) + 0.5) \\
& \quad (1500A_2^{0.6} + 15000) + (0.5 \tanh(P(10 - A_2)) + 0.5)(2750A_2^{0.6} + 3000) \\
& \quad - (600A_2^{0.6} + 46500)) + (600A_2^{0.6} + 46500) \\
& CP_3 = (0.5 \tanh(P(25 - A_3)) + 0.5)((0.5 \tanh(P(A_3 - 10)) + 0.5) \\
& \quad (1500A_3^{0.6} + 15000) + (0.5 \tanh(P(10 - A_3)) + 0.5)(2750A_3^{0.6} + 3000) \\
& \quad - (600A_3^{0.6} + 46500)) + (600A_3^{0.6} + 46500) \\
& T_1^{\text{lo}} \leq T_1 \leq T_1^{\text{up}} \\
& T_2^{\text{lo}} \leq T_2 \leq T_2^{\text{up}} \\
& T_l \in \mathbb{R} \quad l = 1, 2 \\
& CP_i^{\text{lo}} \leq CP_i \leq CP_i^{\text{up}} \quad i = 1, 2, 3 \\
& CP_i \in \mathbb{R} \quad i = 1, 2, 3 \\
& A_i \in \mathbb{R} \quad i = 1, 2, 3
\end{aligned}$$



---

# Bibliography

- [1] Q. Zhang and I. E. Grossmann. Enterprise-wide optimization for industrial demand side management: Fundamentals, advances, and perspectives. *Chemical Engineering Research and Design*, 116:114–131, dec 2016. doi: 10.1016/j.cherd.2016.10.006. URL <https://doi.org/10.1016%2Fj.cherd.2016.10.006>.
- [2] I. Staffell, D. Scamman, A. V. Abad, P. Balcombe, P. E. Dodds, P. Ekins, N. Shah, and K. R. Ward. The role of hydrogen and fuel cells in the global energy system. feb 2018. doi: 10.31224/osf.io/rzm4g. URL <https://doi.org/10.31224%2Fosf.io%2Frzm4g>.
- [3] D. Pélerin, K. Gaukel, M. Härtl, E. Jacob, and G. Wachtmeister. Potentials to simplify the engine system using the alternative diesel fuels oxymethylene ether OME<sub>1</sub> and OME<sub>3-6</sub> on a heavy-duty engine. *Fuel*, 259:116231, jan 2020. doi: 10.1016/j.fuel.2019.116231. URL <https://doi.org/10.1016%2Fj.fuel.2019.116231>.
- [4] M. Härtl, K. Gaukel, D. Pélerin, and G. Wachtmeister. Oxymethylenether als potenziell CO<sub>2</sub>-neutraler kraftstoff für saubere dieselmotoren teil 1: Motorenuntersuchungen. *MTZ - Motortechnische Zeitschrift*, 78(2):52–59, jan 2017. doi: 10.1007/s35146-016-0170-9. URL <https://doi.org/10.1007%2Fs35146-016-0170-9>.
- [5] A. García, J. Monsalve-Serrano, D. Villalta, R. L. Sari, V. G. Zavaleta, and P. Gailard. Potential of e-fischer tropsch diesel and oxymethyl-ether (OME<sub>x</sub>) as fuels for the dual-mode dual-fuel concept. *Applied Energy*, 253:113622, nov 2019. doi: 10.1016/j.apenergy.2019.113622. URL <https://doi.org/10.1016%2Fj.apenergy.2019.113622>.
- [6] M. Härtl, P. Seidenspinner, E. Jacob, and G. Wachtmeister. Oxygenate screening on a heavy-duty diesel engine and emission characteristics of highly oxygenated oxymethylene ether fuel OME<sub>1</sub>. *Fuel*, 153:328–335, aug 2015. doi: 10.1016/j.fuel.2015.03.012. URL <https://doi.org/10.1016%2Fj.fuel.2015.03.012>.
- [7] A. Omari, B. Heuser, and S. Pischinger. Potential of oxymethylenether-diesel blends for ultra-low emission engines. *Fuel*, 209:232–237, dec 2017. doi: 10.1016/j.fuel.2017.07.107. URL <https://doi.org/10.1016%2Fj.fuel.2017.07.107>.
- [8] S. E. Iannuzzi, C. Barro, K. Boulouchos, and J. Burger. POMDME-diesel blends: Evaluation of performance and exhaust emissions in a single cylinder heavy-duty diesel engine. *Fuel*, 203:57–67, sep 2017. doi: 10.1016/j.fuel.2017.04.089. URL <https://doi.org/10.1016%2Fj.fuel.2017.04.089>.
- [9] A. Omari, B. Heuser, S. Pischinger, and C. Rüdinger. Potential of long-chain oxymethylene ether and oxymethylene ether-diesel blends for ultra-low emission en-

- gines. *Applied Energy*, 239:1242–1249, apr 2019. doi: 10.1016/j.apenergy.2019.02.035. URL <https://doi.org/10.1016%2Fj.apenergy.2019.02.035>.
- [10] IEA, International Energy Agency. Energy efficiency indicators – highlights, 2020.
- [11] L. Ding, T. Shi, J. Gu, Y. Cui, Z. Zhang, C. Yang, T. Chen, M. Lin, P. Wang, N. Xue, L. Peng, X. Guo, Y. Zhu, Z. Chen, and W. Ding. CO<sub>2</sub> hydrogenation to ethanol over cu@na-beta. *Chem*, 6(10):2673–2689, oct 2020. doi: 10.1016/j.chempr.2020.07.001. URL <https://doi.org/10.1016%2Fj.chempr.2020.07.001>.
- [12] N. Mahbub, A. O. Oyedun, A. Kumar, D. Oestreich, U. Arnold, and J. Sauer. A life cycle assessment of oxymethylene ether synthesis from biomass-derived syngas as a diesel additive. *Journal of Cleaner Production*, 165:1249–1262, nov 2017. doi: 10.1016/j.jclepro.2017.07.178. URL <https://doi.org/10.1016%2Fj.jclepro.2017.07.178>.
- [13] A. O. Oyedun, A. Kumar, D. Oestreich, U. Arnold, and J. Sauer. The development of the production cost of oxymethylene ethers as diesel additives from biomass. *Biofuels, Bioproducts and Biorefining*, 12(4):694–710, may 2018. doi: 10.1002/bbb.1887. URL <https://doi.org/10.1002%2Fbbb.1887>.
- [14] X. Zhang, A. O. Oyedun, A. Kumar, D. Oestreich, U. Arnold, and J. Sauer. An optimized process design for oxymethylene ether production from woody-biomass-derived syngas. *Biomass and Bioenergy*, 90:7–14, jul 2016. doi: 10.1016/j.biombioe.2016.03.032. URL <https://doi.org/10.1016%2Fj.biombioe.2016.03.032>.
- [15] S. Schemme, R. C. Samsun, R. Peters, and D. Stolten. Power-to-fuel as a key to sustainable transport systems – an analysis of diesel fuels produced from CO<sub>2</sub> and renewable electricity. *Fuel*, 205:198–221, oct 2017. doi: 10.1016/j.fuel.2017.05.061. URL <https://doi.org/10.1016%2Fj.fuel.2017.05.061>.
- [16] D. Bongartz, J. Burre, and A. Mitsos. Production of oxymethylene dimethyl ethers from hydrogen and carbon dioxide—part I: Modeling and analysis for OME<sub>1</sub>. *Industrial & Engineering Chemistry Research*, 58(12):4881–4889, mar 2019. doi: 10.1021/acs.iecr.8b05576. URL <https://doi.org/10.1021%2Facs.iecr.8b05576>.
- [17] J. Burre, D. Bongartz, and A. Mitsos. Production of oxymethylene dimethyl ethers from hydrogen and carbon dioxide—part II: Modeling and analysis for OME<sub>3-5</sub>. *Industrial & Engineering Chemistry Research*, 58(14):5567–5578, mar 2019. doi: 10.1021/acs.iecr.8b05577. URL <https://doi.org/10.1021%2Facs.iecr.8b05577>.
- [18] M. Held, Y. Tönges, D. Pélerin, M. Härtl, G. Wachtmeister, and J. Burger. On the energetic efficiency of producing polyoxymethylene dimethyl ethers from CO<sub>2</sub> using electrical energy. *Energy & Environmental Science*, 12(3):1019–1034, 2019. doi: 10.1039/c8ee02849d. URL <https://doi.org/10.1039%2Fc8ee02849d>.
- [19] S. Deutz, D. Bongartz, B. Heuser, A. Kätelhön, L. S. Langenhorst, A. Omari, M. Walters, J. Klankermayer, W. Leitner, A. Mitsos, S. Pischinger, and A. Bardow. Cleaner production of cleaner fuels: wind-to-wheel – environmental assessment of CO<sub>2</sub>-based oxymethylene ether as a drop-in fuel. *Energy & Envi-*

- ronmental Science*, 11(2):331–343, 2018. doi: 10.1039/c7ee01657c. URL <https://doi.org/10.1039%2Fc7ee01657c>.
- [20] L. Lautenschütz, D. Oestreich, P. Seidenspinner, U. Arnold, E. Dinjus, and J. Sauer. Physico-chemical properties and fuel characteristics of oxymethylene dialkyl ethers. *Fuel*, 173:129–137, jun 2016. doi: 10.1016/j.fuel.2016.01.060. URL <https://doi.org/10.1016%2Fj.fuel.2016.01.060>.
- [21] D. Bongartz, L. Doré, K. Eichler, T. Grube, B. Heuser, L. E. Hombach, M. Robinius, S. Pischinger, D. Stolten, G. Walther, and A. Mitsos. Comparison of light-duty transportation fuels produced from renewable hydrogen and green carbon dioxide. *Applied Energy*, 231:757–767, dec 2018. doi: 10.1016/j.apenergy.2018.09.106. URL <https://doi.org/10.1016%2Fj.apenergy.2018.09.106>.
- [22] Z. P. Cano, D. Banham, S. Ye, A. Hintennach, J. Lu, M. Fowler, and Z. Chen. Batteries and fuel cells for emerging electric vehicle markets. *Nature Energy*, 3(4): 279–289, apr 2018. doi: 10.1038/s41560-018-0108-1. URL <https://doi.org/10.1038%2Fs41560-018-0108-1>.
- [23] K. D. Vertin, J. M. Ohi, D. W. Naegeli, K. H. Childress, G. P. Hagen, C. I. McCarthy, A. S. Cheng, and R. W. Dibble. Methylal and methylal-diesel blended fuels for use in compression-ignition engines. SAE Technical Paper Series, may 1999.
- [24] J. Schröder and K. Görsch. Storage stability and material compatibility of poly(oxymethylene) dimethyl ether diesel fuel. *Energy & Fuels*, 34:450–459, jan 2020. doi: 10.1021/acs.energyfuels.9b03101. URL <https://doi.org/10.1021%2Facs.energyfuels.9b03101>.
- [25] G. Reuss, W. Disteldorf, A. Gamer, and A. Hilt. Formaldehyde. Ullmann’s Encyclopedia of Industrial Chemistry, jun 2000.
- [26] J. Burger, E. Ströfer, and H. Hasse. Production process for diesel fuel components poly(oxymethylene) dimethyl ethers from methane-based products by hierarchical optimization with varying model depth. *Chemical Engineering Research and Design*, 91(12):2648–2662, dec 2013. doi: 10.1016/j.cherd.2013.05.023. URL <https://doi.org/10.1016%2Fj.cherd.2013.05.023>.
- [27] N. Schmitz, J. Burger, E. Ströfer, and H. Hasse. From methanol to the oxygenated diesel fuel poly(oxymethylene) dimethyl ether: An assessment of the production costs. *Fuel*, 185:67–72, dec 2016. doi: 10.1016/j.fuel.2016.07.085. URL <https://doi.org/10.1016%2Fj.fuel.2016.07.085>.
- [28] A. Peter, S. M. Fehr, V. Dybbert, D. Himmel, I. Lindner, E. Jacob, M. Ouda, A. Schaadt, R. J. White, H. Scherer, and I. Krossing. Towards a sustainable synthesis of oxymethylene dimethyl ether by homogeneous catalysis and uptake of molecular formaldehyde. *Angewandte Chemie*, 130(30):9605–9608, jul 2018. doi: 10.1002/ange.201802247. URL <https://doi.org/10.1002%2Fange.201802247>.
- [29] A. Peter, G. Stebens, J. F. Baumgärtner, E. Jacob, F. K. Mantei, M. Ouda, and I. Krossing. Facile two-phase catalysis: From dimethoxymethane and monomeric

- formaldehyde towards oxymethylene ethers (OMEs). *ChemCatChem*, 12(9):2416–2420, mar 2020. doi: 10.1002/cctc.201902343. URL <https://doi.org/10.1002%2Fcctc.201902343>.
- [30] S. Schemme, J. L. Breuer, M. Köller, S. Meschede, F. Walman, R. C. Samsun, R. Peters, and D. Stolten. H<sub>2</sub>-based synthetic fuels: A techno-economic comparison of alcohol, ether and hydrocarbon production. *International Journal of Hydrogen Energy*, jun 2019. doi: 10.1016/j.ijhydene.2019.05.028. URL <https://doi.org/10.1016%2Fj.ijhydene.2019.05.028>.
- [31] R. Sun, I. Delidovich, and R. Palkovits. Dimethoxymethane as a cleaner synthetic fuel: Synthetic methods, catalysts, and reaction mechanism. *ACS Catalysis*, 9(2): 1298–1318, jan 2019. doi: 10.1021/acscatal.8b04441. URL <https://doi.org/10.1021%2Facscatal.8b04441>.
- [32] J. M. Douglas. A hierarchical decision procedure for process synthesis. *AIChE Journal*, 31(3):353–362, mar 1985. doi: 10.1002/aic.690310302. URL <https://doi.org/10.1002%2Faic.690310302>.
- [33] A. W. Zimmermann and R. Schomäcker. Assessing early-stage CO<sub>2</sub> utilization technologies-comparing apples and oranges? *Energy Technology*, 5(6):850–860, apr 2017. doi: 10.1002/ente.201600805. URL <https://doi.org/10.1002%2Fente.201600805>.
- [34] J. A. Bergerson, A. Brandt, J. Cresko, M. Carbajales-Dale, H. L. MacLean, H. S. Matthews, S. McCoy, M. McManus, S. A. Miller, W. R. Morrow, I. D. Posen, T. Seager, T. Skone, and S. Sleep. Life cycle assessment of emerging technologies: Evaluation techniques at different stages of market and technical maturity. *Journal of Industrial Ecology*, 24(1):11–25, oct 2019. doi: 10.1111/jiec.12954. URL <https://doi.org/10.1111%2Fjiec.12954>.
- [35] G. Thomassen, M. V. Dael, S. V. Passel, and F. You. How to assess the potential of emerging green technologies? towards a prospective environmental and techno-economic assessment framework. *Green Chemistry*, 21(18):4868–4886, 2019. doi: 10.1039/c9gc02223f. URL <https://doi.org/10.1039%2Fc9gc02223f>.
- [36] S. Su, P. Zaza, and A. Renken. Catalytic dehydrogenation of methanol to water-free formaldehyde. *Chemical Engineering & Technology*, 17(1):34–40, feb 1994. doi: 10.1002/ceat.270170106. URL <https://doi.org/10.1002%2Fceat.270170106>.
- [37] Z. Fan, H. Guo, K. Fang, and Y. Sun. Efficient v2o5/TiO<sub>2</sub> composite catalysts for dimethoxymethane synthesis from methanol selective oxidation. *RSC Advances*, 5(31):24795–24802, 2015. doi: 10.1039/c4ra16727a. URL <https://doi.org/10.1039%2Fc4ra16727a>.
- [38] K. Thenert, K. Beydoun, J. Wiesenthal, W. Leitner, and J. Klankermayer. Ruthenium-catalyzed synthesis of dialkoxymethane ethers utilizing carbon dioxide and molecular hydrogen. *Angewandte Chemie*, 128(40):12454–12457, sep 2016. doi: 10.1002/ange.201606427. URL <https://doi.org/10.1002%2Fange.201606427>.

- [39] B. G. Schieweck and J. Klankermayer. Tailor-made molecular cobalt catalyst system for the selective transformation of carbon dioxide to dialkoxymethane ethers. *Angewandte Chemie*, 129(36):10994–10997, jul 2017. doi: 10.1002/ange.201702905. URL <https://doi.org/10.1002%2Fange.201702905>.
- [40] M. Siebert, M. Seibicke, A. F. Siegle, S. Kräh, and O. Trapp. Selective ruthenium-catalyzed transformation of carbon dioxide: An alternative approach toward formaldehyde. *Journal of the American Chemical Society*, 141(1):334–341, dec 2019. doi: 10.1021/jacs.8b10233. URL <https://doi.org/10.1021%2Fjacs.8b10233>.
- [41] R. Sun, C. Mebrahtu, J. P. Hofmann, D. Bongartz, J. Burre, C. H. Gierlich, P. J. Hausoul, A. Mitsos, and R. Palkovits. Hydrogen-efficient non-oxidative transformation of methanol into dimethoxymethane over a tailored bifunctional cu catalyst. *Sustainable Energy and Fuels*, in press.
- [42] O. Osterthun. *Tailored catalysts for the synthesis of SynFuels via methanol dehydrogenation and transfer-hydrogenation*. PhD thesis, RWTH Aachen University, 2021.
- [43] É. S. Van-Dal and C. Bouallou. Design and simulation of a methanol production plant from CO<sub>2</sub> hydrogenation. *Journal of Cleaner Production*, 57:38–45, oct 2013. doi: 10.1016/j.jclepro.2013.06.008. URL <https://doi.org/10.1016%2Fj.jclepro.2013.06.008>.
- [44] M. Pérez-Fortes, J. C. Schöneberger, A. Boulamanti, and E. Tzimas. Methanol synthesis using captured CO<sub>2</sub> as raw material: Techno-economic and environmental assessment. *Applied Energy*, 161:718–732, jan 2016. doi: 10.1016/j.apenergy.2015.07.067. URL <https://doi.org/10.1016%2Fj.apenergy.2015.07.067>.
- [45] J.-O. Weidert, J. Burger, M. Renner, S. Blagov, and H. Hasse. Development of an integrated reaction–distillation process for the production of methylal. *Industrial & Engineering Chemistry Research*, 56(2):575–582, jan 2017. doi: 10.1021/acs.iecr.6b03847. URL <https://doi.org/10.1021%2Facs.iecr.6b03847>.
- [46] J. Walker. Formaldehyde. Reinhold Publishing, 1944.
- [47] A. Fredenslund, R. L. Jones, and J. M. Prausnitz. Group-contribution estimation of activity coefficients in nonideal liquid mixtures. *AIChE Journal*, 21(6):1086–1099, nov 1975. doi: 10.1002/aic.690210607. URL <https://doi.org/10.1002%2Faic.690210607>.
- [48] G. Maurer. Vapor-liquid equilibrium of formaldehyde-and water-containing multi-component mixtures. *AIChE Journal*, 32(6):932–948, jun 1986. doi: 10.1002/aic.690320604. URL <https://doi.org/10.1002%2Faic.690320604>.
- [49] H. Hasse, I. Hahnenstein, and G. Maurer. Revised vapor-liquid equilibrium model for multicomponent formaldehyde mixtures. *AIChE Journal*, 36(12):1807–1814, dec 1990. doi: 10.1002/aic.690361204. URL <https://doi.org/10.1002%2Faic.690361204>.

- [50] I. Hahnenstein, H. Hasse, C. G. Kreiter, and G. Maurer. 1h- and 13c-NMR-spectroscopic study of chemical equilibria in solutions of formaldehyde in water, deuterium oxide, and methanol. *Industrial & Engineering Chemistry Research*, 33(4):1022–1029, apr 1994. doi: 10.1021/ie00028a033. URL <https://doi.org/10.1021%2Fie00028a033>.
- [51] M. Albert, B. C. García, C. Kreiter, and G. Maurer. Vapor-liquid and chemical equilibria of formaldehyde-water mixtures. *AIChE Journal*, 45(9):2024–2033, sep 1999. doi: 10.1002/aic.690450919. URL <https://doi.org/10.1002%2Faic.690450919>.
- [52] M. Albert, B. C. García, C. Kuhnert, R. Peschla, and G. Maurer. Vapor-liquid equilibrium of aqueous solutions of formaldehyde and methanol. *AIChE Journal*, 46(8):1676–1687, aug 2000. doi: 10.1002/aic.690460818. URL <https://doi.org/10.1002%2Faic.690460818>.
- [53] M. Albert, H. Hasse, C. Kuhnert, and G. Maurer. New experimental results for the vapor-liquid equilibrium of the binary system (trioxane + water) and the ternary system (formaldehyde + trioxane + water). *J. Chem. Eng. Data*, 50:1218–1223, 2005.
- [54] Y.-Q. Liu, H. Hasse, and G. Maurer. Enthalpy change on vaporization of aqueous and methanolic formaldehyde solutions. *AIChE J.*, 38(11):1693–1702, 1992.
- [55] J. Burre and D. Bongartz. Aspen Plus implementations of process models for the production of OME<sub>n</sub> from H<sub>2</sub> and CO<sub>2</sub>. URL <http://permalink.avt.rwth-aachen.de/?id=661625>. 2019.
- [56] A. Otto. *Chemical, procedural and economic evaluation of carbon dioxide as feedstock in the chemical industry*. PhD thesis, RWTH Aachen University, 2015.
- [57] J.-O. Drunsel, M. Renner, and H. Hasse. Experimental study and model of reaction kinetics of heterogeneously catalyzed methylal synthesis. *Chemical Engineering Research and Design*, 90(5):696–703, may 2012. doi: 10.1016/j.cherd.2011.09.014. URL <https://doi.org/10.1016%2Fj.cherd.2011.09.014>.
- [58] E. Jacob and W. Maus. Oxymethylenether als potenziell CO<sub>2</sub>-neutraler Kraftstoff für saubere Dieselmotoren Teil 2: Erfüllung des Nachhaltigkeitsanspruchs. *MTZ-Motortechnische Zeitschrift*, 78(3):54–61, 2017.
- [59] C. J. Baranowski, A. M. Bahmanpour, and O. Kröcher. Catalytic synthesis of polyoxymethylene dimethyl ethers (OME): A review. *Applied Catalysis B: Environmental*, 2017.
- [60] N. Schmitz, J. Burger, E. Ströfer, and H. Hasse. From methanol to the oxygenated diesel fuel poly (oxymethylene) dimethyl ether: An assessment of the production costs. *Fuel*, 185:67–72, 2016.
- [61] N. Schmitz, E. Ströfer, J. Burger, and H. Hasse. Conceptual design of a novel process for the production of poly (oxymethylene) dimethyl ethers from formaldehyde and methanol. *Industrial & Engineering Chemistry Research*, 56(40):11519–11530, 2017.



- [62] M. Ouda, F. Mantei, M. Elmehlawy, R. White, H. Klein, and S.-E. Fateen. Describing oxymethylene ether synthesis based on the application of non-stoichiometric gibbs minimisation. *Reaction Chemistry & Engineering*, 3(3):277–292, 2018.
- [63] M. Ouda, F. Mantei, K. Hesterwerth, E. Bargiacchi, H. Klein, and R. J. White. A hybrid description and evaluation of oxymethylene dimethyl ethers synthesis based on the endothermic dehydrogenation of methanol. *Reaction Chemistry & Engineering*, 3(5):676–695, 2018.
- [64] Z.-J. Ai, C.-Y. Chung, and I.-L. Chien. Design and control of poly (oxymethylene) dimethyl ethers production process directly from formaldehyde and methanol in aqueous solutions. *IFAC-PapersOnLine*, 51(18):578–583, 2018.
- [65] X. Zhang, A. O. Oyedun, A. Kumar, D. Oestreich, U. Arnold, and J. Sauer. An optimized process design for oxymethylene ether production from woody-biomass-derived syngas. *Biomass and Bioenergy*, 90:7–14, 2016.
- [66] X. Zhang, A. Kumar, U. Arnold, and J. Sauer. Biomass-derived oxymethylene ethers as diesel additives: A thermodynamic analysis. *Energy Procedia*, 61:1921–1924, 2014.
- [67] N. Mahbub, A. O. Oyedun, A. Kumar, D. Oestreich, U. Arnold, and J. Sauer. A life cycle assessment of oxymethylene ether synthesis from biomass-derived syngas as a diesel additive. *Journal of Cleaner Production*, 165:1249–1262, 2017.
- [68] K. Hackbarth, P. Haltenort, U. Arnold, and J. Sauer. Recent progress in the production, application and evaluation of oxymethylene ethers. *Chemie Ingenieur Technik*, 90(10):1520–1528, 2018.
- [69] J. Mahieux. Make trioxane continuously. *Hydrocarbon Processing, International Edition*, 48(5):163, 1969.
- [70] M. Held, Y. Tönges, D. Pélerin, M. Härtl, G. Wachtmeister, and J. Burger. On the energetic efficiency of producing polyoxymethylene dimethyl ethers from CO<sub>2</sub> using electrical energy. *Energy & Environmental Science*, 2019.
- [71] M. Ouda, G. Yarce, R. White, M. Hadrich, D. Himmel, A. Schaadt, H. Klein, E. Jacob, and I. Krossing. Poly (oxymethylene) dimethyl ether synthesis—a combined chemical equilibrium investigation towards an increasingly efficient and potentially sustainable synthetic route. *Reaction Chemistry & Engineering*, 2(1):50–59, 2017.
- [72] J. Zhang, M. Shi, D. Fang, and D. Liu. Reaction kinetics of the production of polyoxymethylene dimethyl ethers from methanol and formaldehyde with acid cation exchange resin catalyst. *Reaction Kinetics, Mechanisms and Catalysis*, 113(2):459–740, 2014.
- [73] J. Zhang, D. Fang, and D. Liu. Evaluation of zr–alumina in production of polyoxymethylene dimethyl ethers from methanol and formaldehyde: performance tests and kinetic investigations. *Industrial & Engineering Chemistry Research*, 53(35):13589–13597, 2014.

- [74] N. Schmitz, F. Homberg, J. Berje, J. Burger, and H. Hasse. Chemical equilibrium of the synthesis of poly (oxymethylene) dimethyl ethers from formaldehyde and methanol in aqueous solutions. *Industrial & Engineering Chemistry Research*, 54(25):6409–6417, 2015.
- [75] N. Schmitz, J. Burger, and H. Hasse. Reaction kinetics of the formation of poly (oxymethylene) dimethyl ethers from formaldehyde and methanol in aqueous solutions. *Industrial & Engineering Chemistry Research*, 54(50):12553–12560, 2015.
- [76] D. Oestreich, L. Lautenschütz, U. Arnold, and J. Sauer. Reaction kinetics and equilibrium parameters for the production of oxymethylene dimethyl ethers (OME) from methanol and formaldehyde. *Chemical Engineering Science*, 163:92–104, 2017.
- [77] N. Schmitz, C. F. Breitzkreuz, E. Ströfer, J. Burger, and H. Hasse. Separation of water from mixtures containing formaldehyde, water, methanol, methylal, and poly (oxymethylene) dimethyl ethers by pervaporation. *Journal of Membrane Science*, 564:806–812, 2018.
- [78] X. Y. Li, H. B. Yu, Y. M. Sun, H. B. Wang, T. Guo, Y. L. Sui, J. Miao, X. J. Zeng, and S. P. Li. Synthesis and application of polyoxymethylene dimethyl ethers. In *Applied Mechanics and Materials*, volume 448, pages 2969–2973. Trans Tech Publ, 2014.
- [79] D. Oestreich, L. Lautenschütz, U. Arnold, and J. Sauer. Production of oxymethylene dimethyl ether (OME)-hydrocarbon fuel blends in a one-step synthesis/extraction procedure. *Fuel*, 214:39–44, 2018.
- [80] F. Liu, T. Wang, Y. Zheng, and J. Wang. Synergistic effect of brønsted and lewis acid sites for the synthesis of polyoxymethylene dimethyl ethers over highly efficient so 4 2-/tio 2 catalysts. *Journal of Catalysis*, 355:17–25, 2017.
- [81] G.-F. Shi, J. Miao, G.-Y. Wang, J.-M. Su, and H.-X. Liu. Synthesis of polyoxymethylene dimethyl ethers catalyzed by rare earth compounds. *Asian Journal of Chemistry*, 27(6), 2015.
- [82] Y. Zhao, Z. Xu, H. Chen, Y. Fu, and J. Shen. Mechanism of chain propagation for the synthesis of polyoxymethylene dimethyl ethers. *Journal of Energy Chemistry*, 22(6):833–836, 2013.
- [83] Y. Zheng, Q. Tang, T. Wang, Y. Liao, and J. Wang. Synthesis of a green fuel additive over cation resins. *Chemical Engineering & Technology*, 36(11):1951–1956, 2013.
- [84] Y. Zheng, Q. Tang, T. Wang, and J. Wang. Kinetics of synthesis of polyoxymethylene dimethyl ethers from paraformaldehyde and dimethoxymethane catalyzed by ion-exchange resin. *Chemical Engineering Science*, 134:758–766, 2015.
- [85] G. Reuss, W. Disteldorf, A. O. Gamer, and A. Hilt. Formaldehyde. *Ullmann’s Encyclopedia of Industrial Chemistry*, 2000.

- 
- [86] J. Burger, M. Siegert, E. Ströfer, and H. Hasse. Poly (oxymethylene) dimethyl ethers as components of tailored diesel fuel: Properties, synthesis and purification concepts. *Fuel*, 89(11):3315–3319, 2010.
- [87] J. Burger. *A novel process for the production of diesel fuel additives by hierarchical design*. PhD thesis, Techn. Univ. Kaiserslautern, 2012.
- [88] J. Burger, E. Ströfer, and H. Hasse. Chemical equilibrium and reaction kinetics of the heterogeneously catalyzed formation of poly (oxymethylene) dimethyl ethers from methylal and trioxane. *Industrial & Engineering Chemistry Research*, 51(39):12751–12761, 2012.
- [89] J. Burger and H. Hasse. Multi-objective optimization using reduced models in conceptual design of a fuel additive production process. *Chemical Engineering Science*, 99:118–126, 2013.
- [90] J. Burger, E. Ströfer, and H. Hasse. Production process for diesel fuel components poly (oxymethylene) dimethyl ethers from methane-based products by hierarchical optimization with varying model depth. *Chemical Engineering Research and Design*, 91(12):2648–2662, 2013.
- [91] L. Wang, W.-T. Wu, T. Chen, Q. Chen, and M.-Y. He. Ion-exchange resin-catalyzed synthesis of polyoxymethylene dimethyl ethers: A practical and environmentally friendly way to diesel additive. *Chemical Engineering Communications*, 201(5):709–717, 2014.
- [92] Q. Wu, M. Wang, Y. Hao, H. Li, Y. Zhao, and Q. Jiao. Synthesis of polyoxymethylene dimethyl ethers catalyzed by brønsted acid ionic liquids with alkanesulfonic acid groups. *Industrial & Engineering Chemistry Research*, 53(42):16254–16260, 2014.
- [93] J. Wu, H. Zhu, Z. Wu, Z. Qin, L. Yan, B. Du, W. Fan, and J. Wang. High si/al ratio hzsm-5 zeolite: an efficient catalyst for the synthesis of polyoxymethylene dimethyl ethers from dimethoxymethane and trioxymethylene. *Current Green Chemistry*, 17(4):2353–2357, 2015.
- [94] Y. Wu, Z. Li, and C. Xia. Silica-gel-supported dual acidic ionic liquids as efficient catalysts for the synthesis of polyoxymethylene dimethyl ethers. *Industrial & Engineering Chemistry Research*, 55(7):1859–1865, 2016.
- [95] L. P. Lautenschütz. *Neue Erkenntnisse in der Syntheseoptimierung oligomerer Oxymethylen dimethylether aus Dimethoxymethan und Trioxan*. PhD thesis, Ruprecht-Karls-Universität Heidelberg, 2015.
- [96] L. Lautenschütz, D. Oestreich, P. Haltenort, U. Arnold, E. Dinjus, and J. Sauer. Efficient synthesis of oxymethylene dimethyl ethers (OME) from dimethoxymethane and trioxane over zeolites. *Fuel Processing Technology*, 165:27–33, 2017.
- [97] T. Grützner, H. Hasse, N. Lang, M. Siegert, and E. Ströfer. Development of a new industrial process for trioxane production. *Chemical Engineering Science*, 62(18):5613–5620, 2007.

- [98] T. Grützner. *Entwicklung eines destillationsbasierten Verfahrens zur Herstellung von Trioxan*. PhD thesis, Techn. Univ. Kaiserslautern, 2007.
- [99] Q. Zhang, Y. Tan, G. Liu, J. Zhang, and Y. Han. Rhenium oxide-modified h 3 pw 12 o 40/tio 2 catalysts for selective oxidation of dimethyl ether to dimethoxy dimethyl ether. *Green Chemistry*, 16(11):4708–4715, 2014.
- [100] Q. Zhang, W. Wang, Z. Zhang, Y. Han, and Y. Tan. Low-temperature oxidation of dimethyl ether to polyoxymethylene dimethyl ethers over cnt-supported rhenium catalyst. *Catalysts*, 6(3):43, 2016.
- [101] P. Haltenort, K. Hackbarth, D. Oestreich, L. Lautenschütz, U. Arnold, and J. Sauer. Heterogeneously catalyzed synthesis of oxymethylene dimethyl ethers (OME) from dimethyl ether and trioxane. *Catalysis Communications*, 109:80–84, 2018.
- [102] C. F. Breitzkreuz, N. Schmitz, E. Ströfer, J. Burger, and H. Hasse. Design of a production process for poly (oxymethylene) dimethyl ethers from dimethyl ether and trioxane. *Chemie Ingenieur Technik*, 90(10):1489–1496, 2018.
- [103] O. Ryll, S. Blagov, and H. Hasse. inf/inf-analysis of homogeneous distillation processes. *Chemical Engineering Science*, 84:315–332, 2012.
- [104] T. Grützner and H. Hasse. Solubility of formaldehyde and trioxane in aqueous solutions. *Journal of Chemical & Engineering Data*, 49(3):642–646, 2004.
- [105] J. Chen, H. Song, C. Xia, X. Zhang, and Z. Tang. Method for synthesizing poly-oxymethylene dimethyl ethers by ionic liquid catalysis. Google Patents, March 2010. US Patent App. 12/548,807.
- [106] J. Chen, H. Song, C. Xia, and Z. Li. Method for synthesizing polyoxymethylene dimethyl ethers catalyzed by an ionic liquid. Google Patents, November 2011. US Patent App. 13/154,359.
- [107] Z. Xue, H. Shang, C. Xiong, C. Lu, G. An, Z. Zhang, C. Cui, and M. Xu. Synthesis of polyoxymethylene dimethyl ethers catalyzed by sulfonic acid-functionalized mesoporous sba-15. *RSC Advances*, 7(33):20300–20308, 2017.
- [108] E. Strofer, H. Schelling, H. Hasse, and S. Blagov. Method for the production of polyoxymethylene dialkyl ethers from trioxan and dialkylethers. Google Patents, August 2011. US Patent 7,999,140.
- [109] M. Arvidson, M. Fakley, and M. Spencer. Lithium halide-assisted formation of poly-oxymethylene dimethyl ethers from dimethoxymethane and formaldehyde. *Journal of molecular catalysis*, 41(3):391–393, 1987.
- [110] G. Maurer. Vapor-liquid equilibrium of formaldehyde-and water-containing multi-component mixtures. *AIChE journal*, 32(6):932–948, 1986.
- [111] A. Gruznov, E. Oreshenkova, V. Klyuchnikov, and P. Curtis. Kinetic studies of the formation of methanol and formic acid in aqueous formaldehyde solutions in the presence of acids. *International polymer science and technology*, 24(4):39–43, 1997.

- 
- [112] A. Balashov, V. Krasnov, S. Danov, A. Y. Chernov, and A. Sulimov. Formation of cyclic oligomers in concentrated aqueous solutions of formaldehyde. *Journal of Structural Chemistry*, 42(3):398–403, 2001.
- [113] K. A. Bernard and J. D. Atwood. Evidence for carbon-oxygen bond formation, aldehyde decarbonylation, and dimerization by reaction of formaldehyde and acetaldehyde with trans-roir (co)(pph3) 2. *Organometallics*, 7(1):235–236, 1988.
- [114] M. Albert, B. C. García, C. Kreiter, and G. Maurer. Vapor-liquid and chemical equilibria of formaldehyde-water mixtures. *AIChE Journal*, 45(9):2024–2033, 1999.
- [115] M. Albert. *Thermodynamische Eigenschaften formaldehydhaltiger Mischungen*. PhD thesis, Techn. Univ. Kaiserslautern, 1998.
- [116] I. Hahnenstein, H. Hasse, C. G. Kreiter, and G. Maurer. 1h-and 13c-nmr-spectroscopic study of chemical equilibria in solutions of formaldehyde in water, deuterium oxide, and methanol. *Industrial & engineering chemistry research*, 33(4):1022–1029, 1994.
- [117] I. Hahnenstein, M. Albert, H. Hasse, C. G. Kreiter, and G. Maurer. Nmr spectroscopic and densimetric study of reaction kinetics of formaldehyde polymer formation in water, deuterium oxide, and methanol. *Industrial & engineering chemistry research*, 34(2):440–450, 1995.
- [118] C. Kuhnert, M. Albert, S. Breyer, I. Hahnenstein, H. Hasse, and G. Maurer. Phase equilibrium in formaldehyde containing multicomponent mixtures: experimental results for fluid phase equilibria of (formaldehyde+(water or methanol)+ methylal)) and (formaldehyde+ water+ methanol+ methylal) and comparison with predictions. *Industrial & engineering chemistry research*, 45(14):5155–5164, 2006.
- [119] M. Ott. *Reaktionskinetik und Destillation formaldehydhaltiger Mischungen*. PhD thesis, Techn. Univ. Kaiserslautern, 2004.
- [120] A. Fredenslund, R. L. Jones, and J. M. Prausnitz. Group-contribution estimation of activity coefficients in nonideal liquid mixtures. *AIChE Journal*, 21(6):1086–1099, 1975.
- [121] H. Renon and J. M. Prausnitz. Local compositions in thermodynamic excess functions for liquid mixtures. *AIChE journal*, 14(1):135–144, 1968.
- [122] A. Mitsos, G. M. Bolas, and P. I. Barton. Bilevel optimization algorithm for rigorous & robust parameter estimation in thermodynamics BOARPET. <http://www.avt.rwth-aachen.de/cms/AVT/Wirtschaft/SoftwareSimulation/~kvkz/BOARPET/?lidx=1>. Accessed: 2018-03-22.
- [123] A. Mitsos, G. M. Bolas, and P. I. Barton. Bilevel optimization formulation for parameter estimation in liquid–liquid phase equilibrium problems. *Chemical Engineering Science*, 64(3):548–559, 2009.

- [124] G. M. Bollas, P. I. Barton, and A. Mitsos. Bilevel optimization formulation for parameter estimation in vapor–liquid (–liquid) phase equilibrium problems. *Chemical Engineering Science*, 64(8):1768–1783, 2009.
- [125] D. H. König, N. Baucks, R.-U. Dietrich, and A. Wörner. Simulation and evaluation of a process concept for the generation of synthetic fuel from CO<sub>2</sub> and H<sub>2</sub>. *Energy*, 91:833–841, 2015.
- [126] É. S. Van-Dal and C. Bouallou. Design and simulation of a methanol production plant from CO<sub>2</sub> hydrogenation. *Journal of Cleaner Production*, 57:38–45, 2013.
- [127] A. Ursua, L. M. Gandia, and P. Sanchis. Hydrogen production from water electrolysis: current status and future trends. *Proceedings of the IEEE*, 100(2):410–426, 2012.
- [128] T. Smolinka, M. Günther, and J. Garche. Stand und Entwicklungspotenzial der Wasserelektrolyse zur Herstellung von Wasserstoff aus regenerativen Energien. *Kurzfassung des Abschlussberichtes NOW-Studie, Freiburg im Breisgau*, 2011.
- [129] U. Lee, J. Burre, A. Caspari, J. Kleinekorte, A. M. Schweidtmann, and A. Mitsos. Techno-economic optimization of a green-field post-combustion CO<sub>2</sub> capture process using superstructure and rate-based models. *Industrial & Engineering Chemistry Research*, 55(46):12014–12026, 2016.
- [130] K. Wagemann and F. Ausfelder. E-fuels – Mehr als eine Option. *DECHEMA*, 2017.
- [131] C. Kuhnert, M. Albert, S. Breyer, I. Hahnenstein, H. Hasse, and G. Maurer. Phase equilibrium in formaldehyde containing multicomponent mixtures: experimental results for fluid phase equilibria of (formaldehyde + (water or methanol) + methylal)) and (formaldehyde + water + methanol + methylal) and comparison with predictions. *Industrial & Engineering Chemistry Research*, 45(14):5155–5164, jul 2006. doi: 10.1021/ie060131u. URL <https://doi.org/10.1021%2Fie060131u>.
- [132] H. Liu, H. Gao, Y. Ma, Z. Gao, and W. Eli. Synthesis of high-purity methylal via extractive catalytic distillation. *Chemical Engineering & Technology*, 35(5):841–846, apr 2012. doi: 10.1002/ceat.201100446. URL <https://doi.org/10.1002%2Fceat.201100446>.
- [133] Q. Wang, B. Yu, and C. Xu. Design and control of distillation system for methylal/methanol separation. part 1: Extractive distillation using DMF as an entrainer. *Industrial & Engineering Chemistry Research*, 51(3):1281–1292, jan 2012. doi: 10.1021/ie201946d. URL <https://doi.org/10.1021%2Fie201946d>.
- [134] B. Yu, Q. Wang, and C. Xu. Design and control of distillation system for methylal/methanol separation. part 2: Pressure swing distillation with full heat integration. *Industrial & Engineering Chemistry Research*, 51(3):1293–1310, jan 2012. doi: 10.1021/ie201949q. URL <https://doi.org/10.1021%2Fie201949q>.
- [135] X. Zhang, S. Zhang, and C. Jian. Synthesis of methylal by catalytic distillation. *Chemical Engineering Research and Design*, 89(6):573–580, jun 2011. doi: 10.1016/j.cherd.2010.09.002. URL <https://doi.org/10.1016%2Fj.cherd.2010.09.002>.

- [136] R. Smith. *Chemical process: design and integration*. John Wiley & Sons, 2005.
- [137] K. Kraemer, S. Kossack, and W. Marquardt. Efficient optimization-based design of distillation processes for homogeneous azeotropic mixtures. *Industrial & Engineering Chemistry Research*, 48(14):6749–6764, jul 2009. doi: 10.1021/ie900143e. URL <https://doi.org/10.1021%2Fie900143e>.
- [138] J. Bausa, R. v. Watzdorf, and W. Marquardt. Shortcut methods for nonideal multicomponent distillation: I. simple columns. *AIChE Journal*, 44(10):2181–2198, oct 1998. doi: 10.1002/aic.690441008. URL <https://doi.org/10.1002%2Faic.690441008>.
- [139] Process Systems Engineering (AVT.SVT). Ee-toolbox, 2017. URL <https://www.avt.rwth-aachen.de/cms/AVT/Forschung/Software/~iptv/Shortcut-Toolbox/?lidx=1>. Accessed: 2020-03-04.
- [140] S. Kossack, K. Kraemer, and W. Marquardt. Efficient optimization-based design of distillation columns for homogenous azeotropic mixtures. *Industrial & Engineering Chemistry Research*, 45(25):8492–8502, dec 2006. doi: 10.1021/ie060117h. URL <https://doi.org/10.1021%2Fie060117h>.
- [141] J. Burre, D. Bongartz, L. Brée, K. Roh, and A. Mitsos. Power-to-x: Between electricity storage, e-production, and demand side management. *Chemie Ingenieur Technik*, 92(1-2):74–84, nov 2019. doi: 10.1002/cite.201900102. URL <https://doi.org/10.1002%2Fcite.201900102>.
- [142] J. Burre, D. Bongartz, S. Deutz, C. Mebrahtu, O. Osterthun, R. Sun, S. Völker, A. Bardow, J. Klankermayer, R. Palkovits, and A. Mitsos. Comparing pathways for electricity-based production of dimethoxymethane as a sustainable fuel. *Energy & Environmental Science*, 14(7):3686–3699, 2021. doi: 10.1039/d1ee00689d. URL <https://doi.org/10.1039%2Fd1ee00689d>.
- [143] International Organization for Standardization. *ISO 14040: Environmental Management: Life Cycle Assessment: Principles and Framework*. ISO, 2006.
- [144] International Organization for Standardization. *ISO 14044: Environmental Management: Life Cycle Assessment: Requirements and Guidelines*. ISO, 2006.
- [145] L. J. Müller, A. Kätelhön, M. Bachmann, A. Zimmermann, A. Sternberg, and A. Bardow. A guideline for life cycle assessment of carbon capture and utilization. *Frontiers in Energy Research*, 8:15, 2020. ISSN 2296-598X. doi: 10.3389/fenrg.2020.00015. URL <https://www.frontiersin.org/article/10.3389/fenrg.2020.00015>.
- [146] J. Guinée. Handbook on life cycle assessment — operational guide to the ISO standards. *The International Journal of Life Cycle Assessment*, 6(5):255–255, sep 2001. doi: 10.1007/bf02978784. URL <https://doi.org/10.1007%2Fbf02978784>.
- [147] D. Bongartz, J. Burre, A. L. Ziegler, and A. Mitsos. Power-to-ome1 via direct oxidation of methanol: Process design and global flowsheet optimization. In *Computer Aided Chemical Engineering*, volume 50, pages 273–278. Elsevier, 2021.

- [148] T. Grube, L. Doré, A. Hoffrichter, L. E. Hombach, S. Rath, M. Robinius, M. Nobis, S. Schiebahn, V. Tietze, A. Schnettler, G. Walther, and D. Stolten. An option for stranded renewables: electrolytic-hydrogen in future energy systems. *Sustainable Energy & Fuels*, 2(7):1500–1515, 2018. doi: 10.1039/c8se00008e. URL <https://doi.org/10.1039/c8se00008e>.
- [149] M. Bui, C. S. Adjiman, A. Bardow, E. J. Anthony, A. Boston, S. Brown, P. S. Fennell, S. Fuss, A. Galindo, L. A. Hackett, J. P. Hallett, H. J. Herzog, G. Jackson, J. Kemper, S. Krevor, G. C. Maitland, M. Matuszewski, I. S. Metcalfe, C. Petit, G. Puxty, J. Reimer, D. M. Reiner, E. S. Rubin, S. A. Scott, N. Shah, B. Smit, J. P. M. Trusler, P. Webley, J. Wilcox, and N. M. Dowell. Carbon capture and storage (CCS): the way forward. *Energy & Environmental Science*, 11(5):1062–1176, 2018. doi: 10.1039/c7ee02342a. URL <https://doi.org/10.1039/c7ee02342a>.
- [150] W. L. Luyben. Design and control of the ethyl benzene process. *AIChE Journal*, 57(3):655–670, apr 2010. doi: 10.1002/aic.12289. URL <https://doi.org/10.1002/aic.12289>.
- [151] W. D. Seider, J. D. Seader, and D. R. Lewin. *Product & Process Design Principles: Synthesis, Analysis and Evaluation*. John Wiley & Sons, 2009.
- [152] K. M. Guthrie. Capital cost estimation. *Chem. Engng.*, 24:114–142, 1969.
- [153] R. Turton, R. C. Bailie, W. B. Whiting, and J. A. Shaeiwitz. *Analysis, synthesis and design of chemical processes*. Pearson Education, 2008.
- [154] H. Li, Z. Song, X. Zhang, Y. Huang, S. Li, Y. Mao, H. J. Ploehn, Y. Bao, and M. Yu. Ultrathin, molecular-sieving graphene oxide membranes for selective hydrogen separation. *Science*, 342(6154):95–98, oct 2013. doi: 10.1126/science.1236686. URL <https://doi.org/10.1126/science.1236686>.
- [155] A. Linzenich, K. Arning, D. Bongartz, A. Mitsos, and M. Ziefle. What fuels the adoption of alternative fuels? examining preferences of german car drivers for fuel innovations. *Applied Energy*, 249:222–236, sep 2019. doi: 10.1016/j.apenergy.2019.04.041. URL <https://doi.org/10.1016/j.apenergy.2019.04.041>.
- [156] R. Socolow, M. Desmond, R. Aines, J. Blackstock, O. Bolland, T. Kaarsberg, N. Lewis, M. Mazzotti, A. Pfeffer, K. Sawyer, et al. Direct air capture of CO<sub>2</sub> with chemicals: a technology assessment for the aps panel on public affairs. Technical report, American Physical Society, 2011.
- [157] ecoinvent. ecoinvent Database Version 3.01. URL <https://ecoquery.ecoinvent.org/Search/Index>. Accessed: 2020-07-09.
- [158] IEA, International Energy Agency. Energy technology perspectives 2017: Catalysing energy technology transformation, 2017.
- [159] A. Mitsos, I. Palou-Rivera, and P. I. Barton. Alternatives for micropower generation processes. *Industrial & Engineering Chemistry Research*, 43(1):74–84, jan 2004. doi: 10.1021/ie0304917. URL <https://doi.org/10.1021/ie0304917>.



- [160] E. C. Carlson. Don't gamble with physical properties for simulations. *Chemical engineering progress*, 92(10):35–46, 1996.
- [161] J. Gross. An equation-of-state contribution for polar components: Quadrupolar molecules. *AIChE Journal*, 51(9):2556–2568, 2005. ISSN 0001-1541. doi: 10.1002/aic.10502.
- [162] J. Gross and J. Vrabec. An equation-of-state contribution for polar components: Dipolar molecules. *AIChE Journal*, 52(3):1194–1204, 2006. ISSN 0001-1541. doi: 10.1002/aic.10683.
- [163] M. Kleiner and G. Sadowski. Modeling of polar systems using PCP-SAFT: An approach to account for induced-association interactions. *The Journal of Physical Chemistry C*, 111(43):15544–15553, aug 2007. doi: 10.1021/jp072640v. URL <https://doi.org/10.1021%2Fjp072640v>.
- [164] D. Bongartz, J. Najman, S. Sass, and A. Mitsos. MAiNGO – McCormick-based Algorithm for mixed-integer Nonlinear Global Optimization. Technical report, Process Systems Engineering (AVT.SVT), RWTH Aachen University, 2018. URL <http://permalink.avt.rwth-aachen.de/?id=729717>.
- [165] K. M. Thenert. *Maßgeschneiderte Ruthenium-Katalysatoren für die stoffliche Nutzung von CO<sub>2</sub> in Kombination mit molekularem Wasserstoff*. PhD thesis, Universitätsbibliothek der RWTH Aachen, 2018.
- [166] J. Gross and G. Sadowski. Perturbed-chain saft: An equation of state based on a perturbation theory for chain molecules. *Industrial & Engineering Chemistry Research*, 40(4):1244–1260, 2001. ISSN 0888-5885. doi: 10.1021/ie0003887.
- [167] M. Aigner, A. Echtermeyer, S. Kaminski, J. Viell, K. Leonhard, A. Mitsos, and A. Jupke. Ternary system CO<sub>2</sub>/2-mthf/water—experimental study and thermodynamic modeling. *Journal of Chemical & Engineering Data*, 2019. ISSN 0021-9568. doi: 10.1021/acs.jced.9b00315.
- [168] F. Tumakaka, J. Gross, and G. Sadowski. Thermodynamic modeling of complex systems using pc-saft. *Fluid Phase Equilibria*, 228-229:89–98, 2005. ISSN 03783812. doi: 10.1016/j.fluid.2004.09.037.
- [169] J. Burre, C. Kabatnik, M. Al-Khatib, D. Bongartz, A. Jupke, and A. Mitsos. Global flowsheet optimization for reductive dimethoxymethane production using data-driven thermodynamic models. *Computers & Chemical Engineering*, 2022. Accepted for publication.
- [170] A.-D. Leu, S. Y.-K. Chung, and D. B. Robinson. The equilibrium phase properties of (carbon dioxide + methanol). *The Journal of Chemical Thermodynamics*, 23(10): 979–985, 1991. ISSN 00219614. doi: 10.1016/S0021-9614(05)80178-8.
- [171] P. Gillespie and G. Wilson. *Vapor-liquid equilibrium data on water-substitute gas components: N<sub>2</sub>-H<sub>2</sub>O, H<sub>2</sub>-H<sub>2</sub>O, CO-H<sub>2</sub>O, H<sub>2</sub>-CO-H<sub>2</sub>O, and H<sub>2</sub>S-H<sub>2</sub>O*. 1980. doi: 10.2172/6782591.

- [172] G. Kling and G. Maurer. Solubility of hydrogen in aqueous ethanolamine solutions at temperatures between 323 and 423 K. *Journal of Chemical & Engineering Data*, 36(4):390–394, 1991. ISSN 0021-9568. doi: 10.1021/jc00004a014.
- [173] W. DeVaney, J. M. Berryman, P. L. Kao, and B. Eakin. High temperature vLE measurements for substitute gas components. gas processors association.
- [174] E. Brunner, W. Hültenschmidt, and G. Schlichthärle. Fluid mixtures at high pressures iv. isothermal phase equilibria in binary mixtures consisting of (methanol + hydrogen or nitrogen or methane or carbon monoxide or carbon dioxide). *The Journal of Chemical Thermodynamics*, 19(3):273–291, 1987. ISSN 00219614. doi: 10.1016/0021-9614(87)90135-2.
- [175] Institute of Physical Chemistry, University of Cologne. Thermoc, 2018. URL <http://thermoc.uni-koeln.de/index.html>. Accessed: 2021-11-15.
- [176] A. M. Schweidtmann and A. Mitsos. Deterministic global optimization with artificial neural networks embedded. *Journal of Optimization Theory and Applications*, 180(3):925–948, oct 2018. doi: 10.1007/s10957-018-1396-0. URL <https://doi.org/10.1007/s10957-018-1396-0>.
- [177] A. M. Schweidtmann, D. Bongartz, D. Grothe, T. Kerkenhoff, X. Lin, J. Najman, and A. Mitsos. Deterministic global optimization with gaussian processes embedded. *Mathematical Programming Computation*, jun 2021. doi: 10.1007/s12532-021-00204-y. URL <https://doi.org/10.1007/s12532-021-00204-y>.
- [178] K. Hornik, M. Stinchcombe, and H. White. Multilayer feedforward networks are universal approximators. *Neural Networks*, 2(5):359–366, jan 1989. doi: 10.1016/0893-6080(89)90020-8. URL [https://doi.org/10.1016/0893-6080\(89\)90020-8](https://doi.org/10.1016/0893-6080(89)90020-8).
- [179] C. Nentwich, C. Varela, and S. Engell. Optimization of chemical processes applying surrogate models for phase equilibrium calculations. In *2019 International Joint Conference on Neural Networks (IJCNN)*. IEEE, jul 2019. doi: 10.1109/ijcnn.2019.8851816. URL <https://doi.org/10.1109/ijcnn.2019.8851816>.
- [180] A. Cozad, N. V. Sahinidis, and D. C. Miller. Learning surrogate models for simulation-based optimization. *AIChE Journal*, 60(6):2211–2227, mar 2014. doi: 10.1002/aic.14418. URL <https://doi.org/10.1002/aic.14418>.
- [181] C. E. Rasmussen. Gaussian processes in machine learning. In *Advanced Lectures on Machine Learning*, pages 63–71. Springer Berlin Heidelberg, 2004. doi: 10.1007/978-3-540-28650-9\_4. URL [https://doi.org/10.1007/978-3-540-28650-9\\_4](https://doi.org/10.1007/978-3-540-28650-9_4).
- [182] H. Yeomans and I. E. Grossmann. A systematic modeling framework of superstructure optimization in process synthesis. *Computers & Chemical Engineering*, 23(6):709–731, jun 1999. doi: 10.1016/s0098-1354(99)00003-4. URL [https://doi.org/10.1016/s0098-1354\(99\)00003-4](https://doi.org/10.1016/s0098-1354(99)00003-4).

- 
- [183] H. Yeomans and I. E. Grossmann. Nonlinear disjunctive programming models for the synthesis of heat integrated distillation sequences. *Computers & Chemical Engineering*, 23(9):1135–1151, nov 1999. doi: 10.1016/s0098-1354(99)00279-3. URL <https://doi.org/10.1016%2Fs0098-1354%2899%2900279-3>.
- [184] L. Mencarelli, Q. Chen, A. Pagot, and I. E. Grossmann. A review on superstructure optimization approaches in process system engineering. *Computers & Chemical Engineering*, 136:106808, may 2020. doi: 10.1016/j.compchemeng.2020.106808. URL <https://doi.org/10.1016%2Fj.compchemeng.2020.106808>.
- [185] J. Burre, D. Bongartz, and A. Mitsos. Comparison of MINLP formulations for global superstructure optimization. *Optimization and Engineering*, jan 2022. doi: 10.1007/s11081-021-09707-y. URL <https://doi.org/10.1007%2Fs11081-021-09707-y>.
- [186] A. J. V. Underwood. Fractional distillation of multicomponent mixtures. *Chemical Engineering Progress*, 44(8):603–614, 1948.
- [187] G. Liu, M. Jobson, R. Smith, and O. M. Wahnschafft. Shortcut design method for columns separating azeotropic mixtures. *Industrial & Engineering Chemistry Research*, 43(14):3908–3923, jul 2004. doi: 10.1021/ie030678y.
- [188] D. Bongartz and A. Mitsos. Deterministic global optimization of process flowsheets in a reduced space using McCormick relaxations. *Journal of Global Optimization*, 69(4):761–796, aug 2017. doi: 10.1007/s10898-017-0547-4. URL <https://doi.org/10.1007%2Fs10898-017-0547-4>.
- [189] J. Najman, D. Bongartz, and A. Mitsos. Linearization of McCormick relaxations and hybridization with the auxiliary variable method. *Journal of Global Optimization*, 80(4):731–756, feb 2021. doi: 10.1007/s10898-020-00977-x. URL <https://doi.org/10.1007%2Fs10898-020-00977-x>.
- [190] J. Najman, D. Bongartz, and A. Mitsos. Relaxations of thermodynamic property and costing models in process engineering. *Computers & Chemical Engineering*, 130:106571, nov 2019. doi: 10.1016/j.compchemeng.2019.106571. URL <https://doi.org/10.1016%2Fj.compchemeng.2019.106571>.
- [191] B. Chachuat, B. Houska, R. Paulen, N. Peric, J. Rajyaguru, and M. E. Villanueva. Set-theoretic approaches in analysis, estimation and control of nonlinear systems. *IFAC-PapersOnLine*, 48(8):981–995, 2015. doi: 10.1016/j.ifacol.2015.09.097. URL <https://doi.org/10.1016%2Fj.ifacol.2015.09.097>.
- [192] G. P. McCormick. Computability of global solutions to factorable nonconvex programs: Part i — convex underestimating problems. *Mathematical Programming*, 10(1):147–175, dec 1976. doi: 10.1007/bf01580665. URL <https://doi.org/10.1007%2Fbf01580665>.
- [193] A. Tsoukalas and A. Mitsos. Multivariate McCormick relaxations. *Journal of Global Optimization*, 59(2-3):633–662, apr 2014. doi: 10.1007/s10898-014-0176-0. URL <https://doi.org/10.1007%2Fs10898-014-0176-0>.

- [194] J. J. E. Kelley. The cutting-plane method for solving convex programs. *Journal of the Society for Industrial and Applied Mathematics*, 8(4):703–712, dec 1960. doi: 10.1137/0108053. URL <https://doi.org/10.1137%2F0108053>.
- [195] E. M. Smith and C. C. Pantelides. Global optimisation of nonconvex MINLPs. *Computers & Chemical Engineering*, 21:S791–S796, may 1997. doi: 10.1016/s0098-1354(97)87599-0. URL <https://doi.org/10.1016%2Fs0098-1354%2897%2987599-0>.
- [196] M. Tawarmalani and N. V. Sahinidis. *Convexification and Global Optimization in Continuous and Mixed-Integer Nonlinear Programming*. Springer US, 2002. doi: 10.1007/978-1-4757-3532-1. URL <https://doi.org/10.1007%2F978-1-4757-3532-1>.
- [197] R. Misener and C. A. Floudas. ANTIGONE: Algorithms for coNTinuous / integer global optimization of nonlinear equations. *Journal of Global Optimization*, 59(2-3): 503–526, mar 2014. doi: 10.1007/s10898-014-0166-2. URL <https://doi.org/10.1007%2Fs10898-014-0166-2>.
- [198] T. Achterberg. SCIP: solving constraint integer programs. *Mathematical Programming Computation*, 1(1):1–41, Jul 2009. ISSN 1867-2957. doi: 10.1007/s12532-008-0001-1. URL <https://doi.org/10.1007/s12532-008-0001-1>.
- [199] J. Voggenreiter and J. Burger. Side products in the water-tolerant synthesis of poly(oxymethylene) dimethyl ethers: Formation kinetics and implications for process design. *Industrial & Engineering Chemistry Research*, 60(6):2418–2429, feb 2021. doi: 10.1021/acs.iecr.0c05780. URL <https://doi.org/10.1021%2Facs.iecr.0c05780>.
- [200] D. Oestreich, L. Lautenschütz, U. Arnold, and J. Sauer. Reaction kinetics and equilibrium parameters for the production of oxymethylene dimethyl ethers (OME) from methanol and formaldehyde. *Chemical Engineering Science*, 163:92–104, may 2017. doi: 10.1016/j.ces.2016.12.037. URL <https://doi.org/10.1016%2Fj.ces.2016.12.037>.
- [201] N. W. Ockwig and T. M. Nenoff. Membranes for hydrogen separation. *Chemical Reviews*, 107(10):4078–4110, oct 2007. doi: 10.1021/cr0501792. URL <https://doi.org/10.1021%2Fcr0501792>.
- [202] A. K. Prabhu and S. Oyama. Highly hydrogen selective ceramic membranes: application to the transformation of greenhouse gases. *Journal of Membrane Science*, 176(2):233–248, aug 2000. doi: 10.1016/s0376-7388(00)00448-8. URL <https://doi.org/10.1016%2Fs0376-7388%2800%2900448-8>.
- [203] A. Singh, J. Forbes, P. Vermeer, and S. Woo. Model-based real-time optimization of automotive gasoline blending operations. *Journal of process control*, 10(1):43–58, 2000. doi: 10.1016/S0959-1524(99)00037-2. URL [https://doi.org/10.1016/S0959-1524\(99\)00037-2](https://doi.org/10.1016/S0959-1524(99)00037-2).
- [204] E. Ahmetović and I. E. Grossmann. Global superstructure optimization for the design of integrated process water networks. *AIChE Journal*, 57(2):434–457, jan 2011. doi: 10.1002/aic.12276. URL <https://doi.org/10.1002%2Faic.12276>.

- [205] I. E. Grossmann. Review of nonlinear mixed-integer and disjunctive programming techniques. *Optimization and engineering*, 3(3):227–252, 2002. URL <https://doi.org/10.1023/A:1021039126272>.
- [206] R. Raman and I. Grossmann. Modelling and computational techniques for logic based integer programming. *Computers & Chemical Engineering*, 18(7):563–578, jul 1994. doi: 10.1016/0098-1354(93)e0010-7. URL <https://doi.org/10.1016/2F0098-1354%2893%29e0010-7>.
- [207] S. Lee and I. E. Grossmann. New algorithms for nonlinear generalized disjunctive programming. *Computers & Chemical Engineering*, 24(9-10):2125–2141, oct 2000. doi: 10.1016/s0098-1354(00)00581-0. URL <https://doi.org/10.1016/2Fs0098-1354%2800%2900581-0>.
- [208] M. Türkay and I. E. Grossmann. Logic-based MINLP algorithms for the optimal synthesis of process networks. *Computers & Chemical Engineering*, 20(8):959–978, aug 1996. doi: 10.1016/0098-1354(95)00219-7. URL <https://doi.org/10.1016/2F0098-1354%2895%2900219-7>.
- [209] I. E. Grossmann and F. Trespalacios. Systematic modeling of discrete-continuous optimization models through generalized disjunctive programming. *AIChE Journal*, 59(9):3276–3295, may 2013. doi: 10.1002/aic.14088. URL <https://doi.org/10.1002/2Faic.14088>.
- [210] G. Nemhauser and L. Wolsey. *Integer and Combinatorial Optimization*. John Wiley & Sons, Inc., jun 1988. doi: 10.1002/9781118627372. URL <https://doi.org/10.1002/2F9781118627372>.
- [211] S. Lee and I. E. Grossmann. Global optimization of nonlinear generalized disjunctive programming with bilinear equality constraints: applications to process networks. *Computers & Chemical Engineering*, 27(11):1557–1575, nov 2003. doi: 10.1016/s0098-1354(03)00098-x. URL <https://doi.org/10.1016/2Fs0098-1354%2803%2900098-x>.
- [212] J. P. Ruiz and I. E. Grossmann. Strengthening of lower bounds in the global optimization of bilinear and concave generalized disjunctive programs. *Computers & Chemical Engineering*, 34(6):914–930, jun 2010. doi: 10.1016/j.compchemeng.2009.10.016. URL <https://doi.org/10.1016/2Fj.compchemeng.2009.10.016>.
- [213] Z.-Q. Luo, J.-S. Pang, and D. Ralph. *Mathematical Programs with Equilibrium Constraints*. Cambridge University Press, nov 1996. doi: 10.1017/cbo9780511983658. URL <https://doi.org/10.1017/2Fcbo9780511983658>.
- [214] C. Chen and O. L. Mangasarian. A class of smoothing functions for nonlinear and mixed complementarity problems. *Computational Optimization and Applications*, 5(2):97–138, mar 1996. doi: 10.1007/bf00249052. URL <https://doi.org/10.1007/2Fbf00249052>.
- [215] D. Bongartz. *Deterministic Global Flowsheet Optimization for the Design of Energy Conversion Processes*. PhD thesis, RWTH Aachen University, 2020.

- [216] R. P. Byrne and I. D. L. Bogle. Global optimization of modular process flowsheets. *Industrial & Engineering Chemistry Research*, 39(11):4296–4301, nov 2000. doi: 10.1021/ie990619d. URL <https://doi.org/10.1021%2Fie990619d>.
- [217] D. Bongartz and A. Mitsos. Deterministic global flowsheet optimization: Between equation-oriented and sequential-modular methods. *AIChE Journal*, 65(3):1022–1034, jan 2019. doi: 10.1002/aic.16507. URL <https://doi.org/10.1002%2Faic.16507>.
- [218] A. Mitsos, B. Chachuat, and P. I. Barton. McCormick-based relaxations of algorithms. *SIAM Journal on Optimization*, 20(2):573–601, jan 2009. doi: 10.1137/080717341. URL <https://doi.org/10.1137%2F080717341>.
- [219] J. K. Scott, M. D. Stuber, and P. I. Barton. Generalized McCormick relaxations. *Journal of Global Optimization*, 51(4):569–606, feb 2011. doi: 10.1007/s10898-011-9664-7. URL <https://doi.org/10.1007%2Fs10898-011-9664-7>.
- [220] M. D. Stuber, J. K. Scott, and P. I. Barton. Convex and concave relaxations of implicit functions. *Optimization Methods and Software*, 30(3):424–460, jun 2014. doi: 10.1080/10556788.2014.924514. URL <https://doi.org/10.1080%2F10556788.2014.924514>.
- [221] A. Wechsung, J. K. Scott, H. A. J. Watson, and P. I. Barton. Reverse propagation of McCormick relaxations. *Journal of Global Optimization*, 63(1):1–36, apr 2015. doi: 10.1007/s10898-015-0303-6. URL <https://doi.org/10.1007%2Fs10898-015-0303-6>.
- [222] K. Roh, A. Bardow, D. Bongartz, J. Burre, W. Chung, S. Deutz, D. Han, M. Heßelmann, Y. Kohlhaas, A. König, J. S. Lee, R. Meys, S. Völker, M. Wessling, J. H. Lee, and A. Mitsos. Early-stage evaluation of emerging CO<sub>2</sub> utilization technologies at low technology readiness levels. *Green Chemistry*, 22(12):3842–3859, 2020. doi: 10.1039/c9gc04440j. URL <https://doi.org/10.1039%2Fc9gc04440j>.
- [223] B. Baumrucker, J. Renfro, and L. Biegler. MPEC problem formulations and solution strategies with chemical engineering applications. *Computers & Chemical Engineering*, 32(12):2903–2913, dec 2008. doi: 10.1016/j.compchemeng.2008.02.010. URL <https://doi.org/10.1016%2Fj.compchemeng.2008.02.010>.
- [224] A. Wechsung and P. I. Barton. Global optimization of bounded factorable functions with discontinuities. *Journal of Global Optimization*, 58(1):1–30, mar 2013. doi: 10.1007/s10898-013-0060-3. URL <https://doi.org/10.1007%2Fs10898-013-0060-3>.
- [225] F. Trespalacios and I. E. Grossmann. Improved big-m reformulation for generalized disjunctive programs. *Computers & Chemical Engineering*, 76:98–103, may 2015. doi: 10.1016/j.compchemeng.2015.02.013. URL <https://doi.org/10.1016%2Fj.compchemeng.2015.02.013>.
- [226] S. Ceria and J. Soares. Convex programming for disjunctive convex optimization. *Mathematical Programming*, 86(3):595–614, dec 1999. doi: 10.1007/s101070050106. URL <https://doi.org/10.1007%2Fs101070050106>.

- 
- [227] N. Sawaya. *Reformulations, relaxations and cutting planes for generalized disjunctive programming*. PhD thesis, Carnegie Mellon University, 2006.
- [228] K. C. Furman, N. W. Sawaya, and I. E. Grossmann. A computationally useful algebraic representation of nonlinear disjunctive convex sets using the perspective function. *Computational Optimization and Applications*, pages 1–26, 2020.
- [229] I. E. Grossmann and S. Lee. Generalized convex disjunctive programming: Nonlinear convex hull relaxation. *Computational optimization and applications*, 26(1):83–100, 2003. URL <https://doi.org/10.1023/A:1025154322278>.
- [230] S. Scholtes. Convergence properties of a regularization scheme for mathematical programs with complementarity constraints. *SIAM Journal on Optimization*, 11(4):918–936, jan 2001. doi: 10.1137/s1052623499361233. URL <https://doi.org/10.1137%2Fs1052623499361233>.
- [231] V. Gopal and L. T. Biegler. Smoothing methods for complementarity problems in process engineering. *AIChE Journal*, 45(7):1535–1547, jul 1999. doi: 10.1002/aic.690450715. URL <https://doi.org/10.1002%2Faic.690450715>.
- [232] A. M. Sahlodin, H. A. J. Watson, and P. I. Barton. Nonsmooth model for dynamic simulation of phase changes. *AIChE Journal*, 62(9):3334–3351, jul 2016. doi: 10.1002/aic.15378. URL <https://doi.org/10.1002%2Faic.15378>.
- [233] W. R. Huster, A. M. Schweidtmann, J. T. Lüthje, and A. Mitsos. Deterministic global superstructure-based optimization of an organic rankine cycle. *Computers & Chemical Engineering*, 141:106996, oct 2020. doi: 10.1016/j.compchemeng.2020.106996. URL <https://doi.org/10.1016%2Fj.compchemeng.2020.106996>.
- [234] M. R. Kılınç and N. V. Sahinidis. Exploiting integrality in the global optimization of mixed-integer nonlinear programming problems with BARON. *Optimization Methods and Software*, 33(3):540–562, jul 2017. doi: 10.1080/10556788.2017.1350178. URL <https://doi.org/10.1080%2F10556788.2017.1350178>.
- [235] T. G. W. Epperly and E. N. Pistikopoulos. *Journal of Global Optimization*, 11(3):287–311, 1997. doi: 10.1023/a:1008212418949. URL <https://doi.org/10.1023%2Fa%3A1008212418949>.
- [236] M. Dür and R. Horst. Lagrange duality and partitioning techniques in nonconvex global optimization. *Journal of Optimization Theory and Applications*, 95(2):347–369, nov 1997. doi: 10.1023/a:1022687222060. URL <https://doi.org/10.1023%2Fa%3A1022687222060>.
- [237] A. Ben-Tal, G. Eiger, and V. Gershovitz. Global minimization by reducing the duality gap. *Mathematical Programming*, 63(1-3):193–212, jan 1994. doi: 10.1007/bf01582066. URL <https://doi.org/10.1007%2Fbf01582066>.
- [238] R. Kannan and P. I. Barton. Convergence-order analysis of branch-and-bound algorithms for constrained problems. *Journal of Global Optimization*, 71(4):753–813, jun 2017. doi: 10.1007/s10898-017-0532-y. URL <https://doi.org/10.1007%2Fs10898-017-0532-y>.

- [239] M. Türkay and I. E. Grossmann. Disjunctive programming techniques for the optimization of process systems with discontinuous investment costs-multiple size regions. *Industrial & Engineering Chemistry Research*, 35(8):2611–2623, jan 1996. doi: 10.1021/ie9600856. URL <https://doi.org/10.1021%2Fie9600856>.
- [240] M. Langiu, D. Y. Shu, F. J. Baader, D. Hering, U. Bau, A. Xhonneux, D. Müller, A. Bardow, A. Mitsos, and M. Dahmen. COMANDO: A next-generation open-source framework for energy systems optimization. *Computers & Chemical Engineering*, 152:107366, sep 2021. doi: 10.1016/j.compchemeng.2021.107366. URL <https://doi.org/10.1016%2Fj.compchemeng.2021.107366>.
- [241] Q. Chen, E. S. Johnson, J. D. Siirola, and I. E. Grossmann. Pyomo.GDP: Disjunctive models in python. In *13th International Symposium on Process Systems Engineering (PSE 2018)*, pages 889–894. Elsevier, 2018. doi: 10.1016/b978-0-444-64241-7.50143-9. URL <https://doi.org/10.1016%2Fb978-0-444-64241-7.50143-9>.
- [242] Q. Chen, Y. Liu, G. Seastream, J. D. Siirola, and I. E. Grossmann. Pyosyn: A new framework for conceptual design modeling and optimization. *Computers & Chemical Engineering*, 153:107414, oct 2021. doi: 10.1016/j.compchemeng.2021.107414. URL <https://doi.org/10.1016%2Fj.compchemeng.2021.107414>.
- [243] K. Kraemer, A. Harwardt, M. Skiborowski, S. Mitra, and W. Marquardt. Shortcut-based design of multicomponent heteroazeotropic distillation. *Chemical Engineering Research and Design*, 89(8):1168–1189, aug 2011. doi: 10.1016/j.cherd.2011.02.026. URL <https://doi.org/10.1016%2Fj.cherd.2011.02.026>.
- [244] J. Bausa and W. Marquardt. Quick and reliable phase stability test in VLLE flash calculations by homotopy continuation. *Computers & Chemical Engineering*, 24(11):2447–2456, nov 2000. doi: 10.1016/s0098-1354(00)00604-9. URL <https://doi.org/10.1016%2Fs0098-1354%2800%2900604-9>.
- [245] Rohm and Haas Company. Amberlyst polymeric catalysts. Data Sheet, 2005.
- [246] M. Albert, I. Hahnenstein, H. Hasse, and G. Maurer. Vapor-liquid and liquid-liquid equilibria in binary and ternary mixtures of water, methanol, and methylal. *Journal of Chemical & Engineering Data*, 46(4):897–903, jul 2001. doi: 10.1021/je000352l. URL <https://doi.org/10.1021%2Fje000352l>.
- [247] C. B. Dirk-Faitakis, W. An, T.-B. Lin, and K. T. Chuang. Catalytic distillation for simultaneous hydrolysis of methyl acetate and etherification of methanol. *Chemical Engineering and Processing: Process Intensification*, 48(5):1080–1087, may 2009. doi: 10.1016/j.cep.2009.03.001. URL <https://doi.org/10.1016%2Fj.cep.2009.03.001>.
- [248] C. F. Breitzkreuz, N. Schmitz, E. Ströfer, J. Burger, and H. Hasse. Design of a production process for poly(oxymethylene) dimethyl ethers from dimethyl ether and trioxane. *Chemie Ingenieur Technik*, 90(10):1489–1496, aug 2018. doi: 10.1002/cite.201800038. URL <https://doi.org/10.1002%2Fcite.201800038>.



- 
- [249] M. S. Peters and K. D. Timmerhaus. *Plant design and economics for chemical engineers*. McGraw-Hill, Inc., 1980.
- [250] N. Mimura and M. Saito. Dehydrogenation of ethylbenzene to styrene over  $\text{Fe}_2\text{O}_3/\text{Al}_2\text{O}_3$  catalysts in the presence of carbon dioxide. *Catalysis Today*, 55(1-2): 173–178, jan 2000. doi: 10.1016/S0920-5861(99)00236-9. URL [https://doi.org/10.1016/S0920-5861\(99\)00236-9](https://doi.org/10.1016/S0920-5861(99)00236-9).
- [251] A. Ghosh, W. G. Chapman, and R. N. French. Gas solubility in hydrocarbons—a soft-based approach. *Fluid Phase Equilibria*, 209(2):229–243, 2003. ISSN 03783812. doi: 10.1016/S0378-3812(03)00147-X.
- [252] M. K. Kozłowska, B. F. Jürgens, C. S. Schacht, J. Gross, and T. W. de Loos. Phase behavior of hyperbranched polymer systems: experiments and application of the perturbed-chain polar soft equation of state. *The journal of physical chemistry. B*, 113(4):1022–1029, 2009. doi: 10.1021/jp804459x.
- [253] V. Pokorný, V. Štejfá, J. Pavlíček, M. Klajmon, M. Fulem, and K. Růžička. Vapor pressures and thermophysical properties of dimethoxymethane, 1,2-dimethoxyethane, 2-methoxyethanol, and 2-ethoxyethanol: Data reconciliation and perturbed-chain statistical associating fluid theory modeling. *Journal of Chemical & Engineering Data*, 66(6):2640–2654, 2021. ISSN 0021-9568. doi: 10.1021/acs.jced.1c00229.
- [254] J. Gross and G. Sadowski. Application of the perturbed-chain soft equation of state to associating systems. *Industrial & Engineering Chemistry Research*, 41(22):5510–5515, 2002. ISSN 0888-5885. doi: 10.1021/ie010954d.